UPGRADING OF PGM-RICH LEACH RESIDUE BY HIGH PRESSURE CAUSTIC LEACHING

by

Brian Mwewa

Thesis presented in partial fulfilment
of the requirements for the Degree

of

MASTER OF ENGINEERING

(EXTRACTIVE METALLURGICAL ENGINEERING)

in the Faculty of Engineering
at Stellenbosch University

Supervisor

Johann Steyl

Co-Supervisor

Steven Bradshaw

December, 2015

Declaration

By submitting this thesis electronically, I declare that the entirety of the work contained therein is my own, original work, that I am the sole author thereof (save to the extent explicitly otherwise stated), that reproduction and publication thereof by Stellenbosch University will not infringe any third party rights and that I have not previously in its entirety or in part submitted it for obtaining any qualification.

31st August, 2015
Date

ABSTRACT

There is a lack of clear understanding of the rate of selenium (Se), arsenic (As) and sulphur (S) dissolution during caustic (NaOH) batch leaching of PGM-rich leach residue in the presence of oxygen. This has been a limitation in the optimisation of hydrometallurgical processes for the upgrading of PGM concentrates before refining the precious metals. Conditions to improve the rate of leaching of amphoteric elements while minimizing PGM losses were examined to enhance the performance of the leaching process. Development of intrinsic leaching rate equations represent the core of the overall batch leaching model developed in this study. The robustness of the model was assessed by its ability to accurately simulate the effects of changing operating parameters on the reaction extents. The effects of the interfacial oxygen mass transfer rate and temperature on the leaching rates were therefore also included in the overall model.

The first part of the experimental program focussed on the interfacial oxygen mass transfer rate in the test autoclave. This enabled an accurate mathematical description of the interfacial mass transfer rate of the primary oxidant, diatomic oxygen (O_2) molecule from the gas to the liquid phase. Mass transfer tests were conducted using the sodium sulphite method at 60°C, 100 kPa oxygen partial pressure and agitation speed of between 500 to 1000 rev/min. Cobalt(II) was used as the catalyst with a concentration range of 1 to 5 mg/L.

Oxidation of amphoteric elements was investigated by leaching of PGM-rich leach residue (residue from sulphuric acid leaching of converter matte) in caustic solution. The test work was conducted to determine the intrinsic leaching rates in 0.125, 0.25 and 0.5 mol/L NaOH solutions in the 160° to 190°C temperatures range over a period of 6 hours. Oxygen partial pressure was maintained at 11 atm in the factorial experiments. The effect of oxygen partial pressure was quantified by conducting tests with oxygen partial pressure ranging from 7 to 16 atm. The intrinsic rate constants and activation energies derived from this test work were incorporated in the overall kinetic model to simulate the batch leaching profiles under real plant conditions.

During the caustic pressure oxidation of amphoteric elements, the rate of oxidation was rapid during the first 10 minutes and decreased steadily over the course of

experiment. The experimental results suggest that the oxidation kinetics are controlled by product layer diffusion with sulphur, selenium and arsenic (Arrhenius) activation energies of 31.8 kJ/mol, 26.1 kJ/mol and 10.7 kJ/mol respectively over the temperature range of 160 to 190°C. The reaction mechanism, as well as the observed kinetic behaviour, is most likely due to the base metal/PGMs hydroxide layer that formed as a result of precipitation. An increase in temperature increased the sulphur and arsenic reaction rates. The selenium reaction rate also increased as the temperature was increased from 160 to 175°C. A further increase in temperature above 175°C did not yield a significant increase in the reaction rate. An increase in the caustic concentration increased the reaction rates of all the elements. Increased oxygen partial pressure also improved the reaction rates, with the most significant change observed for sulphur oxidation; the extent of sulphur oxidation increased from 75 to 85% when oxygen partial pressure was increased from 7 to 16 atm. Reaction orders of 0.25, 0.12 and 0.21 with respect to hydroxide concentration and 0.37, 0.29 and 0.36 with respect to dissolved oxygen concentration were obtained for sulphur, selenium and arsenic respectively. Kinetic models were developed for sulphur, selenium and arsenic extraction. The sulphur and selenium simulation gave better agreement between the experimental and model predicted values, while the arsenic simulation gave a relatively poor prediction of the extractions.

The caustic concentration had a notable effect on the dissolution of the PGMs. An increase in the caustic concentration increased the dissolution of platinum, palladium and ruthenium. Ruthenium dissolution also increased with an increase in temperature. To the contrary, platinum and palladium dissolution decreased with an increase in temperature. Rhodium and iridium precipitated and did not report in the solution phase while osmium could not be traced. The oxygen partial pressure did not have a significant effect on the dissolution rate of platinum, palladium and ruthenium.

OPSOMMING

Daar is ‘n tekort aan die begrip van die tempo van seleen (Se), arseen (As) en swawel (S) oplosbaarheid gedurende bytsoda (NaOH) enkelladingsloging van platinum groep metaal (PGM)-ryk oorskot materiaal in die teenwoordigheid van suurstof. Hierdie inligting word benodig wanneer die optimisering van tipiese hidrometallurgiese prosesse wat PGM oorskot materiaal opgradeer verlang word. Hierdie bytsoda druklogingsproses vind tipies voor raffinering van die PGM metale plaas. Kondisies wat die tempo van amfoteriese element-loging verbeter, terwyl die PGM verliese geminimaliseer word, was in hierdie werk geondersoek om sodoende die effektiwiteit van die logingsproses te verbeter. Die ontwikkeling van intrinsieke logingtempo vergelykings vorm die kern van die algemene enkelladingsloging model wat ontwikkel was. Die robuustheid van hierdie model word geevalueer op sy vermoë om akkuraat die effekte van veranderende bedryfstelsel parameters op die logingstempo van betrokke reaksies te simuleer. Die effekte van suurstof tussenvlak massaoordrag en temperatuur was ook in die algehele model ingesluit.

Die eerste deel van die eksperimentele program het gefokus op die suurstof tussenvlak massaoordrag in die outoklaaf. ‘n Akkurate wiskundige model wat die massaoordrag van die primêre oksidant, diatomiese suurstof (O_2), van die gas fase na die vloeistof fase beskryf, was gebruik om die suurstof oordragtempo te kwantifiseer. Suurstof massaoordrag toetse het van die natrium sulfiet metode gebruik gemaak by 60°C, 100 kPa suurstof parsiële druk en tussen 500 en 1000 rev/min roerspoed. Kobalt(II) het gedien as katalis wat tussen 1 tot 5 mg/L gevarieer was.

Die amfoteriese element oksidasie was volgende ondersoek deur die PGM-ryk oorskot materiaal te loog met bytsoda (wat stroomop onderwerp was aan swawelsuur loging van omskakelaar mat). Die toetswerk wou die intrinsieke logingtempo’s met 0.125, 0.25 en 0.5 mol/L NaOH oplossings by temperature 160 en 190°C oor 6 uur residensie tyd vasstel. Die suurstof parsiële druk was konstant gehou op 11 atm in hierdie faktoriale eksperimente. Die effek van suurstof parsiële druk was apart vasgestel, deur die suurstof parsiële druk te varieër vanaf 6 tot 16 atm. Die intrinsieke tempokonstantes en aktiveringsenergieë wat in hierdie toetswerk afgelei is, was in ‘n algehele kinetiese model ingekorporeer wat die enkellading logingsprofiele gesimuleer het by aanleg kondisies.

Die tempo van oksidasie was vinnig in die eerste 10 minute en het geleidelik afgeplat, gedurende die bytsoda druk oksidasie van amfoteriese elemente. Die eksperimentele resultate suggereer dat produklaagdiffusie die oksidasie kinetika beheer met swawel, seleen en arseen (Arrhenius) aktiveringsenergieë as volg bereken in die temperatuur interval 160 tot 190°C: 31.8 kJ/mol, 26.1 kJ/mol en 10.7 kJ/mol. Die reaksie meganisme en kinetiese gedrag word hoogs waarskynlik veroorsaak deur die onedelmetaal/PGM hidroksied laag wat deur middel van presipitasie gevorm het. Temperatuur toename het die swawel en arseen se reaksietempo's verhoog. Met seleen het die reaksietempo met temperatuur toename tussen 160 en 175°C ook verhoog, maar afplatting het by 175°C opwaarts plaasgevind. Oor die algemeen het die bytsoda konsentrasie die amfoteriese elemente se reaksietempo's verhoog. Die verhoging van die suurstof parsiële druk het ook die reaksietempo's verhoog. Swawel oksidasie het van 75 tot 85% verhoog vanaf 6 tot 16 atm, wat die mees noemenswaardige verandering was. Swawel, seleen en arseen reaksieordes van 0.25, 0.12 en 0.21 met hidroksied konsentrasie en 0.37, 0.29 en 0.36 met opgeloste suurstof konsentrasie het die beste paslyn op die eksperimentele data tot gevolg gehad. Hierdie data was gebruik om die kinetiese modelle van swawel, seleen en arseen ekstraksie te ontwikkel. Terwyl swawel en seleen 'n goeie paslyn vir die eksperimentele data tot gevolg gehad het, kon passing van arseen ekstraksie nie 'n goeie model oplewer nie.

Varierende bytsoda konsentrasie het 'n noemenswaardige effek op die PGM ontbinding gehad. Wanneer die bytsoda se konsentrasie vermeerder word, los daar meer platinum, palladium en rutenium op. Rutenium ontbinding het tydens 'n temperatuur toename verhoog. In kontras het platinum en palladium ontbinding velaag tydens temperatuur toename. Rodium en iridium het gepresipiteer en was nie ontbind nie. Osmium kon nie gemeet word nie. Die suurstof parsiële druk het nie 'n noemenswaardige effek op platinum, palladium en rutenium ontbinding gehad nie.

ACKNOWLEDGEMENTS

My appreciation goes to;

- The Almighty God for giving me the strength to utilise the God given intelligence to do the research.
- Dr Johann Steyl and Professor Steven Bradshaw for the tireless effort, dedication, inspiration and guidance rendered to me to successfully complete my research.
- Lonmin BMR for the material and financial support for this research.
- Department of Process Engineering staff at Stellenbosch University for administrative and technical assistance.
- My Mother Theresa Nsemba Mwila Mwewa, My siblings and all my friends for the support and encouragements showered on me.
- My fiancée Iris Ndina Astalavista Lumano for the encouragement and patience during the time of study.

For "I can do all things through Christ who strengths me".

TABLE OF CONTENTS

LIST OF FIGURES

LIST OF TABLES

NOMENCLATURE

a	gas-liquid interfacial area per unit volume	m^2/m^3
A	Area	m^2
C_A	Bulk concentration of A in solution	mol/m^3
C_i	Molal concentration of species	mol/kg
C	Dissolved oxygen concentration	mol/kg
C*	Saturation concentration of oxygen	mol/kg
Cp	Heat capacity	J/kg°C
D	particle diameter	m
D_s	Effective diffusion coefficient	m^2/s
D*	Normalised particle size	m
Ea	Activation energy	J/mol
E_h	Oxidation reduction potential	mV
f(D)	Cumulative distribution function	-
$F(D)_i$	Weight fraction of particles in size class i	-
ΔG	Gibbs free energy change	J/mol
ΔG_r	Gibbs free energy change of reaction	J/mol
h	time step in Euler method	minutes
ΔH	Enthalpy change	J/kg
J	Flux	$mol/m^2/s$
K	equilibrium constant	-
k_c	rate constant for chemically controlled processes	mol/L.min
k_G	Gas side mass transfer coefficient	m/s
k_d	rate constant for diffusion controlled processes	mol/L.min
k_H	Henry's constant	mol/m.atm
kLa	Volumetric mass transfer coefficient	min^{-1}
ℓ	particle length	m
m	mass	kg
m_D	weight fraction of species	-

Mw	Molecular weight	g/mol
n_i	Molar amount of species i	mol
n_0	Molar amount at time 0	mol
p	Molar density	Mol/m_3
P	Pressure	atm
Po_2	Oxygen partial pressure	atm
pH	Negative log of H^+ activity	-
R	Ideal gas constant	J/mol.K
R^2	Coefficient of determination	-
S	Specific surface area	m^2/m^3
r	Rate of reaction	mol/L.min
r	radius of particle	m
T	Temperature	K
T_r	Reference temperature	K
t	Time	minutes
v	stoichiometric coefficient	-
V	Volume	m^3
V_m	Molar volume of species	m^3/mol
X	Conversion of solid species	-

Acronym

BMR	Base Metal Refinery
CAF	Central analytical facility
ICP-AES	Inductive Coupled Plasma Atomic Emission Spectroscopy
ppm	Parts per million
rpm	revolutions per minute
SEM	Scanning Electron Microscope
XRD	X-Ray Diffraction

1 INTRODUCTION

Lonmin Plc is among the largest platinum producing companies in the world. Since it is a primary precious metals refinery, it is essential that prior to refining, there is an intermediate process to remove the bulk of the base metal and deleterious elements. This is vital in lieu of the different types of ore bodies mined. This bulk impurity removal process provides the feed material to the Precious Metal Refinery and makes the subsequent stages in the precious metal separation process more economical and efficient.

Platinum and palladium are the most abundant platinum group metals (PGMs) while rhodium is a distant third. The PGMs nearly always occur as native metal alloys in nature (Christie and Challis, 1990). Platinum occurs as isoferroplatinum (Pt_3Fe) with iron, or as mineral sulphides such as cooperite (Pt,Pd)S and braggite (Pt,Pd,Ni). Platinum also occurs in arsenides as sperrylite $PtAs_2$, bismuthide monchelite $(Pt,Pd)(Te,Bi)_2$ or as antimonides, i.e., geversite ($PtSb_2$) as well as stabio-palladinite (Pd_3Sb). The principal platinum minerals worldwide are platinum-iron alloy, sperrylite, braggite cooperite, osmiridium (IrOs), laurite (RuS_2) and iridosmine (OsIr). Typically, PGMs occur as small grains and inclusions in mineral sulphides (nickel-copper sulphide) and chromite, and as flattened, rounded detrital grains in placer deposits (Christie and Challis, 1990). Table 1.1 shows a selection of the more common platinum group minerals.

The PGM bearing ores processed at Lonmin plc are mined from Upper Group 2 (UG-2) and Merensky reefs. The UG-2 ore body lies 40-140 meters below the Merensky reef in the Bushveld igneous complex. The major base metal sulphides associated with the occurrence of PGMs in both the UG-2 and Merensky reefs include chalcopyrite ($CuFeS_2$), pentlandite $(Ni,Fe,Co)_9S_8$ and pyrrhotite (Fe_8S_9). In the Merensky reef, the dominant PGM bearing minerals include cooperite (PtS), sperrylite ($PtAs_2$), Pt-Pd bismuthtelluride and braggite (Pt-Pd)S. Ru-Os-Ir-bearing laurites, cooperite, Rh sulphides, braggite, and unnamed Pt-Rh-Ir-Cu-S are the dominant PGM bearing minerals in the UG-2 reef. The PGMs are found along the sulphide/silicate grain boundaries or as inclusions in silicate and chromite in the Merensky reef. In the UG-2 reef, PGMs occur interstitially, along chromite grain

boundaries and locked in chromites (Lamya, 2007). Table 1.2 below shows the typical Merensky and UG-2 concentrate composition.

Table 1.1: A selection of the more common platinum group minerals

Group	Name	Formula	Group	Name	Formula
Alloys	Atokite	$(Pd,Pt)_3Sn$	Arsenides	Sperrylite	$PtAs_2$
	Isoferroplatinum	Pt_3Fe		Stillwaterite	Pd_8As_3
	Osmiridium	OsIr		Genkinite	$(Pt,Pd,Rh)_4Sb_3$
	Potarite	PdHg		Isomertieite	$Pd_{11}As_2Sb_2$
	Rustenburgite	$(Pt,Pd)_3Sn$		Stibiopalladinite	Pd_5Sb_2
	Tulameenite	Pt_2FeCu		Sudburyite	(Pd,Ni)Sb
Sulphides	Braggite	(Pt,Pd)S		Geversite	$Pt(Sb,Bi)_2$
	Cooperite	PtS	Bismuthides	Froodite	$PdBi_2$
	Erlichmanite	OsS_2	Tellurides	Kotulskite	PdTe
	Hollingworthite	RhAsS		Merenskyite	$(Pd,Pt)(Te,Bi)_2$
	Laurite	$(Ru,Os)S_2$		Michenerite	Pd(Bi,Sb)Te
	Ruarsite	(Ru,Os)AsS		Moncheite	$(Pt,Pd)(Te,Bi)_2$

(Gunn et al., 2009)

Table 1.2: Typical Merensky and UG-2 concentrate analysis for Lonmin Operations

	Al_2O_3 (%)	CaO (%)	Cr_2O_3 (%)	Cu+Ni (%)	Fe (%)	MgO (%)	S (%)	SiO_2 (%)	PGM (g/t)
Merensky	1.8	2.8	0.4	5.0	18.0	18.0	9.0	41	130
UG-2 blend	3.6	2.7	2.8	3.3	15.0	21.0	4.1	47	340

(Nell, 2004)

These metal sulphide flotation concentrates are treated in several ways. These include high temperature smelting, where sulphur is oxidised with oxygen or air to sulphur dioxide, producing molten matte in the process. Due to environmental concerns, the sulphur dioxide produced has to be captured and is converted into sulphuric acid. The alternative to the smelting of sulphide mineral flotation concentrates would be to employ hydrometallurgy, where the metal sulphide is

dissolved in an aqueous solution. Other processes involve the combination of both smelting and leaching, which is the case for the process of producing PGMs at Lonmin Plc. This processing involves comminution, flotation, smelting, and converter treatment of the furnace matte. After the pyrometallurgical treatment of the concentrate, hydrometallurgy separates and recovers the base metals (primarily nickel, cobalt, copper and any residual iron) associated with the PGMs. The leach solutions are processed further to recover the base metals. These processes represent significant consideration by themselves; nonetheless this is not the focus of this study. Figure 1.1 shows the general process flow sheet for Lonmin base metal refinery (BMR).

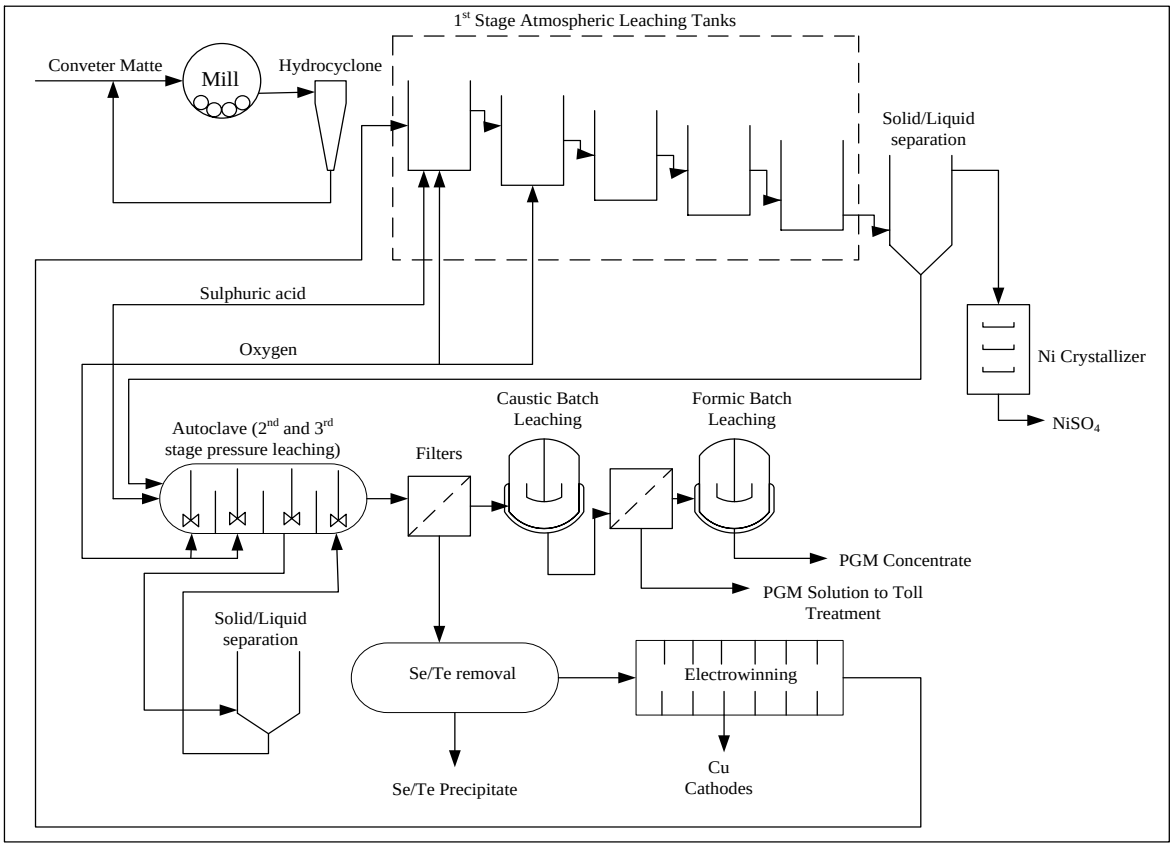

Figure 1.1: Process flow sheet for Lonmin BMR (redrawn from Bircumshaw, 2008).

1.1 Motivation

The pyrometallurgical upgrading of PGM containing minerals in the furnaces ultimately produces a sulphide matte containing base metal sulphides, predominantly as nickel (Ni) and copper (Cu), PGMs albeit at low concentrations and some gangue minerals.

Although the pierce-smith converter reduces the iron (Fe) levels to below 5%, notable amounts of other impurities remain in the main stream, including sulphur (S), selenium (Se) and arsenic (As) which make up 15% of the matte. The matte is first subjected to three stages of leaching under increasing oxidation power in sulphuric acid medium (Figure 1.1). The leaching sequence essentially replaces nickel in the matte with copper in the return electrolyte via various metathesis and oxidative reactions after which the nickel-rich solution is separated from the residue. The copper sulphide concentrating in the solid phase is then oxidised in the final autoclave stages to produce a copper-rich solution, leaving a PGM-containing residue. The PGM concentrate is recovered from the discharge slurry by means of filtering. It is then subjected to a high temperature batch oxidation process in a caustic environment prior to further upgrading in a formic acid leaching process to remove any residual nickel and iron.

Several investigations have been conducted on the mechanisms and kinetics of sulphuric acid leaching of the PGM matte (Dorfling, 2012; Lamya, 2007). However, the kinetics of the high pressure caustic leaching process are poorly understood due to the complex nature of the leaching chemistry and the diverse mineralogy of the residue from the preceding sulphuric acid leach process. Very little work has been done in this regard. It was thus the aim of this work to study the high pressure caustic leaching kinetics of the PGM-rich residue, i.e., the residue from the preceding sulphuric acid leaching process.

1.2 Objective and scope

In order to develop a better understanding of the high pressure caustic leaching of the PGM-rich residue, the following objectives were set:

(i) Study the chemistry, leaching mechanism and kinetics of high pressure caustic leaching by performing batch leaching test work.
(ii) Develop a model that can simulate the leaching process under plant operating conditions.
(iii) Improve the fundamental understanding of the high pressure caustic leaching process.

1.3 Deliverables

The following deliverables were set for the study:

(i) A literature review of the sulphur, selenium and arsenic chemistry in a caustic solution environment, backed by a paper-based thermodynamic study of the most important species and stability regions at high temperature as a function of pH and E_h.

(ii) Coarse grid optimal operating conditions and the associated sulphur, selenium and arsenic dissolution extents, as well as the associated PGM losses to the solution phase.

(iii) Batch kinetic dissolution curves of sulphur, selenium and arsenic, as well as the rates of the associated PGM losses in the solution phase.

(iv) Insights into the leaching chemistry of the sulphur, arsenic and selenium in a high temperature caustic environment over varying parameter space.

2 THERMODYNAMIC BACKGROUND

2.1 Fundamentals of mineral oxidation

The efficiency of hydrometallurgical processes depends on the selectivity and kinetics (reaction rates). In low temperature processes, where the reaction rates are normally slow, kinetic considerations may be of primary importance. However, at high temperatures, activation barriers are more easily overcome. Under such conditions, thermodynamic parameters, which determine the relative chemical stability of the various aqueous species present, are of predominant importance. This chapter focuses on these thermodynamic considerations.

Leaching may be conducted under oxidising or reducing conditions in either acidic or alkaline solutions. The particular leaching conditions are governed primarily by the nature of the material to be treated and the degree of selectivity required in the leaching process. This implies that by using the appropriate leaching conditions, it is possible to dissolve certain metal compounds from a complex feed material and leaving others behind in the residue. Thermodynamic relationships of species in an aqueous environment are conveniently illustrated by using potential/pH (E_h-pH) diagrams. These diagrams map out stable (equilibrium) phases and their relative predominant areas. For an oxidation-reduction reaction (Brookins, 2012):

$$\text{oxidised state} + n\,e^- = \text{reduced state} \qquad 2.1$$

The free energy of reaction determines whether the forward reaction is favoured or the reverse reaction will occur. The free energy of the reaction is represented by (Brookins, 2012):

$$\Delta G_{298} = \Delta G^{\circ}_{298} + RT\ln K \qquad 2.2$$

where ΔG_{298} denotes the standard free energy

T denotes temperature (K)

R denotes universal gas constant

K is equilibrium constant

The relationship between standard free energy and standard half-cell potential E° is represented by (Brookins, 2012; Zemaitis et al., 1986):

$$\Delta G^\circ = -nFE^\circ \qquad 2.3$$

In the above expression, n is the number of electrons involved in the half-reaction while F is the Faraday constant. The free energy change for the reaction can be related to the half-cell potential by:

$$\Delta G = -nFE \qquad 2.4$$

From Equations 2.3 and 2.4, $E_h=E^o$ and oxidation potential can thus be expressed as:

$$Eh = E^\circ - \frac{RT}{nF}\ln K \qquad 2.5$$

Equation 2.5 is the Nernst equation (Rieger, 2012) relating E_h to the activities of species involved in a chemical process. In pressure oxidation processes, the basis is the manipulation of the relative stabilities of different species in solution at varying conditions. In order to achieve selectivity of species during pressure oxidation of a PGM-rich concentrate, knowledge of predominant species such as platinum, palladium, ruthenium, sulphur, selenium and arsenic in aqueous systems is required. The solubility of all the above mentioned species in alkaline aqueous media is dependent on the prevailing conditions (E_h and pH).

2.2 Development of E_h-pH diagrams for the sulphur-selenium-arsenic water system

E_h-pH (Pourbaix) diagrams, despite their limitations, are excellent tools for the study of the thermochemistry of metal-ligand-water systems. This section focusses on the construction of E_h-pH diagrams for the sulphur-selenium-arsenic-water system at 25 and 160°C, the latter being one of the temperatures at which tests were conducted. Species sets and thermodynamic data are presented in Appendix I. The diagrams were generated using HSC Chemistry 7.1(Roine, 2002).

2.2.1 Thermodynamics of aqueous sulphur species

Sulphur chemistry has been studied extensively and is particularly important in metallurgical leaching and corrosion systems. An example is the study conducted by Hamilton and Woods (1981) who studied the effects of sulphur oxidation products on pyrite and pyrrhotite oxidation rates.

Sulphur commonly exists in one of three oxidation states in natural systems. In oxidising environments, the +6 state with sulphur as a sulphate (SO_4^{2-}) ion predominates. Under reducing conditions, sulphur exists in the -2 valence state in the form of bisulphide (HS^-) in solutions with pH values less than 7, and in the form of hydrogen sulphide (H_2S) in more acidic conditions. Sulphur can also occur in solutions as elemental sulphur (S^0). Other sulphur valence states may also be present, such as sulphite (SO_3^{2-}) and the thiosulphate ($S_2O_3^{2-}$).

In the E_h-pH diagram, solid sulphur appears stable in a narrow triangular domain (Figure 2.1). Sulphur is therefore relatively unstable in oxidative aqueous solutions, but is stabilised by the presence of hydrogen ion. In alkaline conditions, sulphur tends to disproportionate to produce HS^-, S^{2-}, SO_4^{2-}, and other oxidation products. In industrial applications, these reactions are slow and take place only in hot and very alkaline media. However, because of kinetic constraints, the sulphur stability range is considerably larger than that depicted by thermodynamics (Peters, 1992).

From a thermodynamic perspective, sulphur is expected to oxidise to +6 oxidation state over a wide range of conditions, i.e., to predominantly bisulphate and sulphate ions in acidic and alkaline solutions, respectively. Figure 2.1 below clearly indicates the small sulphur stability region. With increased temperature, the sulphur stability regions are reduced even further (discussed further in Section 2.3), confirming the rapid oxidation of sulphur over a wide range of conditions (higher pH and E_h).

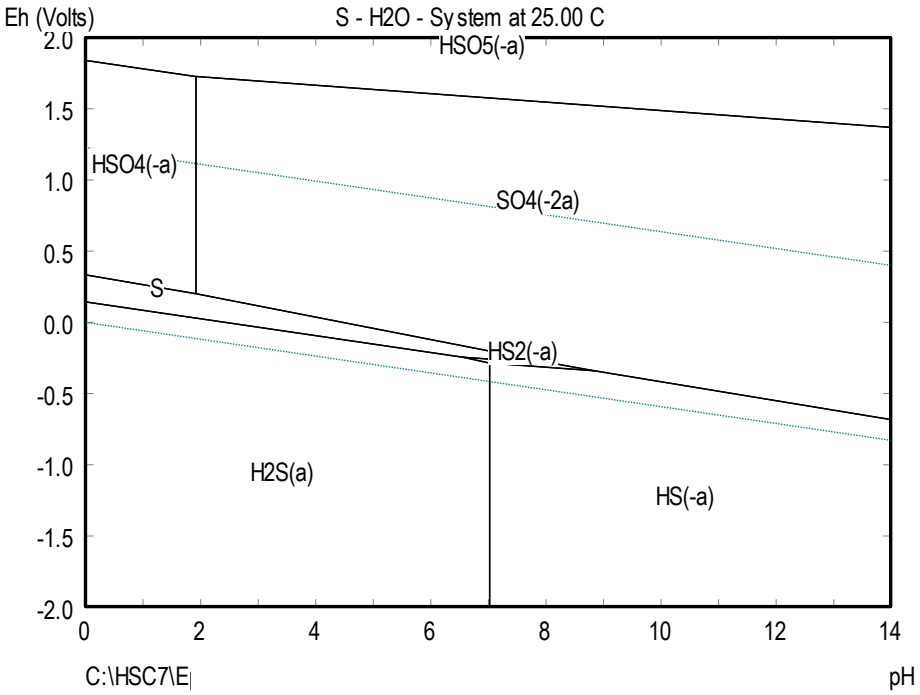

Figure 2.1: S-H_2O at 25°C (using HSC chemistry 7.1)

Elemental sulphur is the primary end product of iron sulphide oxidation in acid media (low pH), but it is unstable in alkaline solutions. Thiosulphate was detected as an intermediate in anodic dissolution of pyrite (Mishra and Osseo-Asare, 1988). Electrochemical oxidation studies of pyrite conducted by Mycroft et al. (1990) confirm the formation of sulphur and polysulphide in near neutral aqueous solutions. However, in alkaline solutions, the formation of sulphur and polysulphide was only detected at lower potentials while sulphite and sulphate species were detected at higher potentials.

2.2.2 Thermodynamics of aqueous selenium species

Selenium belongs to Group VI of the periodic table and is a non-metallic element. Selenium geochemistry is similar in most respects to that of sulphur, with oxidation states of +6, +4, 0, and -2 being important in natural systems under different redox conditions. Selenium in the +6 oxidation state forms the diprotic acid of the oxyanion selenate, SeO_4^{2-}, and like sulphate, selenate is the predominant selenium species in natural systems. Selenium in the +4 oxidation state forms the diprotic acid of the

oxyanion selenite, SeO_3^{2-}. Most selenite salts are less soluble than the corresponding selenates (National Research Council ,U.S., 1976)

Selenium is thermodynamically stable in water and in aqueous solutions over the entire pH range of 0 to 14, albeit in the absence of any oxidising or reducing agent (National Research Council ,U.S., 1976). Selenium solution chemistry is principally anionic, with selenite, SeO_3^{2-} and selenate, SeO_4^{2-} corresponding to sulphite and sulphate respectively being the main forms in aqueous solutions. At high electrochemical potential (as is the case in this study), selenate species are predominant while selenite predominate at moderate potentials. Therefore, oxidation of selenium would be expected to be oxidised to selenate rather than to remain as selenite. Figure 2.2 illustrates the E_h-pH diagram of the predominant species of the selenium-water system at 25°C. The solubility and oxidation states of selenium are influenced by the pH and E_h. As can be seen from the diagram below, fully deprotonated selenium species are formed at higher E_h and pH.

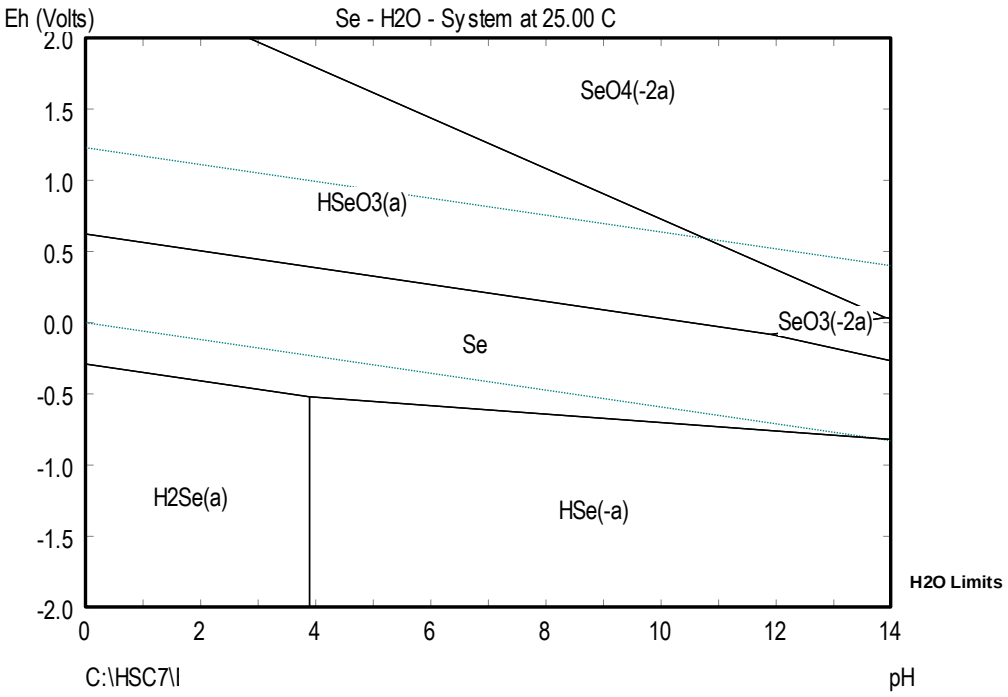

Figure 2.2: Se-H_2O 25°C (Using HSC chemistry 7.1)

The E_h has a key effect on the chemical form of dissolved selenium produced. In a study conducted by Masscheleyn et al. (1990), it was reported that the solubility of selenium increases with an increase in E_h (approximately 450 mV) regardless of the pH.

2.2.3 Thermodynamics of aqueous arsenic species

Arsenic belongs to Group V of the periodic table, is a metalloid, and is known to be toxic to plants and animals. There are four oxidation states of arsenic in inorganic compounds: +5, +3, 0, -3. In natural waters, arsenic occurs in oxidation states +3 (arsenite) and +5 (arsenate). Cherry et al. (1979) reviewed the thermodynamics of inorganic arsenic as an indicator of the redox potential in groundwater. The solubility of arsenic species in natural water is dependent on the environmental conditions i.e., E_h and pH (Rubidge, 2007; Ferguson and Gavis, 1972). However, in hydrometallurgical systems and in this study in particular, only arsenic in +3 and +5 oxidation states is of interest. Arsenic in -3 oxidation state is only stable at extremely low E_h values which do not apply to this study. The pentavalent form is the thermodynamically stable species under oxidising conditions. The trivalent form is much less common because of the small stability range (Figure 2.3). In a system where it exists with other species, its stability tends to be influenced by interactions with these species. For example, these interactions may lead to co-precipitation with metal oxides or adsorption on metal sulphides (if present) (Buckley and Walker, 1988). The E_h-pH diagram for the arsenic-water system is presented Figure 2.3.

Figure 2.3 illustrates that oxidising conditions in an alkaline solution are required to dissolve arsenic to form either arsenate (AsO_4^{3-}) or arsenite (AsO_3^{3-}). Native arsenic and arsenide minerals form under the most reducing conditions in the water stability region (Dow and Rimstidt, 1985).

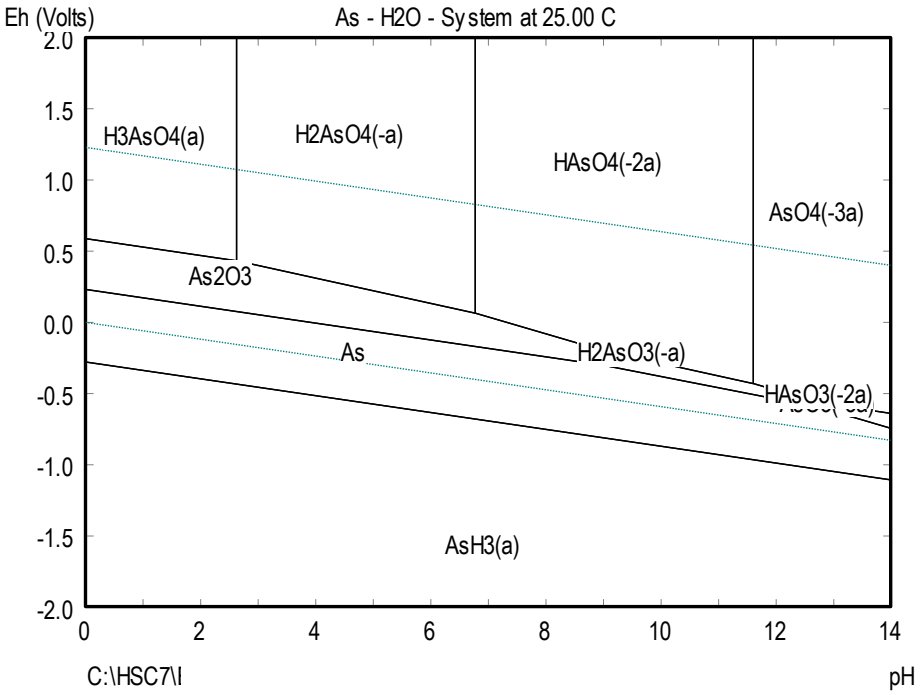

Figure 2.3 As-H_2O 25°C (Using HSC chemistry 7.1)

2.3 E_h-pH diagrams at elevated temperatures

Most mineral oxidation processes are efficient at elevated temperature. This has led to the development of the high pressure leaching processes (Fassel, 1962). It is thus important to carry out a theoretical investigation of mineral oxidation systems at high temperature. It must be remembered that the stability of a chemical species is dependent on the equilibrium constant (K) of the reactions of concern. To calculate the equilibrium state of the system, it is necessary to know the change of the standard Gibbs energy, ΔG^o in the pure and ionic state. Since attention is focused on the higher temperature E_h-pH diagrams, the main prerequisite for constructing these diagrams is the availability of Gibbs free energy of formation data of substances in the pure and ionic states. These data needs to be known not only at standard state, but also at elevated temperature. Although values of ΔG^o_T for pure substances have been tabulated and published in literature, it is more difficult to determine these values for the ions. There are several procedures which can be applied to obtain the required values. Criss and Cobble (Criss and Cobble, 1964; Criss and Cobble, 1964b) laid the foundation for the extrapolation of the thermodynamic values required to calculate E_h-pH diagrams at elevated temperatures.

A system at constant temperature and pressure only reaches equilibrium when the Gibbs free energy is minimised. Gibbs free energy is a state variable that provides the criteria for whether any change to the system is favourable. The Gibbs free energy is defined as (Zemaitis et al., 1986; Brookins, 2012; Rieger, 2012):

$$\Delta G_T^o = \Delta H_T^o - T\Delta S_T^o \qquad 2.6$$

where ΔH^o_T is the standard enthalpy of reaction, T is temperature and ΔS^o_T is the standard reaction entropy. Negative values of ΔG indicate that the process is spontaneous, positive values indicate that the reverse process is spontaneous and a value of zero indicates that the system is at equilibrium.

At temperatures other than 25°C, the change in ΔH^o_T and ΔS^o_T can be expressed as (Brookins, 2012; Rieger, 2012):

$$\Delta H_T^o = \Delta H_{298}^o + \int_{298}^{T} \Delta C_p^o dT \qquad 2.7$$

and

$$\Delta S_T^o = \Delta S_T^o + \int_{298}^{T} \frac{\Delta C_p^o}{T} dT \qquad 2.8$$

where ΔC_p^o is the standard heat capacity of a reaction. Partial molar heat capacities are often expressed in the form of power functions such as (Criss and Cobble, 1964b):

$$C_{p,i}^o = a_i + b_i + c_i T^{-2} \qquad 2.9$$

Equation 2.9 is not a linear function. Therefore, the value of ΔC_p^o is over an interval T_1 and T_2 and can be obtained using the equation:

$$\Delta G_{T2}^o = \Delta G_{T1}^o - \Delta S_{T1}^o (T_2 - T_1) + \overline{C_p}\Big]_{T1}^{T2} (T_2 - T_1) - T_2 \overline{C_p}\Big]_{T1}^{T2} \ln \frac{T_1}{T_2} \qquad 2.10$$

The Criss and Cobble's corresponding principle is based on the experimental observation that a standard state can be selected so that the specific molar entropies of the ions are linearly related at the temperature under consideration. If the entropy of $H^{+}_{(aq)}$ for every temperature is defined, the partial molal ionic entropies at another temperature are linearly related to their corresponding entropies at the same reference temperature (the reference temperature is conventionally taken as 298.15 K).

The corresponding principle is generally described by the following equation:

$$\Delta\overline{S^{o}_{T2}}(abs) = a_{T2} + b_{T2}.\overline{S^{o}_{298}}(abs) \qquad 2.11$$

where a_{T2} and b_{T2} are the constants which depend on the type of ion, i.e., whether cation, anion, oxyanion or acid oxyanion. $\overline{S}^{o}_{298}(abs)$ is the ionic partial molal entropies on an "absolute" scale, corresponding to the entropy for the hydrogen ion of -5 cal/mol deg or -20.97 J/mol deg and is described by the following equation:

$$\Delta\overline{S^{o}_{298}}(abs) = \Delta\overline{S^{o}_{298}}(conv) - 20.97z \qquad 2.12$$

and z is the ion charge. Table 2.1 summarises the values of the constants a_{T2} and b_{T2} (Criss and Cobble, 1964b).

Table 2.1 Entropy constants a_{T2} and b_{T2}

Temperature	Simple cations		Simple anions and OH^{-}		Oxyanions		acid oxyanions (MeO_n^{-m})		Standard state
					MeO_n^{-m}		$MeO_n(OH)^{-m}$		entropy
	a_T	b_T	a_T	b_T	a_T	b_T	a_T	b_T	$H^{+}_{(aq)}$
298	0	4.184	0	4.184	0	4.14	0	4.184	-20.92
333	16.318	3.996	-21.338	4.054	-58.576	5.02	-56.484	5.774	-10.46
398	43.095	3.665	-54.392	14.184	129.74	6.16	126.775	7.924	8.368
423	67.78	3.314	-89.119	4.138	-194.14	7.08	-209.2	9.962	27.196
473	97.487	2.975	126.357	4.104	-280.33	8.42	-298.88	12.385	53.724

Values in Jmol/deg

Applying these considerations to the change in the partial molal heat capacity between the reference temperature (298K) and temperature of interest (T_2) gives:

$$\Delta\overline{C}^{o\,T2}_{p\,298} = \Delta\overline{S}^{o}_{T2}(abs) - \frac{\overline{\Delta S}^{o}_{298}(abs)}{\ln\frac{T}{298}} \qquad 2.13$$

and from equation 2.13, it follows that:

$$\Delta\overline{C}^{o\,T2}_{p\,298} = \alpha_{T2} + \beta_{T2}.\Delta\overline{S}^{o}_{298}(abs) \qquad 2.14$$

where α_{T2} and β_{T2} are constants which depend on the type of ion and the considered temperature.

Table 2.2 summarises α_{T2} and β_{T2} values. For temperatures up to 200°C there is a linear relationship between the entropy constants a_{T2} and b_{T2} with temperature. Therefore, Criss-Cobble method can be modified to calculate the power function coefficients (Equation 2.9) for ions. With this modification of the Correspondence Principle, the standard partial molal heat capacities of aqueous ions can be written as:

$$C^{o}_{p}(T) = bT \qquad 2.15$$

where,

$$b = e + g\overline{\Delta S}^{o}_{298}(abs) \qquad 2.16$$

The constants e and g are the ion type specific. These constants are presented in Table 2.3. However, the application of the modified Correspondence Principle is limited to the ion types listed in the table below.

Table 2.2 Correspondence Principle Heat Capacity Parameters (centimetre-gram-seconds (c.g.s) system of Units) (Zemaitis et al., 1986)

Temperature	Simple cations		Simple aniona and OH^-		Oxyanions		acid oxyanions (MeO_n^{-m})		$C^o_p(T,T_r)$
					MeO_n^{-m}		$MeO_n(OH)^{-m}$		$H^+_{(aq)}$
T(K)	α(T)	β(T)	α(T)	β(T)	α(T)	β(T)	α(T)	β(T)	
333	35	-0.41	-46	-0.28	-127	1.96	-122	3.44	23
373	46	-0.55	-58	0.00	-138	2.24	-135	3.97	31
423	46	-0.59	-61	-0.03	-133	2.27	-143	3.95	33
473	(-50)	(-0.63)	(-0.65)	(-0.04)	(-145)	(-2.53)	(-152)	(-4.24)	(-35)

Table 2.3 Heat Capacity Parameters for Aqueous Ions (c.g.s. units)

	e	g
Hydrogen ion	0.09225	0
simple cation	0.133	$-1.65x10^{-3}$
Simple anion and OH^-	-0.1726	$-4.73x10^{-3}$
Oxyanions	-0.4366	$7.25x10^{-3}$
Acid Oxyanions	-0.399	$11.25x10^{-3}$

Based on the above estimation techniques, high temperature E_h-pH diagrams can be developed for the different systems at elevated temperatures. The thermodynamic data of the species at high temperature is presented in Appendix I.

Figure 2.4 illustrates the E_h-pH equilibrium diagram for the S-H_2O system at 160°C. In contrast to that at 25°C, stable areas of elemental sulphur, hydrogen sulphide and bisulphide have diminished. On the other hand, stability regions for sulphate and bisulphate have increased. Also, sulphur can be oxidised at lower potentials and high temperature (Figure 2.4) than at lower temperatures (Figure 2.1). Stable areas for selenate and selenite increase at higher temperature (Figure 2.5). Selenium can also be oxidised at lower potential and higher temperature compared to lower temperature.

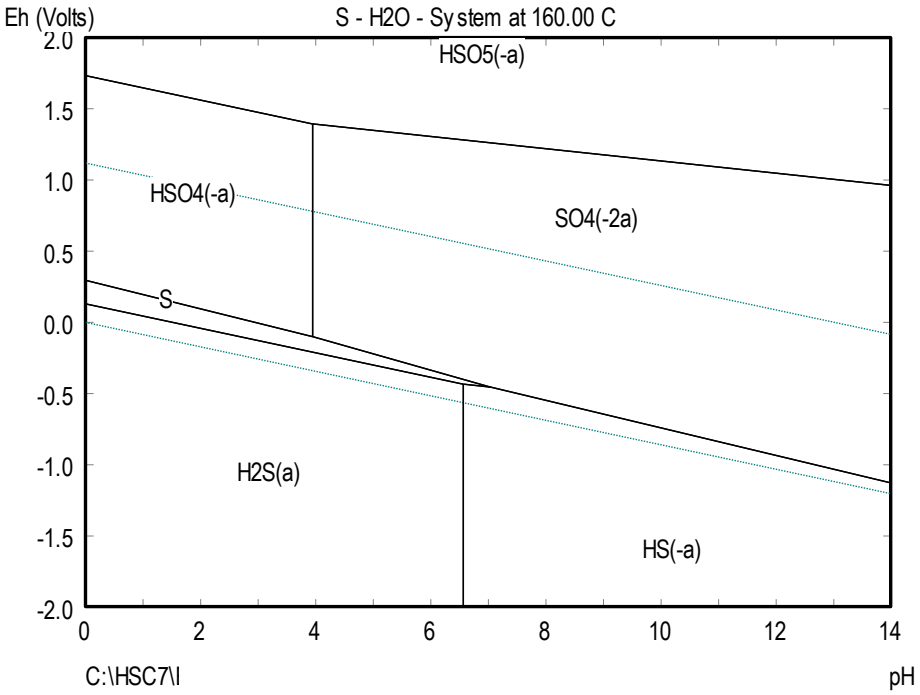

Figure 2.4: S-H_2O at 160°C (using HSC chemistry 7.1)

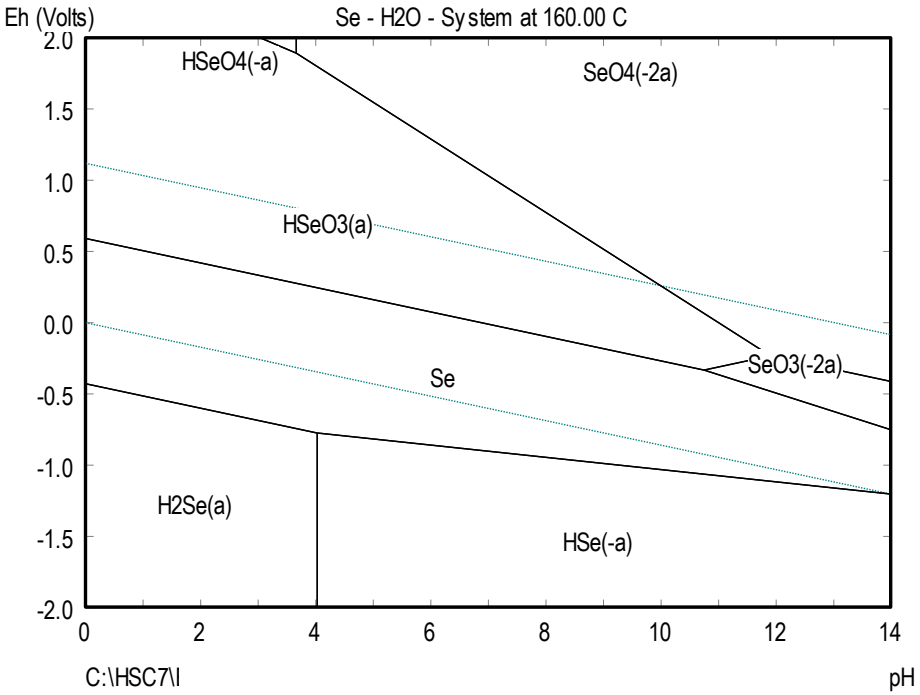

Figure 2.5: Se-H_2O at 160°C (using HSC chemistry 7.1)

Chapter summary

Thermodynamics play a vital role in mineral oxidation. Chemical equilibria of multi-component metallurgical systems are described by thermodynamics. This chapter was devoted to understanding the equilibrium thermodynamics and establishing the dependence of the chemical potential of a given substance on the measurable variables. Thermodynamics formation of the E_h-pH diagrams of species at room temperature was evaluated. However, due to the fact that most metallurgical processes are conducted at conditions other than standard conditions, a framework for the extrapolation of thermodynamic properties from standard conditions (temperature) to other conditions was evaluated.

In any system, phases that are stable at room temperature may differ from the corresponding stable phases at elevated temperature. In the sulphur-water system, the points of interest that become apparent are;

- The area of stability of sulphur is much smaller at elevated temperature than at 298 K. Thus, the oxidation of sulphur is achieved relatively easier at temperatures higher than 298 K.
- Elemental sulphur is thermodynamically unstable at high pH and oxidising conditions and forms HSO_4^- or SO_4^{2-} depending on the prevailing E_h and pH conditions.
- The area of predominance of SO_4^{2-} extends to higher pH values at elevated temperature than at 298 K. The SO_4^{2-} species is formed between pH of 3.9 and 14.
- The area of stability of SO_4^{2-} is much larger at more oxidising than reducing conditions.

In the selenium-water system, the points of interest that become apparent are;

- Elemental selenium is stable in reduced environment with a relatively smaller stability region at elevated temperature as compared to 298 K.
- The selenite, SeO_3^{2-} and selenate, SeO_4^{2-} species are responsible for most selenium compound solubilities.

- Both species are found over a broad pH range. Selenite is found in mildly oxidising conditions while selenate predominates in strongly oxidising conditions.

In the arsenic-water system, redox potential and pH are the most important factors controlling arsenic speciation. The following points are apparent from the thermodynamic equilibria of the arsenic-water system;

- The redox potential of arsenic oxyanions is such that arsenite becomes stable in aqueous forms under moderately reducing conditions at pH 9 while arsenates are stable in oxidised aqueous solutions.
- Under oxidising conditions and pH > 6.9, arsenic exists in the +5 oxidation state and $H_2AsO_4^-$ dominates, while at higher pH, due to ionisation of one or more protons, $HAsO_4^{2-}$ and AsO_4^{3-} predominates.
- Generally, arsenous acid dominates in acidic to neutral conditions while a deprotonated form and stable arsenate anion, AsO_4^{3-} exists in alkaline conditions.

3 CHEMICAL OXIDATION PROCESSES

Extractive metallurgical processes are divided into high temperature (pyrometallurgy) and low-medium temperature (hydrometallurgy) processes. Roasting processes under oxidising conditions are an established commercial technology. Nevertheless, the operating costs that accompany roasting, coupled with stringent environmental control of gases emission, are important limitations in its commercial implementations. Hence, aqueous chemical oxidation processes are attracting increasing attention.

Arsenical and sulphide concentrates have been treated by roasting for many years. This process has its environmental problems due to high arsenic and sulphur dioxide emissions in the roaster off-gasses. This has led to alternative processing routes to treat these concentrates. These processes use soluble oxidants to oxidise the minerals. Pressure oxidation utilises pressures to increase the solubility of oxygen, thereby increasing the rate of mineral oxidation. This, coupled with high temperature, makes the process faster and ideal for increased throughput compared to atmospheric leach processes. This oxidation process usually has acceptable operating costs, although capital associated with pressure leaching plants makes them an expensive option compared to atmospheric oxidation processes. (Linge and Jones; 1993, Bhakta et al., 1989; Nicol and Guresin, 2003).

3.1 Alkaline pressure oxidation

Alkaline oxidation processes dates back to the 1950s when they were first proposed to commercially treat arsenic and sulphur containing minerals (Chilton, 1958; Sill, 1960). These oxidation processes were also utilised in treating sulfidic gold ores (Bhakta et al., 1989; Hiskey and Sanchez, 1995). New alkaline processes have recently been proposed for the oxidation of gold (Mao et al., 1997) and pre-treatment of copper anode slimes (Liu et al., 2014; Kilic et al., 2013; Fernadez et al., 1995). Alkaline oxidation process has several advantages such as reduced corrosion, application of lower temperatures and its suitability for treating high acid consuming minerals. The high cost of caustic may be viewed as a process disadvantage.

3.2 Alkaline oxidation of sulphur containing minerals

A number of chemical extraction processes have been proposed for the extraction of sulphur from sulphide minerals and coal. A review of previous work was done, which focussed mainly on chemical leaching processes that use aqueous solutions containing dissolved oxygen to extract sulphur from pyrite, other sulphide minerals and coal.

One of the most important developments in the field of hydrometallurgy has been the application of elevated pressures and temperatures in the oxidation of complex sulphide and oxide ores. The decomposition of sulphides was investigated as early as 1907. Stokes (1907) concluded that sulphides were decomposed by reacting them with alkaline water, which left hydrated metal oxides and removed the sulphur in the form of thiosulphate and alkali sulphate. Anderson (1951) investigated the oxidation kinetics of galena (PbS) in caustic solution and demonstrated the effects of temperature, oxygen partial pressure, caustic concentration and agitation speed on the oxidation rate. It was concluded that the rate of oxidation of galena was proportional to the square root of the concentration of oxygen. Increasing the caustic concentration from 0.5 to 0.6 N resulted in the decrease of the reaction rate. The reduced rate of reaction was claimed to be due to the decrease in oxygen solubility at the higher caustic concentration. Anderson (1951) reported that monoatomic oxygen participates directly in the rate-controlling step and that the reaction is a heterogeneous process occurring at the galena surface.

Vircikova and Fedor (1991) investigated the effects of temperature and caustic concentration on arsenic and sulphur dissolution in the leaching of arsenic trisulphide (As_2S_3). It was reported that arsenic acid and sulphate ions were produced in the oxidation reaction. The following reaction sequence was proposed for sulphur speciation:

$$As_3S_6^{3-} \rightarrow S_2O_3^{2-} \rightarrow S_3O_6^{2-} \rightarrow SO_4^{2-}$$

However, the parallel sequence of arsenic speciation was not given. Caustic concentration and temperature were found to have a positive effect on the extent of sulphur and arsenic dissolution.

Stenhouse and Armstrong (1952) studied the aqueous oxidation of pyrite (FeS_2) in caustic solutions under positive oxygen pressure. The effects of the caustic concentration, oxygen partial pressure, the average pyrite particle size and temperature on extraction and rate of oxidation where investigated. Stenhouse and Armstrong (1952) also showed that the rate of pyrite oxidation was proportional to the square root of the oxygen concentration. It was also established that the process involved surface dissociation of oxygen followed by diffusion. The pyrite oxidation rate was found to reduce with an increase in the average particle size while caustic concentration increased the oxidation rate up to 2 mol/L. An increase in caustic concentration beyond 2 mol/L was found not to have a marked influence on the oxidation rate. Furthermore, a marginal increase in the temperature increased the pyrite oxidation rate. It was proposed that iron was oxidised by diffusion of oxygen into the oxide product layer. From this investigation, a process model was proposed in which sulphur diffused as a positive ion through an oxide product layer which formed on the particle and then it was subsequently oxidised to sulphate ion. The final products of the oxidation reaction in the caustic solutions were iron oxides and sulphate ions. Hamilton and Woods (1981) investigated the effect of pH on sulphur oxidation. The investigation showed that sulphur is a major product of sulphur mineral oxidation at pH of 4.6. An increase in the pH to 9 accompanied by an increase in the oxidation potential resulted in the formation of sulphate ions (Hamilton and Woods, 1981).

Dresher et al. (1956) investigated the leaching kinetics of molybdenite (MoS_2) by potassium hydroxide under an oxygen overpressure. The leaching rate was controlled by both the dissolved oxygen concentration and potassium hydroxide concentration. Dresher et al. (1956) evaluated the solubility of oxygen in solutions of various temperatures and pressures. It was established that both oxygen partial pressure and alkali concentration controlled the rate of leaching. Similar findings on the effect of temperature, caustic concentration, residence time and mineral particle size on sulphur extraction from different minerals have been reported by other researchers

(Rimstidt and Vaughan, 2003; Mikloš and Fröhlich, 2002; Lowson, 1982; Chiriţă et al., 2014).

3.2.1 Mechanism of sulphide mineral dissolution

The interaction of sulphur bearing minerals with oxygen in acidic or alkaline solutions has been discussed in several publications. The dissolution of these minerals has been explained by two mechanisms, oxidative and non-oxidative.

Non-oxidative mechanisms are usually observed for monosulfides (such as FeS, ZnS) according to the equation below (Nicol and Scott, 1979, Filmer and Nicol, 1980):

$$MeS+2H^{+}= Me^{2+}+ H_2S \qquad 3.1$$

where Me is the metal (Cu, Zn, Fe etc.)

Sulphide oxidative dissolution mechanism is usually a multi-step process, which involves intermediate species. Non-oxidative dissolution involves the following scheme (Equation 3.2):

$$\begin{array}{l} MeS \rightarrow Me^{2+} + S^{2-}; \quad S_8 \\ \qquad\quad \downarrow \qquad\quad \uparrow \\ HS^{-} \rightarrow HS_n^{-} \rightarrow S_2O_3^{2-} \rightarrow SO_4^{2-} \end{array} \qquad 3.2$$

(Karastelev et al, 2013).

where Me and S are metal and sulphur, respectively. Oxidative dissolution involves changes in the oxidation states of atoms. The mechanism of electrochemical dissolution of metal sulphides can be represented by Equation 3.3 (Karastelev et al., 2013).

$$\begin{array}{ccccccc} \text{In solution} & & & & S_2O_3^{2-} \rightarrow SO_4^{2-} \rightarrow \text{In solution} & & \\ \uparrow & & & & \uparrow & & \\ Me_kS_m \rightarrow Me^{2+} + 2e^{-} + & Me_{k-1}S_m & \rightarrow & Me_{k-1-x}S_m & + 2xe^{-} + & Me^{2+} & \\ & \uparrow & & \downarrow & & \downarrow & \\ & Me_{k-1}S_m + S_8 & & & & \text{In solution} & \end{array} \qquad 3.3$$

where Me and S have already been defined, k and m are valence electrons.

This oxidative mechanism involves two coupled reactions: anodic oxidation of the sulphide and cathodic reduction of the oxidant. When used as an oxidant, oxygen reduction results in the formation of water.

3.2.2 Kinetics of sulphur oxidation

Kinetic studies on sulphur oxidation have been conducted for a number of sulphide bearing minerals. However, most of these were based on pyrite oxidation since it is the most abundant sulphide mineral. In most ores and concentrates, pyrite is rarely of economic importance, hence, it is viewed as a gangue mineral (Long and Dixon, 2004). However, its presence in the ores or concentrate largely influences the recovery of high value metals associated with it, e.g., copper, gold and zinc. As such, its oxidation mechanism has been studied extensively due to its significance in leaching, mineral flotation and generation of acid in mine waters.

In alkaline oxidative dissolution of pyrite, the oxidation rate can be described by the rate equation 3.4 below:

$$-\left(\frac{1}{S}\right)\frac{dN_{FeS_2}}{dt} = K\exp\left(\frac{-Ea}{RT}\right)\left[OH^-\right]^a PO_2^b \qquad 3.4$$

where N is the number of moles, Ea is activation energy (J/mol), T is temperature (K), R is the universal gas constant, *a* is reaction order with respect to hydroxide ion and *b* is reaction order with respect to oxygen partial pressure while S is the mineral surface area (Koslides and Ciminelli, 1992). A 0.5 order dependence on oxygen partial pressure on sulphur dissolution in both acidic and alkaline media has been reported by several researchers (Mikloš and Fröhlich, 2002; Smith and Shumate, 1970; Nicol, 1993, Crundwell, 2013). However, Koslides and Ciminelli (1992) found a reaction order of 0.31 with respect to oxygen in alkaline oxidation of pyrite. A 0.23 reaction order with respect to hydroxyl ion concentration was reported while Asare Ciminelli and Osseo-Asare (1995) obtained a value of 0.25. A wide range of activation energies (20-90 kJ/mol) have been reported for alkaline oxidation of sulphur bearing minerals

(Koslides and Ciminelli, 1992; Ciminelli and Osseo-Asare, 1995; Lowson, 1982). Anderson (1951) reported 26 kJ/mol in the study of the oxidation kinetics of galena (PbS) while Stenhouse and Armstrong (1952) reported an activation energy of 20 kJ/mol for the alkaline oxidation of pyrite. Koslides and Ciminelli (1992) suggested that during alkaline oxidation of sulphides, there is a change from chemical (activation energy > 40 kJ/mol) to diffusion (activation energy < 40 kJ/mol) control as the rate determining step when temperature is above 100°C. This led them to conclude that the oxidation is a mixed controlled reaction.

3.3 Alkaline oxidation of arsenic bearing minerals

Arsenopyrite (FeAsS) is the most abundant arsenic containing sulphide mineral. Other arsenic bearing minerals include enargite (Cu_3AsS_4), cobaltite (CoAsS), niccolite (NiAs) and arsenolite (As_2O_3). In gold industry, arsenopyrite is of economic importance when it has a significant portion of gold integrated in the ore. It is usually an unwanted mineral in concentrates and ores.

Oxidative leaching of arsenic containing minerals, which proceed via an electrochemical pathway, is a commercial process for gold recovery from refractory sulphide ores (Mikhlin and Shipin, 2003). A number of electrochemical studies have been devoted to arsenic electrochemistry. Kostina and Chernyak (1976) investigated the oxidation of arsenic in arsenopyrite in alkaline solutions and established that an increase in temperature has a stronger accelerating effect on arsenopyrite oxidation. A -0.2 V potential was reported as the point at which oxidation starts. A positive effect of caustic concentration was observed.

The lower potential needed for arsenic oxidation is also supported by Taylor and Amoah-Forson (2008) who reported that in alkaline media, diatomic oxygen oxidises arsenopyrite at lower potential (value not stated) to form soluble arsenic species of higher oxidation states. The oxidation of arsenopyrite in alkaline solution was expressed as follows (Taylor and Amoah-Forson, 2008):

$$FeAsS_{(s)} + 3.5O_{2(g)} + 5OH^-_{(aq)} \rightarrow 0.5Fe_2O_{3(S)} + AsO^{3-}_{4(aq)} + SO^{2-}_{4(aq)} + 2.5H_2O_{(l)} \qquad 3.5$$

Taylor and Amoah-Forson (2008) presents the reaction mechanism as follows:

Oxygen gas dissolves in the aqueous phase:

$$O_{2(g)} \rightarrow 2O_{2(aq)} \quad 3.6$$

Hydroxide ions are adsorbed on the particle and provide oxygen and electrons:

$$2OH^-_{(aq)} \rightarrow O_{(aq)} + 2e^- + H_2O_{(l)} \quad 3.7$$

FeAsS reacts with the electrons and oxygen to yield soluble ions:

$$FeAsS_{(s)} + 2e^- + 8O_{2(aq)} \rightarrow Fe^{3+}_{(aq)} + AsO^{3-}_{4(aq)} + SO^{2-}_{4(aq)} \quad 3.8$$

Ferric ions react with water to yield solid metal oxide (or hydroxide), most likely on the surface and hydrogen ions.

$$Fe^{3+}_{(aq)} + 1.5H_2O_{(l)} \rightarrow 0.5Fe_2O_{3(s)} + 3H^+_{(aq)} \quad 3.9$$

The hydrogen ions react with the hydroxide ion to form water.

$$H^+_{(aq)} + OH^-_{(aq)} \rightarrow H_2O_{(l)} \quad 3.10$$

The cathodic reaction can be expressed as follows:

$$FeAsS_{(s)} + 8O_{(aq)} + 3OH^-_{(aq)} + 2e^- \rightarrow 0.5Fe_2O_{3(s)} + AsO^{3-}_{4(aq)} + SO^{2-}_{4(aq)} + 1.5H_2O_{(l)} \quad 3.11$$

And the anodic reaction as:

$$2OH^-_{(aq)} \rightarrow O_{(aq)} + H_2O_{(l)} + 2e^- \quad 3.12$$

In the alkaline oxidation of enargite (Cu_3AsS_4), two treatment techniques have been proposed for arsenic removal (Curreli et al., 2005).

a) Leaching of enargite concentrate using sodium sulphide (Baláž et al., 2000).
b) Alkaline leaching of enargite using sodium hypochlorite under oxidising conditions (Viñals et al., 2003).

Ruiz et al. (2014) used the former to investigate the selective leaching of arsenic from enargite by alkaline digestion. The process consisted of alkaline digestion with concentrated Na_2S-NaOH followed by water leaching. The dissolution of arsenic was observed to increase with an increase in both the temperature and caustic concentration. Yu et al. (2014) also reported similar effects of temperature and caustic concentration during extraction of arsenic from arsenic-containing cobalt and nickel slag. Curreli et al. (2005) observed that the later method (leaching with sodium hypochlorite) was more effective. This was due to the ease with which arsenic was dissolved at lower potential to form arsenate ion. The oxidation reaction was fast and chemically controlled. In both methods, it was found that pH had a significant influence on arsenic extraction. Castro and Baltierra (2005) in the study of surface properties of enargite showed that arsenic dissolution is sensitive to pH due to several simultaneous ionisation and dissolution reactions. The same study illustrated that at a potential of between 0.2 V and 0.6 V, arsenic species were detected in solution. The effect of pH on arsenic dissolution was explained by Castro and Baltierra (2005). Figure 3.1 is an illustration of the equilibrium diagram of the arsenic-water system as a function of pH. The diagram shows the hydrolysis of H_3AsO_4 with the release of H^+ ions subsequently forming AsO_4^{3-} at a pH value of around 12. This illustrates the positive effect of pH on arsenic extraction.

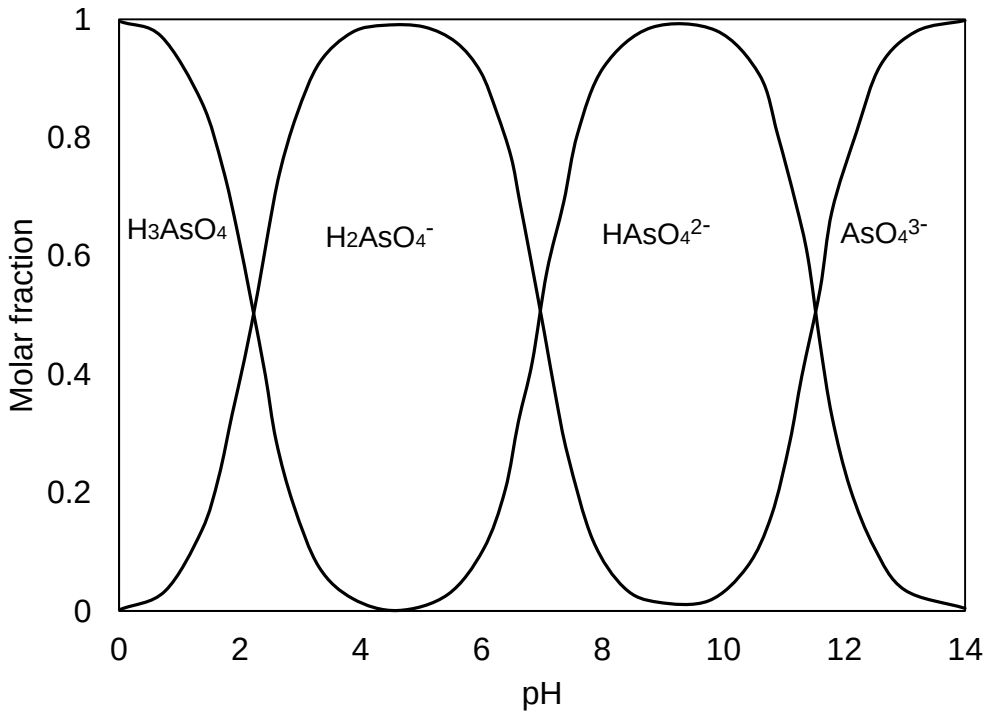

Figure 3.1: Equilibrium diagram of arsenic –water system as a function of pH at 25°C (Castro and Baltierra, 2005, Scott, 1991)

3.3.1 Kinetics of arsenic oxidation

Kinetics studies of the pressure oxidation of arsenopyrite have been conducted by several researchers. Papangelakis et al. (1990) conducted detailed studies on pressure oxidation of arsenopyrite in acid solutions. Several other studies were conducted in alkaline media (Bhakta et al., 1989; Taylor and Amoah-Forson, 2008; Koslides and Ciminelli, 1992; Mikloš and Fröhlich, 2002). The factors affecting the oxidation rate of arsenopyrite include caustic concentration, oxygen partial pressure, temperature, mineral surface area, slurry density, agitation speeds, as well as the reaction times. The initial oxidation rate of arsenopyrite was found to be a function of the mineral surface area, hydroxide ion concentration and the oxygen partial pressure (dissolved oxygen concentration). This can be described by the following rate equation (Taylor and Amoah-Forson, 2008):

$$-\left(\frac{1}{S}\right)\frac{dN_{FeAsS}}{dt} = K\exp\left(\frac{-Ea}{RT}\right)\left[OH^{-}\right]^{c}PO_2^{d} \qquad 3.13$$

where dN/dt is the number of moles of arsenopyrite per unit time, c is reaction order with respect to hydroxide ion concentration and d is reaction order with respect to oxygen while S is the mineral surface area.

Koslides and Ciminelli (1992) obtained a reaction order of 0.27 with respect to hydroxide ion concentration. A zero order dependency on the oxygen partial pressure was obtained. Taylor and Amoah-Forson (2008) obtained an activation energy value of 23.8 kJ/mol while Koslides and Ciminelli (1992) obtained 15.1 kJ/mol. Ruiz et al. (2014) obtained an activation energy of 22 kJ/mol during arsenic removal from enargite by alkaline digestion. Such low activation energy is indicative of a diffusion controlled reaction mechanism (Levenspiel, 1972, Dreisinger and Abed, 2002). This was claimed to be due to the formation of passivation oxide on the mineral surface. Bhakta et al. (1989) and Miklos and Frohlich (2002) observed that longer reaction times resulted in higher arsenic extraction (Koslides and Ciminelli, 1992). The

oxidation rate of arsenopyrite was found to increase with agitation up to 900 rev/min. An increase in agitation speed above 900 rev/min did not result in an increase in oxidation rate.

3.4 Alkaline oxidation of selenium bearing minerals

Selenium concentration in the earth's crust is similar to antimony and cadmium which are approximately 0.08 mg each per kilogram of ore. Selenium is found in most sulphide minerals largely due to similarities with sulphur such as ionic radii (Harold et al., 1965). Table 3.1 illustrates the similarities between selenium and sulphur. Sulphide (S^{2-}) ion has a radius of 184 pm while a selenide has a radius of 198 pm (Harold et al., 1965). Though in small quantities, selenium occurs in different minerals i.e., galena (PbS), chalcopyrite ($CuFeS_2$) arsenopyrite (FeAsS), sphalerite (Zn,Fe)S, pyrrhotite Fe(1-x)S [where x = 0 to 0.2] and pyrite FeS_2.

Other minerals with naturally occurring selenium are eucairite (CuAgSe), clausthalite (PbSe), crookesite ($Cu_7(Tl,Ag)Se_4$), and berzelianite (Cu_2Se). However, these minerals contain low quantities of selenium and are too rare to be used for selenium production**.** Thus, the study of selenium chemistry of these minerals has received little attention.

Table 3.1: Similarities between selenium and sulphur

	Sulphur	Selenium
Tetrahedral covalent radius	1.04Å	1.14Å
Ionic radius (divalent)[2]	1.81Å	1.98Å
Electronegativity	2.5	2.4

(Harold et al., 1965)

Kilic et al. (2013) conducted investigations of copper and selenium recovery from copper anode slimes. The process consisted of two hydrometallurgical steps; decopperisation in sulphuric acid media and dissolution of selenium in a caustic solution. Temperature, caustic concentration, oxygen partial pressure and reaction time were all found to increase selenium dissolution. The caustic concentration was varied between 0.36 and 5 mol/L. Maximum selenium extraction was obtained with 4 mol/L caustic concentration. The maximum temperature of 90°C used in the

investigation yielded the maximum selenium dissolution. The following reactions were proposed for the dissolution of selenium producing sodium selenite and sodium selenate respectively (Kilic et al., 2013):

$$Se_{(s)} + O_{2(g)} + NaOH_{(aq)} \rightarrow Na_2SeO_{3(aq)} + H_2O_{(l)}$$

$$2Se_{(s)} + 3O_{2(g)} + 4NaOH_{(aq)} \rightarrow 2Na_2SeO_{4(aq)} + 2H_2O_{(l)}$$

Figure 3.2 and Figure 3.3 illustrate the speciation of selenate and selenite as a function of pH (Scott, 1991). The fully deprotonated selenate is formed at a pH of about 2-14. On the other hand, selenite is only formed at a pH of about 8. The redox potential determines which species will predominate over the other (Baur and Johnson 2003). Cornelis et al. (2008) obtained 79% selenate and 21% selenite during geochemical modelling of selenium leaching in alkaline media at a pH value of 11. Baur and Johnson (2003) also showed that the thermodynamic stability of the selenate increases with pH, as can also be seen from the E_h-pH diagram (Figure 2.2). Other researchers have also shown that an increase in pH results in increased selenium dissolution (Zheng and Chen, 2013; Otero-Rey et al., 2005). Zheng and Chen (2013) and Otero-Rey et al. (2005) obtained results that showed a relative influence of temperature on selenium and arsenic dissolution. The selenium leaching extent also improved with an increase in reaction time.

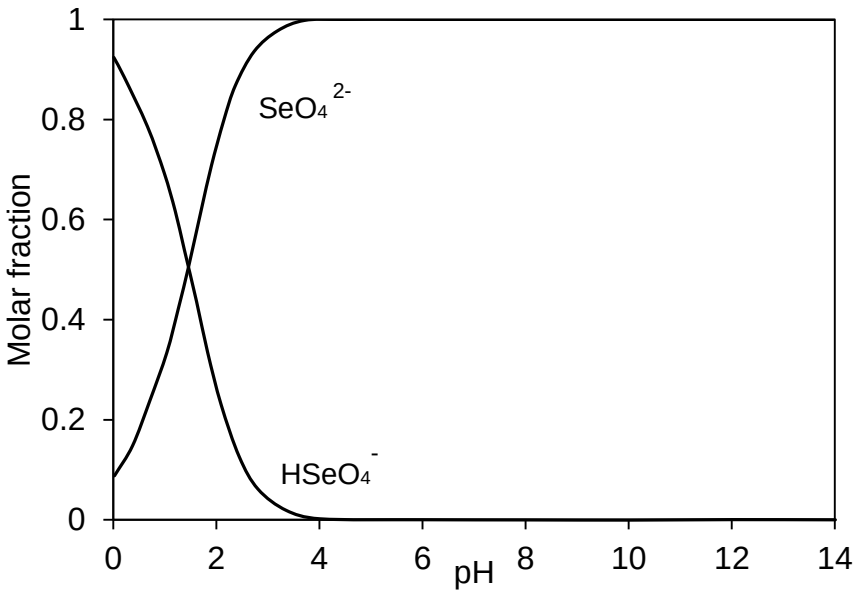

Figure 3.2: Equilibrium diagram of selenate as a function of pH at 25°C (Scott, 1991)

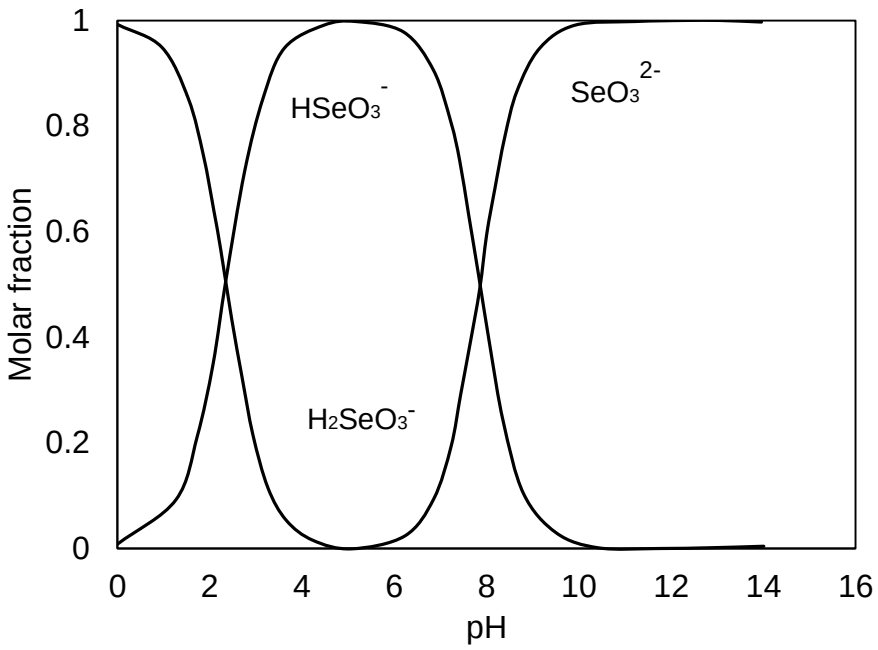

Figure 3.3: Equilibrium diagram of selenite as a function of pH at 25°C (Scott, 1991)

3.4.1 Kinetics of selenium oxidation

Kinetic studies on the oxidation of selenium and selenium bearing minerals in acidic, neutral and alkaline conditions have been conducted by a number of researchers.

Kilic et al. (2013) conducted kinetic studies on the dissolution of selenium from copper anode slimes. The experimental data fitted the ash diffusion model. However, 62 kJ/mol activation energy was obtained which is typical of a chemical controlled reaction. No further discussion was made on this effect. Zheng and Chen (2013) conducted a kinetic study on the leaching of selenium-tellurium rich material in 1 to 2.5 mol/L sodium sulphite solution and 25-95°C. It was reported that the dissolution reaction was controlled by diffusion through a boundary layer with an activation energy of about 20 kJ/mol. Leaching kinetics of selenium from nickel-molybdenum smelter dust using sodium chlorate, in a mixture of hydrochloric and sulphuric acid was studied by Hou et al. (2010). 98% leaching efficiency of selenium was obtained at 95°C, initial H^+ concentration of 8 mol/L and 150 rev/min in 150 minutes. The apparent activation energy for the dissolution of selenium was 44.4 kJ/mol and is consistent with surface chemical reaction control.

3.5 Other studies on alkaline oxidative leaching of sulphur, selenium and arsenic bearing materials

Hoffmann (1984) studied the caustic leaching of selenium from copper anode slimes. He stipulated a leaching temperature of approximately 200°C and caustic concentration in the range 2.5 to 12.5 mol/L. The concentration of the caustic solution was based on the concentration of the selenium in the slimes and the solids content of the slimes in the leach slurry. Due to the importance of oxygen in the dissolution rate of selenium, the oxygen partial pressures were varied from 200 to 2000 kPa. The reaction time was varied between 4 to 7 hours. Under these operating conditions, the conversion of selenium to the hexavalent form is represented by Reaction 3.14:

$$Se_{(s)} + \frac{3}{2}O_{2(g)} + 2NaOH_{(aq)} \rightarrow Na_2SeO_{4(aq)} + H_2O_{(l)} \qquad 3.14$$

All the metal sulphides present in the slimes were converted to sodium sulphate and their respective oxides, hydroxides or sodium salts. Although no attempt was made to determine the various factors affecting the leaching rate or the various factors that might affect the downstream operations e.g. the precious metal recoveries, the alkaline leaching process was rated as appropriate.

A caustic leaching process is described in a European patent (Thomas et al., 1986) for the leaching of selenium and platinum selenide (PtSe) from a product of sulphur dioxide reduction process of selenium and PGMs. Selenium was dissolved and tellurium remained in the residue. In this process, the filter cake from the sulphur dioxide reduction step was slurried in a caustic solution between 100 and 250 g/L solids. The amount of caustic used for the leach was 1 mol/L in excess of the stoichiometric amount with respect to selenium. A caustic pressure leach was conducted at 180 to 220°C and a total gauge pressure of 1725 to 2410 kPa (gauge). The oxygen partial pressure was maintained between 340 to 690 kPa. Sufficient oxygen was provided to oxidise selenium and tellurium to the hexavalent state. The maximum selenium extraction was yielded at the optimal operating conditions of 200°C, oxygen partial pressure of 690 kPa and an excess of 1 mol/L.

Steenekamp and Dunn (1999) showed that tellurium and selenium can be selectively leached from a copper selenide/telluride precipitate, leaving the PGMs as part of the residue. The treatment consisted of two leaching stages; first to leach tellurium, followed by the leaching of selenium. The approximate leach conditions for the first stage were as follows:

Temperature	80°C
Oxygen partial pressure	65 kPa
Time	15-20 minutes
NaOH	0.5 mol/L

Tellurium was recovered in solution as sodium tellurate according to the stoichiometry of the following reaction:

$$CuTe_{(s)} + 2O_{2(g)} + 2NaOH_{(aq)} \rightarrow Na_2TeO_{4(aq)} + 2CuO_{(s)} + H_2O_{(l)} \qquad 3.15$$

It was also noted that increased caustic concentration and residence time resulted in an insoluble sodium tellurate (Na_2TeO_4). The residue was then subjected to another stage of caustic leaching, although the leaching conditions were not stated. The extent of the selenium, sulphur and arsenic leaching was 90%, 90% and 75%, respectively.

Rappas and Waterman (1990) utilised alkali solutions to leach smelter flue dust. This resulted in the separation of metals in a water-insoluble or solid group, containing bismuth and several oxides, and a water-soluble or liquid group containing soluble oxyanions, including arsenic. Additionally, a large fraction of the sulphur was removed as sodium sulphate. This selective caustic leaching of flue dust yielded a solid residue containing most of the valuable metals, i.e., copper, gold and silver, which was suitable for recycling back to the smelter, and a caustic solution containing soluble sodium salts of the oxy-anion forming elements. Concentrated caustic solution of approximately 2 mol/L, leaching temperature of 50° to 100°C and a residence time of one hour were utilised. It was found that in order to achieve good leaching of sulphur and arsenic in the flue dust, without dissolving the valuable elements, the caustic mass ratio had to be kept between 0.3 and 1.4 g NaOH per gram flue dust. This

conclusion is supported by Subramanian et al. (1980) who found the optimum dosage of caustic to be 0.5 to1.07 g NaOH per g flue dust.

According to a study conducted by Saydut et al (2011) on the chemical leaching of sulphur and mineral matter from asphaltite (a mixture of hydrocarbons), a total of about 83% dissolution of sulphur was achieved after 16 hours in 1 mol/L caustic solution at 180°C. Bhakta et al. (1989) investigated the kinetics of alkaline oxidative leaching of gold arsenopyrite ores. The test conditions of the study were 100°C, 2 mol/L NaOH, oxygen pressure of 276 kPa, 10% solids loading and 4 hours residence time. Under these conditions 90% arsenic extraction was achieved.

The following reactions have been proposed (Subramanian et al., 1979) for elemental selenium, tellurium, sulphur and arsenic oxidation, respectively.

$$2Se_{(s)} + 3O_{2(g)} + 4NaOH_{(aq)} \rightarrow 2Na_2SeO_{4(aq)} + 2H_2O_{(l)} \quad 3.16$$

$$2Te_{(s)} + 3O_{2(g)} + 4NaOH_{(aq)} \rightarrow 2Na_2TeO_{4(aq)} + 2H_2O_{(l)} \quad 3.17$$

$$2S_{(s)} + 3O_{2(g)} + 4NaOH_{(aq)} \rightarrow 2Na_2SO_{4(aq)} + 2H_2O_{(l)} \quad 3.18$$

$$4As_{(s)} + 5O_{2(g)} + 12NaOH_{(aq)} \rightarrow 4Na_3AsO_{4(aq)} + 6H_2O_{(l)} \quad 3.19$$

3.6 Platinum group metals chemistry

3.6.1 General properties

The six platinum group metals (PGMs), ruthenium (Ru), rhodium (Rh), palladium (Pd), iridium (Ir), osmium (Os) and platinum (Pt) are grouped with gold and silver as ‘precious metals’. These elements possess a silvery white colour with an exception of osmium, which is bluish white. These metals are highly resistant to attack by most chemical reagents, yet, when employed as catalysts, they accelerate many oxidation, reduction, and hydrogenation reactions. Renner et al. (2001) gave an overview of the physical and mechanical properties of these metals. The elements have many other

uses and moreover, they exhibit extremely varied chemical behaviour, depending on their state of oxidation and chemical environment.

The inorganic chemistry of PGMs, particularly coordination chemistry has been dealt by Hartley (2013, 1973a) and Livingstone (1975). PGMs are kinetically inert in relation to other transition-metal ions. According to Giandomenico (1996), palladium, rhodium and ruthenium are more labile in their higher oxidation states than platinum, osmium and iridium. These elements have several stable oxidation states. The extreme case is represented by ruthenium and osmium, which have oxidation states ranging from −2 to +8. However, their principle oxidation states are +3/+4 and +4, respectively. Rhodium, palladium, platinum and Iridium have +3, +2, +4 and +2/+4 as their principle oxidation states, respectively. The relative ease of conversion between oxidation states gives rise to a rich catalytic chemistry (Giandomenico, 1996). Their metallic properties suggest classification by pairs, i.e., Ru and Os, Rh and Ir, and Pt and Pd.

3.6.2 Ruthenium species in alkaline media

Ruthenium is not attacked by acids below 100°C but more easily dissolves in alkaline oxidising environments. The +6 oxidation state is the most common form in which ruthenium species exist under oxidative conditions in alkaline solutions (Goldberg and Hepler, 1968). In potassium solutions, the formal species would be K_2RuO_4 in an oxidising environment (Renner et al., 2001). The oxidative dissolution reaction in caustic solution can be represented by Equation 3.20 below:

$$2Ru_{(s)} + 3O_{2(aq)} + 4OH^-_{(aq)} \rightarrow 2RuO^{2-}_{4(aq)} + 2H_2O_{(l)} \qquad 3.20$$

3.6.3 Osmium species in alkaline media

As already mentioned in the previous section, the chemistry of osmium involves a variety of species in oxidation states from -2 to +8. The tetraoxide, OsO_4, is probably the most important osmium compound with an oxidation state +8. This osmium compound is very volatile and poisonous (Goldberg and Hepler, 1968). In oxidising alkaline conditions, it forms what is known as ‘perosmate’ ion which is represented by $OsO_4^-(OH)_2^{2-}{}_{(aq)}$. Alkaline oxidation of osmium in metallic form also yields osmates

such as K_2OsO_4. The osmate ion $OsO_4^{2-}{}_{(aq)}$ is realistically represented as $[OsO_2(OH)_4]^{2-}{}_{(aq)}$ (Hartley, 2013).

3.6.4 Rhodium species in alkaline media

Unlike ruthenium and osmium, rhodium does not dissolve in alkaline solutions. However, it is soluble in aqua regia or hot concentrated sulphuric acid (Goldberg and Hepler, 1968). The reaction of rhodium, either in metallic form or as a hydrated oxide $Rh_2O_3.5H_2O$ yields $Rh(H_2O)_6^{3+}$. According to Goldberg and Hepler (1968), the oxidation of metallic rhodium in caustic solutions yield RhO_2. In addition, $Rh^{3+}{}_{(aq)}$ is precipitated as $Rh_2O_3.5H_2O$ when it is treated with a strong oxidising agent in a basic solution. The reaction of rhodium with caustic solution can be represented by the equation below:

$$Rh_{(s)} + O_{2(aq)} + OH^-_{(aq)} \rightarrow RhO_2.XH_2O_{(s)} + H_2O_{(l)} \qquad 3.21$$

with X being the number of water molecules in the precipitated hydrate salt. Shukla (1958) in his study of rhodium oxidation of Na_2RhCl_5 in caustic solution also observed the formation of a rhodium hydroxide precipitate.

3.6.5 Iridium species in alkaline media

Iridium is commonly found in +3 oxidation state. Similarly to rhodium, it is soluble in acid solutions, but precipitates in basic solutions. The oxide Ir_2O_3 which also exists as a hydrate is the predominant species formed when iridium reacts with a NaOH in the presence of an oxidant (Goldberg and Hepler, 1968). Renner et al. (2001) also shows that in the treatment of scrap containing PGMs, dissolution of scrap with potassium hydroxide leaves iridium in the residue as an oxide. From the redox potential diagrams by Pourbaix (Pourbaix et al., 1956) anhydrous IrO_2 is insoluble in acids and bases as well as in aqua regia, but soluble in hydrated form when freshly prepared.

3.6.6 Palladium species in alkaline media

Although the principle oxidation state of palladium is +4, it is also known to exist in the 0 and +2 states. Palladium is known to resist attack by alkaline solutions even in the presence of oxidising agents. Although this is not in agreement with the theories of Goldberg and Hepler (1968) who observed the formation of soluble palladites, this

may be due to the formation of a protective film on the surface of palladium, possibly as the more stable PdO compound (Pourbaix et al., 1956). Pourbaix cites other studies from the literature were palladium was polarised anodically in caustic solutions at high pH (13.7). It was observed that palladium takes several steps during polarisation as the potential changes. Several steps were observed during the polarisation, which can be presented as follows:

$$Pd - Pd_2O - PdO - PdO_2 - PdO_3 \qquad 3.22$$

These changes in the species during oxidation may imply that palladium dissolves and then precipitates as the oxidation process proceeds. However, no other information was found in the open literature to support this theory.

3.6.7 Platinum species in alkaline media

One of the most common oxidation states of platinum is +4. It is known to be resistant to chemical attack at most pH levels. However, in very concentrated solutions (acidic/basic) at high redox potential, platinum may dissolve appreciably (Renner et al., 2001; Goldberg and Hepler, 1968). Some of the complex ions that platinum form includes $Pt(OH)^{3+}$, PtO^{2+}, PtO^{2-} and PtO_3^{2-}.

Platinum also forms hydroxides and hydrated oxides in alkaline media. The species depend on the redox potential. $Pt(OH)_2$ is predominant at lower potential 0.4mV. As the potential increases, $PtO_2.XH_2O$ is formed while $PtO_3.XH_2O$ is formed at higher potential (X denotes degree of hydration). Therefore, the degree of dissolution of platinum depends on the degree of hydration. Due to lack thermodynamic properties, the formation of these hydrates is difficult to quantify.

Chapter summary

The literature review conducted showed a significant number of publications available on the subject of PGM-matte pressure leaching under sulphuric acid conditions. However, relatively few studies have focussed on the caustic leaching of PGM concentrates. Some of this literature addressed the recovery of the precious metals from anode slimes while others focused on the recovery of sulphur, selenium and arsenic from copper anode slimes and different forms of smelter flue dust. The lack of published information confirms the need to conduct leaching studies on these types of materials.

PGM ores or concentrates that contain sulphides, arsenides and selenides usually need to undergo some form of purification to remove these deleterious elements. Alkaline oxidation has long been a preferred process for the oxidation of sulphide/arsenide/selenide minerals due to the instability of these minerals at high pH and E_h values. However, little attention has been given to alkaline oxidation as compared to conventional acidic oxidation. Sulphur and selenium bearing minerals are more easily oxidised by oxygen than arsenic minerals in alkaline media. The oxidation chemistry and mechanism of arsenic remain largely unknown, even though a number of electrochemical studies have been conducted on arsenopyrite.

The alkaline oxidation of sulphur, arsenic and selenium minerals containing base metals (Fe, Cu, Ni) by oxygen yields, sulphates, arsenates, selenates ions and base metal hydroxides (or oxides). The oxidation process may also produce species such as polythionates, sulphites, arsenites, and selenites. The dissolution rate of these minerals may be influenced by pH, oxygen partial pressure, temperature, mineral particle size, agitation speed, as well as reaction time.

There are a few studies that have been carried out on the kinetics of amphoteric elements dissolution in various alkaline solutions by other researchers, most of who concluded that the pattern of dissolution was by diffusion through a product layer. Moreover, most of the studies agree that the rate of reactions of the amphoteric elements is proportional to between 0.2 to 0.5 reaction order with respect to dissolved

oxygen concentration and hydroxide ion concentration. The activation energy values have been consistent with diffusion through a product layer with values of between 10 and 40 kJ/mol reported.

However, despite all the investigations that have been carried out on the alkaline oxidation chemistry and kinetics of amphoteric elements of different mineral species, no study has been conducted on the PGM concentrate. Thus, a number of questions remain unanswered with regards the behaviour of amphoteric elements and PGMs during alkaline oxidation of the PGM concentrate/leach residue, some of which are;

- The relationship between amphoteric elements dissolution rate, caustic concentration and temperature.
- The relationship between PGM dissolution rates (losses) and caustic concentration.
- The relationship between temperature and PGMs dissolution rates.

4 INTERFACIAL OXYGEN MASS TRANSFER

4.1 Background

Oxygen gas is utilised as the primary oxidant in various hydrometallurgical processes. However, because diatomic oxygen is sparingly soluble in aqueous electrolytes, an accurate mathematical description of the interfacial mass transfer rate from the gas to the liquid phase was required for this study and is covered in this chapter.

Oxygen use is hindered by its low solubility in water and aqueous solutions. The dissolution of a gas in a liquid may be described by two sequential steps. The first step is the dissolution of the gas in the solution at the gas liquid interface, followed by the diffusion of the dissolved gas through the solution boundary layer. (Kimweri, 2001; Filippou et al., 2000)

Oxygen transfer kinetics are dependent on temperature, pressure and liquid-phase properties (ionic strength, density, surface tension, viscosity etc.), as well as the specific features of the reactor, e.g., agitation speed, agitator configuration (Filippou et al., 2000). The rate of oxygen transfer across a gas-liquid interface is dependent upon the mass-transfer characteristics of boundary layers that are formed next to the interface, and the total interfacial area available. The liquid-side volumetric mass-transfer coefficient, $k_L a$ is generally used as a quantitative measure of the mass-transfer capability of a given reactor. The volumetric mass transfer coefficient is the product of mass-transfer coefficient, k_L and the specific gas-liquid interfacial area, a expressed per unit volume of liquid, per unit reactor volume or, more often, per unit volume of gas-liquid mixture (Filippou et al., 2000).

The following oxygen mass balance equation of a stirred reactor describes the dissolved oxygen concentration, C in the electrolyte solution:

$$\frac{dC}{dt} = k_L a\left[C^* - C\right] \qquad 4.1$$

The overall $k_L a$ term is not easily separated into the individual k_L and *a* term. The area, *a* is closely related to the reactor configuration and degree of agitation, whereas, k_L is closely related to the turbulence and liquid properties (Yang and Wang, 1992a). C* is the dissolved oxygen concentration in the liquid phase at equilibrium with the gas. C* is a temperature-dependent thermodynamic property that can be estimated by Henry's Law, which is a function of the oxygen partial pressure (Tromans, 1998a).

Equation 4.1 follows directly from the 'film model' (Whitman, 1962), and assumes the presence of a laminar fluid film adjacent to the interface, and poses a resistance to the gas diffusion process. This is expressed by the following equation:

$$k_L = \frac{D}{\delta} \qquad 4.2$$

where k_L is the liquid-side mass transfer coefficient (ms^{-1}), D is the effective diffusivity (m^2s^{-1}) of the dissolved gas in the stagnant film layer and δ is the film thickness (m).

The oxygen concentration in the film falls from saturation or equilibrium concentration, C* at the solution interface between the gas and the liquid, to its bulk solution value, [C]. There is no convection in the stagnant film and the dissolved gas crosses it by molecular diffusion alone. The driving force for the interfacial mass transfer of oxygen from the gas to the liquid phase is the difference in its chemical potential between the two phases (Filippou et al., 2000).

Equation 4.1 neglects the gas-side resistance of the two-film theory because it has been experimentally proven to be of minor importance for the O_2-H_2O system. Figure 4.1 below presents a schematic illustration of the film theory, where L, G and i represent liquid, gas and interface, respectively.

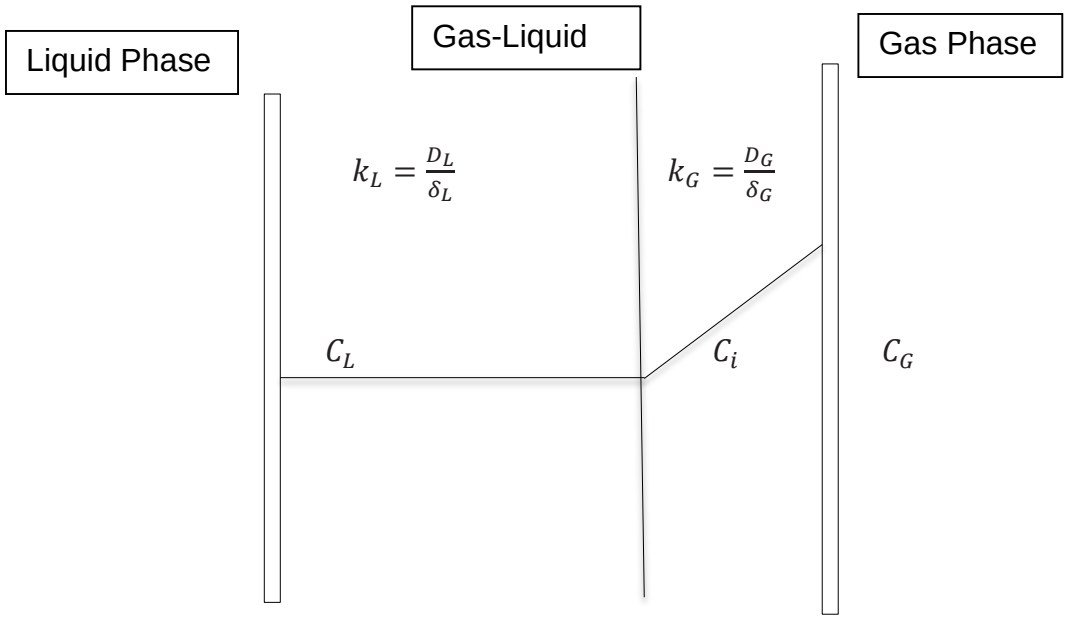

Figure 4.1 Schematic representation of the gas–liquid interface, concentrations and mass transfer coefficients k_L and k_G according to film theory (Garcia-Ochoa and Gomez, 2009)

4.2 Methods of measurement of oxygen mass transfer rates

Different methods are available to determine k_La and can be divided into physical and chemical methods. Some of the chemical methods used include the sodium sulphite, hydrazine oxidation, absorption of CO_2 and bio-oxidation of catechol methods while dynamic gassing out is one of the physical methods (Garcia-Ochoa and Gomez, 2009; Onken et al., 1985; Hermann et al., 2001; Suresh et al., 2009). One of the most commonly used methods of determining the k_La is the sodium sulphite method as proposed by Cooper et al. (1944). This method is preferred due to its experimental simplicity, and was therefore adopted in this study. Section 4.2.1 gives a brief discussion of the method.

4.2.1 Sulphite-oxidation method

This method relies on the oxidation of sulphite to sulphate by diatomic oxygen in the presence of a catalyst according to the following equation:

$$2SO_3^{2-} + O_2 \xrightarrow{\text{Catalyst}} 2SO_4^{2-} \qquad 4.3$$

The oxidation reaction is zero order with respect to the sulphite concentration, provided the sulphite concentration is higher than some threshold value (see below). The reaction rate is controlled by the rate of mass transfer, especially in the presence of a catalyst. In the procedure given by Cooper et al. (1944), the sulphite solution is agitated for a measured period of time. A sample is taken and excess iodine is then added to react with the unoxidised sulphite. The unreacted iodine is titrated using sodium thiosulphate. The detailed procedure is given in Appendix III

In the sulphite-oxidation method, the reaction rate is a complex function of the catalyst concentration and the operational conditions (Yang and Wang, 1992). Cobalt(II) and copper(II) ions (of varying concentrations) have been the widely used catalysts. Fuller and Crist (1941) studied the sulphite oxidation reaction with copper(II) catalyst. They found that the uncatalysed reaction is first order with respect to sulphite concentration. Westerterp et al. (1963) found the reaction to be zero order with respect to sulphite concentration and first order with respect to dissolved oxygen concentration in a copper catalysed system. Murphy et al. (1959) studied the aeration of tower-type fermenters. The gas (air) was injected at the bottom of the fermenter via porous discs. The rate of copper catalysed sulphite oxidation was found to be strongly dependent on total sulphite and sulphate concentration. For the initial sulphite concentration of between 0.1 mol/L to 0.2 mol/L, the rate was found to be dependent on the sulphite concentration. This was attributed to bubble size dependency on molar concentration.

In cobalt catalysed sulphite oxidation processes, Phillips and Johnson (1959) studied the effect of oxygen partial pressure on the rate of oxidation in sparged and unsparged vessels. The rate of oxidation was found to vary proportionally with the oxygen partial pressure in sparged systems, as well as unsparged systems at high turbulent levels.

Roxburgh (1962) investigated the effect of different catalysts on the oxidation rate of sulphite solutions. The effect of copper, cobalt, iron and nickel catalyst was found to be very different at similar concentrations. Roxburgh (1962) also found that the oxidation rate depended appreciably on the pH of the sulphite solution. Similarly, the study by Fuller and Crist (1941) showed that the pH of the sulphite solution had an

effect on the sulphite oxidation rate. It was established that at a pH between 8.2 and 8.8 the oxidation rate was independent of the pH, but decreased between 3.2 and 5.9. They also found that the sulphite oxidation was sensitive to catalyst concentration. Using copper as a catalyst, cupric ion concentration above 10^{-4} mol/L had no effect on reaction rate. To the contrary, Robinson and Engel (1967) found that the uncatalysed reaction rate was faster than the copper catalysed reaction. This led to a recommendation of the use of cobalt instead of copper catalyst.

Filippou et al. (2000), Steyl (2012) and Olle et al. (2006) studied the application of the sulphite method to determine the $k_L a$ in stirred tank reactors. The sulphite oxidation process was found not suitable at low pH as established by Fuller and Crist (1941). There have also been arguments on the mass transfer enhancement at higher pH values (>9) as shown by Olle et al. (2006) and Linek and Vacek (1981). Since this study focusses on determining the kLa value in the absorption regime, the effect of pH on the intrinsic sulphite oxidation rate will not be investigated further. Studies by Steyl (2012) and Olle et al. (2006) established the cobalt catalyst concentration range where the catalyst does not enhance the mass transfer. In both studies, cobalt(II) concentration range of 1 to 5 mg/L was high enough to accelerate the intrinsic kinetics so that the chemical reaction rate was not limiting, whilst, at the same time, being low enough to prevent chemical enhancement of the physical absorption process. Cobalt(II) catalyst in this concentration range was therefore also used in this study.

4.3 Effect of different operating parameters on $\mathbf{k_L a}$

4.3.1.1 Effect of Temperature on $k_L a$

The effect of temperature on the volumetric mass transfer coefficient $k_L a$ can be explained by the variation in the physical properties of the gas and liquid phases, i.e., viscosity, surface tension and diffusivity. It has been shown by many researchers that raising the temperature typically causes the reduction in the solution viscosity, surface tension and liquid density while increasing the diffusivity (Filippou et al., 2000). According to Equation 4.2, an increase in the dissolved oxygen diffusivity causes an increase in the k_L value and therefore, an increase in the $k_L a$ value. However, an increase in the temperature decreases the density, which in turn, favours an increase

in the average bubble diameter, thus, reducing the specific interfacial area (Jin et al., 2004). A decrease in surface tension at higher temperature aids bubble growth and coalescence, thereby decreasing the interfacial surface area. The same effect is observed for the viscosity at higher temperature, which promotes coalescence of small bubbles into larger ones and a reduction in the interfacial area (Jin et al., 2004). Therefore, the overall effect of temperature on $k_L a$ will ultimately depend on the competition between the effects of temperature on the diffusivity (k_L) and the interfacial area (*a*).

The correlation:

$$k_L a(T) = k_L a(T)_r . \theta^{T-T_r} \qquad 4.4$$

is used to correlate the temperature effect on the volumetric mass transfer coefficient. T_r is the reference temperature; T is temperature and is θ is the theta factor. Equation 4.4 has been used for the temperature correction of the $k_L a$ with the generally accepted θ value of 1.024 (Stenstrom and Gilbert, 1981).

4.3.2 Effect of Pressure on $k_L a$

In hydrometallurgical processes, reactions are often conducted under pressure. According to the literature, the effect of pressure on $k_L a$ can be different depending on the nature of the interfacial mass transfer system and the operating conditions. Some investigators have reported an increase in the kLa value with increase in pressure (Jin et al., 2004; Yang, 1982), while others have reported that the kLa value remain unaffected by pressure. Filippou et al. (2000) cited studies which have shown that the kLa value is not affected by changes in pressure.

4.3.3 Effect of Solids on $k_L a$

Literature (Alba et al., 1983; Inga and Morsi, 1997; Deimling, 1984; Filippou et al., 2000) has shown that addition of solid particles to the liquid-phase can have different effects on the $k_L a$ value. The influence of solids depends on many parameters related either to solids (shape, size, and concentration) or to interfacial properties i.e.,

wettability, adsorption capacity, etc. (Hichri et al., 1992). Particular cases have shown low solid concentration to have a minor influence or increase in the kLa value (Alba et al., 1983, Inga and Morsi, 1997) whereas at high solid concentrations, kLa values have been shown to decrease (Alba et al., 1983; Deimling, 1984; Filippou et al., 2000). When the solids concentration is low, particles only have a limited impact on the slurry viscosity and can inhibit the coalescence tendency or promote the breakup of gas bubbles by interacting directly with the gas-liquid interface, resulting in a small increase of the $k_L a$ values. High solid concentrations, on the other hand, are more likely to increase the slurry viscosity, which, in turn, will promote gas bubble coalescence and will lead to a decrease in the gas-liquid interfacial area. Increasing bubble size, however, can increase the mass transfer coefficient k_L and as a result the $k_L a$ value may increase, decrease or remain unaffected by the solid concentration.

4.4 Solubility of oxygen

The solubility of oxygen in water and aqueous electrolyte solutions, and its variation with pressure, temperature, and electrolyte concentration, is of paramount importance in hydrometallurgical oxidation processes. The thermodynamic relationship relating oxygen solubility with partial pressure is given by the following thermodynamic expression:

$$K^\circ = \frac{a}{f} = \frac{\gamma m}{\Phi p} \qquad 4.5$$

where K° is the equilibrium constant, Φ is the fugacity coefficient and γ is the activity coefficient. At a low solute concentration and moderate partial pressure of oxygen, the fugacity coefficient, Φ is close to unity. Since diatomic oxygen is a non-polar gas, it exhibits a very low solubility in water. Hence, the activity coefficient, γ, is also close to unity. Diatomic oxygen, therefore exhibits Henry-type behaviour:

$$K^\circ \approx K_H \text{ (Henry's law constant).} \qquad 4.6$$

Tromans (1998a, 1998b) determined empirical relationships for oxygen solubility in water and electrolyte solutions. These relationships are also adopted in this work:

$$C_{aq} = P_{O_2} f(T) \tag{4.7}$$

$$(C_{aq})_I = \Phi P_{O_2} f(T) \tag{4.8}$$

where C_{aq}, $(C_{aq})_I$ and P_{O_2} are the solubility of diatomic oxygen in water, inorganic solution and partial pressure of oxygen, respectively, and f(T) and Φ are defined by the equations below:

$$f(T) = \exp\left\{\frac{\left(A_1 T^2 + A_2 T \ln\left(\frac{T}{298}\right) - (A_3 - A_4 T)(T - 298) - A_5\right)}{RT}\right\} \tag{4.9}$$

$$\Phi = \left\{\frac{1}{1 + \kappa(C_I)^y}\right\}^{\eta} \tag{4.10}$$

where T is the temperature, R is universal gas constant, C_I is the solute concentration (mol/kg) and the other constants are given in Table 4.1 and Table 4.2 below.

The coefficient κ and exponents y and η in Equation 4.10 are solute specific empirical parameters. Due to lack of published data on the sodium sulphite solutions, the parameters for sodium sulphate where adopted in this study. The error due to this assumption has been reported to be less than 2% (Filippou et al., 2000).

Table 4.1 Constants for solubility of oxygen in water

A_1	0.046
A_2	203.35
A_3	299.378
A_4	0.092
A_5	20591

Table 4.2 Constants for oxygen solubility in Na_2SO_4 solutions

κ	0.629498
y	0.911841
η	1.440175

Chapter summary

Oxygen supply is a critical factor in many hydrometallurgical processes. It is no wonder then that the study of oxygen mass transfer and reaction has attracted significant attention in leaching reactors. There has been a tendency, however, in treating reaction chemistry and oxygen transfer in isolation. This may lead to catastrophic failure in reactor design due to inadequate supply of oxygen to hydrometallurgical systems.

The understanding of the volumetric mass transfer coefficient and oxygen consumption for a particular system is important to determine the optimal operating conditions (pressure and agitation speed) that would ensure that there is minimum amount of dissolved oxygen (stoichiometric oxygen demand) available for the oxidation reactions. This avoids oxygen gas becoming a reaction limiting factor. The two factors; oxygen supply and demand, are summarised by the differential equation below:

$$\frac{d[O_2]}{dt} = kLa\left[[O_2]^* - [O_2]\right] - xQ_{O_2}$$

where x is mass fraction of oxygen consuming mineral and Q_{O_2} is the oxygen demand, while the other parameters have been defined before. From the above equation, it is clear that the oxygen transfer rate of the reactor $\left(kLa\left[[O_2]^* - [O_2]\right]\right)$ must exceed the oxygen consumption rate $\left(xQ_{O_2}\right)$ of the mineral in order to maintain the dissolved oxygen above a particular concentration. This may be achieved by:

I. Controlling the mineral feed
II. Controlling the oxygen mass transfer rate
III. A combination of (I) and (II)

The above review emphasises the importance of oxygen mass transfer in oxidative leaching processes because it may affect the overall performance of the process. The potential limiting role of the interfacial mass transfer rate will be dictated by the nature of mineral, reactor configuration and the scale of operation. In this regard, this chapter

has highlighted the importance of temperature, pressure, agitation and pulp density on oxygen solubility.

5 REACTION KINETICS

Reaction rate studies conducted at conditions similar to industrial conditions provide valuable engineering data for full scale reactor design.

In a typical oxidative pressure leaching process, the mass transfer that is required to sustain a heterogeneous reaction takes place at the boundary between two phases, which is called the reaction interface**.** Obviously one of the phases is solid, so it is the reaction at the solid surface. The total reaction rate of heterogeneous processes is controlled by the rate of the slowest step. Figure 5.1 below presents a schematic diagram of the sequential process (1 to 6) for the leaching reaction of a solid particle

1. Dispersion of oxygen into the pulp
2. Fluid film mass transfer
3. Diffusion of dissolved oxygen through a product layer
4. Chemical reaction
5. Diffusion of reaction product through product layer
6. Diffusion of reaction product through fluid film into the bulk solution

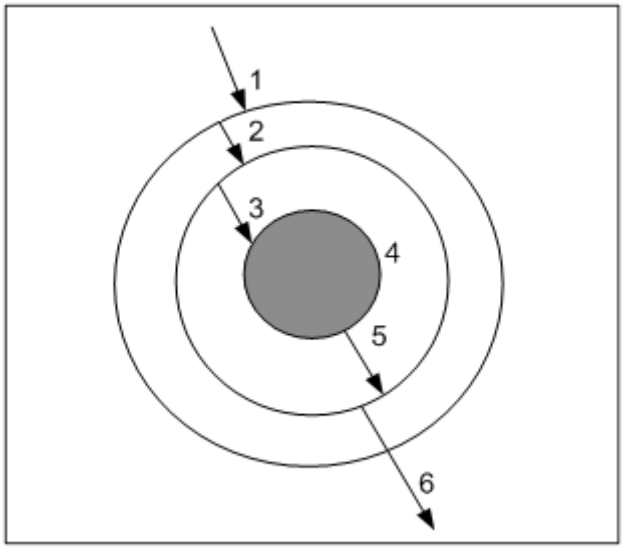

Figure 5.1: Schematic diagram of sequential process steps of leaching of a solid particle

In an irreversible leaching reaction involving a solid particle and a liquid species, the reaction equation may be written as follows:

$$aA_{(s)} + bB_{(aq)} \rightarrow cC_{(s)} + dD_{(aq)} \qquad 5.1$$

When no product layer is formed, the rate determining step may be a chemical reaction at the solids-fluid interface, diffusion through the fluid boundary layer or both.

5.1 Kinetic Models

The two most commonly used leaching models are described in this section, i.e., the shrinking particle and unreacted shrinking core models.

5.1.1 The shrinking particle model

For the shrinking particle model, reactions are confined at the surface of the particle and the size of the particle is reduced by flaking off the solid products. The development of this model is based on a non-porous particle in an agitated fluid medium with no product layer formation, such that the radius decreases with time as the reaction proceeds. This is illustrated in the diagrams below:

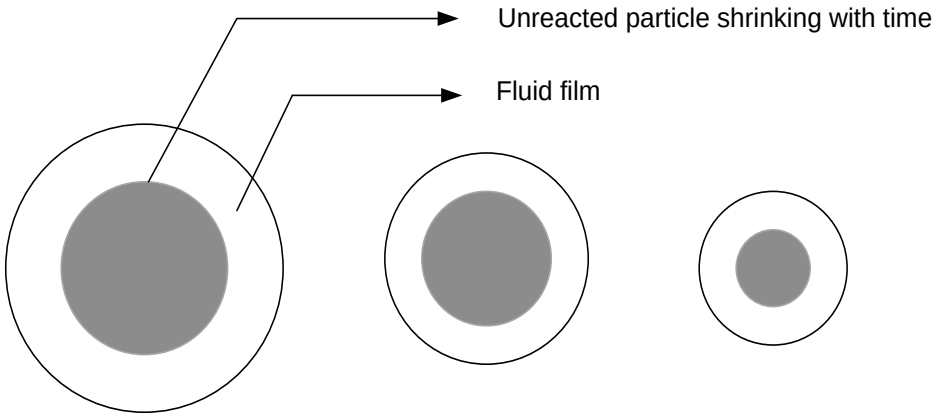

Figure 5.2: Schematic diagram of the shrinking particle model

Considering a particle with initial radius r_o and containing n_o moles of a certain solid species A of molecular volume V. A reacts with an aqueous species B to give an aqueous soluble reaction product, C.

$$aA_{(s)} + bB_{(aq)} \rightarrow cC_{(aq)} \qquad 5.2$$

The rate of the heterogeneous Equation 5.2 of a mineral with a dissolved reagent may be expressed as (Levenspiel, 1972):

$$\frac{dn}{dt} = -AkC = -4\pi r^2 kC \qquad 5.3$$

where n is the number of moles of solid species A at any time point t

A = surface area of the mineral particle

C = concentration of reactant B

k = the rate constant

r= particle radius

When n is expressed in terms of the molar volume, yields:

$$n = \frac{\frac{4}{3}\pi r^3}{V} \qquad 5.4$$

where V is the molar volume. Because the radius of the solid particle under dissolution changes over time, differentiating Equation 5.4 yields:

$$\frac{dn}{dt} = \frac{4\pi r^2}{V} \cdot \frac{dr}{dt} \qquad 5.5$$

Combining Equation 5.3 and 5.5

$$\frac{dr}{dt} = -k'' CV \qquad 5.6$$

Considering the fact that at time t=0, r=r_o. Integrating Equation 5.6 with initial boundary conditions and r= r_o at time t=t_o yields:

$$r_o - r = -k'' CVt \qquad 5.7$$

Defining X, the fraction of solid reacted in time t, as:

$$X = \frac{(n_o - n)}{n_o} \qquad 5.8$$

then from Equation 5.4 and 5.7 we obtain;

$$r = r_o(1-X)^{\frac{1}{3}} \qquad 5.9$$

Substituting Equation 5.9 into Equation 5.7 yields:

$$1-(1-X)^{\frac{1}{3}} = \frac{k''CVt}{r_o} \qquad 5.10$$

If the aqueous phase concentration is kept constant, the Equation 5.10 may be written as:

$$1-(1-X)^{\frac{1}{3}} = \frac{kt}{r_o} \qquad 5.11$$

where $k= k''CV$ (linear rate constant) refers to the rate of the movement of the reaction interface.

Equation 5.10 describes the chemical reaction rate and the plot of $1-(1-X)^{\frac{1}{3}}$ against reaction time, t should give a straight line, if the overall leaching kinetics is controlled by the intrinsic reaction rate.

5.1.2 Unreacted shrinking core model

The unreacted shrinking core model is applied when the reactant is converted to another solid material, leaving behind a product layer around the unreacted particle core.

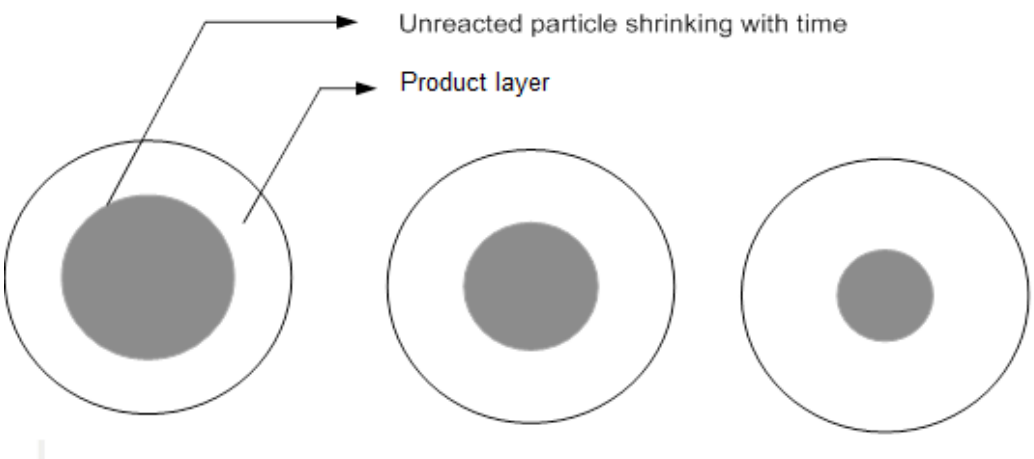

Figure 5.3: Schematic diagram of the shrinking core model

The mathematical description of the shrinking core model under product diffusion control is based on the following assumptions

1. The particle is considered to maintain its shape and size during the entire leaching process
2. The low reagent and product concentrations in solution means the net flux due to diffusion is considered negligible
3. The surface reaction is assumed to be first order and irreversible with respect to the reacting reagent
4. The reaction reagent is in excess and its concentration may be considered constant during the entire leaching process
5. The system may be considered to be in quasi steady state

Considering J to be the flux of B in Reaction 5.2 through a product layer in time, t then from Fick's law:

$$J = -4\pi r^2 D_s \frac{dC}{dr} \qquad 5.12$$

where D_s is the effective diffusion coefficient of B through a product layer and C is the concentration of B.

Based on assumption 5, J may be considered constant. Using the boundary conditions at which $C=C_c$ when $r=r_c$ and $C=C_o$ when $r=r_o$, Equation 5.12 can be integrated to yield:

$$J = -\frac{4\pi r^2 D_s (C_c - C_o) r_c r_o}{r_c - r_o} \qquad 5.13$$

Under steady state conditions, the rate of disappearance of the core volume of A (Equation 5.2) can be related to J by:

$$J = -\frac{V dV_c}{dt} \qquad 5.14$$

where V is the number of moles of solute per unit volume.

Equating Equations 5.13 and 5.14:

$$-V\left(\frac{dV_c}{dt}\right) = -4\pi\left\{\frac{D_s(C_c - C_o)r_c r_o}{r_c - r_o}\right\} \quad 5.15$$

Rearranging and integrating both sides of Equation 5.15 yields:

$$\int_{V_o}^{V_c}\left\{\frac{r_c - r_o}{r_c}\right\}dV_C = \int_0^t \frac{4\pi D_s(C_c - C_o)r_o}{V}dt \quad 5.16$$

We know that $\frac{r_c}{r_o} = \left(\frac{V_o}{V_c}\right)^{\frac{1}{3}}$. Equation 5.16 can be written as:

$$\int_{V_o}^{V_c}\left\{1 - \left(\frac{V_o}{V_c}\right)\right\}dV_C = \int_0^t \frac{4\pi D_s(C_c - C_o)r_o}{V}dt \quad 5.17$$

After integrating,

$$V_v + \frac{1}{2}V_o - \frac{3}{2}V_c^{\frac{1}{3}}V_c^{\frac{2}{3}} = \frac{4\pi D_s(C_c - C_O)r_o t}{V} \quad 5.18$$

From Equation 5.8 we obtain:

$$X = \frac{(n_o - n)}{n_o} = \frac{(V_o - V_c)}{V_o} \quad 5.19$$

or

$$1 - X = \frac{V_c}{V_o} \quad 5.20$$

where X is the fraction of solid reacted in time t. Then Equation 5.20 becomes:

$$1 - \frac{2}{3}X - (1 - X)^{\frac{2}{3}} = \frac{2D_s(C_c - C_o)t}{r_o^2 V} \quad 5.21$$

Therefore, for reactions controlled by diffusion of reacting species through a product layer, the plot left hand side of Equation 5.21 against reaction time should yield a straight line.

5.2 Rate expressions

To develop a relatively simple kinetic model to capture the effects of both [OH^-] and [O_2], the rate equation can be expressed so that the driving force for dissolution

depends on the difference between its current concentration in the ore/concentrate and its respective concentration after infinite leaching time.
A simple case for a solute reagent reacting with a leachable solid is given in Equation 5.22 (Peters, 1991).

$$Rate = k_r . C_{reagent} . C_{solids} \qquad 5.22$$

where k_r is the rate constant, $C_{reagent}$ and C_{solids} are the concentration of reagents and solids respectively. Equation 5.22 is plausible when the mineral surface area is proportional to concentration of the unleached solids. This can be represented by the equation below:

$$Rate = k_r A C_{reagent} \qquad 5.23$$

where A is the mineral surface area. For a constant volume in a batch reactor (neglecting the volume change due to sampling) Choo et al., (2006) gives the rate equation which can be written as follows:

$$\frac{dC}{dt} = \nu_i A k_r \prod C_r^{\alpha_r} \qquad 5.24$$

where C_r and α_r are the concentration and reaction order with respect to any reactant respectively while ν is the stoichiometric coefficient.

5.3 Mineral surface area

Allen (1990) presents the derivation for the specific surface of a powder (mineral) during weathering. The method described by Allen (1990) is also adopted in this study and is discussed next.

There are two particularly important properties of particles, namely surface area and volume. These properties are proportional to the square and cube, respectively. The proportionality constant depends upon the dimension chosen to characterise the particle. Assuming the particles in question are spherical, the mass of a single particle is given by Equation 5.25 below:

$$m_s = k_v \ell^3 \rho \qquad 5.25$$

where m_s mass of a single particle, k_v is the volume shape factor (π/6 for spherical particles), ℓ is the diameter of the particle and ρ is the density of the particle. The mass of multiple particles within a size range will be:

$$m_m = k_v \ell^3 \rho f \qquad 5.26$$

where m_m is the mass of particles and *f* is the number of particles in the size range. The mass fraction of size range (m_i) will be the mass of size range divided mass of the entire distribution as given by Equation 5.27 below:

$$m_i = \frac{k_v \ell_i^3 \rho f_i}{\sum k_v \ell_i^3 \rho f_i} = \frac{\ell_i^3 f_i}{\sum \ell_i^3 f_i} \qquad 5.27$$

Equation 5.27 assumes the volume shape factor and mineral density to remain constant in all the different size ranges. The analogue expression for area to Equation 5.27 is given in Equation 5.28 below:

$$m_i = \frac{k_p \ell_i^3 \rho f_i}{\sum k_p \ell_i^3 \rho f_i} = \frac{\ell_i^3 f_i}{\sum \ell_i^3 f_i} \qquad 5.28$$

where k_p is area shape factor (π for spherical particles). The surface area of a single sphere is area of single particle (πx^2) divided by the volume ($\pi x^3/6$). The specific surface area for a single particle becomes:

$$A_i = \frac{6}{\ell} \qquad 5.29$$

The specific surface area per unit volume A_v for the full size distribution is the total area divided by total volume as given by equation below:

$$A_v = \frac{\pi \sum \ell_i^2 f_i}{\frac{\pi}{6} \sum \ell_i^3 f_i} = \frac{6 \sum \ell_i^2 f_i}{\sum \ell_i^3 f_i} \qquad 5.30$$

In many instances, the particle size distribution data is in mass rather than number. It is therefore important to find a correlation between mass and number.

Considering Equation 5.27 and rearranging:

$$\ell_i^2 f_i = \frac{m_i}{\ell_i} \sum \ell_i^3 f_i \qquad 5.31$$

Replacing the Equation 5.31 into 5.30 yields the equation for calculating surface area using distribution data given in terms of mass (Equation 5.32 below).

$$A_v = 6 \sum \frac{m_i}{\ell_i} \qquad 5.32$$

The surface area per unit mass becomes:

$$A = \frac{6}{\rho} \sum \frac{m_i}{\ell_i} \qquad 5.33$$

where A is surface area per unit mass, m_i is the mass fraction between size classes and ℓ_i is the geometric mean of size classes. This formula (Equation 5.33) is used to calculate the area exposed to lixiviant during the course of the leaching process.

5.3.1 Overall rate expressions

Given the apparent role of both the hydroxide ions and oxygen in the alkaline leaching of the PGM concentrate, it is of interest to generate a rate equation that would describe the importance of each reactant for selenium, arsenic and sulphur extraction. The following rate expressions are proposed to capture the combined effect of caustic solution and oxygen on the dissolution extent of the amphoteric species:

$$r_{Se} = \frac{d[Se]}{dt} = k_{Se} A [OH^-]^a [O_2]^b \qquad 5.34$$

$$r_{As} = \frac{d[As]}{dt} = k_{As} A [OH^-]^c [O_2]^d \qquad 5.35$$

$$r_S = \frac{d[S]}{dt} = k_{Se} A [OH^-]^e [O_2]^f \qquad 5.36$$

where a, b,c,d,e and f are the reaction orders with respect to the respective reagents and k is the intrinsic rate constant of a species.

5.4 Factors influencing reaction kinetics

Pressure oxidation involves various consecutive and parallel reactions that yield different product species. The abundance of the various products depends on the conditions applied. These conditions are summarised by Prosser (1996) and include temperature, pressure (oxygen partial pressure in this case), acidity or alkalinity, degree of agitation, particle size, and residence time among others.

5.4.1 Effect of temperature

The rate of oxidation generally increases with temperature (Papangelakis and Demopoulos, 1991, Long, 2000). The activation energy (Ea) of sulphur, selenium and arsenic dissolution can be derived by measuring the temperature dependence of the leach rate. The activation energy can also be used to suggest the dominant leaching mechanism. Chemical controlled processes rates can be enhanced by increasing temperature by only a few degrees. If the influence of temperature is weak, together with a mild effect of agitation speed, it can be inferred that the kinetics of leaching is controlled by diffusion rather than chemical reaction (Dreisinger and Abed, 2002). It should be noted that a value of Ea over 40 kJ mol^{-1} implies chemical controlled process whilst less than 40 kJ mol^{-1} suggests that the leaching process is controlled by diffusion (Dreisinger and Abed, 2002, Li et al., 2013). The upper limit of temperature (and pressure) may be restricted by mechanical constraints and increased capital and operating costs.

5.4.2 Effect of oxygen partial pressure

An increase in the oxygen partial pressure increases the rate of oxidation processes. This is due to the increase in dissolved oxygen concentration. However, high temperature reduces the solubility of oxygen in solutions, especially when the temperature approaches the boiling point of the solution (Deng et al., 2001). The reduced oxygen solubility at high temperatures is usually offset by operating at high oxygen partial pressures.

5.4.3 Effect of lixiviant concentration

The concentration of the lixiviant is usually selected based on a number of factors. These include the composition of the raw material. Generally, the concentration is maintained at sufficient free lixiviant concentration to retain the species of interest in the solution, to avoid precipitation and sustain a target oxidation potential. In most chemical oxidation processes, increased lixiviant concentration (e.g., H_2SO_4 and NaOH) increases the reaction rate. Concentration of caustic solution has been known to increase the reaction rates of sulphur, selenium and arsenic in many investigations carried out by several researchers (Virčíkova and Fedor, 1991;Kilic et al., 2013; Yu et al., 2014;Ruiz et al., 2014).

5.4.4 Degree of agitation

As discussed in Chapter 4, adequate agitation is required to provide suitable heat and mass transfer in the reactor. Oxygen absorption rate into the liquid phase largely depends on the conditions of mixing. Other characteristics such as the reactor and impeller design, impeller tip speed and mixing power have an influence on the intensity of agitation. An increase of the agitation speed results in higher dispersion and retention of oxygen bubbles in the slurry. Certain processes, however, do not show a significant dependence on the agitation intensity. Long and Dixon (2004b) conducted test work and showed that agitation speed had no substantial effect on pyrite oxidation rate when the agitation speed was higher than 800 rev/min.

5.4.5 Pulp density

In chemical oxidation processes, the optimum pulp density is usually a compromise between minimising the reactor size by maximising pulp density and oxygen mass transfer rate. The high slurry density leads to increased productivity (especially in low grade ores). However, mass transfer conditions deteriorate and the load on the mixing device is increased. This leads to slow oxidation rates and ultimately results in poor reactor performance.

5.4.6 Particle size

Particle size has a direct effect on leaching chemistry as small particle sizes result in increased mineral exposure (surface area). Reduced particle size, therefore results in higher oxidation rates and higher degree of oxidation in shorter reaction time. The optimum particle size is influenced by many other factors especially the costs associated with comminution. Comminution process is energy intensive and over grinding of material might not be cost effective. When material is overground, other difficulties might appear in downstream processes in the separation and clarification of the solutions.

5.4.7 Residence time

The reaction time required to obtain the desired conversion depends fundamentally on reactor conditions (discussed above) such as temperature, pressure of the reaction mixture, degree of mixing, properties of slurry such as type and amount of minerals and the particle size distribution of material. Longer residence times are required for certain processes due to slow intrinsic reaction kinetics, larger particle sizes and poor mineral liberation. This results in higher operating and capital costs.

5.5 Modelling of reactors

Leaching reactions are carried out in a number of different types of reactors.
Table 5.1 presents a list of the reactor types (Taylor and Martins, 1986).

Table 5.1: Reactor types

Agitated - Solids mechanically agitated or by Sparger. Process can be batch or continuous, co-current or counter current
Columns - Solids are stationary or flow agitated, batch or semi batch, counter-current or co-current
Vat - Solids stationary and batch, maybe treated co-current or counter-current
In-situ - Solids stationary and batch
Dump or Heap - Solids stationary and batch

The major differences in the various reactors are related to whether the solids are stationary or moving and whether there is mechanical agitation or not. These reactors consist of various model components. They can be divided into fluid properties (which include viscosity, density, temperature, gas solubilities etc.), solid properties (which include particle size distribution, particle shape, structure, porosity, thermal conductivity etc.), reaction properties (which include reaction mechanisms, stoichiometry, mass transfer coefficient, heat transfer coefficient, enthalpy of reaction etc.) and reactor properties (including type of reactor, residence time distribution, heat loss or input, number of stages, degree of agitation etc.).

5.5.1 General approach to reactor design for leaching reactions

The ability to describe metallurgical leaching reactors mathematically requires an understanding of the various model components as well as the types of reactors used. The best place to start in reactor modelling is to consider of how the process model will be developed. Figure 5.4 gives a schematic representation of the process model development.

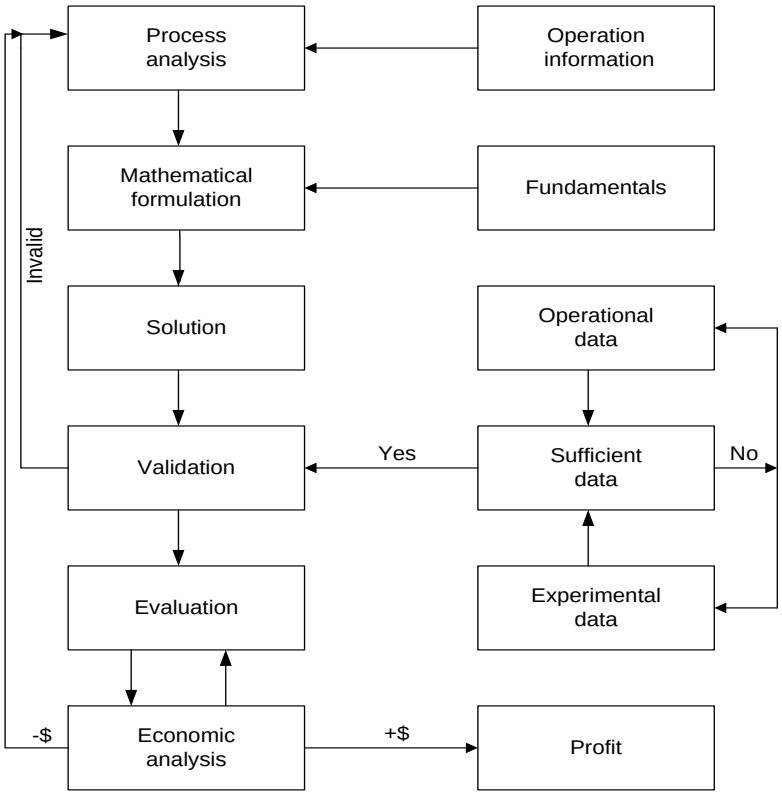

Figure 5.4: Schematic diagram for general process model development

Chapter summary

The main difficulty in deriving a predictive model for heterogeneous reactions is the complexity of such system. There are two types of complexities in reactor modelling; one is mainly the computational while the second is concerned with the identification of the system and the quantitative description of the reaction rates of the process taking place within the system.

Heterogeneous reactions are complex reactions determined by the interaction of various factors. Depending on the reaction conditions, one must apply different models of various complexities. A complete process model should be able to:

- Account for the effect of the full range of process variables (e.g., pressure, temperature, particle size or mineral surface area, residence time and solution composition)
- Encompass the effects of hydrodynamics on reaction extents
- Pass the test of comparison with lab or plant scale data

The first point is captured in the expressions for time-conversion relationships for the two most common leaching models (shrinking particle and unreacted shrinking core) and the overall rate expressions derived. This is further expanded in Chapter 8. The second point has largely to do with mass transfer effects (captured in Chapter 4) while the last point is discussed in Chapter 8 where the experimental results and model prediction are discussed.

6 EXPERIMENTAL

6.1 Mass transfer tests

The mass transfer tests in the test reactor (2 L Büchi autoclave) were conducted using the sodium sulphite method. The experimental procedure (detailed in Section 6.1.3) consisted of filling the reactor with approximately 1.2 mol/L sodium sulphite solution containing 1 to 5 mg/L cobalt(II) ion. The oxidation reaction was allowed to continue for a predetermined time. The oxygen supply was turned on. The initial 'time zero' sample was taken and the clock was also started at this point. Samples were taken at regular time intervals. Each sample was mixed with an excess standard iodine solution and titrated with a standard sodium thiosulfate solution ($Na_2S_2O_3$) using a starch indicator. The reactions are (Jeffrey et al., 1989):

$$SO_3^{2-} + I_2 + H_2O \rightarrow SO_4^{2-} + 2H^+ + 2I^- \qquad 6.1$$

$$2S_2O_3^{2-} + I_2 \rightarrow S_4O_6^{2-} + 2I^- \qquad 6.2$$

The residual amount of sulphate was determined by the stoichiometry of Reaction 6.2. The details of solution preparation and experimental procedure are presented in Appendix III.

6.1.1 Reagents

All solutions were prepared with deionised water and grade A chemicals. The reagents used in this investigation were:

Sodium sulphite (Na_2SO_3) (99.9% purity)
Cobalt sulphate ($CoSO_4$)
Iodine resublimed crystals (I_2)
Potassium iodide (KI)
Sodium thiosulphate crystals ($Na_2S_2O_3.5H_2O$)
Hydrochloric acid (HCl)
Starch indicator

Medical grade pressurised oxygen gas with minimum 99.5% purity.

6.1.2 Equipment for pressure leaching

Equipment used in the in the mass transfer tests is the leaching test equipment described in Section 6.2.2.

6.1.3 Procedure

A 1.2 mol/L sodium sulphite solution was prepared with de-mineralised water in a 1 L volumetric flask. The solution was then transferred to the reactor vessel. The required catalyst concentration was then added to the solution. The contents of the vessel were heated to the required (target) temperature of 60°C with the agitator turning slowly. Once the experimental temperature was reached, agitation was increased to the required value and the required oxygen overpressure was supplied. The reaction was allowed to proceed for 3 minutes after which an initial 'time zero' sample was taken and the clock was started. Samples were then taken at regular intervals of 5 minutes for the first 20 minutes and at 10 minute thereafter. A dead sample was taken before each actual sample, to ensure the solution was representative of the reactor contents at that point in time. The samples were then immediately cooled in a water bath to limit further sulphite oxidation. An accurate 4 mL aliquot was pipetted from the cooled sample and immediately added to the standard iodine solution, i.e., to utilise the iodometric back-titration method for residual sulphite concentration determination.

6.2 Leaching tests

The PGM-rich leach residue was subjected to autoclave leaching in caustic medium using oxygen. The feed material was supplied by Lonmin Plc. This is the residue from the 3rd stage sulphuric acid leaching in the Lonmin BMR circuit. The wet material was kept in a container to avoid vaporisation and the loss of moisture to obtain the same weight for each leach test.

6.2.1 Reagents

All solutions were prepared with deionised water and grade A chemicals. The reagents used in this investigation were:

Sodium hydroxide (NaOH) 50%-weight percent

Medical grade pressurised oxygen gas with minimum 99.5% purity

6.2.2 Equipment for mass transfer/pressure leaching

All pressure oxidation tests were conducted in a 2.0 L Büchi pressure reactor. Figure 6.1 presents a schematic diagram for the reactor while Figure 6.2 represents a picture of the experimental setup. The reactor is equipped with a stirrer drive with integrated high torque magnetic coupling to provide agitation. The agitation speeds were manually set and maintained throughout the course of the experimentation. The reactor has an anchor type blade stirrer which was used for slurry agitation in all the tests conducted in this investigation. The pressure inside the reactor was monitored using a fitted pressure gauge. In order to obtain the desired pressure in the reactor vessel, the pressure of oxygen gas added to the reactor vessel and regulated by the pressure regulating valve fitted to the oxygen cylinder.

Heating of the reactor vessel was achieved by electric heating elements placed around the reactor shell. The target operating temperature for each test was maintained by the temperature controller. Besides the heating supplied by the elements, the controller also regulated the cooling water flow through the autoclave. This control system allowed the temperature to be maintained within 0.001% of the target value.

The caustic solution was added at temperature using a reagent cylinder bomb fitted to the reactor vessel. One end of this cylinder bomb was attached to the autoclave while the other end was attached to an oxygen feed line. A slight pressure difference was used to inject the reagents into the autoclave, after which the pressure was set at the desired operating pressure. A dip tube was used to collect slurry samples from the reactor. Each sample was immediately cooled and filtered to prevent any further reactions from taking place.

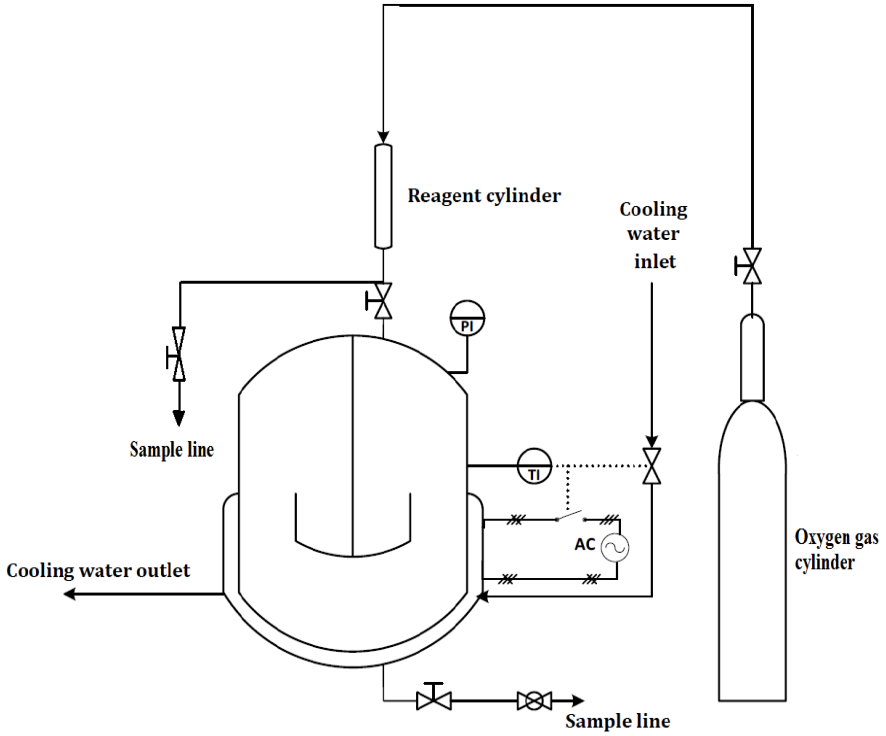

Figure 6.1 Schematic diagram of the experimental setup

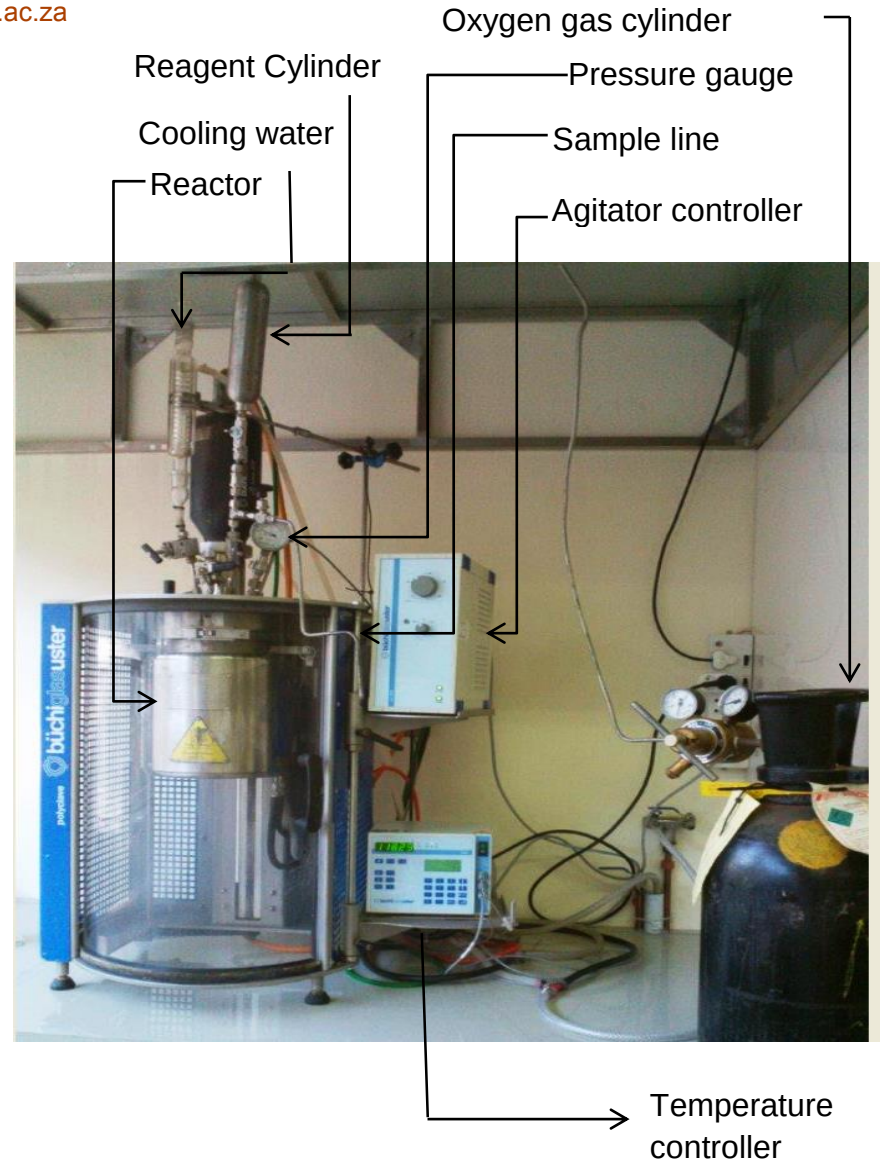

Figure 6.2 Picture of experimental setup

6.2.3 Experimental Leaching procedure

The experimental leaching testwork was divided into two phases. The first phase focused on low pulp density tests that aimed at obtaining kinetic intrinsic leaching rate constant data. A low pulp density of 1% (10 g of leach residue and 1000 mL of leaching solution) was chosen to maintain the concentration of caustic as constant as possible. The second phase focused on high pulp density tests used to validate the overall leaching reactor model. All experiments were carried out using a similar experimental procedure, but with different initial conditions and operating parameters.

After filling the autoclave with the required amount of water, the predetermined mass of solid material was added to the reactor. The required amount of caustic was then prepared and added to the reagent cylinder. The temperature controller was switched on and set to the target temperature. The reactor was then heated to the setpoint temperature while stirring slowly. Once the set temperature was reached, the reagent cylinder was pressurised, allowing the caustic solution to flow into the reactor. The pressure was adjusted to the required oxygen overpressure and the agitation was then set at the required speed.

The autoclave dip tube was used to take approximately 30 mL samples from the reactor. 15 mL was taken as a dead sample before each sample to flush the sampling line. Samples were taken every 10, 20, 30, 45, 60, 120, 180, and 360 minutes from the time of the reagent addition. The pH, E_h, and density were measured and recorded immediately after taking each particular sample. The samples were immediately filtered using a 0.2 µm syringe filter.

6.2.4 Experimental Tests

In order to generate the rate constants from the batch leach tests, a 2^3 factorial design was employed to evaluate the effects of the variables on the leaching process and to identify possible interaction effects between the control variables. A total of 18 experiments were conducted. The variables investigated and their respective levels are summarised in Table 6.1.

.

Table 6.1 : Process variables investigated

Fixed parameters	**Value**
Residence time, min	360
Agitation, rev/min	750
O_2 partial pressure, atm	11
Variables	**Value**
Caustic concentration, mol/L	0.125, 0.25, 0.5
Temperature, °C	160, 175, 190

12 other tests were conducted at 0.25 mol/L caustic, 160°C and 7 to 16 atm oxygen partial pressure to determine the effect of oxygen pressure on the reaction extents.

6.3 Analytical Methods

The following analytical techniques were used in this study:

- Scanning electron microscope (SEM) analysis was used to study the morphology of the feed and leached mineral particles. This was performed using a MA 15 EVO SEM ZEISS instrument with accelerating voltage of 20KV. This instrument uses INCA software to identify the compositions of the samples. These analyses were conducted by the Central Analytical Facility of Stellenbosch University.
- Inductive coupled plasma atomic emission spectroscopy (ICP-AES) analysis was used to obtain the concentrations of selenium, arsenic, sulphur, platinum, palladium, rhodium, ruthenium, iridium, gold, copper, iron, and nickel and lithium in the solution samples.
- X-ray powder diffraction (XRD) analyses of the solid samples were conducted to identify the mineral phases of the residue compounds. XRD analyses of the samples were conducted by the Central Analytical Facility of Stellenbosch University.

- Particle size distribution analyses were conducted using the Saturn DigiSizer 5200 particle size analyser.

Details of analytical methods are presented in Appendix II.

7 EXPERIMENTAL RESULTS AND DISCUSSION

7.1 Mass transfer test results

The $k_L a$ value provides an overall measure of the gas absorbing capacity of a reactor. The figures in the next section present the measured oxygen absorption test results. These oxygen absorption rate values were subsequently used in the modelling part of the study (see Chapter 8)

7.1.1 Identification of the absorption regime

In these tests, the temperature was limited to 60°C.The temperature was selected to allow for quick sample taking without significant flushing. The cobalt(II) catalyst concentration and the impeller speed were varied in the first series of tests, while keeping the other conditions constant. These results are summarised in Table 7.1 and are illustrated in Figure 7.1 to Figure 7.5.

Table 7.1: Mass transfer tests at different impeller speed and Cobalt(II) concentrations

Test No	Feed Gas (% O_2)	P_g (kPa)	Agitation, rev/min	Co(II), mg/L	Temp, °C	Slope, mg/kg.min	$[O_2]^*$ mg/kg	k_La 1/min
MT1	100	100	500	1	60	231.6	22.4	10.3
$MT2_A$	100	100	500	5	60	276.9	22.4	12.36
$MT2_B$	100	100	500	5	60	271.1	22.4	12.1
$MT3_A$	100	100	750	1	60	364.7	22.4	16.28
$MT3_B$	100	100	750	5	60	356.1	22.4	15.89

Figure 7.2 and Figure 7.3 illustrate the test results obtained at the same operating conditions. As can be seen from the $k_L a$ value obtained, there is good reproducibility of tests results. However, comparing the results obtained at low catalyst concentration, presented in Figure 7.1, it can clearly be seen that at low agitation, there is a mass transfer enhancement by the chemical reaction (see Section 7.1.2)

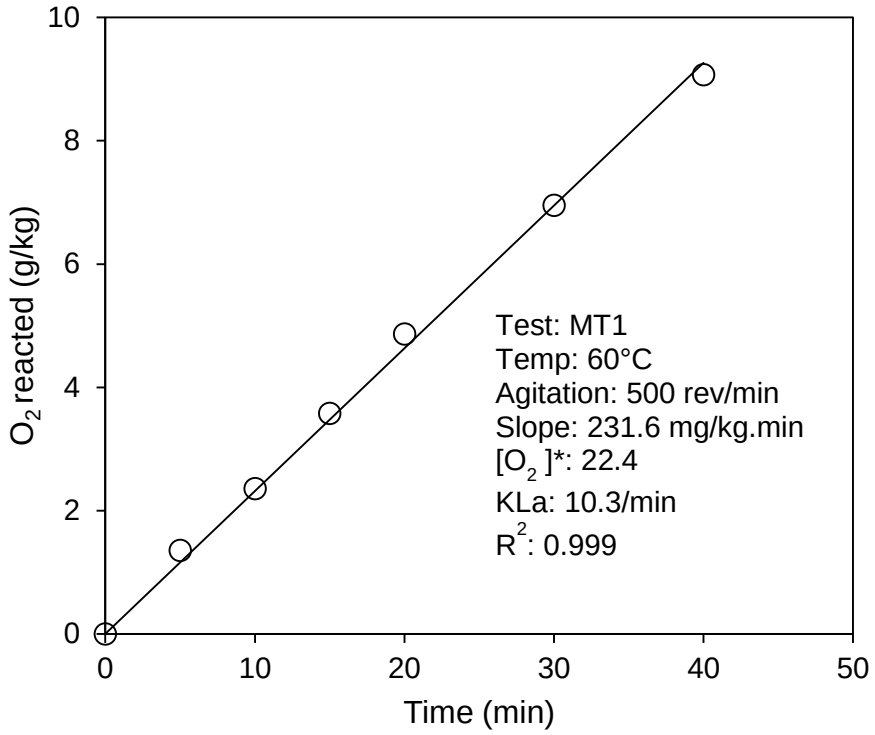

Figure 7.1: Mass transfer test with 1 mg/L cobalt(II) at 500 rev/min

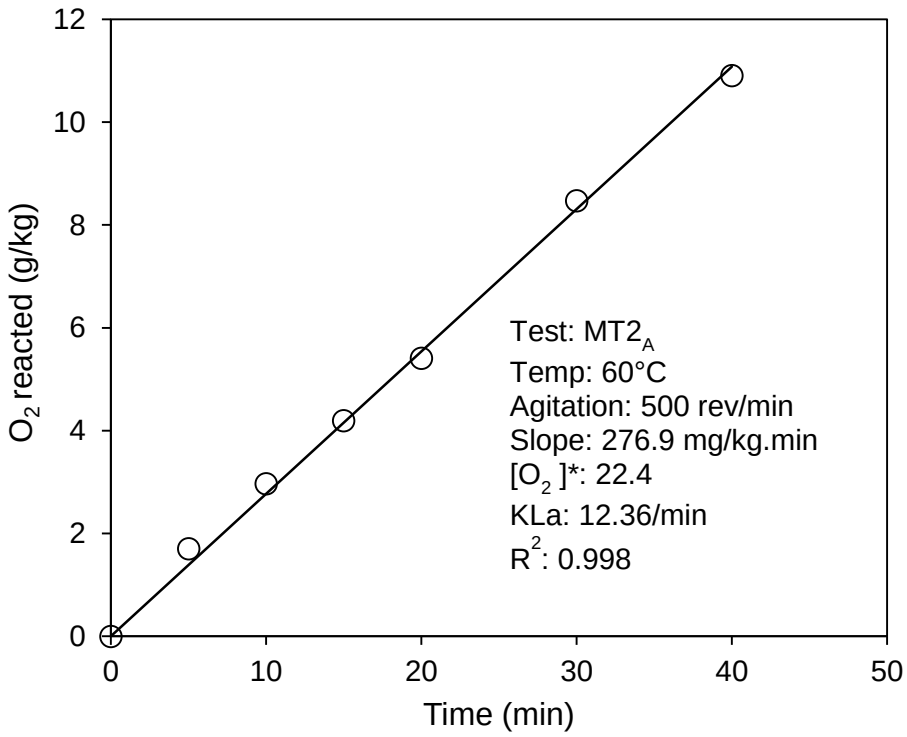

Figure 7.2: Mass transfer test with 5 mg/L cobalt(II) at 500 rev/min

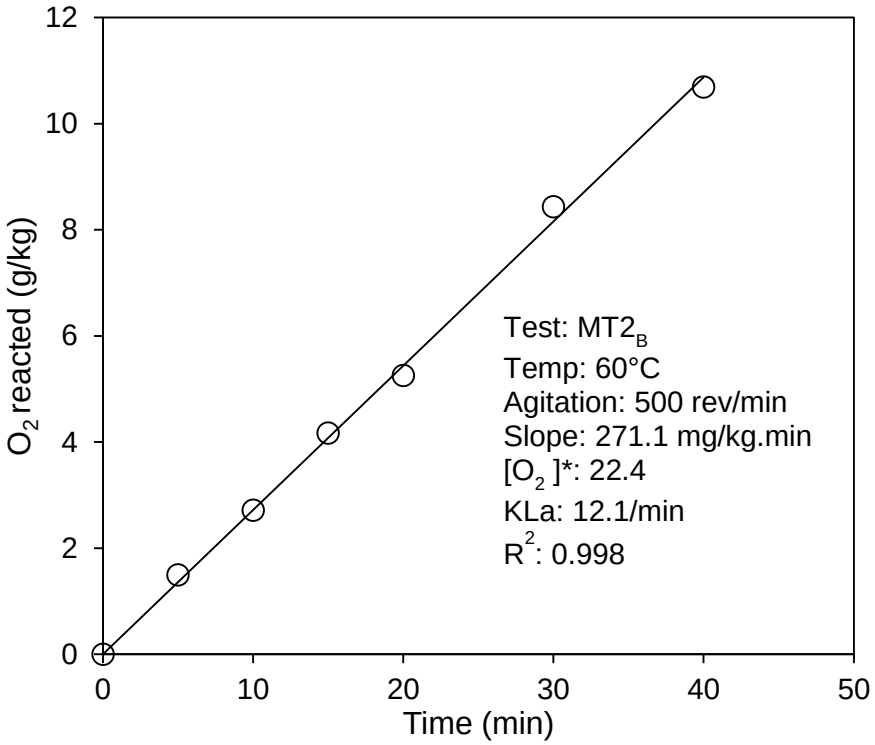

Figure 7.3: Mass transfer test with 5 mg/L cobalt(II) at 500 rev/min (repeat)

Figure 7.4 and Figure 7.5 illustrate the absorption test results obtained at 750 rev/min and different cobalt(II) concentrations. At increased agitation (750 rev/min) the k_La values obtained at 1 mg/L and 5 mg/L catalyst concentrations are very close with only 2.5% deviation. Figure 7.6 illustrates that there is an exponential increase in the k_La values with increasing impeller speed. This can be explained by the combined increase of both k_L and *a* with the change of the hydrodynamics of the system. The increased impeller speed results in increased shear between the impeller and the fluid, which in turn, results in more turbulent conditions and therefore increased interfacial mass transfer rates. An increase in agitation also increases the gas liquid film renewal rate (Machon and Linek, 1974), as well as the surface renewal frequency (Lewis and Whitman, 1924).

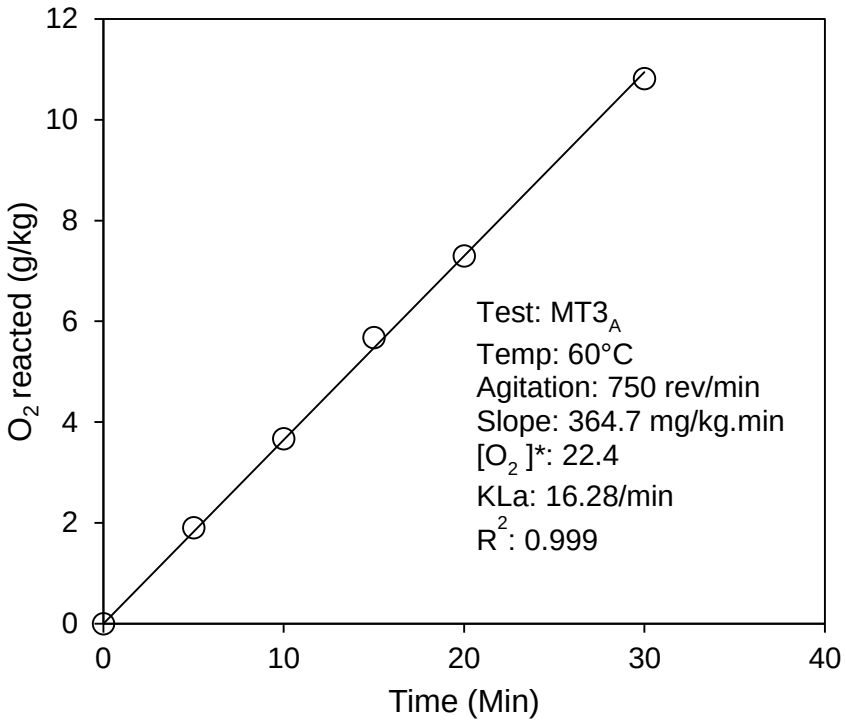

Figure 7.4: Mass transfer test with 1 mg/L cobalt(II) at 750 rev/min

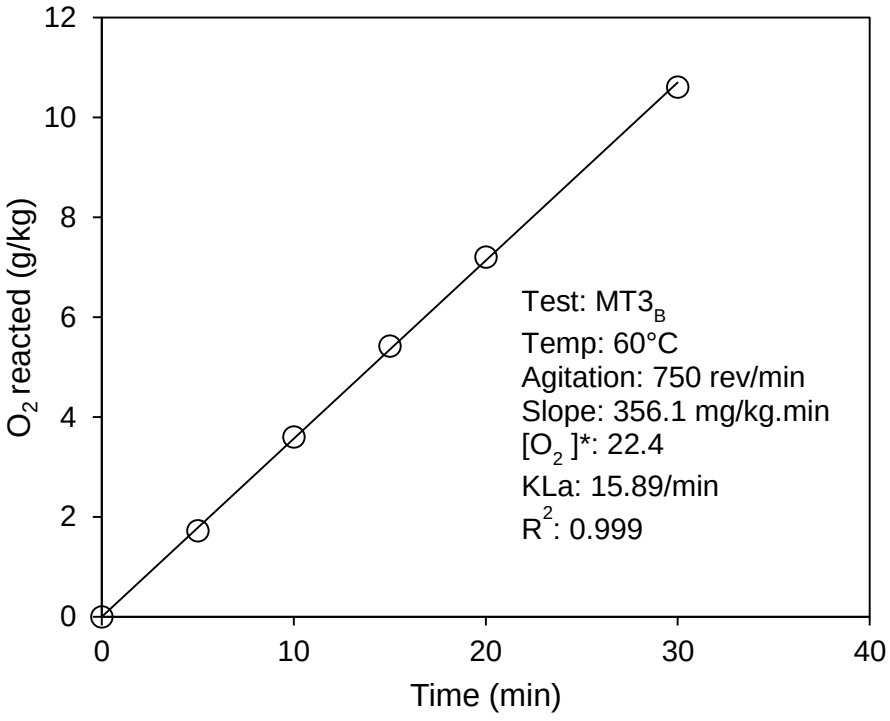

Figure 7.5: Mass transfer tests with 5 mg/L cobalt(II) at 750 rev/min

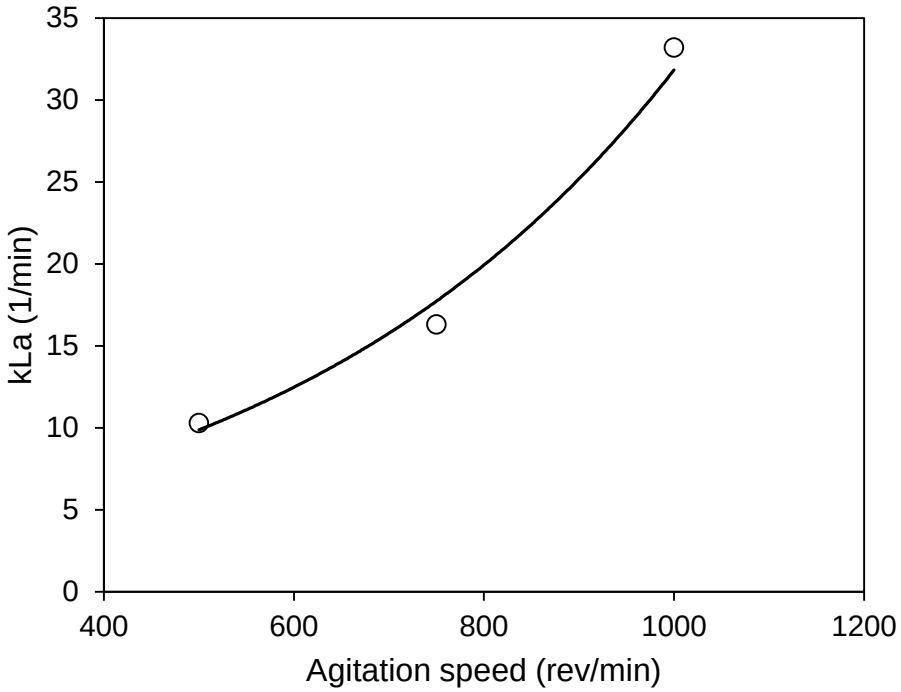

Figure 7.6: Relationship between kLa value and agitation speed

7.1.2 Effect of cobalt(II) on the absorption rate

To re-emphasise, this mass transfer measurement method depends on the oxidation of sulphite to sulphate by oxygen in the presence of a catalyst. The rate of oxidation is a strong function of the catalyst concentration (Olle et al., 2006, Steyl, 2012) This entails operating at the right catalyst concentration, such that the rate of reaction is fast enough to maintain the dissolved oxygen levels in the bulk solution at zero, $C_{O2,bulk}$ =0.

To ensure that the right concentration of catalyst was used in the oxidation reactions, experiments were conducted for a range of different cobalt(II) concentrations, i.e., to determine the regime where the absorption rates are not chemically enhanced. The results are illustrated in Figure 7.7 below. These results confirm that the absorption rate was not significantly enhanced by the chemical reaction in the 1 to 5 mg/L cobalt(II) concentration range. This is in agreement with the results obtained by Olle et al. (2006) presented in Figure 7.8. However, as explained in Section 7.1.1 above, at low agitation speed, there is mass transfer enhancement by the chemical reaction when the catalyst concentration is increased, as can be seen in Figure 7.7. In this case the kLa values obtained at 1 mg/L and 5 mg/L are notably different (17%).

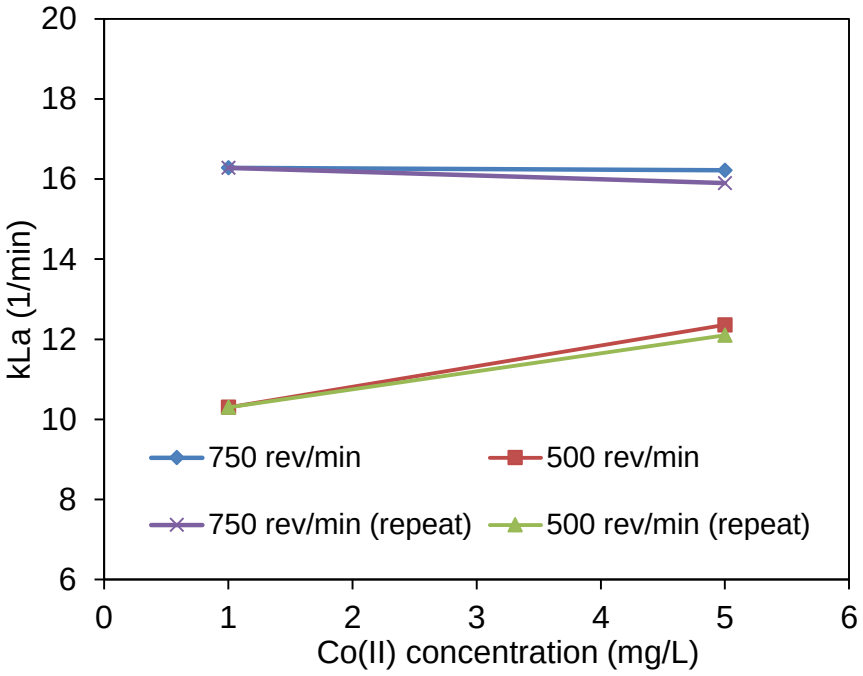

Figure 7.7: Absorption rate as a function of cobalt ion concentration

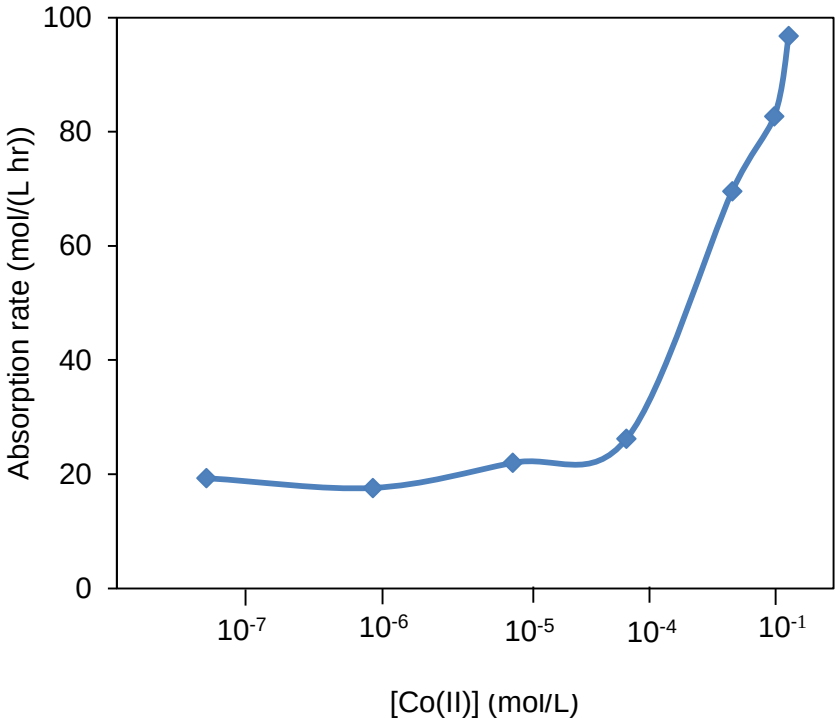

.

Figure 7.8: Absorption rate as a function of cobalt ion concentration (redrawn from from Olle et al., 2006)

7.2 Leaching test results and discussion

Table 7.2 below summarises the elemental composition of the feed material used in the autoclave caustic leaching tests. It can clearly be seen from the analysis that the material is rich in PGMs. It also contains base metals, albeit at low concentrations. The amphoteric elements make up 11.9% of the material. The feed material also contains some lead (Pb).

Table 7.2: Elemental analysis of feed material

Element	S	As	Se	Cr	Ni	Cu	Ru
Weight %	5.5	1.9	4.4	0.9	1.5	0.9	7.6

Element	Rh	Pd	Ag	Ir	Pt	Au	Pb
Weight %	3.0	13.2	1.0	0.9	28.5	0.4	2.5

No information was found in the open literature on the behaviour of the amphoteric elements during aqueous oxidation of PGM-rich concentrate in caustic solution at high temperatures (>150°C). The results presented in this chapter contribute towards a better understanding of the oxidation of PGM-rich concentrate in sodium hydroxide solution.

7.2.1 Effect of caustic concentration

The effect of caustic concentration on the reaction rate was studied in a series of experiments at 10 g/L solids concentration, 0.125, 0.250 and 0.500 mol/L caustic concentrations with temperatures ranging from 160°C to 190°C and at an oxygen partial pressure of 11 atm. The results obtained from these experiments are presented as elemental conversion versus time plots.

These figures illustrate the similar extraction trends for the different elements. The observed reaction rates clearly increase with an increase in caustic concentration from 0.125 to 0.5 mol/L. A further increase in caustic concentration to 0.5 mol/L does not

significantly increase the reaction rate. This effect may be due the decrease in oxygen solubility with increased caustic concentration (Bhakta et al., 1989, Ciminelli and Osseo-Asare, 1995). This observation is supported by Figure 7.12 generated using Tromans correlation (Tromans, 1998b) showing a decrease in oxygen solubility with an increase in caustic concentration.

The effect of the caustic concentration on the leaching rate of the amphoteric elements has been studied by several researchers (Vircikova and Fedor, 1991; Kilic et al., 2013; Yu et al., 2014; Ruiz et al., 2014) . The results obtained in this work agree with what has been reported by these researchers. The results in Figure 7.9 to Figure 7.11 illustrate that caustic concentration appears to have a stronger effect on the sulphur and arsenic leaching extents. Extraction of sulphur increases from 82 to 89% when caustic concentration increases from 0.125 to 0.5 mol/L while arsenic extraction increases from 72 to 79%. There is less significant change in reaction rates of selenium with increased sodium hydroxide concentration.

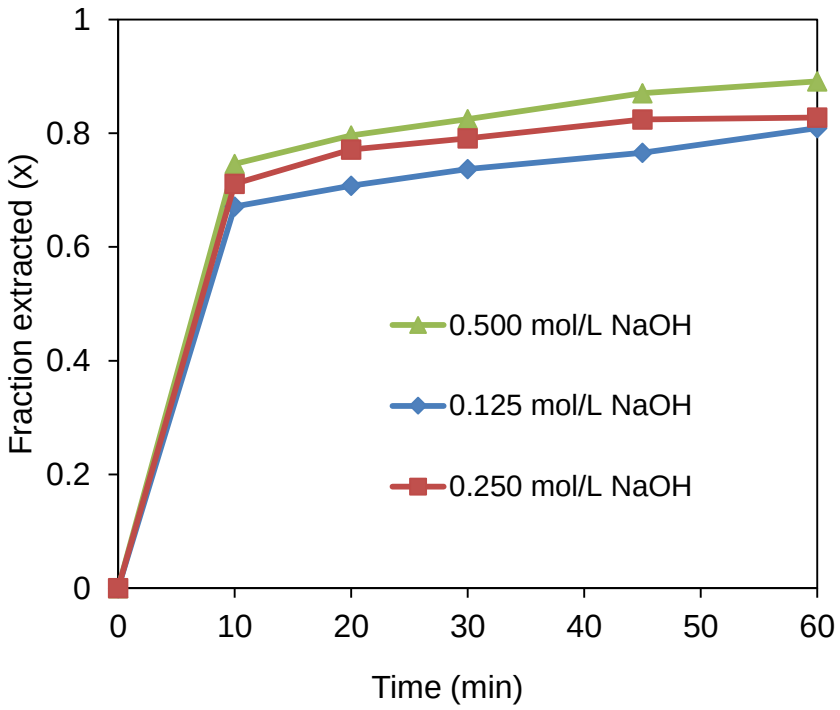

Figure 7.9: Effect of NaOH concentration on sulphur extraction (Temperature 175°C; 10 g/L solids; 750 rev/min; 11 atm O_2 partial pressure)

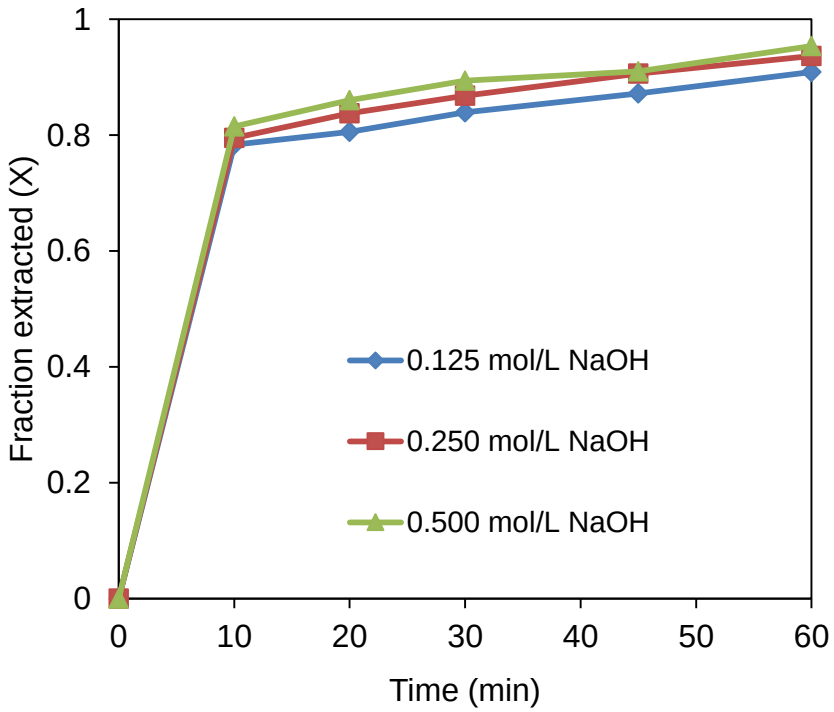

Figure 7.10: Effect of NaOH concentration on selenium extraction (Temperature 175°C; 10 g/L solids; 750 rev/min; 11 atm O_2 partial pressure)

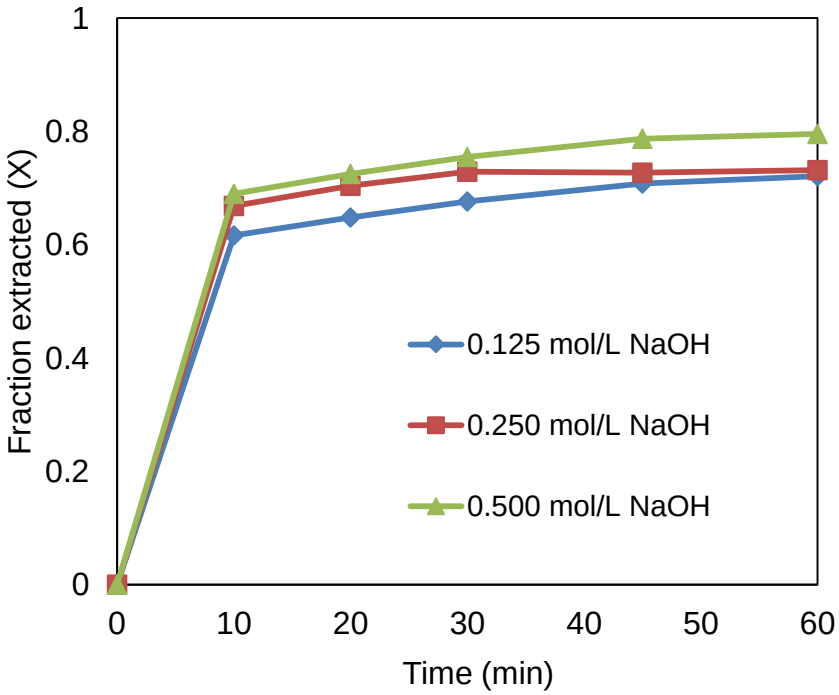

Figure 7.11: Effect of NaOH concentration on arsenic extraction (Temperature 175°C; 10 g/L solids; 750 rev/min; 11 atm O_2 partial pressure)

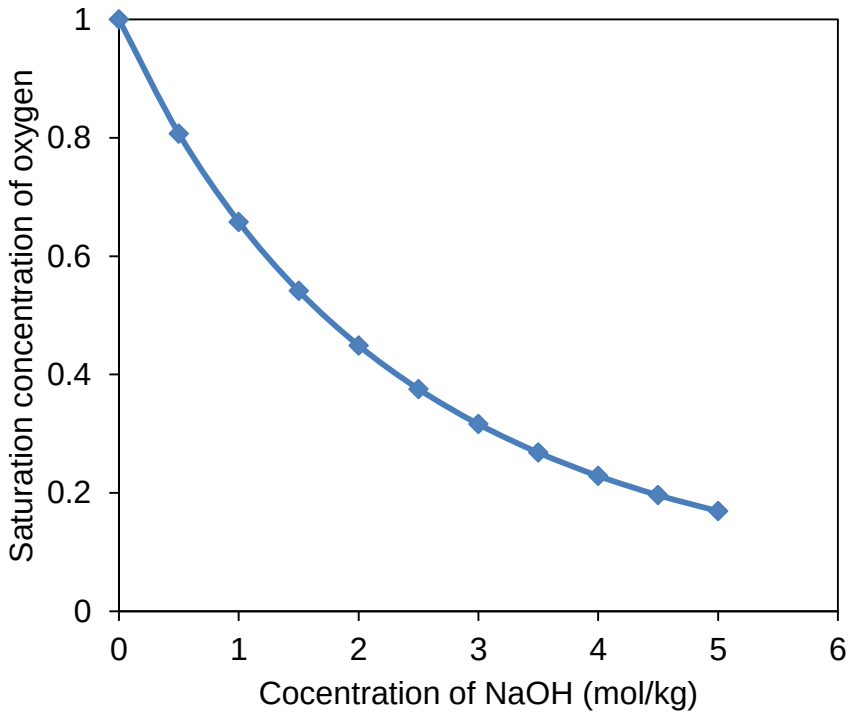

Figure 7.12: Effect of caustic concentration on oxygen solubility (Tromans, 1998b)

7.2.2 Effect of temperature

The effect of temperature on the reaction rate was studied in a series of experiments at 160°C, 175°C and 190°C at an oxygen partial pressure of 11 atm, under varying caustic concentration. The results obtained from these experiments are presented in Figure 7.13 to Figure 7.15.

It is evident from the dissolution profile of sulphur in Figure 7.13 that its leaching rate is strongly dependent on temperature. 95% oxidation of sulphur was achieved within 60 min at 190°C. However, at lower temperature, sulphur conversion reached only about 83% after 60 minutes. The influence of temperature on the oxidative dissolution of selenium is illustrated in Figure 7.14. The temperature had a strong effect on selenium extraction from 160°C to 175°C. However, a further increase in temperature did not yield any substantial increase in the leaching extent of selenium.

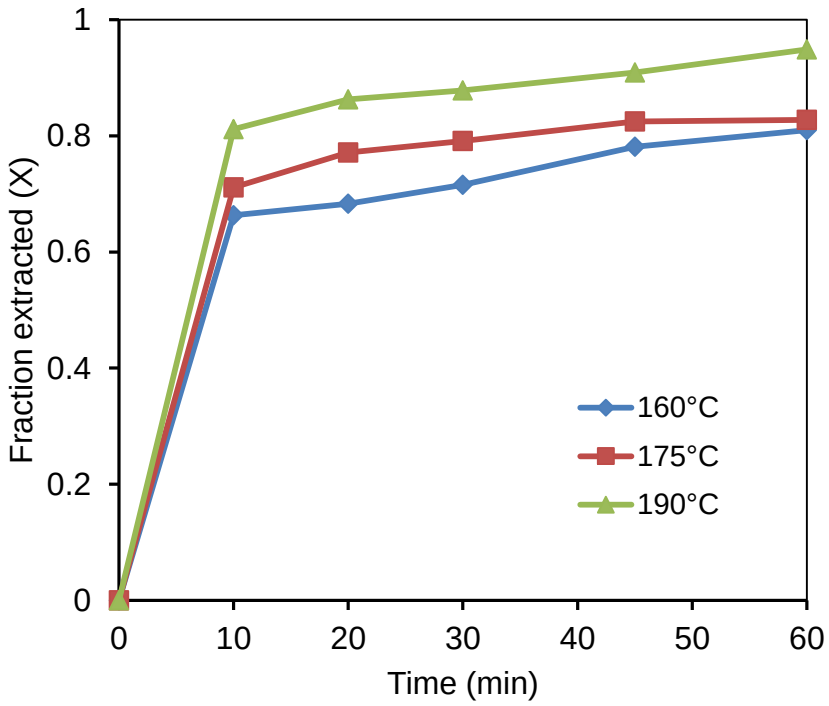

Figure 7.13: Effect of temperature on sulphur extraction with 0.25 mol/L NaOH (10 g/L solids; 750 rev/min; 11 atm O_2 partial pressure)

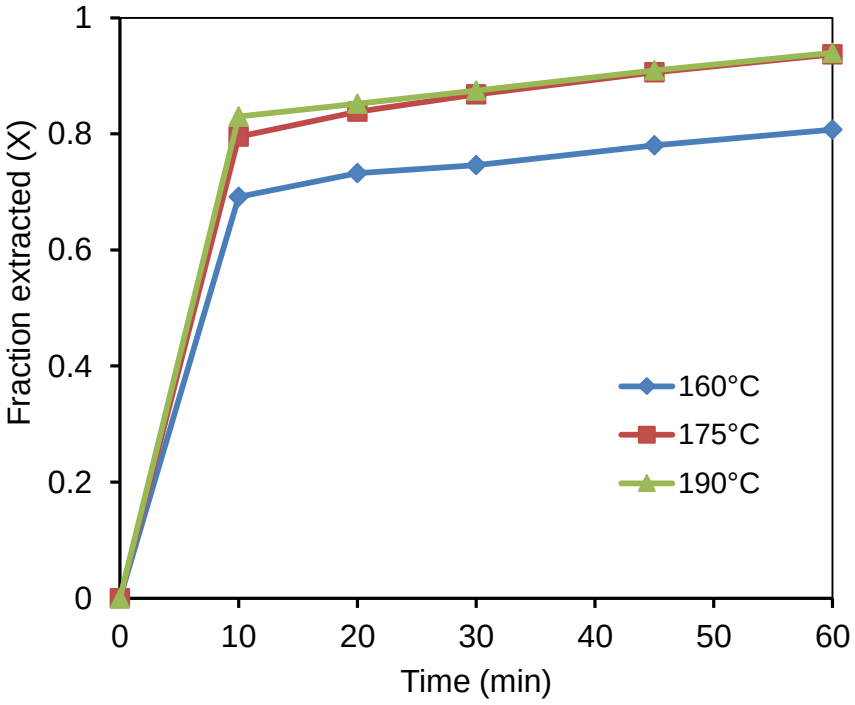

Figure 7.14: Effect of temperature on selenium extraction with 0.25 mol/L NaOH (10 g/L solids; 750 rev/min; 11 bars O_2 partial pressure)

It is well known from the literature that chemically controlled processes are more sensitive to temperature changes (Levenspiel, 1972). Even though the temperature effect was notable between 160 and 175°C in this study, this does not automatically imply that the reaction was chemically controlled.

Figure 7.15 illustrates the effect of temperature on arsenic extraction. There is clearly a weak dependency of the arsenic extraction on the temperature. The weak temperature dependence is a strong indication that the leaching mechanism is not controlled by the intrinsic dissolution reaction on the particle surface. In an attempt to gain more knowledge on the reaction mechanism, Arrhenius plots were constructed and activation energies of the different species were calculated and is presented in the next Chapter.

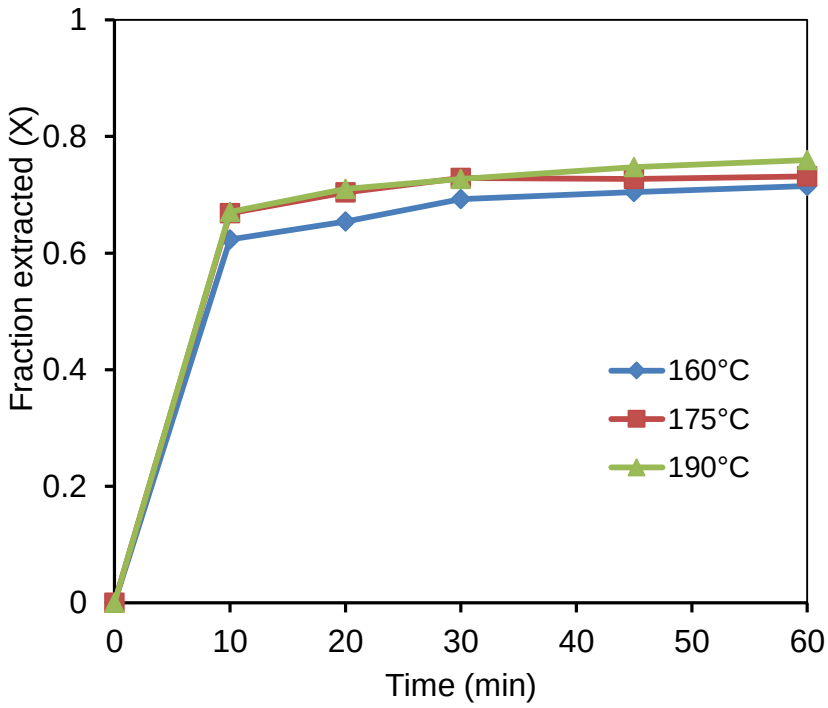

Figure 7.15: Effect of temperature on arsenic extraction with 0.25 mol/L NaOH (10 g/L solids; 750 rev/min; 11 atm O_2 partial pressure)

7.2.3 Statistical analysis

Statistical analyses of the results were conducted (detailed results presented in Section Appendix VII) The surface plots presented in Figure 7.16 to Figure 7.18 are

used to explain the combined effect of the process parameters (temperature and caustic concentration) on the degree of species extraction. Figure 7.16 illustrates that maximum extraction of sulphur was achieved at the highest tested temperature and caustic concentration. Figure 7.17 illustrates that the temperature had the most beneficial effect on the selenium extraction. Regardless of the caustic concentration, the lowest tested temperature of 160°C yielded the lowest selenium extraction. The surface plot for arsenic is presented in Figure 7.18. It can be seen that both the caustic concentration and temperature had a positive effect on the arsenic extraction.

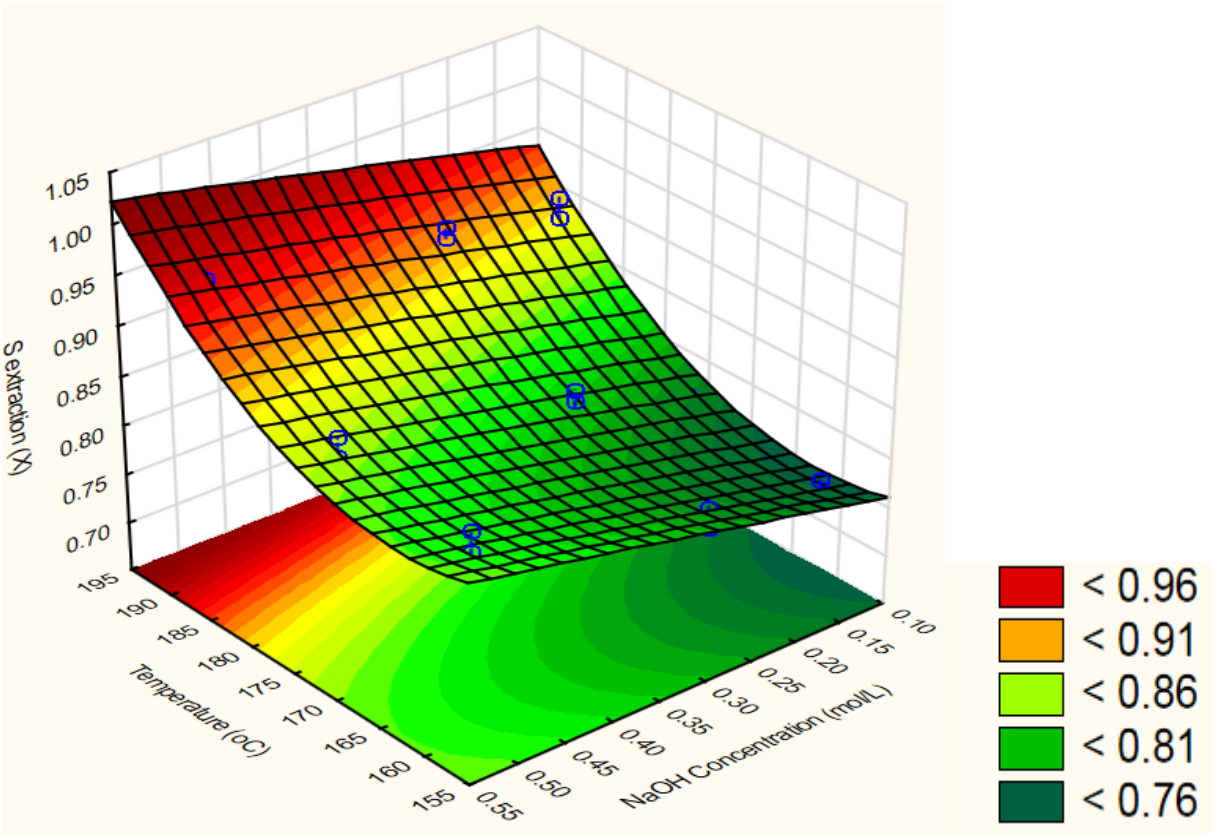

Figure 7.16: Response surface plot for sulphur dissolution at 60 minutes

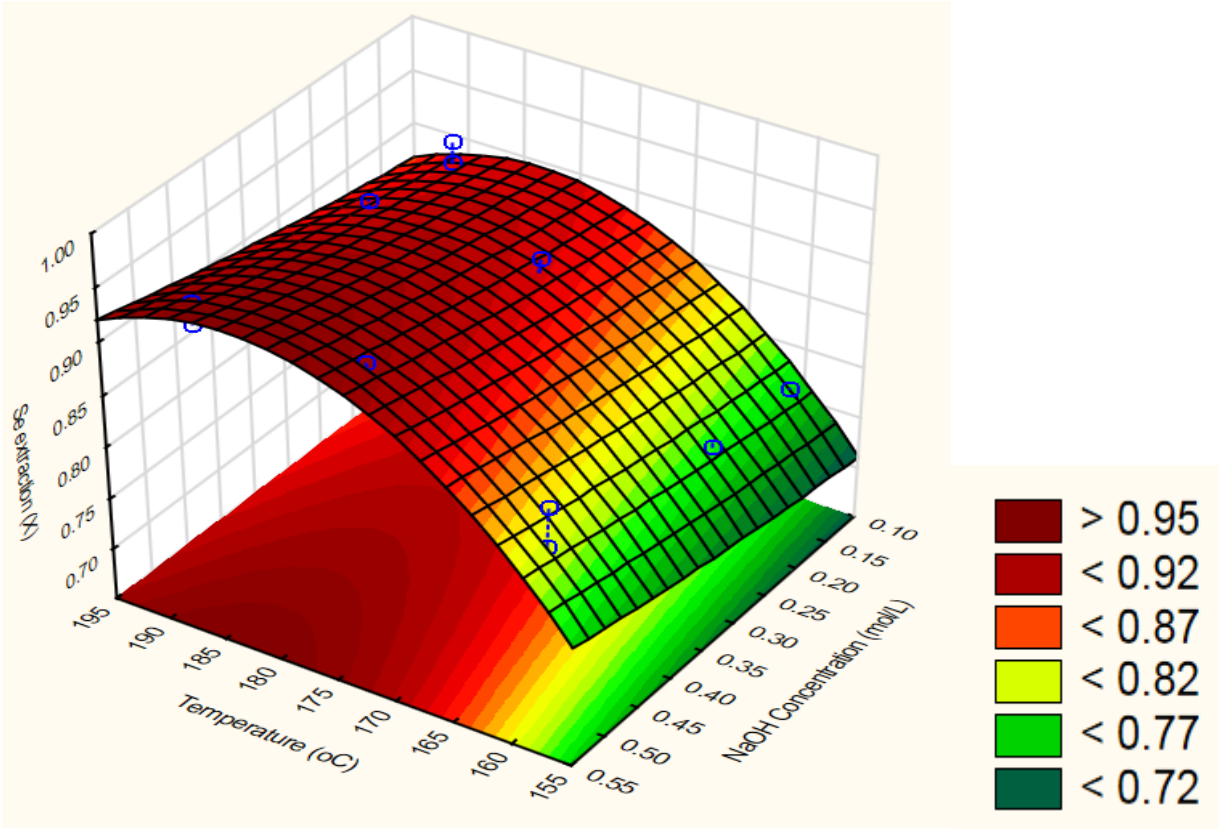

Figure 7.17: Response surface plot for selenium dissolution at 60 minutes

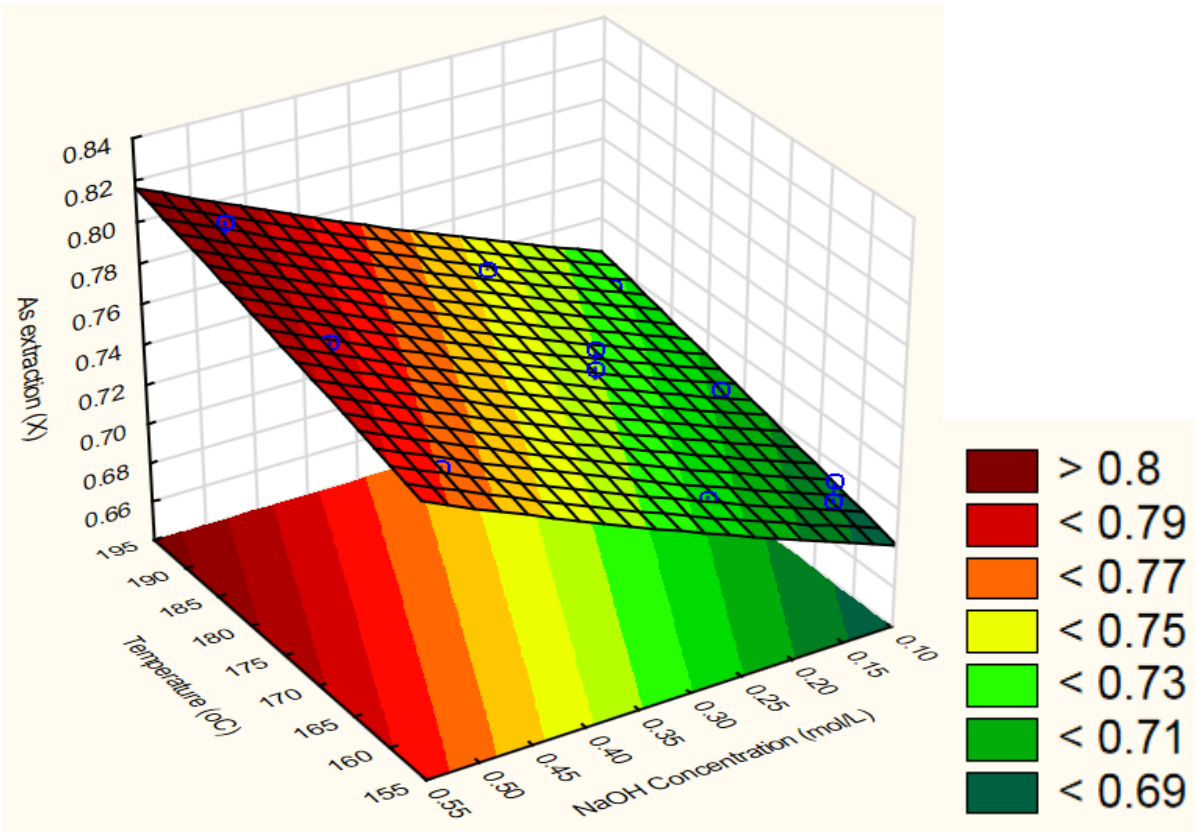

Figure 7.18: Response surface plot for arsenic dissolution at 60 minutes

7.2.4 Effect of oxygen partial pressure

The influence of oxygen on the chemical reaction is dependent on the dissolved oxygen concentration during the process. The oxygen only participates in the reaction when in contact with the mineral surface. However, the solubility of oxygen is affected by temperature, pressure and solution composition. Increasing oxygen partial pressure increases its solubility. The relationship between the oxygen partial pressure and temperature is illustrated in Figure 7.19 (based on correlation of Tromans, 1998b). The solubility of oxygen decreases as the temperature increases up to about 100°C (373K), after which it increases appreciably with increased temperature.

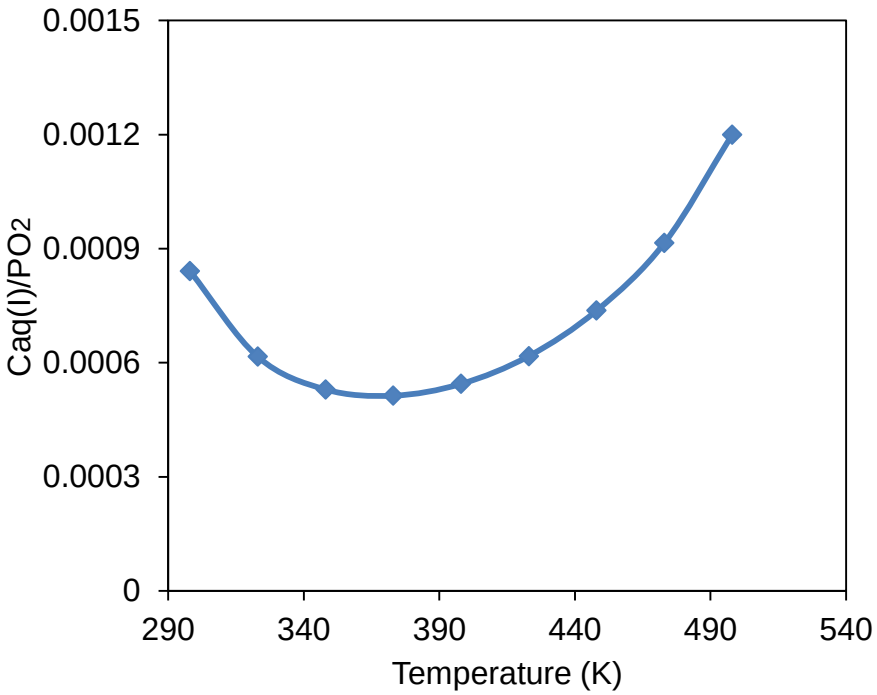

Figure 7.19: Effect of temperature on O_2 solubility at 1 atm O_2 partial pressure and 1 mol/kg NaOH

The effect of oxygen partial pressure on the reaction extents was determined over the range of 7 to 16 atm under the standard conditions (0.25 mol/L NaOH, 160°C and 60 minutes reaction time) The extraction for all the species followed similar trends. High sensitivity of vapour pressure of water above the solution, especially at high

temperatures, means that temperature had to be controlled within+/-0.001%. A slight change in temperature resulted in a significant change in the pressure. In order to avoid this problem, an internal reactor-jacket cooling system was used to carefully control the temperature and maintain the desired pressure. The desired oxygen overpressure was added based on the vapour pressure at the particular leaching temperature.

Figure 7.20 illustrates that the leaching extent of sulphur increased gradually with increasing oxygen partial pressure. When the oxygen partial pressure was increased from 7 to 16 atm, sulphur extraction increased from 75% to 85%. As expected, the intrinsic leaching mechanism is dependent on the dissolved oxygen concentration. Figure 7.21 and Figure 7.22 below illustrate the similar trends for selenium and arsenic, respectively.

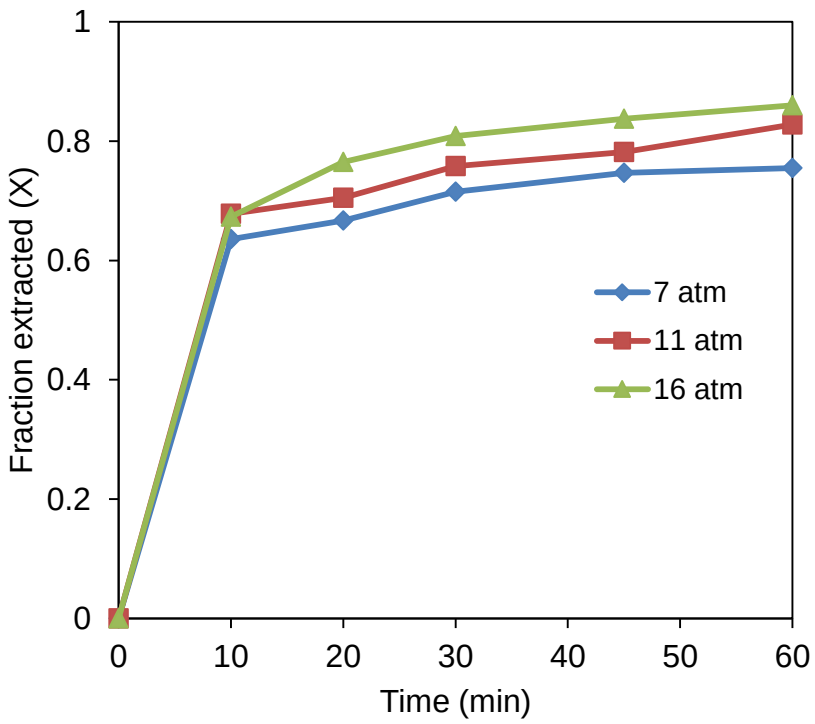

Figure 7.20: Effect of O_2 partial pressure on sulphur extraction (160°C, 0.25 mol/L NaOH 10 g/L solids; 750 rev/min)

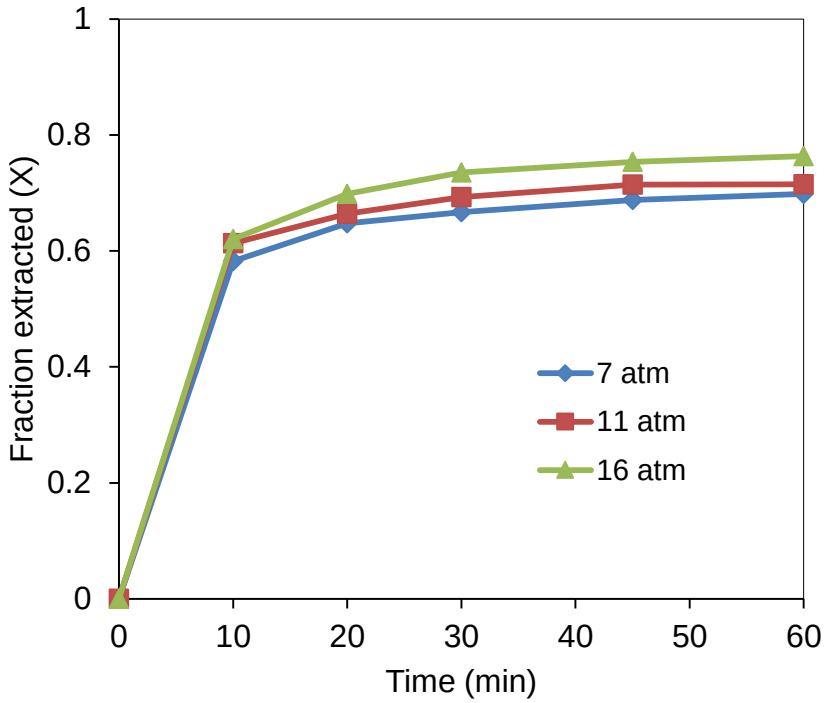

Figure 7.21: Effect of O_2 partial pressure on selenium extraction (160°C, 0.25 mol/L NaOH 10 g/L solids; 750 rev/min)

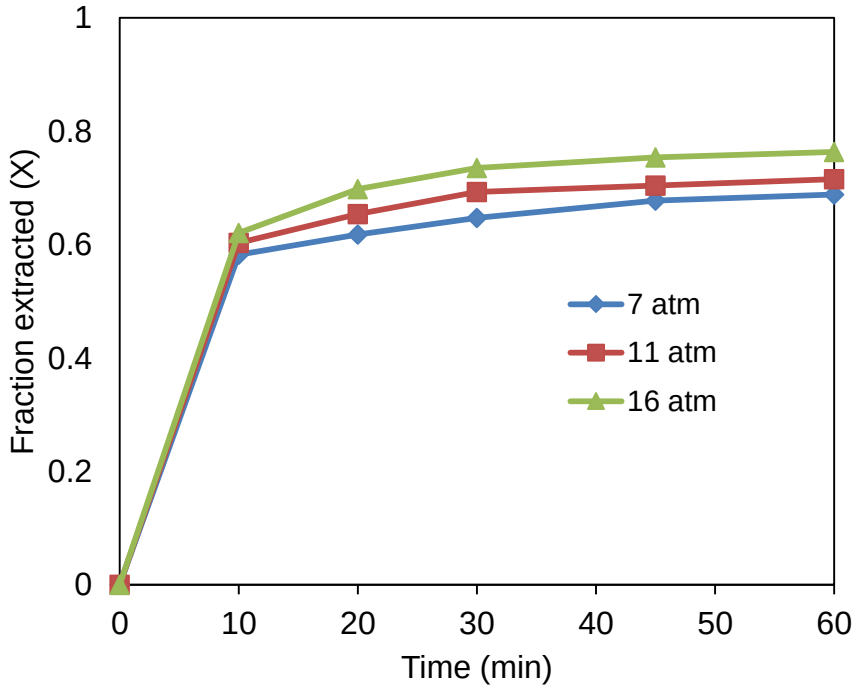

Figure 7.22: Effect of O_2 partial pressure on selenium extraction (160°C, 0.25 mol/L NaOH 10 g/L solids; 750 rev/min)

7.3 Qualitative analyses of feed and leached residues by SEM-EDX

The feed and leach residue particles were analysed for major phase composition using Scanning electron microscopy with energy dispersive X-ray spectroscopy (SEM-EDX). The surface morphology of the feed particles is presented in Figure 7.23. A digital image of leached grains in Figure 7.24 reveals the formation of pores and cracks at the surface. The cracks and pores were present at all the conditions tested. Figure 7.23 and Table 7.3 illustrates that the oxide layers were detected across the residual particle surface.

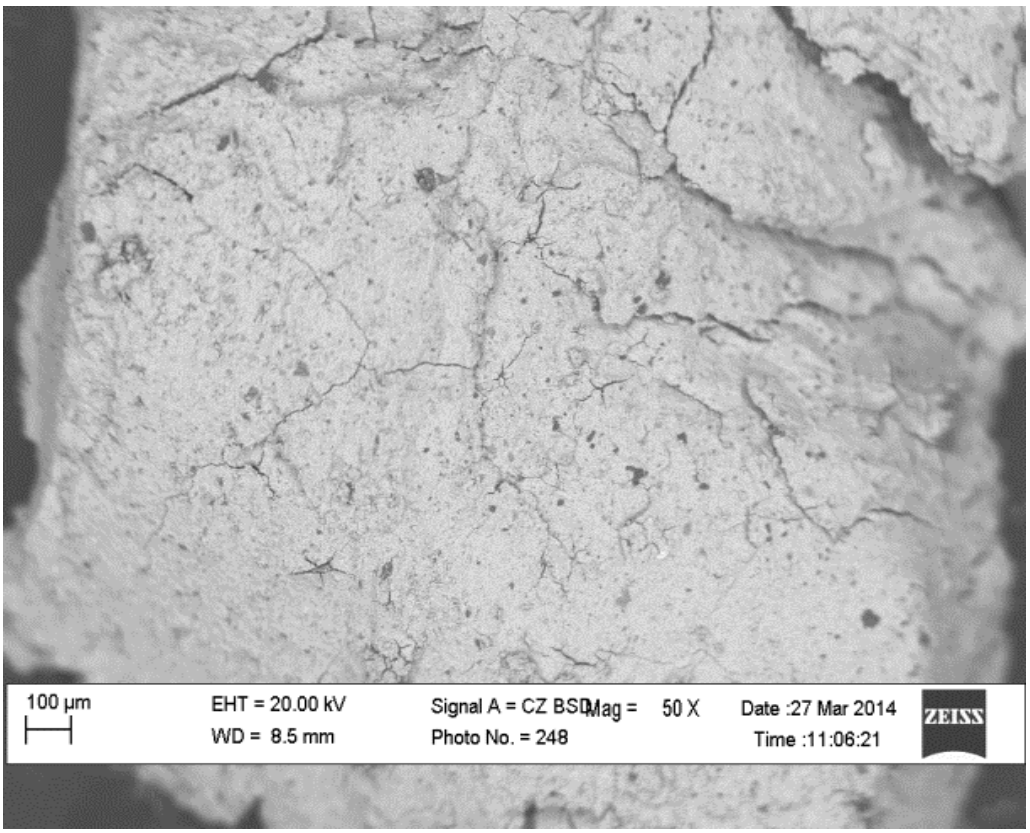

Figure 7.23: Backscattered electron image of the feed grains of PGM rich concentrate sample

As can be seen from Figure 7.25, the results obtained from the XRD analyses showed PGMs to be the dominant constituent with chromite ($FeCr_2O_4$), quartz (SiO_2) and anglesite ($PbSO_4$) being the other phases. Palladium represents the composition of all the PGMs. Although not dominant, the iron oxide is seen across the mineral surface. The XRD probe analyses of points A to D is summarised in Table 7.3.

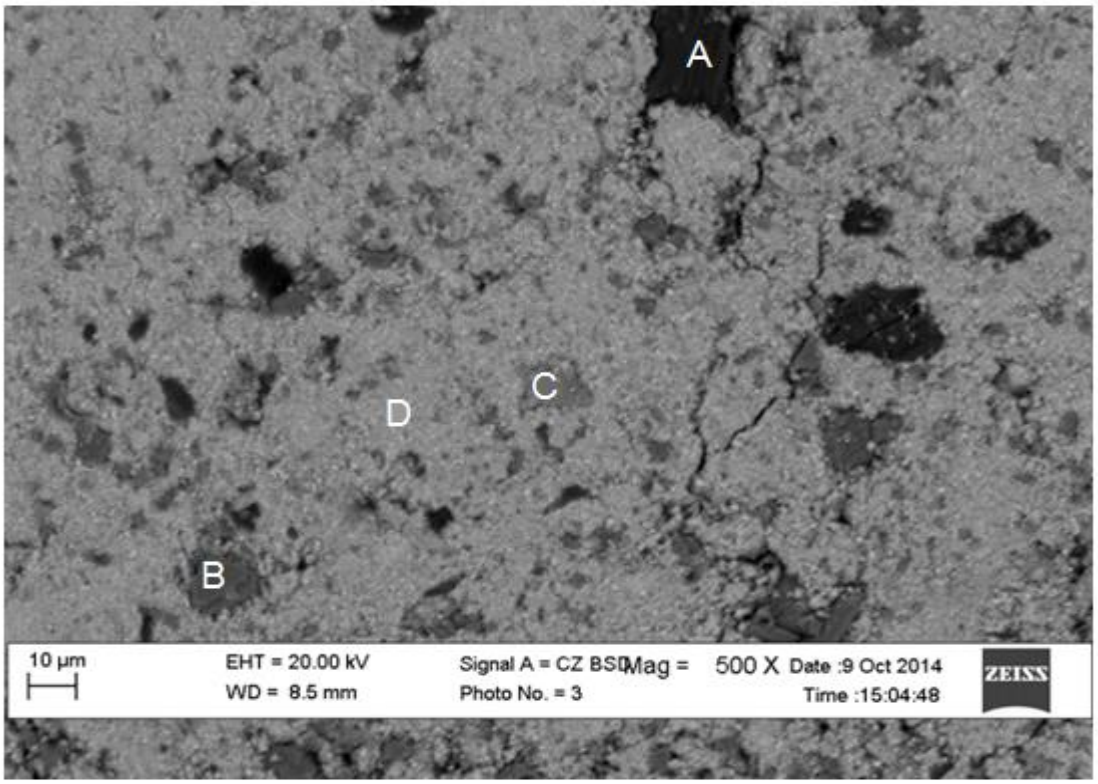

Figure 7.24: Backscattered electron image of the leached residue grains of PGM rich leach residue after 95% extraction at 190°C, 0.5 mol/L NaOH, 11 atm O_2 partial pressure

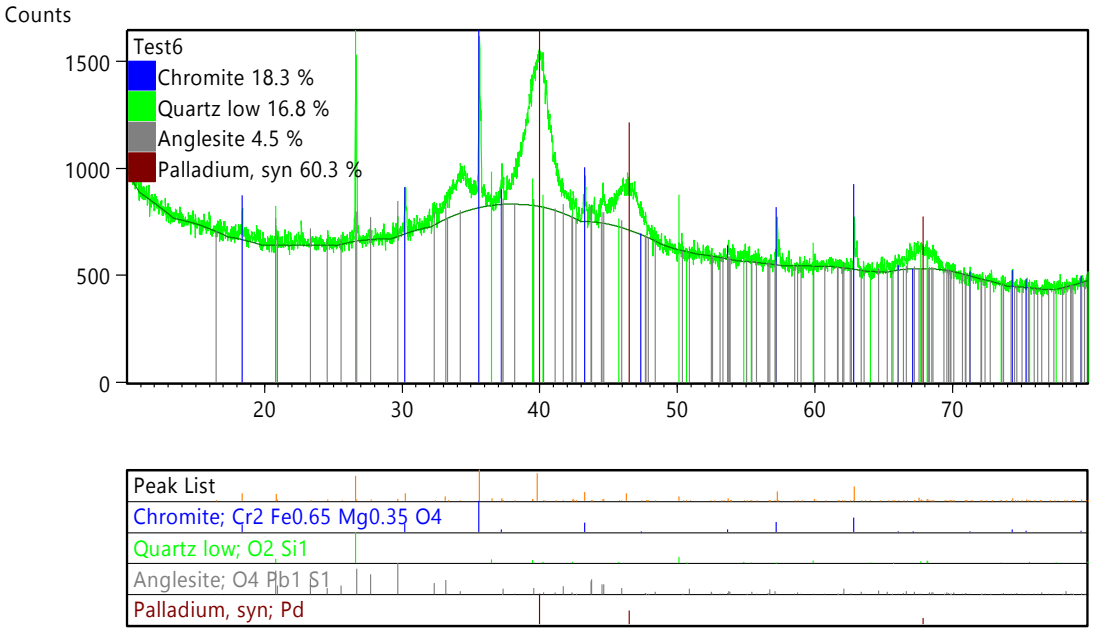

Figure 7.25: XRD analysis of residue at 160°C, 0.25 mol/L NaOH, 750 rev/min and 11 atm O_2 partial pressure

Table 7.3 summarises the different phases of the leach residue. A major alloy phase consisting of PGMs is represented by point D. The Fe, Ni oxide, which is formed during alkaline oxidation, is seen forming an oxide/hydroxide layer on the surface of the residue. Other images of residue as well as XRD analysis results are presented in Appendix VI.

Table 7.3: Summary of qualitative analyses of the leached residues by SEM

Spot ID	Elemental composition	Remarks
A	Si, O	Composition consistent with oxidised quartz
B	Fe, Ni, O	Trevorite- a Fe, Ni mineral
C	Fe, O	Hematite
D	Pt,Pd,Ir,Rh,Ru	Major phase which is an alloy of PGM's with traces of other impurities imbedded in them.

7.4 Platinum group metals

The primary focus of the Lonmin Plc base metal refinery is to produce the PGMs. However, before the precious metal refinery, there are a number of the preceding processes to remove the bulk of other elements as discussed in Chapter 1. These processes lead to losses of the PGMs. It is thus important to operate at conditions where PGM losses are minimised. In this chapter, the behaviour of PGMs during caustic batch leaching is presented.

7.4.1 Effect of NaOH concentration on dissolution of PGMs

The solubility of platinum is dependent on various factors, including the free hydrogen concentration as reflected by the pH (Azaroual et al., 2001). Figure 7.26 illustrates the effect of caustic concentration on the platinum solution tenor. It can be seen that the dissolution extent increases with increasing caustic concentration. At 0.125 mol/L concentration, a final concentration of 50 mg/L platinum was obtained while 229 mg/L was recorded with 0.5 mol/L caustic concentration. As the leaching progressed, a downward trend (possibly precipitation) of platinum is observed. This trend is observed at low (0.125 mol/L) and medium (0.25 mol/L) caustic concentration.

However, at high caustic concentration, no precipitation of platinum would likely have occurred due to excess caustic in solution.

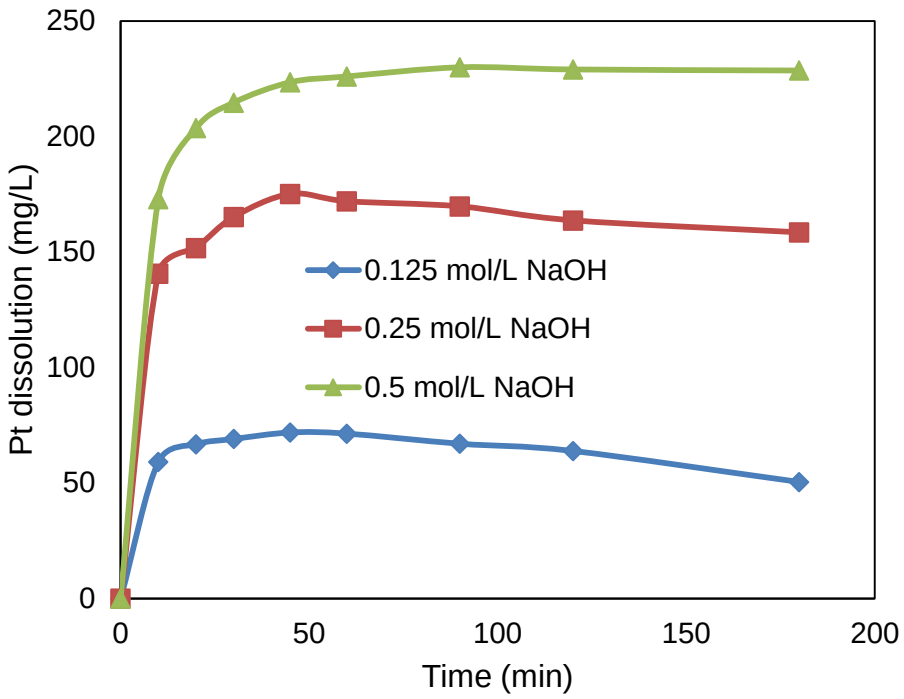

Figure 7.26: Effect of NaOH concentration on Pt dissolution at 160°C (10 g/L solids; 750 rev/min; 11 atm O_2 partial pressure)

Other studies from the open literature have also reported similar results (Azaroual et al., 2001; Wood, 1991). Wood (1991) determined platinum solubility at 25°C in caustic solution of variable ionic strength (10^{-4} to 10) and obtained solubilities ranging between 14 and 36 mg/L. The experimental results therefore clearly illustrate the effect of hydroxide ions on platinum solubility; an increase in caustic concentration results in increased platinum dissolution.

Figure 7.27 illustrates the effect of caustic concentration on the palladium solution tenor. Again, these results indicate an increase in the palladium solution tenor from 2.5 to 19 mg/L when the caustic concentration is increased from 0.125 to 0.5 mol/L. Again, at increased reaction time, palladium appears to have precipitated. Precipitation at low (0.125 mol/L) and medium (0.25 mol/L) caustic concentration

resulted in 99% palladium precipitation based on the metal that had dissolved during the first ten minutes.

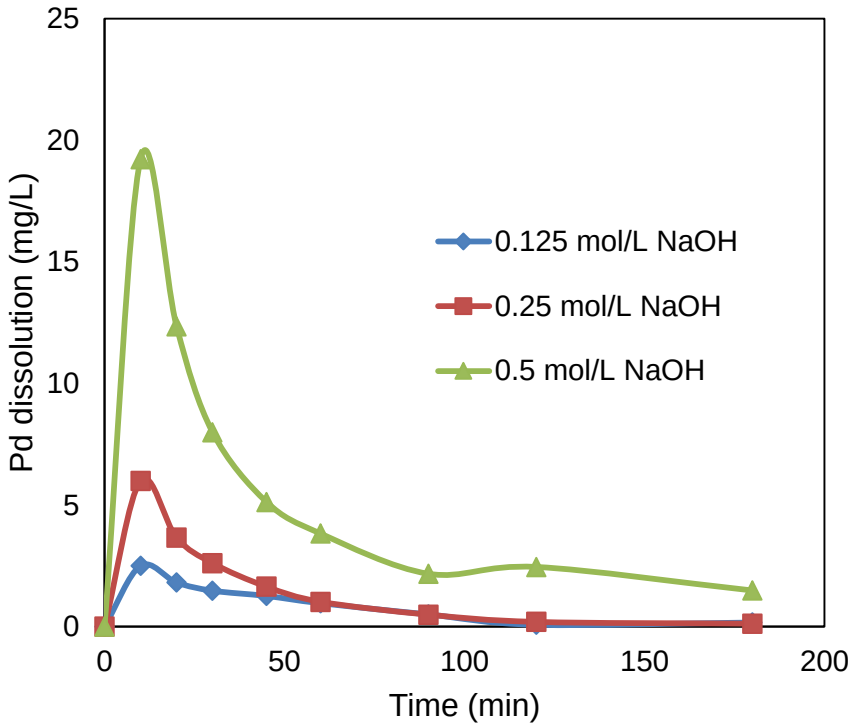

Figure 7.27: Effect of NaOH concentration on Pd dissolution at 160°C (10 g/L solids; 750 rev/min; 11 atm O_2 partial pressure)

Pourbaix et al. (1956) reported several changes in potential in a palladium/water system at high pH (>13.7). In the investigation, palladium was observed to take several oxidation steps as the potential changes leading to a more stable palladium oxide (PdO) from $Pd(OH)_2$. This can possibly explain the dissolution/precipitation trend observed as palladium initially dissolved at lower potential but precipitated as the potential changed. Nevertheless, would need to be validated in follow-up investigations.

The dissolution of ruthenium increases with increase in caustic concentration. As explained in Section 3.6, ruthenium and osmium form soluble ruthanate (RuO_4^{2-}) and osmate (OsO_4^{2-}), respectively, in oxidative alkaline conditions. These species are relatively stable in strong alkaline medium. Other studies also illustrated the effect of caustic concentration on the ruthenium dissolution extent (Goldberg and Hepler, 1968; Watari et al., 1994) where ruthenium dissolution was noted to increase with an increase in sodium hydroxide concentration. The results presented in Figure 7.28

illustrate the dissolution extents at different caustic concentrations, e.g., 175 mg/L ruthenium dissolved at 0.125 mol/L caustic concentration after 180 minutes.

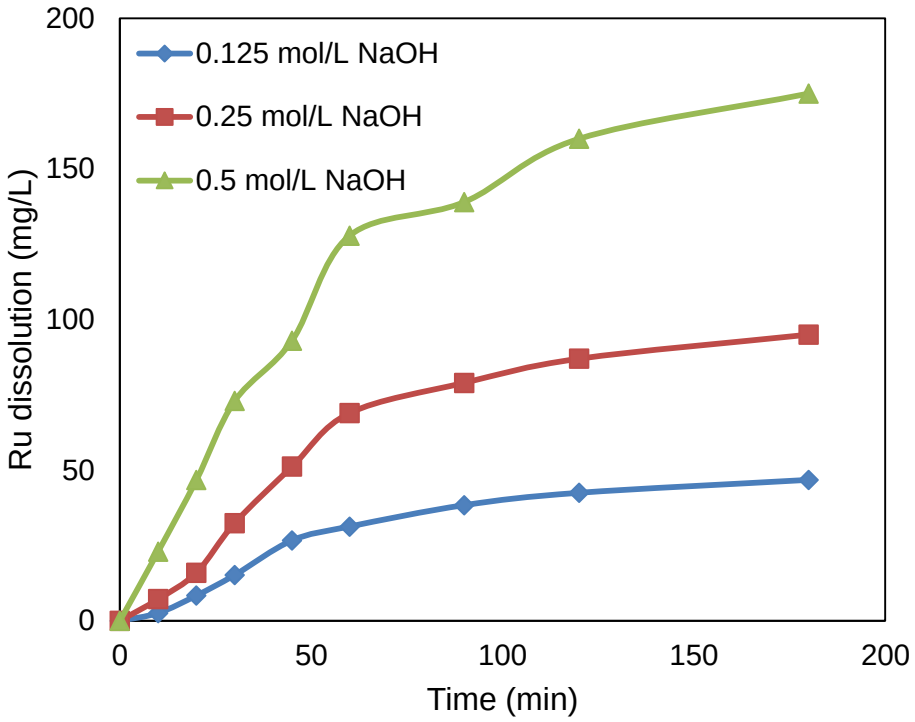

Figure 7.28: Effect of NaOH concentration on Ru dissolution at 160°C (10 g/L solids; 750 rev/min; 11 atm O_2 partial pressure)

7.4.2 Effect of Temperature on dissolution of PGMs

The general leachability of PGMs was compared at different temperatures for 3 hours. Final extractions are based on solutions analyses and dissolution profiles. The tests were performed in the range 160°C to 190°C, and are presented in Figure 7.29 to Figure 7.31.

It can be seen from Figure 7.29 and Figure 7.30 that low temperature favours the higher solubility of platinum and palladium. However, as the temperature is increased, the solubility reduces. This can be explained by the effect of temperature on the dielectric properties of water. For example, the dielectric constant of water, which is indicative of the ability of water to act as a solvent, changes from 88 at 0°C to 44 at 150°C (Heger et al., 1980). The higher the temperature, the less the ability of the water molecules has to act as a solvent (Chamberlin, 2008). At low temperature (160°C), the water molecules have higher ability to act as a solvent thereby rendering

the platinum and palladium in soluble form. It can be seen from Figure 7.29 that the dissolution reaches 70 mg/L platinum in solution at 160°C. As the temperature increases to 190°C, only 24 mg/L of platinum dissolves. Palladium also exhibits a similar trend as illustrated in Figure 7.30. The relationship between temperature and platinum/palladium dissolution was explained by Mountain and Wood (1988), albeit conducted in chloride media. They demonstrated that the solubility of platinum and palladium as tetrachloro complexes first decreases passing through a minimum at about 200°C and then begins to increase. They also speculated that the solubility decreased dramatically at temperatures greater than 400°C because of the decrease in the dielectric constant of water and subsequent increase in the electrostatic attraction between the metal and ligand.

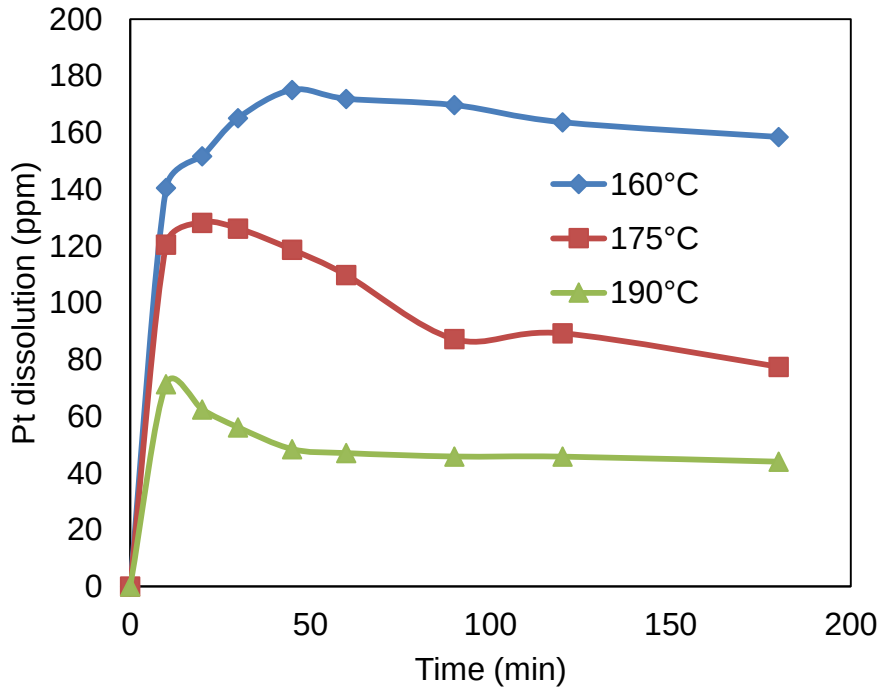

Figure 7.29: Effect of temperature on Pt dissolution with 0.25 mol/L NaOH (10 g/L solids; 750 rev/min; 11 atm O_2 partial pressure)

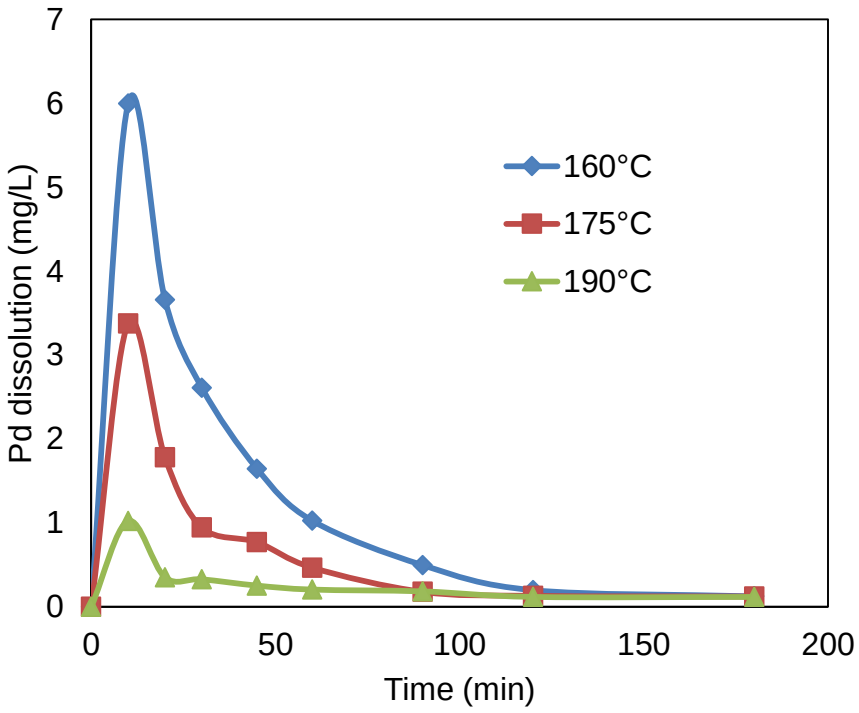

Figure 7.30: Effect of temperature on Pd dissolution with 0.25mol/L NaOH (10 g/L solids; 750rev/min; 11 atm O_2 partial pressure)

Figure 7.31 illustrates the effect of temperature on ruthenium dissolution. From the graph, ruthenium dissolution increases significantly from 0.081 to 0.161 mg/L when the temperature is increased from 175°C to 190°C. The temperature effect is less pronounced when the temperature is increased from 160°C to 170°C with ruthenium dissolution increasing from 47 mg/L to 81 mg/L after 180 minutes of leaching.

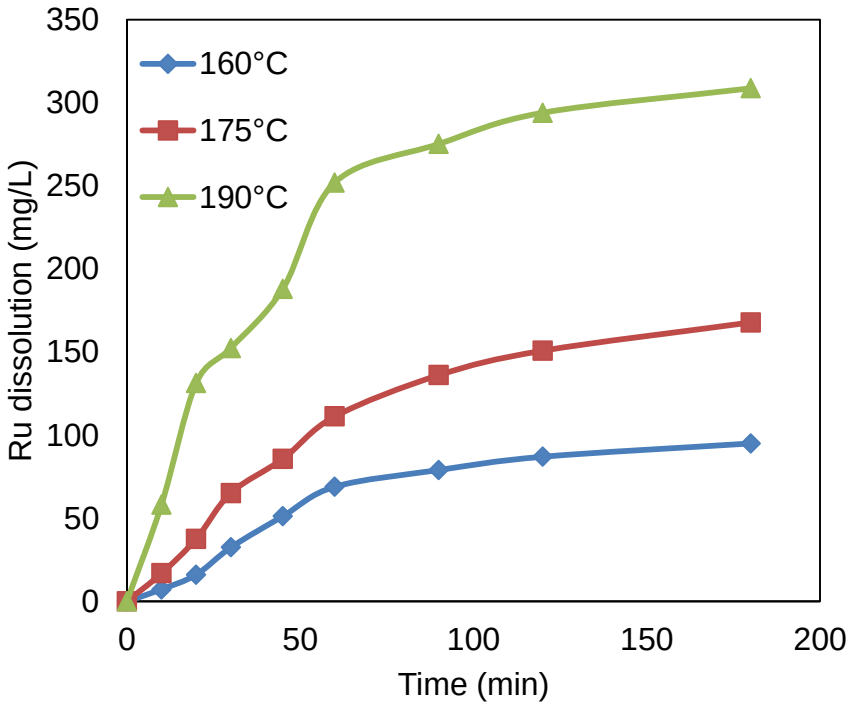

Figure 7.31: Effect of temperature on Ru dissolution with 0.25 mol/L NaOH (10 g/L solids; 750 rev/min; 11 atm O_2 partial pressure)

Figure 7.32 and Figure 7.33 illustrate the surface response plots for platinum and ruthenium dissolution at 180 minutes. It can be seen from Figure 7.32 that minimum platinum dissolution is obtained with low caustic concentration and high temperature. To the contrary, ruthenium dissolution is favoured by both increased temperature and caustic concentration. Minimal dissolution is obtained at low caustic concentration and low temperature. Therefore, a compromise will have to be made during process optmisation as to which element should be allowed to dissolve preferentially.

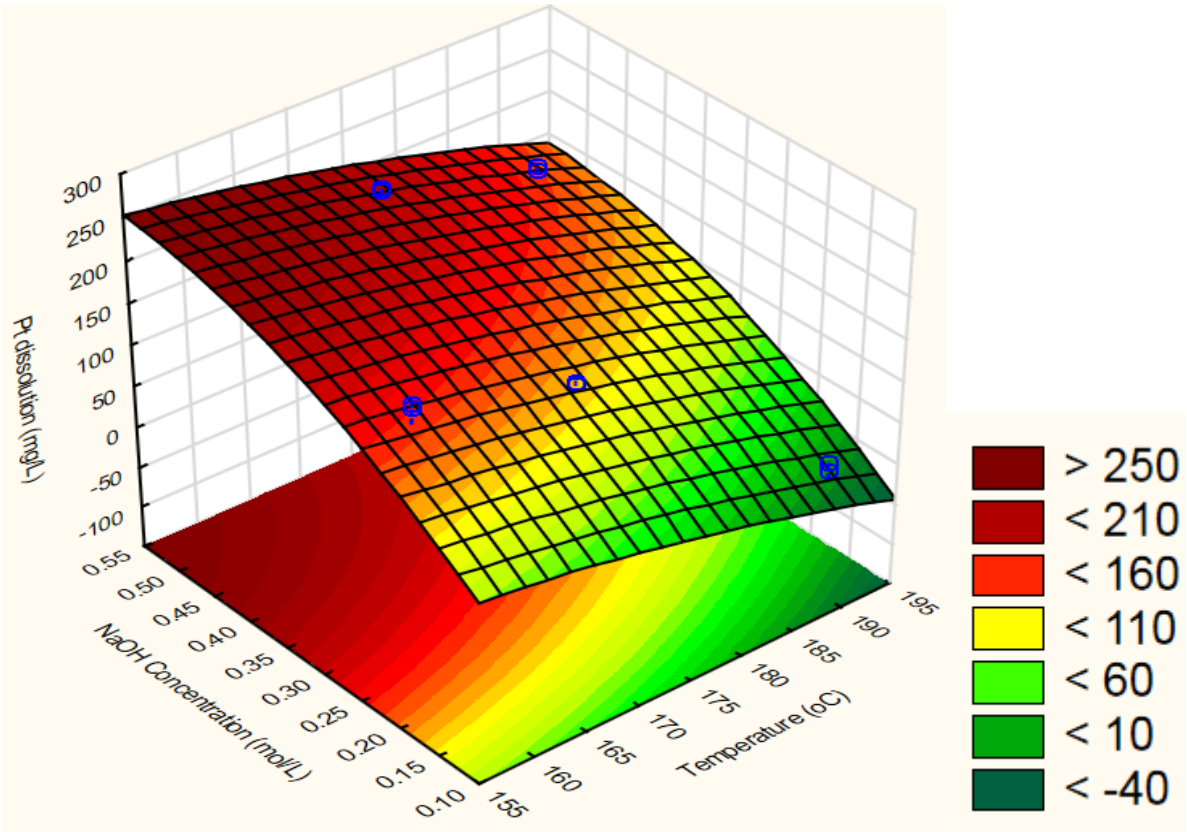

Figure 7.32: Response surface plot for platinum dissolution at 180 minutes

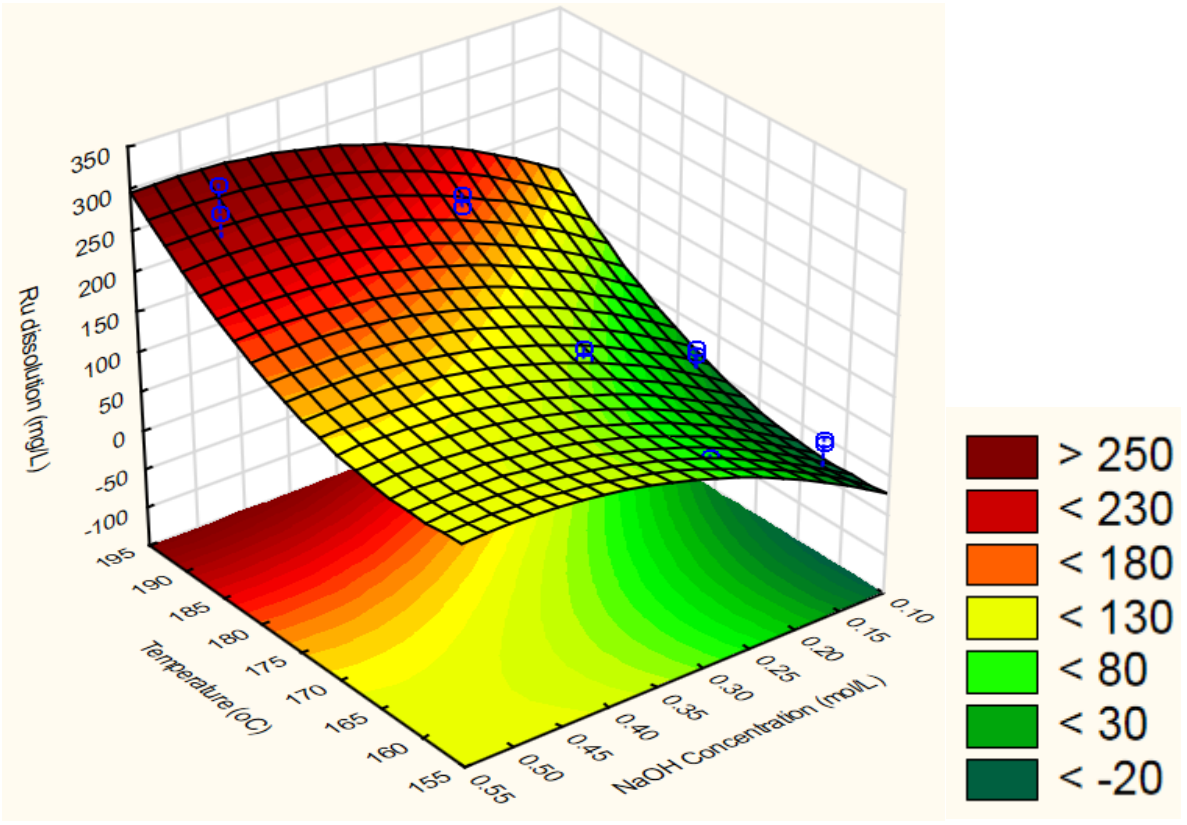

Figure 7.33: Response surface plot for ruthenium dissolution at 180 minutes

7.4.3 Effect of O_2 partial pressure on dissolution of PGMs

The effect of oxygen partial pressure was investigated in the range from 7 to 16 atm. The leaching temperature (160°C), caustic concentration (0.25 mol/L) and 1% solids loading were all kept constant. Figure 7.34 to Figure 7.36 present concentration–leaching time relationships for platinum, palladium and ruthenium. The effect of the oxygen partial pressure on the dissolution of platinum and palladium showed significant increase in dissolution extent when the oxygen partial pressure was increased from 11 to 16 atm. The oxygen partial pressure also had a noticeable effect on the ruthenium dissolution extent. The lowest ruthenium dissolution concentration of 175 mg/L was detected with an oxygen partial pressure of 7 atm. An increase in the oxygen partial pressure increased the amount of ruthenium that dissolved. The effect of the oxygen partial pressure, as explained in Section 3.6.2 may have resulted in the oxidation of ruthenium to ruthanate (RuO_4^{-2}) which is a stable species in strong alkaline conditions.

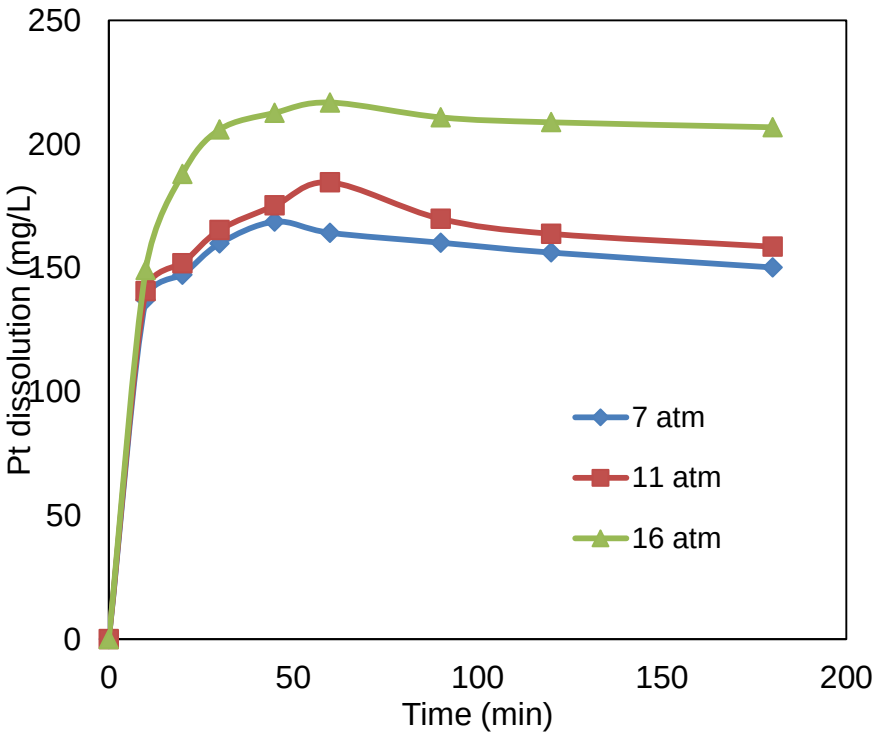

Figure 7.34: Effect of O_2 partial pressure on Pt dissolution (160°C, 0.25 mol/L NaOH 10 g/L solids; 750 rev/min)

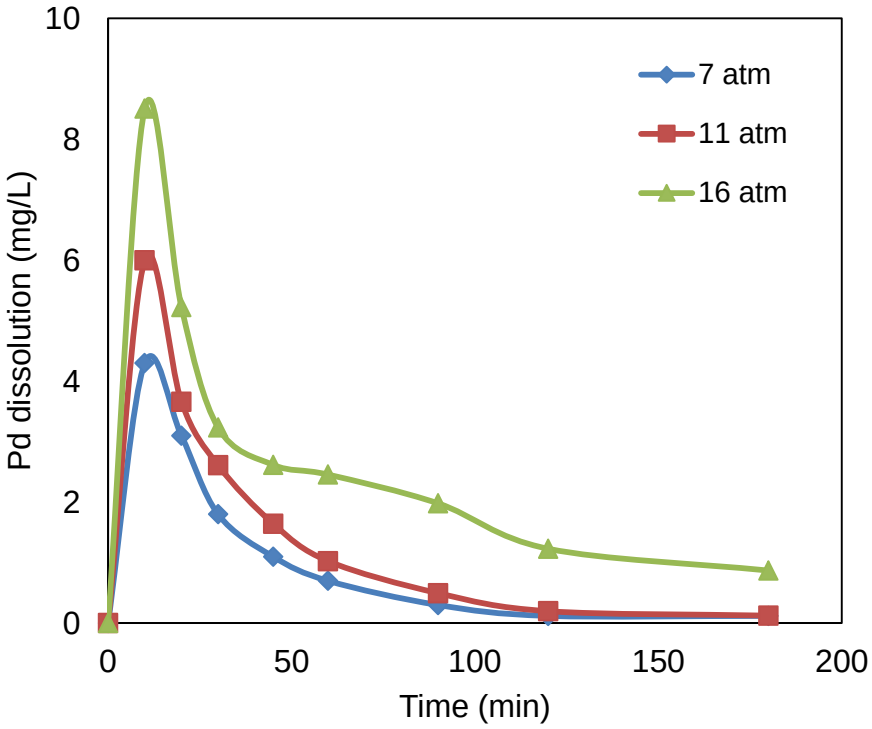

Figure 7.35: Effect of O_2 partial pressure on Pd dissolution (160°C, 0.25 mol/L NaOH 10 g/L solids; 750 rev/min)

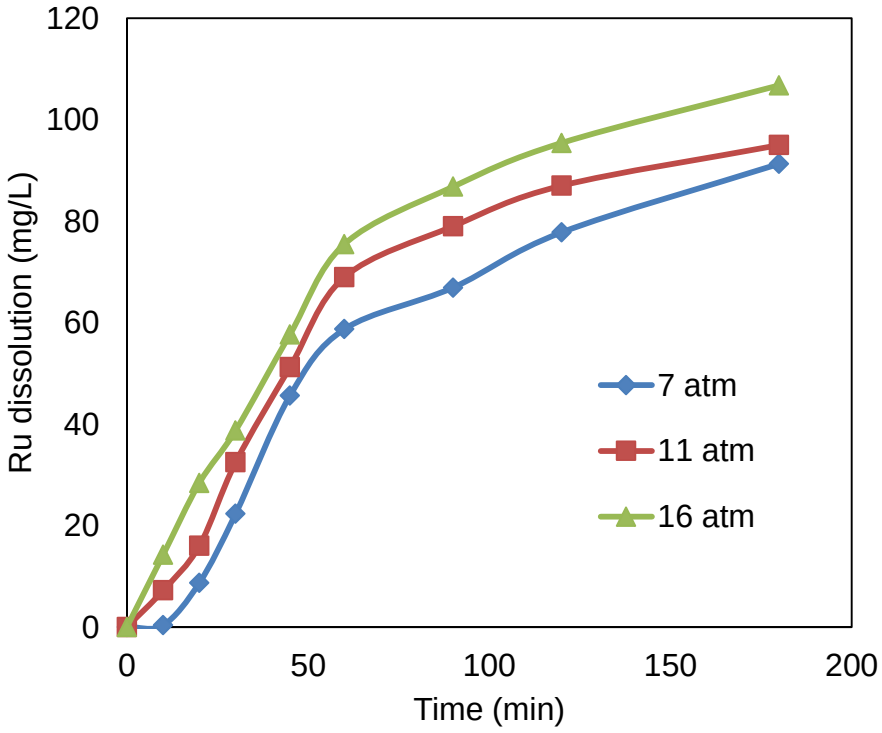

Figure 7.36: Effect of O_2 partial pressure on Ru dissolution (160°C, 0.25 mol/L NaOH 10 g/L solids; 750 rev/min)

7.4.4 Other platinum group metals

The other PGMs, i.e., iridium and rhodium do not dissolve in strong alkaline conditions (Goldberg and Hepler, 1968) Their aqueous solution ions hydrolyse as illustrated by the equation below:

$$Ir(OH)_6^{3-} \xrightarrow{H_2O} Ir_2O_3.XH_2O + 6OH^- \qquad 7.1$$

Therefore, iridium and rhodium precipitates and are recovered in the residue as hydroxides.

The tests conducted at various temperatures and NaOH concentrations provided three general conclusions on PGM dissolution.

1. Caustic concentration affects the dissolution of platinum and ruthenium. However, palladium precipitation occurred at prolonged leaching times, and most (although not 100 percent) of it was recovered in the residue as an oxide.
2. Increased temperature played an important role in minimising platinum and palladium dissolution. On the other hand, ruthenium dissolution increased with an increase in temperature.
3. The oxygen partial pressure had a relative weak effect on the rates of platinum and palladium dissolution up to 11 atm. A noticeable increase in the dissolution was experienced as the partial pressure of O_2 was increased to 16 atm. On the other hand, ruthenium dissolution showed a more significant dependency on the oxygen partial pressure.

7.5 Repeatability of leaching tests results

As explained in Section 6.2.4, a 2^3 factorial design with two replicates was employed to evaluate the effects of the variables on the leaching. A total of 18 tests, to investigate the effect of temperature and caustic concentration on extraction extents were conducted. Figure 7.37 to Figure 7.39 illustrates the results obtained for tests conducted at similar conditions. The results confirm that the leaching tests had good repeatability. The standard deviation obtained for sulphur selenium and arsenic are 0.28, 0.32 and 0.25, respectively.

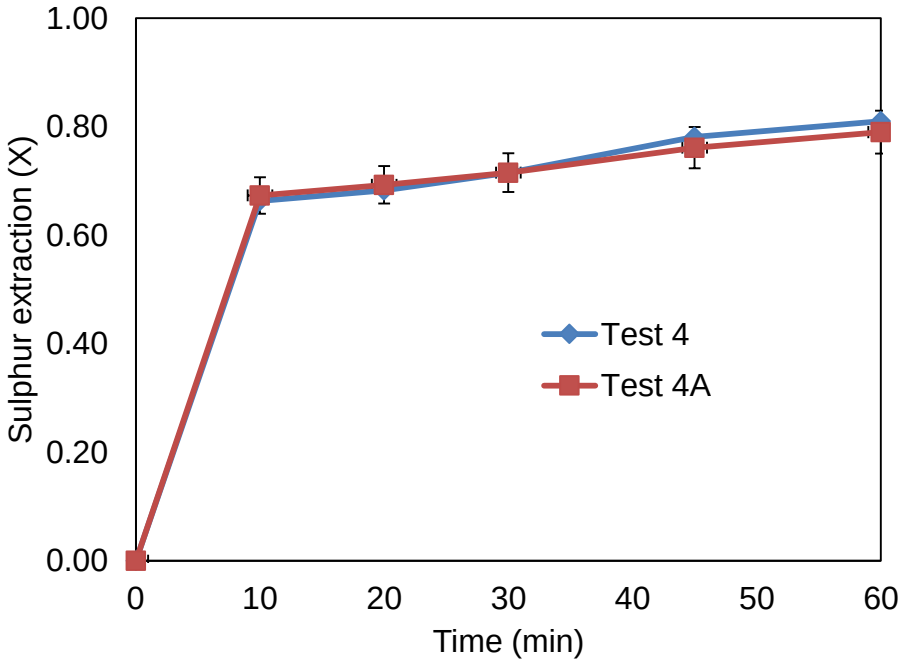

Figure 7.37: Repeatability of sulphur extraction (160°C, 0.25 mol/L NaOH, 11 atm O_2 partial pressure and 10 g/L solids)

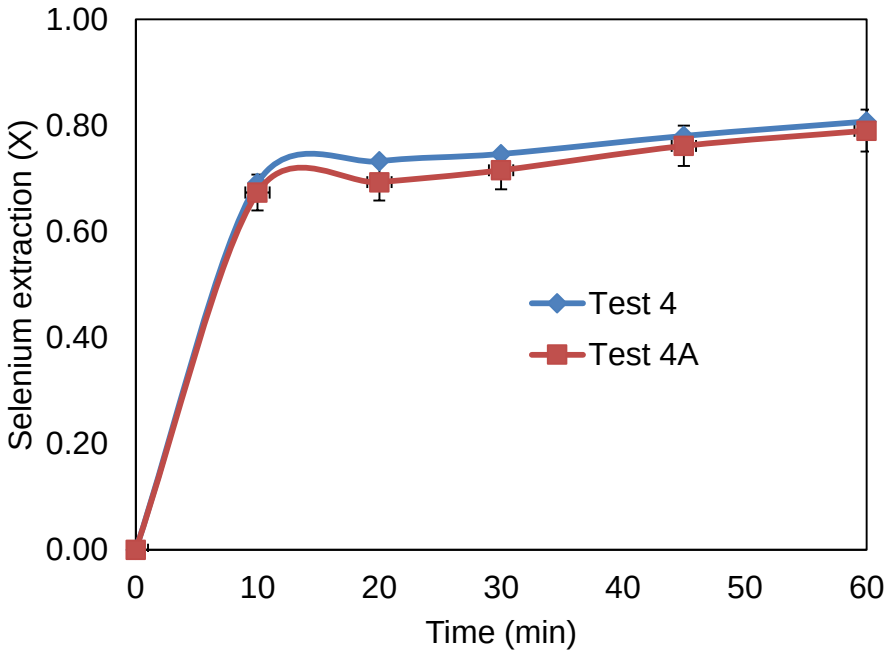

Figure 7.38: Repeatability of selenium extraction (160°C, 0.25 mol/L NaOH, 11 atm O_2 partial pressure and 10 g/L solids)

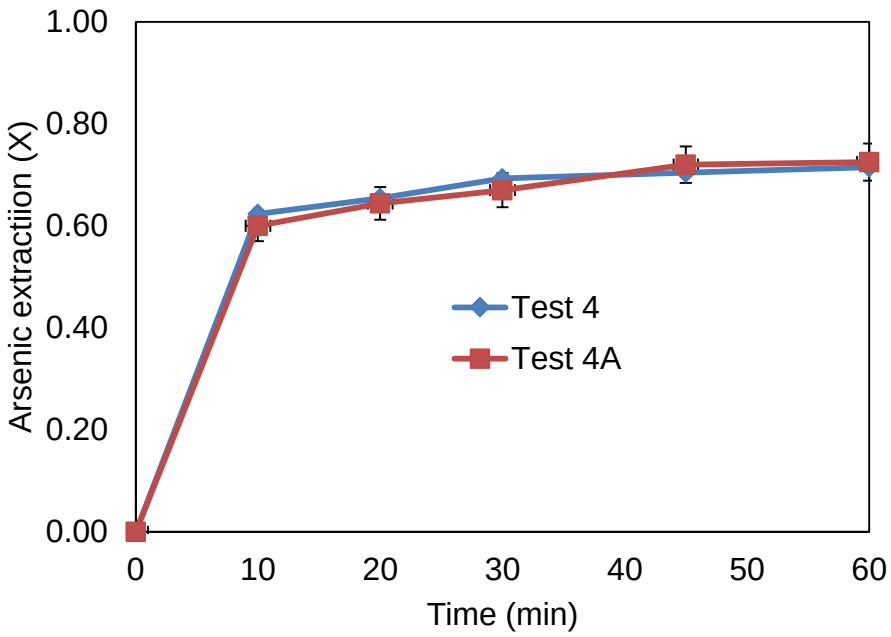

Figure 7.39: Repeatability of arsenic extraction (160°C, 0.25 mol/L NaOH, 11 atm O_2 partial pressure and 10 g/L solids)

8 MODELLING

This chapter focusses on explaining the leaching kinetics of sulphur, selenium and arsenic under varying operating parameter space. The model developed in this work is based on particle leaching theory (Levenspiel, 1972) and adopted by Peters (1991).

8.1 Kinetics analysis

Many metallurgical reactions are heterogeneous in nature. A number of leaching studies have utilised mathematical modelling to simulate the rate of dissolution (Wadsworth, 1979; Levenspiel, 1972). The three most common subsets of the shrinking particle/core model are chemical reaction, liquid film diffusion and product layer diffusion controlled cases (see Chapter 5).

Due to the wide particle size distribution of the feed material (0.07 to 400 µm) used in this investigation (Figure 8.1), the simple application of the kinetic models was not expected to generate satisfactory results, in predicting the mechanism of dissolution and the rate controlling step (Herbst, 1979; Gbor and Jia, 2004; Kacham and Suri, 2014). Foremost, the particle size variation had to be accounted for by integrating the shrinking particle or core models over the feed material distribution by evaluating the fraction that is unreacted for each particle size, L, i.e., for the chemical and diffusion rate controlling regimes presented by Equations 8.2 to 8.4, respectively (Hackl et al., 1995; Parada et al., 2014).

$$1-X_L = \sum_L (f(L,t)).m_L \qquad 8.1$$

$$f(L,t) = 1-X_L = \left(1-\frac{kt}{L}\right)^3 \qquad 8.2$$

$$f(L,t) = 1-3(1-X_L)^{\frac{2}{3}} + 2(1-X_L) = \left(1-\frac{kt}{L^2}\right) \qquad 8.3$$

$$f(L,t) = 1 - X_L = \left(1 - \frac{kt}{L}\right) \qquad 8.4$$

Equation 8.1 represents the fraction material remaining at time, t where 1-X_L is the fraction unreacted, f(L,t) is the function for the rate controlling model and m_L is the mass fraction of feed sample with size L, while Equations 8.2 to 8.4 represent the three equations used for chemical reaction, liquid diffusion and diffusion through product layer controlled mechanisms for particles of size L. Table 8.1 below summarises the mean particle diameter and weight fractions used in the calculations (determined using Saturn DigiSizer 5200; see Appendix VIII for details of instrument).

Table 8.1: Mean particle diameter (L_{av}) and weight fractions (m_L) used in modelling (derived from particle size distribution presented in Appendix IV)

D_{av} (mean particle size)	m_D (weight fraction)
5.35	0.0811
15	0.0652
30	0.1398
45	0.0735
60	0.1323
75	0.0523
85	0.0431
95	0.0370
110	0.0630
135	0.0687
175	0.0829
225	0.0804
275	0.0549
350	0.0234

The above integration was performed using numerical integration of the cumulative particle size distribution.

If f(L) represents the cumulative distribution function, such that F(D) is the fraction of mineral feed particles smaller than size L_i, the discrete probability density function, $f(\overline{D_i})$ is obtained as follows (Hackl, 1995):

$$f(\overline{L_i}) = \frac{F(L_{i+1}) - F(L_l)}{L_{l+1} - L_i} = \frac{\Delta F_i}{\Delta L_i} \qquad 8.5$$

where $F(L_{i+1})$ and $F(L_i)$ are the cumulative fractions of particles smaller than size L_{i+1} and L_i, respectively.

$(\overline{L_i})$ is the arithmetic or geometric mean of particles between size L_i and L_{i+1}

$\Delta F_i = f(\overline{L_i})\Delta L_i$ is the weight fraction of particles of size $(\overline{L_i})$.

It should be noted that the discrete probability density function is normalised, such that:

$$\sum_{i=0}^{n} f(\overline{L_i})\Delta L_i = 1 \qquad 8.6$$

At any size L, the discrete cumulative distribution function is related to the discrete probability density function by:

$$F(L) = \sum_{i=0}^{n} f(\overline{L_i})\Delta L_i \qquad 8.7$$

The particle size distribution data generated by the Saturn DigiSizer 5200 (instrument discussed in Appendix VIII) was used to produce discrete cumulative, distribution and probability density functions (Figure 8.1 and Figure 8.2, respectively).

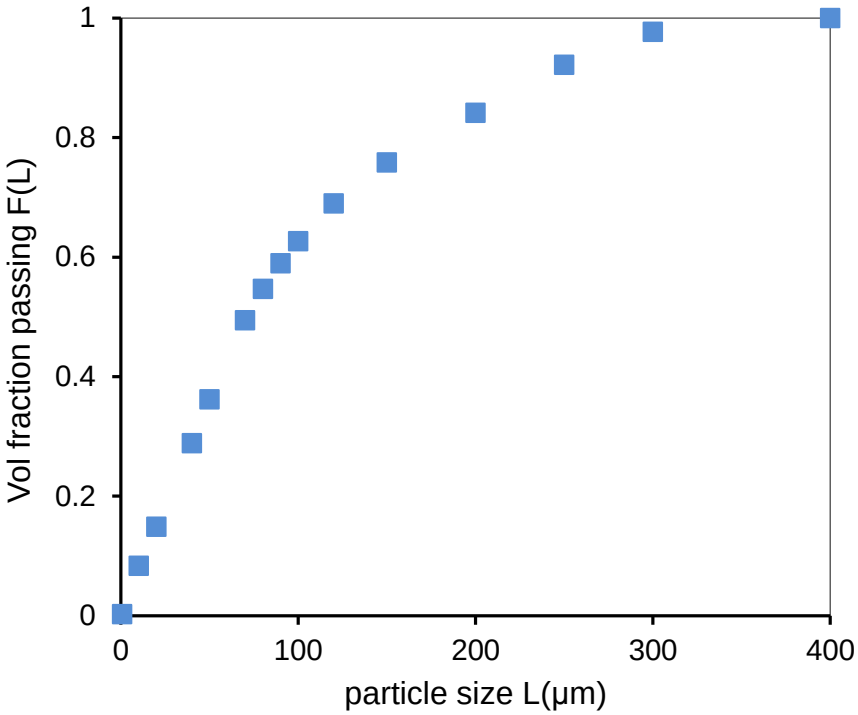

Figure 8.1: Particle size distribution of feed material using Saturn DigiSizer 5200

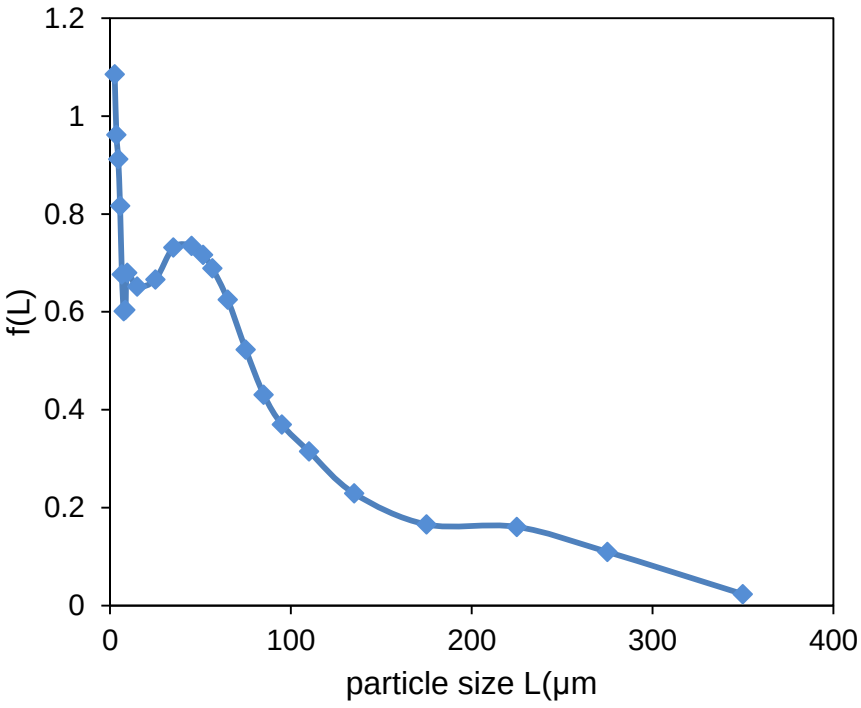

Figure 8.2: Discrete probability density function of feed material

The surface area (see details in Appendix IV) was calculated from the particle size distribution obtained using the Saturn DigiSizer 5200. By assuming that all the particles were spherical and smooth (non-porous), specific surface area, A, was computed using Equation 5.33.

8.2 Model formulation

The important leaching parameters are the surface area, reaction time, solution concentration, temperature and pressure. Particle surface area, reaction time and concentration are related to the extraction in a complex fashion and must include knowledge of the particle size distribution, geometry (i.e., area variation with time) and the solution chemistry. The purpose of modelling is to capture the relationship between the extraction (the fraction of material that has been leached) and the reaction time. Peters (1991) describes the two kinds of models that are used to describe a leaching process: a micromodel and a macromodel.

The changes that occur at the surface of the particle as a result of leaching are described by a micromodel. These include change in size, size distribution and shape. The micromodel in simplistic terms, describes the change in the size distribution of particles being leached. The macromodel on the other hand, describes the macro properties for the process, like temperature change, volume change, pressure change and change in the solution composition. These changes in both macromodel and micromodel are calculated by mean of mass and energy balances.

A batch leaching model thus needs to incorporate macro- and micro- elements. These can be divided into the following:

- A particle reaction model – to describe the reaction rates and the rate determining step for reactions taking place on or within the individual mineral particles
- A mathematical methodology – to calculate the mineral recovery in a batch reactor for a distribution of particle sizes
- Mass balance equations – to calculate the change in all important species concentration (reactants and products); and

- Energy balance equations - to calculate the heat transfer requirements for the system.

The first three parts (particle reaction model, mathematical methodology and mass balance equations) constitute the model developed in this study and is discussed further below.

During leaching, the amount of exposed surface area of the soluble mineral decreases, as the free particles shrinks. For an equiaxed particle, the shape of which does not change with size during leaching, the rate equation is:

$$\frac{dn_i}{dt} = -k(T)f(C)_i A \qquad 8.8$$

where: k = reaction rate constant

$f(C)_i$ = factor accounting for solution condition effect

A = surface area (m^2)

n_i = moles in the particle at time, t

In many instances, the mineral surface area is expressed in terms of the shape factor (γ) and the characteristic length (ℓ). This allows for the area of the particles to be expressed in terms of the characteristic volume (ϑ) and thus the density of the particles (ρ) (Levenspiel, 1972).

$$\gamma = \frac{A}{\ell^2} \qquad 8.9$$

$$\vartheta = \ell^3 \qquad 8.10$$

Rearranging Equation 8.10 gives:

$$\ell = \vartheta^{\frac{1}{3}} \qquad 8.11$$

Defining the molar density (p) as:

$$p = \frac{n}{\vartheta} \tag{8.12}$$

where n is moles, the area can then be expressed by:

$$A = \gamma \ell^2 = \gamma \vartheta^{\frac{2}{3}} = \gamma \left(\frac{n}{p} \right)^{\frac{2}{3}} \tag{8.13}$$

Therefore, the moles, n_i, left at any given time is given by the following expression:

$$\frac{dn_i}{dt} = -k(T) f(C)_i A = -k(T) f(C)_I \gamma \left(\frac{n_i}{p} \right)^{\frac{2}{3}} \tag{8.14}$$

Assuming that the molar density of material remains constant during leaching leads the following equation:

$$p = \frac{n_{i_o}}{\ell_o^3} \tag{8.15}$$

where n_{i_o} is the initial moles of mineral species.

Therefore:

$$\frac{dn_i}{dt} = -k(T) f(C)_i \gamma \left(\frac{\ell_o^3}{n_{i_o}} \right)^{\frac{2}{3}} (n_i)^{\frac{2}{3}} \tag{8.16}$$

If N is the number of particles with an average shape factor (γ) of the total mass F_0, the rate of change of amount of species in a particle is given by:

$$\frac{dn_i}{dt} = -k(T) f(C)_i \gamma N \left(\frac{\ell_o^3}{n_{i_o}} \right)^{\frac{2}{3}} (n_i)^{\frac{2}{3}} \tag{8.17}$$

The total number of particles can be calculated from the total mass of particles and the unit volume, assuming uniform size particles. The unit volume is calculated using Equation 8.10. Therefore:

$$N = \frac{F_o}{\rho \ell_o^3} \tag{8.18}$$

where ρ is the mass density, Equation 8.17 becomes:

$$\frac{dn_i}{dt} = -k(T)f(C)_i \gamma \frac{F_o}{\rho \ell_o^3} \left(\frac{\ell_o^3}{n_{i_o}} \right)^{\frac{2}{3}} (n_i)^{\frac{2}{3}} \tag{8.19}$$

Simplifying Equation 8.19 leads to:

$$\frac{dn_i}{dt} = -k(T)f(C)_i \gamma \frac{F_o}{\rho \ell_o} \left(\frac{n_i}{n_{i_o}} \right)^{\frac{2}{3}} \tag{8.20}$$

The term $\frac{F_o}{\rho \ell}$ is equivalent to the mineral surface area given by Equation 5.33.

Alternative expressions have been derived by other researchers (Dixon and Dreisinger, 2002). The amount of mineral species remaining in a particle at any time point can be expressed in terms of fraction conversion as follows:

$$X = \frac{n_{i_o} - n_i}{n_{i_o}} = 1 - \frac{n_i}{n_{i_o}} \tag{8.21}$$

$$\frac{n_i}{n_{i_o}} = 1 - X \tag{8.22}$$

$$n_i = n_{i_o}(1 - X) \tag{8.23}$$

Therefore:

$$dn_i = n_{i_o} dX \qquad 8.24$$

where X is the fraction reacted, while the other parameters are defined as before. Substituting Equation 8.23 and Equation 8.24 into Equation 8.20 yields:

$$\frac{dX}{dt} = -\frac{k(T)f(C)_i}{n_{i_o}} \gamma \frac{F_o}{\rho \ell_o} (1-X)^{\frac{2}{3}} \qquad 8.25$$

$$\frac{dn_i}{dt} = n_{i_o} \frac{dX}{dt} = -k(T)f(C)_i \gamma \frac{F_o}{\rho \ell_o} (1-X)^{\frac{2}{3}} \qquad 8.26$$

where $\frac{dn_i}{dt}$ is the change in the number of moles of a species.

Equation 8.26 is similar to the general topological leaching rate expression given by Dixon and Dreisinger (2002) as follows:

$$\frac{dX}{dt} = -k(T)f(C)_i(1-X)^{\varphi} \qquad 8.27$$

where k(T) is a rate constant which is a function of temperature and initial particle diameter (or surface area), $f(C)_i$ is as defined before and φ is a constant typically between 0.5 and 2. For the shrinking particle model, φ is equal to 2/3 under chemical reaction control. Equation 8.27 is utilised to determine the fraction of mineral species reacted with time.

8.2.1 Calculation of rate constants k

The intrinsic rate constant, k, was determined by assessing each reaction mechanism using by Equations 8.2 to 8.4 and minimising the sum of squared error between experimental extractions, X_E and calculated extraction, X_C (according to Equation 8.28). These optimisations were conducted using MS Excel solver.

$$\text{Error} = \sum_{1}^{n} (X_E - C_C)^2 \qquad 8.28$$

The best regressed model turned out to be the diffusion through the product layer model presented by Equation 8.3, with a global error of less than 0.02 for all the sample points. Figure 8.3 below illustrates the correlation between the experimental and calculated sulphur extractions. The intrinsic rate constant value of each experimental run was obtained using this regression procedure.

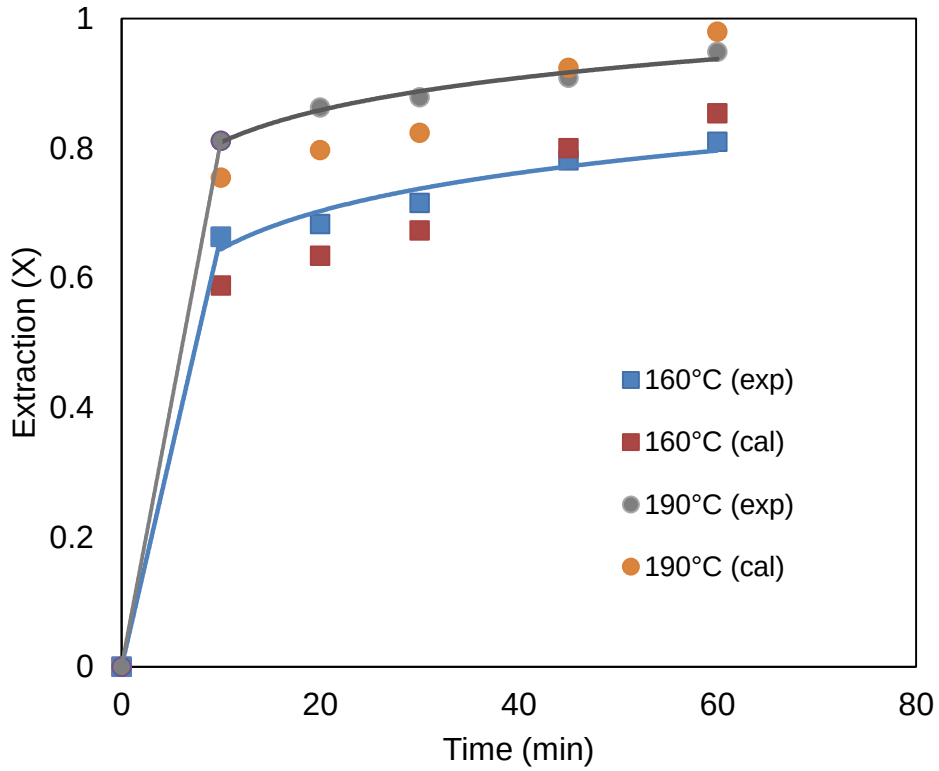

Figure 8.3: Comparison between experimental and calculated extractions for sulphur at different temperatures (0.25 mol/L NaOH, 10 g/L solids; 750 rev/min; 11 atm O2 partial pressure).

8.2.2 Order of reactions with respect to hydroxide ion concentration (OH^-)

Reaction orders of 0.25 with respect to the hydroxide ion for sulphur, 0.21 for arsenic and 0.12 for selenium were obtained as illustrated in Figure 8.4. Coincidentally, these values are comparable to those obtained in the oxidative alkaline leaching of pyrite (0.27 for S) and arsenopyrite (0.23 for As) by Koslides and Ciminelli (1992).

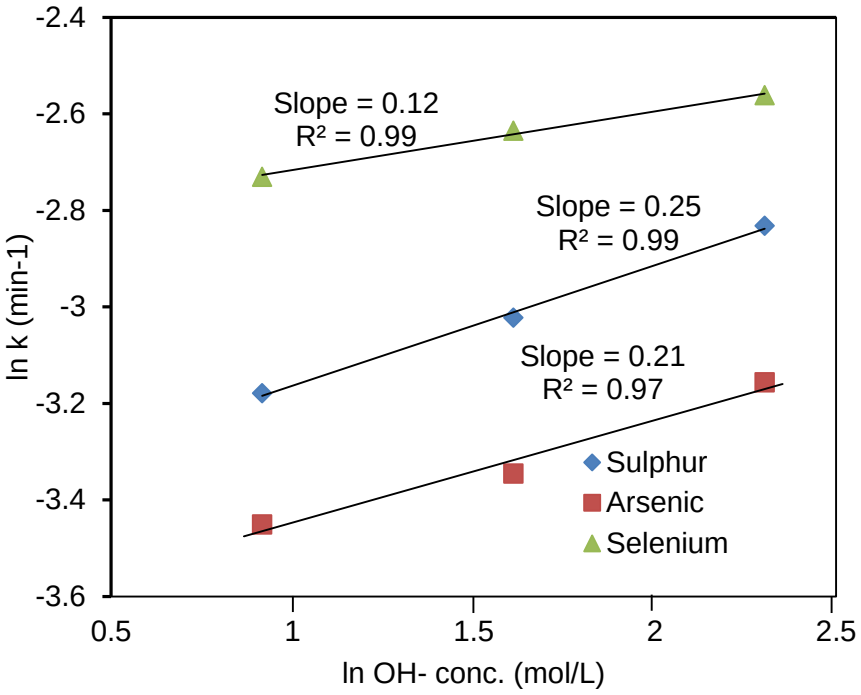

Figure 8.4: Rate constant versus OH^- concentration (175°C; 10 g/L solids; 750 rev/min; 11 atm O_2 partial pressure)

8.2.3 Order of reactions with respect to O_2

The effect of O_2 partial pressure on the rate constant was determined next. Several researchers have reported a 0.5 order dependence on oxygen partial pressure on dissolution in both acidic and alkaline media, under a wide range of temperatures (up to 483K) (Crundwell, 2013; Bailey and Peters; 1976, Smith and Shumate; 1970, Nicol, 1993).

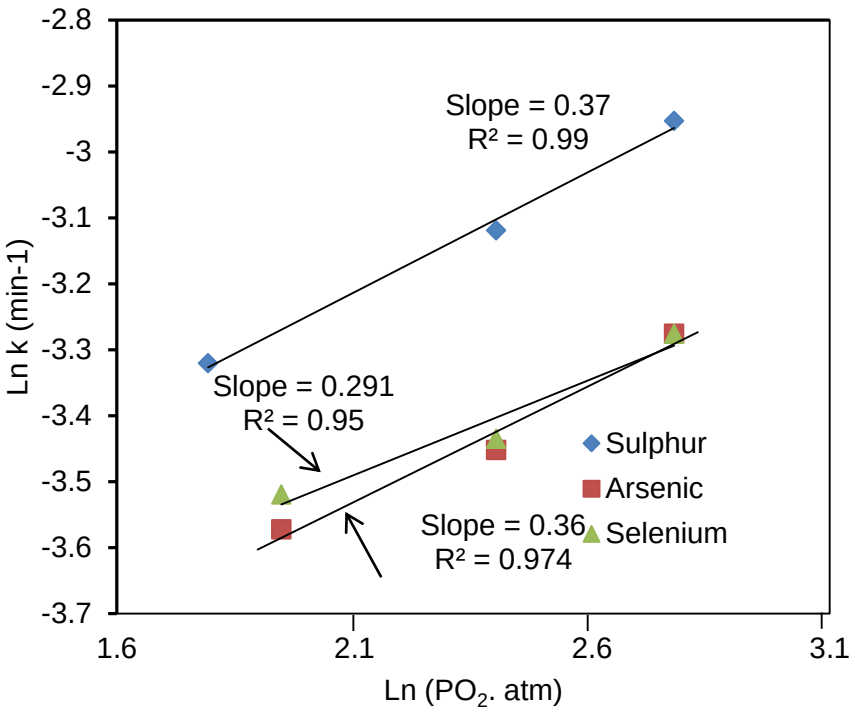

Figure 8.5: Rate constant versus O_2 partial pressure (0.25 mol/L NaOH; 160°C; 10 g/L solids; 750 rev/min)

Reaction orders of 0.37, 0.36 and 0.29 for S, As and Se, respectively for the reactions with respect to oxygen partial pressure was obtained in this investigation. The reaction order value for sulphur is comparable to 0.31 obtained by Koslides and Ciminelli (1992).

8.2.4 Activation energy

The temperature dependence of reaction rates can be used to estimate the apparent activation energy. For a system under chemical reaction control, the activation energy is usually greater than 40 kJ/mol while diffusion (transport) controlled processes typically have activation energies less than 40 kJ/mol. Diffusion can either occur via a product layer or a boundary fluid film barrier (Levenspiel, 1972). The rate constant, k, is related to temperature according to the Arrhenius equation:

$$k = k_o \exp\left(\frac{-Ea}{RT}\right) \quad \text{and} \quad \ln(k) = \ln(k_o) - \frac{Ea}{R}.\frac{1}{T} \qquad 8.29$$

A plot of ln k vs 1/T for the k values determined from the regression procedure (Section 8.2.1) would be expected to yield a straight line where the slope is -Ea/R (Figure 8.6).

The experimental activation energy of 31.8 kJ/mol with a correlation coefficient of 0.95, 10.7 kJ/mol with a correlation coefficient of 0.99 and 26.1 kJ/mol with a correlation coefficient of 0.95 were obtained for S, As and Se, respectively. These values suggest that the kinetics may be controlled by product layer diffusion mechanism. Most research conducted on the oxidative alkaline leaching of iron-bearing sulphides/arsenides has identified the precipitation of iron oxide compounds on the surface of the reacting mineral. Koslides and Ciminelli (1992) have sited many references to this effect. The oxide often forms a coating and the rate of oxidation depends on the mass-transfer through the product layer. The formation of oxides (iron and PGM oxides) on the particle surface supports the product layer diffusion mechanism postulated in this study.

Zheng and Chen (2013) determined the activation energy value of 20.5 kJ/mol for the leaching of selenium from a selenium-tellurium rich material in sodium sulphite solution. This value is slightly lower than 26.1 kJ/mol obtained in this study.

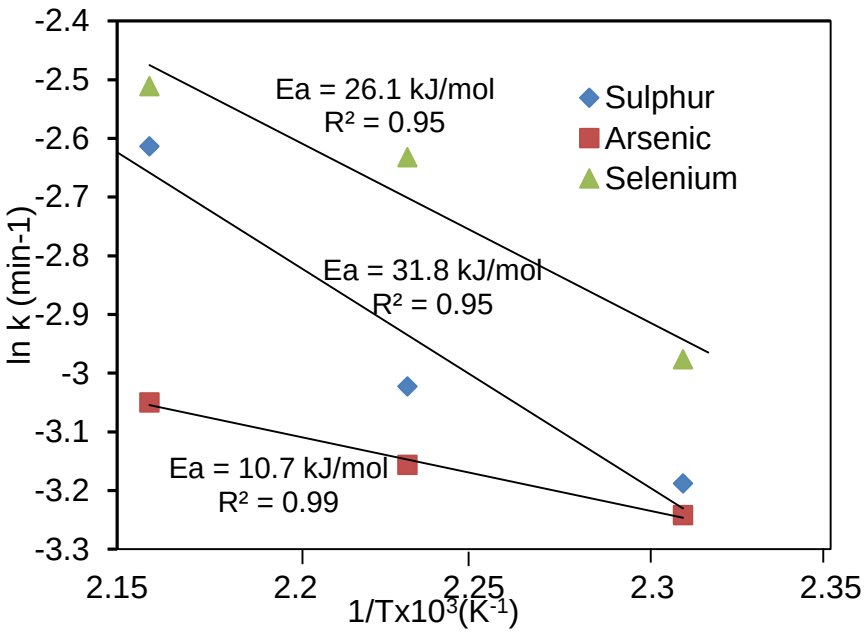

Figure 8.6: Arrhenius plot of ln k vs 1/T (0.25mol/L NaOH; 10 g/L solids; 750 rev/min; 11 atm O_2 partial pressure)

Table 8.2: Summary of kinetic parameters used in the model

Species	Activation energies (kJ/mol)	Pre-exponential factor	Order of OH^- with respect to reactant	Order of O_2 with respect to reactant
S	31.8	269.54	0.25	0.37
Se	26.1	72.11	0.12	0.29
As	10.7	0.75	0.21	0.36

8.3 Model expressions

The analyses conducted in the previous section have suggested that the leaching of the amphoteric elements is limited by the diffusion of the reacting species through a particle product layer, most likely an oxide or hydroxide phase. The optimised regression parameters yielded the following expressions:

$$\frac{dX_S}{dt} = 269.54A_o \exp\left(-\frac{31800}{RT}\right).[OH^-]^{0.25}.[O_2]^{0.37}.(1-X_S)^{1.05} \quad 8.30$$

$$\frac{dX_{Se}}{dt} = 72.11A_o \exp\left(-\frac{26100}{RT}\right).[OH^-]^{0.12}.[O_2]^{0.29}.(1-X_{Se})^{1.05} \quad 8.31$$

$$\frac{dX_{As}}{dt} = 0.75A_o \exp\left(-\frac{10700}{RT}\right).[OH^-]^{0.36}.[O_2]^{0.21}.(1-X_{As})^{2} \quad 8.32$$

where A_0 is the initial surface area, T is temperature and R is universal gas constant. The best fit φ value for sulphur and selenium (Equation 8.27) was 1.05, while a value of 2 was obtained for arsenic.

The rate equations were solved (using Matlab 7.10.1) for the fractions extracted with time. The mathematical modelling approach involved solving the three extraction differential equations coupled with the caustic mass balance (Equation 8.33) and the oxygen mass balance (Equation 8.34), simultaneously.

$$\frac{d[OH^-]}{dt} = -2n_{i_S}\frac{dX_S}{dt} - 2n_{i_{Se}}\frac{dX_{Se}}{dt} - 2n_{i_{As}}\frac{dX_{As}}{dt} \quad 8.33$$

$$\frac{d[O_2]}{dt} = kLa\left([O_2]^* - [O_2]\right) - Q_{O_2}\frac{dX}{dt} \quad 8.34$$

where n_i is the initial number of moles of species (sulphur, selenium or arsenic) while Q_{O2} is the oxygen demand term (total oxygen demand for all the oxygen consuming

species) and dX/dt is the rate of mineral oxidation. Table 8.3 summarises the parameters utilised in the pressure leach model.

Table 8.3: Parameters of pressure leaching model

Input (leaching conditions)	Constants (from laboratory data)	Unknowns (solved for)
Pulp density	Exponential factors	C_{O_2}
Concentrate composition	Activation energies	X_S
Feed temperature	Reaction orders	X_{Se}
Oxygen partial pressure		X_{As}
Alkali strength		$[OH^-]$

8.4 Modelling results

Oxygen transfer is an important aspect during the operation of the autoclave reactor (highlighted in Chapter 4). Figure 8.7 illustrates the trends for the saturation concentration of oxygen at different solids loadings, as calculated by the model. It is evident from the figure that the bulk oxygen consumption would be a limiting factor at higher slurry densities. The figure illustrates that at higher solids loading, there is mass transfer limitation with only 83% saturation reached after 100 minutes. However, at 10% solids loading, 91% saturation is reached after 50 minutes. Figure 8.8 to Figure 8.10 compare the experimental and simulated results. The best regressed model performance was observed for sulphur and selenium extraction while arsenic extraction was poorly fitted.

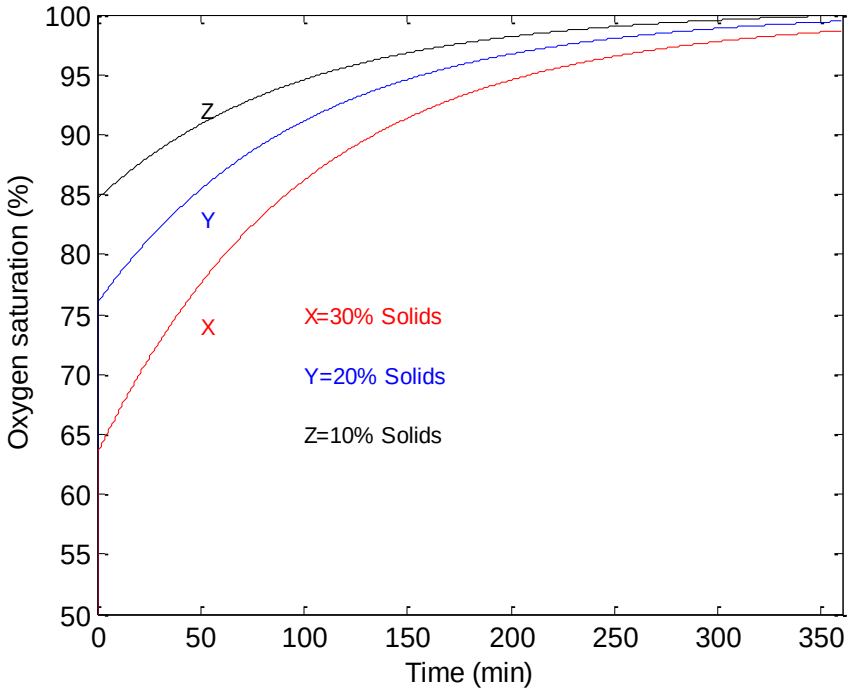

Figure 8.7: Oxygen saturation at 175°C , 11 atm O_2 partial pressure and different solids loading

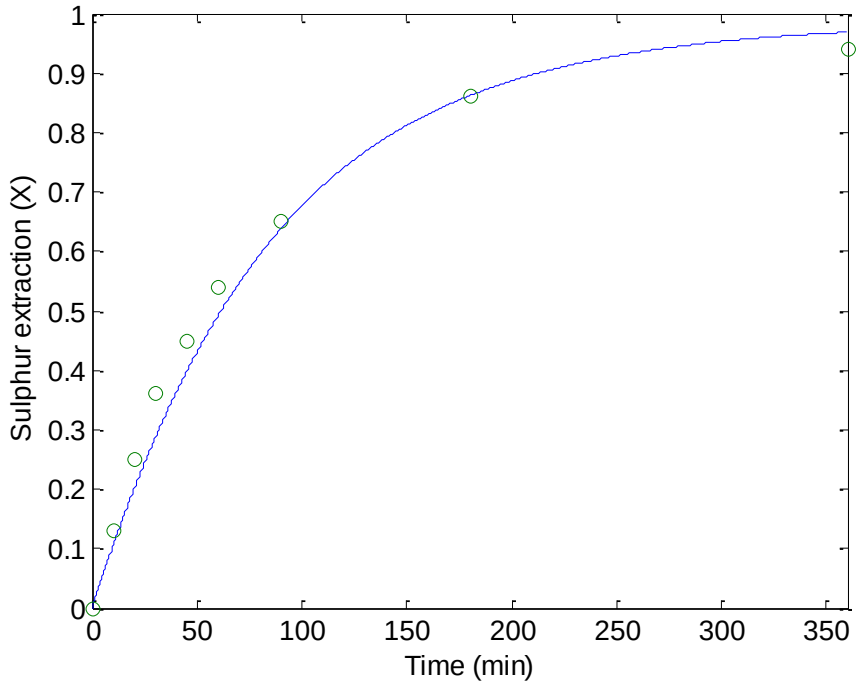

Figure 8.8: Model prediction (-) vs experimental (o) for sulphur extractions at 175°C, 2 mol/L NaOH, 750 rev/min and 11 atm O_2 partial pressure and 250 g/L solids

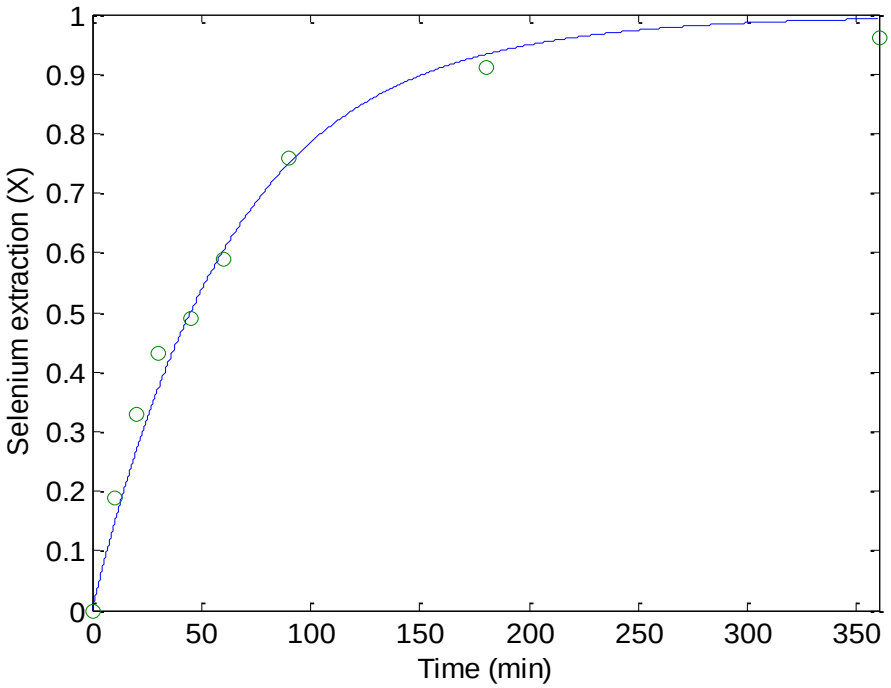

Figure 8.9: Model prediction (-) vs experimental (o) for selenium extractions at 175°C, 2 mol/L NaOH, 750 rev/min, 11 atm O_2 partial pressure and 250 g/L solids

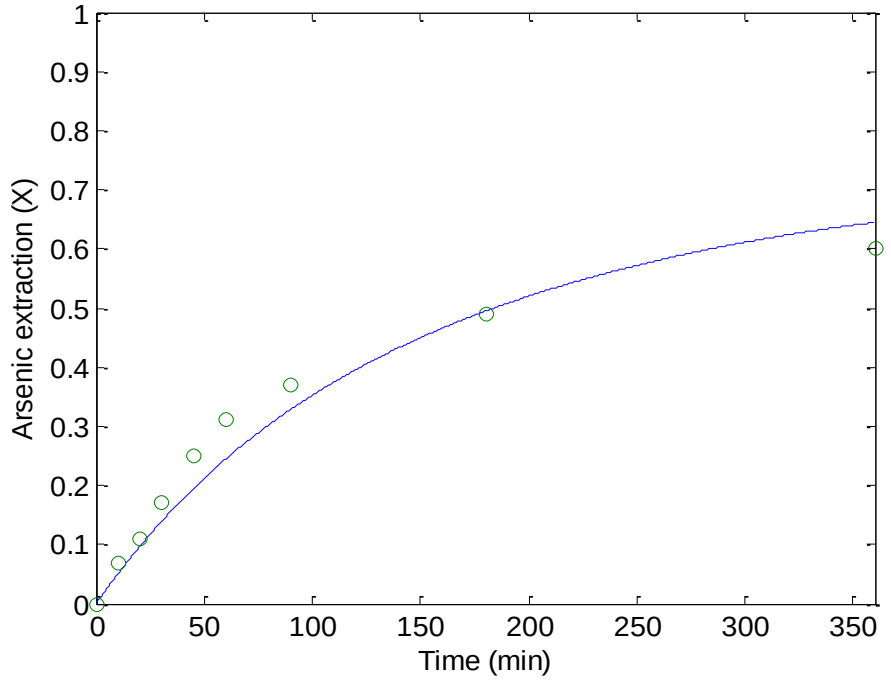

Figure 8.10: Model prediction (-) vs experimental (o) for arsenic extractions at 175°C, 2 mol/L NaOH, 750 rev/min, 11 atm O_2 partial pressure and 250 g/L solids

9 CONCLUSIONS AND RECOMMENDATIONS

9.1 Conclusions

The kinetics of dissolution of amphoteric element bearing minerals in alkaline media have been studied by several researchers. However, little work has been conducted to understand and simulate the kinetics of dissolution of sulphur, selenium and arsenic of the platinum group metals concentrates. Above all, the effects of process parameters on the dissolution extents of PGMs during alkaline leaching of PGM concentrates have not been studied. Therefore, this study focussed on alkaline autoclave oxidation of the PGM concentrate containing sulphur, selenium and arsenic in 0.125 to 0.5 mol/L NaOH, 160 to 190°C and 7 to 16 atm oxygen partial pressure. Also the mathematical description of the interfacial mass transfer rate of the primary oxidant-diatomic oxygen, O_2 molecule from the gas to the liquid phase was evaluated.

The PGM-rich leach residue was subjected to leaching in aqueous caustic solution under oxygen pressure under well-controlled conditions. With these experiments, the effects of several process parameters on the dissolution of sulphur, selenium and arsenic as well as the associated PGM losses were studied. These parameters included caustic concentration, temperature and oxygen partial pressure. Mathematical models were developed for sulphur, selenium and arsenic oxidation kinetics in a batch reactor under alkaline conditions at high temperature and pressure. The models accounted for the effect of temperature, oxygen partial pressure, oxygen mass transfer rate and particle size (or surface area) on the reaction kinetics. The findings from this study can be summarised as follows:

9.1.1 Effect of process parameters on leaching behaviour

- Caustic concentration appeared to have a stronger effect on the extraction extents of all the species. Sulphur and arsenic extraction extents increased from 82 to 89% and 72 to 79%, respectively, when caustic concentration was increased from 0.125 to 0.5 mol/L. However, it was noted that increasing the caustic concentration from 0.25 mol/L to 0.5 mol/L does not significantly improve the reaction rate. This may be attributed to the decrease in oxygen solubility with an increase in the caustic concentration.

- Caustic concentration also affected the dissolution of platinum, palladium and ruthenium which showed an increase in dissolution with increased caustic concentration. It was also noted that platinum and palladium dissolved appreciably in the first ten minutes and then precipitated at longer reaction times. A downward trend was observed for both species with increased reaction time. Rhodium and iridium possibly precipitated and did not report in the solution phase while osmium could not be detected by the analytical instrument used.

- Temperature had a positive effect on the dissolution of sulphur, selenium and arsenic. 95% of sulphur extraction was observed at 190°C while only 80% was extracted at 160°C after 60 minutes. Similarly, 94% selenium was extracted at 190°C after 60 minutes as compared to 80°C at 160°C.

- Platinum and palladium dissolution decreased with increased temperature. This was attributed to the decrease in the dielectric properties of water at increased temperature which reduced the degree of hydration of the platinum and palladium. However, ruthenium dissolution increased with increase in temperature.

- Oxygen partial pressure positively influenced the dissolution of all the species. An increase in partial pressure resulted in the increased dissolution of all species. This was attributed to an increase in dissolved oxygen concentration with an increase in oxygen partial pressure.

9.1.2 Leaching reaction Kinetics

The high pressure alkaline oxidation of PGMs amphoteric elements was described by the shrinking core model for diffusion reaction control. The diffusion reaction control was likely due to the formation of an oxide (Fe/PGM) layer on the mineral surface. By analysing the experimental results with the reaction model, the activation energies for sulphur, selenium and arsenic were estimated as 31.8, 26.1 and 10.7 kJ/mol, respectively. The reaction order with respect to [OH^-] for sulphur, selenium and arsenic were found equal to 0.25, 0.12 and 0.21, respectively, while reaction orders of

0.37, 0.29 and 0.36 with respect to [O_2] were obtained for the same respective species.

The mathematical model for the oxygen balance clearly illustrated that the bulk oxygen interfacial mass transfer rate could be a limiting factor at higher slurry densities. This is due to the significant increase in the oxygen demand at higher slurry densities. The kinetic models for the dissolution of sulphur and selenium showed better agreement between experimental and predicted values while the arsenic model poorly predicted extractions.

9.2 Recommendations

From this investigation, the following recommendations are made:

I. Most of the tests in this study were conducted at a low pulp density. Only a few confirmatory runs were conducted at high pulp densities, i.e., resembling the actual plant conditions. In order to have a high degree of confidence in the developed model, further studies should focus on the leaching behaviour at high pulp densities.
II. In order to improve the accuracy of the model, a detailed study of the effect of the process parameters on PGMs dissolution and precipitation kinetics, coupled with PGM's speciation, should be considered.
III. Investigate possible methods for the recovery of dissolved PGMs.
IV. The kinetic model developed in this study could be used to determine the economic impact of PGM losses against product grade for different autoclave operating conditions.

REFERENCES

Alba, R.S., Shah, Y.T., Schumpe, A., 1983. Mass Transfer in Multiphase Agitated Contactors. The Chemical Engineering Journal, 27 61–80.

Allen, T., 1997. Particle size measurement. 5th edition. Chapman and Hall publishers, USA, 204-215.

Anderson, J., 1951. Aqueous oxidation of galena. PhD dissertation, University of British Columbia, Canada.

Azaroual, M., Romand, B., Freyssinet, P., Disnar, J.-R., 2001. Solubility of platinum in aqueous solutions at 25 C and pHs 4 to 10 under oxidising conditions. Geochim. Cosmochim. Acta 65, 4453–4466.

Bailey, L.K., Peters, E., 1976. Decomposition of pyrite in acids by pressure leaching and anodization: the case for an electrochemical mechanism. Can. Metall. Q. 15, 333–344.

Baláž, P., Achimovičová, M., Bastl, Z., Ohtani, T., Sánchez, M., 2000. Influence of mechanical activation on the alkaline leaching of enargite concentrate. Hydrometallurgy 54, 205–216.

Baur, I., Johnson, C.A., 2003. Sorption of selenite and selenate to cement minerals. Environ. Sci. Technol. 37, 3442–3447.

Bhakta, P., Langhans, J.W., Lei, K.P., 1989. Alkaline oxidative leaching of gold-bearing arsenopyrite ores. Bureau of Mines, US Department of the Interior.

Bircumshaw, L., 2008. Base Metal Refinery Process Overview, Lonmin Internal Communication.

Brookins, D.G., 2012. Eh-pH diagrams for geochemistry. Springer Science & Business Media, Berlin.

Brunauer, S., Emmett, P.H., Teller, E., 1938. Adsorption of gases in multimolecular layers. J. Am. Chem. Soc. 60, 309–319.

Buckley, A.., Walker, G.., 1988. The surface composition of arsenopyrite exposed to oxidising environments. Applied Surface Science 35, 227–240.

Chamberlin, A.C. 2008. The calculation of bulk solvation phenomena. PhD dissertation, University of Minnesota.

Castro, S.H., Baltierra, L., 2005. Study of the surface properties of enargite as a function of pH. Int. J. Miner. Process. 77, 104–115.

Cherry, J.A., Shaikh, A.U., Tallman, D.E., Nicholson, R.V., 1979. Arsenic species as an indicator of redox conditions in groundwater. J. Hydrol. 43, 373–392.

Chilton, C., 1958. Leach licks arsenic bugaboo in metal ore. Chem Eng, New York, 65, 80–82.

Chiriţă, P., Popa, I., Duinea, M.I., Schlegel, M.L., 2014. Electrochemical Investigation of the Mechanism of Aqueous Oxidation of Pyrite by Oxygen. Procedia Earth Planet. Sci. 10, 154–158.

Choo, W.L., Jeffrey, M.I., Robertson, S.G., 2006. Analysis of leaching and cementation reaction kinetics: Correcting for volume changes in laboratory studies. Hydrometallurgy 82, 110–116.

Christie, T., Challis, A., 1990. Mineral Commodity Report 5 —Platinum Group Metals (No. 5). Institute of Geological and Nuclear Sciences Ltd.

Ciminelli, V.S.T., Osseo-Asare, K., 1995. Kinetics of pyrite oxidation in sodium hydroxide solutions. Metall. Mater. Trans. B 26, 677–685.

Cooper, C.M., Fernstrom, G.A., Miller, S.A., 1944. Performance of agitated gas-liquid contactors. Ind. Eng. Chem. 36, 504–509.

Cornelis, G., Poppe, S., Van Gerven, T., Van den Broeck, E., Ceulemans, M., Vandecasteele, C., 2008. Geochemical modelling of arsenic and selenium leaching in alkaline water treatment sludge from the production of non-ferrous metals. J. Hazard. Mater. 159, 271–279.

Criss, C.M., Cobble, J.W., 1964a. The thermodynamic properties of high temperature aqueous solutions. IV. Entropies of the ions up to 200° and the correspondence principle. J. Am. Chem. Soc. 86, 5385–5390.

Criss, C.M., Cobble, J.W., 1964b. The Thermodynamic Properties of High Temperature Aqueous Solutions. V. The Calculation of Ionic Heat Capacities up to 2C0. Entropies and Heat Capacities above 200°. J. Am. Chem. Soc. 86, 5390–5393.

Crundwell, F.K., 2013. The dissolution and leaching of minerals. Hydrometallurgy 139, 132–148.

Curreli, L., Ghiani, M., Surracco, M., Orrù, G., 2005. Beneficiation of a gold bearing enargite ore by flotation and As leaching with Na-hypochlorite. Miner. Eng. 18, 849–854.

Deimling, 1984. Solubility and Mass Transfer of CO and H2 in Fischer-Tropsch liquids and slurries. Chemwal Engineering J. 29 127–140.

Deng, T., Lu, Y., Wen, Z., Liu, D., 2001. Oxygenated chloride-assisted leaching of copper residue. Hydrometallurgy 62, 23–30.

Dixon, D.G., Dreisinger, D.B., 2002. Hydrometallurgical process modeling for design and analysis, part II: Leaching kinetics and associated phenomena. Presented at the EPD Congress 2002 and Fundamentals of Advanced Materials for Energy Conversion as held at the 2002 TMS Annual Meeting, pp. 687–708.

Dorfling, C., 2012. Characterisation and dynamic modelling of the behaviour of platinum group metals in high pressure sulphuric acid/oxygen leaching systems (PhD). Stellenbosch University

Dow, P.M., Rimstidt, D.J., 1985. The solubility and stability of scorodite, FeAsO4.H2O. Am. Mineral. 70, 838–844.

Dreisinger, D., Abed, N., 2002. A fundamental study of the reductive leaching of chalcopyrite using metallic iron part I: kinetic analysis. Hydrometallurgy 66, 37–57.

Dresher, W.H., Wadsworth, M.E., Fassell Jr, W.M., 1956. A kinetic study of the leaching of molybdenite.

Fassel, J.W.M., 1962. hyper-atmospheric extractive metallurgy, its past present and future 5, 683–699.

Ferguson, J.F., Gavis, J., 1972. A review of the arsenic cycle in natural waters. Water Res. 6, 1259–1274.

Fernadez, M.., Segarra, M., Espiell, F., 1995. Selective leaching of arsenic and antimony contained in the anode slimes from copper refining. Elsevier 255–267.

Filippou, D., Cheng, T.C.-M., Demopoulos, G.P., 2000. Gas–Liquid Oxygen Mass-transfer; from Fundamentals to Applications in Hydrometallurgical Systems. Miner. Process. Extr. Metall. Rev. 20, 447–502.

Filmer, A.O., Nicol, M.J., 1980. The non-oxidative dissolution of nickel sulphides in aqueous acidic solutions. J. South Afr. Inst. Min. Metall. 12 415–424.

Fuller, E.C., Crist, R.H., 1941. The rate of oxidation of sulfite ions by oxygen. J. Am. Chem. Soc. 63, 1644–1650.

Garcia-Ochoa, F., Gomez, E., 2009. Bioreactor scale-up and oxygen transfer rate in microbial processes: An overview. Biotechnol. Adv. 27, 153–176.

Gbor, P.K., Jia, C.Q., 2004. Critical evaluation of coupling particle size distribution with the shrinking core model. Chem. Eng. Sci. 59, 1979–1987.

Giandomenico, C.M., 1996. Platinum-Group Metals, Compounds. Kirk-Othmer Encycl. Chem. Technol.

Goldberg, R.N., Hepler, L.G., 1968. Thermochemistry and oxidation potentials of the platinum group metals and their compounds. Chem. Rev. 68, 229–252.

Gunn, G., Benham, A., Minks, A., 2009. Platinum Group Elements. British geological survey.

Hackl, P., Ralph, 1995. The leaching and passivation of chalcopyrite in acid sulphate media. University of British Colombia, Vancouver B.C, Canada.

Hackl, R., Dreisinger, D., Peters, E., King, J., 1995. Passivation of chalcopyrite during oxidative leaching in sulfate media. Hydrometallurgy 39, 25–48.

Hamilton, I.., Woods, R., 1981. An investigation of surface oxidation of pyrite and pyrrhotite by linear potential sweep voltammetry. Elsevier Sequoia SA 327–343.

Harold, D.W., Walter, M.B., Joseph, B.H., 1965. Solid solution in the systems ZnS-ZnSe and PbS-PbSe at 300°C and above. The American mineralogist 50, 802–814.

Hartley, F.., 2013. Chemistry of the Platinum Group Metals: Recent Developments. Elsiever Science.

Hartley, F.., 1973. The chemistry of platinum and palladium: with particular reference to complexes of the elements. Wiley, New York.

Heger, K., Uematsu, M., Franck, E., 1980. The static dielectric constant of water at high pressures and temperatures to 500 MPa and 550 C. Berichte Bunsenges. Für Phys. Chem. 84, 758–762.

Herbst, J.A., 1979. Rate processes in multiparticle metallurgical systems, in: Rate Processes of Extractive Metallurgy. Springer, pp. 53–112.

Hermann, R., Walther, N., Maier, U., Büchs, J., 2001. Optical method for the determination of the oxygen-transfer capacity of small bioreactors based on sulfite oxidation. Biotechnol. Bioeng. 74, 355–363.

Hichri, H., Accary, A., Puaux, J.P., Andrieu, J., 1992. Gas-liquid mass-transfer coefficients in a slurry batch reactor equipped with a self-gas-inducing agitator. Ind. Eng. Chem. Res. 31, 1864–1867.

Hiskey, J.B., Sanchez, V.M., 1995. Alkaline pressure oxidation of a gold-bearing arsenopyrite concentrate. Miner. Process. Extr. Metall. Rev. 15, 61–74.

Hoffmann, J.E., 1984. Recovery of selenium from electrolytic copper refinery slimes. Precious Met. Min. Extr. Process. 495–516.

Hou, X., Xiao, L., Gao, C., Zhang, Q., Zeng, L., 2010. Kinetics of leaching selenium from Ni–Mo ore smelter dust using sodium chlorate in a mixture of hydrochloric and sulfuric acids. Hydrometallurgy 104, 76–80.

Inga, J.R., Morsi, B.I., 1997. Effect of catalyst loading on gasliquid mass transfer in a slurry reactor: A statistical experimental approach. Can. J. Chem. Eng. 75, 872–881.

Jeffrey, G.., Basset, J., Mendahm, J., Denney, R.., 1989. Vogel's Qualitative Chemical Analysis, Fifth edition. ed. Longman Scientif and Technology.

Jin, H., Liu, D., Yang, S., He, G., Guo, Z., Tong, Z., 2004. Experimental Study of Oxygen Mass Transfer Coefficient in Bubble Column with High Temperature and High Pressure. Chem. Eng. Technol. 27, 1267–1272.

Kacham, A.R., Suri, A.K., 2014. Application of a topochemical reaction model to predict leaching behavior of high carbonate uranium ores in alkaline solutions: An experimental case study. Hydrometallurgy 141, 67–75.

Karastelev, N., 2013. Modeling of high pressure pretreatment process for gold leaching. Masters dissertation, Lappeenranta University of Technology

Kilic, Y., Kartal, G., Timur, S., 2013. An investigation of copper and selenium recovery from copper anode slimes. Int. J. Miner. Process. 124, 75–82.

Kimweri, H., 2001. Enhancement of gas-liquid mass transfer in hydrometallurgical leaching systems. PhD dissertation, University of British Colombia.

Koslides, T., Ciminelli, V.S.., 1992. Pressure oxidation of arsenopyrite and pyrite in alkaline solutions. Hydrometallurgy,30 87–106.

Kostina, G., Chernyak, A., 1976. Electrochemical conditions for oxidation of pyrite and arsenopyrite in alkaline and acid-solutions. J. Appl. Chem. USSR 49, 1566–1570.

Lamya, R.M., 2007. A fundamental evaluation of the atmospheric pre-leaching section of the nickel-copper matte treatment process.PhD dissertation, Stellenbosch: University of Stellenbosch.

Levenspiel, O., 1972. Chemical Reaction Engineering, Second Edition. ed. John Wiley and Sons, New York, United States of America.

Lewis, W.K., Whitman, W.G., 1924. Principles of gas absorption. Ind. Eng. Chem. 16, 1215–1220.

Linek, V., Vacek, V., 1981. Chemical engineering use of catalysed sulfite oxidation kinetics for the determination of mass transfer characteristics of gas—liquid contactors. Chem. Eng. Sci. 36, 1747–1768.

Linge, H.., Jones, W.., 1993. Electrolytic oxidation of arsenopyrite slurries. Minerals engineering 6, 873–882.

Liu, W., Yang, T., Zhang, D., Chen, L., Liu, Y., 2014. Pretreatment of copper anode slime with alkaline pressure oxidative leaching. Int. J. Miner. Process. 128, 48–54.

Livingstone, S.E., 1975. The Second- and Third-row Elements of Group VIII A, B and C. Comprehensive Inorganic Chemistry. Pergamon, Oxford, 1163-1170.

Li, Y., Kawashima, N., Li, J., Chandra, A.P., Gerson, A.R., 2013. A review of the structure, and fundamental mechanisms and kinetics of the leaching of chalcopyrite. Adv. Colloid Interface Sci. 197-198, 1–32.

Long, H.., 2000. A fundamental study of the acidic pressure oxidation of orpiment and pyrite at high temperature. PhD dissertation, University of British Colombia.

Long, H., Dixon, D.G., 2004. Pressure oxidation of pyrite in sulfuric acid media: a kinetic study. Hydrometallurgy 73, 335–349.

Lowson, R.T., 1982. Aqueous oxidation of pyrite by molecular oxygen. Chem. Rev. 82, 461–497.

Machoň, V., Linek, V., 1974. Effect of salts on the rate of mass transfer across a plane interface between a gas and mechanically agitated aqueous solutions of inorganic electrolytes. Chem. Eng. J. 8, 53–61.

Mao, A., Qiu, G., Deng, Z., Shi, X., Xu, J., Wang, D., 1997. One-step leaching of some refractory gold concentrate containing arsenic and theory analysis. J. Cent. South Univ. Technol. 4, 92–95.

Masel, R.I., 2001. Chemical kinetics and catalysis. Wiley-Interscience, New York.

Masscheleyn, P.H., Delaune, R.D., Patrick Jr, W.H., 1990. Transformations of selenium as affected by sediment oxidation-reduction potential and pH. Environ. Sci. Technol. 24, 91–96.

Mikhlin, Y., Shipin, D., 2003. Electrochemical study of arsenopyrite in acidic media. Presented at the Electrochemistry in Mineral and Metal Processing VI: Proceedings of the International Symposium, The Electrochemical Society, pp. 121–130.

Mikloš, V., Fröhlich, L., 2002. Decomposition of the pyrite and arsenopyrite by pressure oxidation of tetrahedrite raw materials. Metalurgija 41, 29–32.

Mishra, K., Osseo-Asare, K., 1988. Aspects of the interfacial electrochemistry of semiconductor pyrite (FeS2). J. Electrochem. Soc. 135, 2502–2509.

Mountain, B., Wood, S., 1988. Solubility and Transport of Platinum-Group Elements in Hydrothermal Solutions: Thermodynamic and Physical Chemical Constraints, in: Prichard, H.M., Potts, P.J., Bowles, J.F.W., Cribb, S.J. (Eds.), Geo-Platinum 87. Springer Netherlands, pp. 57–82.

Murphy, D., Clark, D., Lentz, C., 1959. Aeration in tower-type fermenters. Can. J. Chem. Eng. 37, 157–161.

Mycroft, J., Bancroft, G., McIntyre, N., Lorimer, J., Hill, I., 1990. Detection of sulphur and polysulphides on electrochemically oxidised pyrite surfaces by X-ray photoelectron spectroscopy and Raman spectroscopy. J. Electroanal. Chem. Interfacial Electrochem. 292, 139–152.

National Research Council (U.S.), 1976. Selenium. National Academy of Sciences.

Nell, J., 2004. Melting of platinum group metal concentrates in South Africa. J. South Afr. Inst. Min. Metall. 104, 423–428.

Nicol, M.J., 1993. The role of electrochemistry in hydrometallurgy, in: Hydrometallurgy, Fundamentals, Technology and Innovations, Proceedings of the Milton E. Wadsworth Fourth International Symposium on Hydrometallurgy. AIME, Society for Mining, Metallurgy and Exploration, Littleton, Colorado. pp. 43–62.

Nicol, M.J., Guresin, N., 2003. Anodic behaviour of arsenopyrite and cathodic reduction of ferrate (VI) and oxygen in alkaline solutions. J. Appl. Electrochem. 33, 1017–1024.

Nicol, M.J., Scott, P.D., 1979. The kinetics and mechanism of the non-oxidative dissolution of some iron sulphides in aqueous acidic solutions. J. South Afr. Inst. Min. Metall. 79, 298–305.

Olle, B., Bucak, S., Holmes, T.C., Bromberg, L., Hatton, T.A., Wang, D.I.C., 2006. Enhancement of Oxygen Mass Transfer Using Functionalized Magnetic Nanoparticles. Ind. Eng. Chem. Res. 45, 4355–4363.

Onken, U., Sick, R., Weiland, P., 1985. Determination of gas-liquid mass transfer by oxidation of hydrazine. Chem. Eng. Sci. 40, 1990–1993.

Otero-Rey, J.R., Mato-Fernández, M.J., Moreda-Piñeiro, J., Alonso-Rodríguez, E., Muniategui-Lorenzo, S., López-Mahía, P., Prada-Rodríguez, D., 2005. Influence of several experimental parameters on As and Se leaching from coal fly ash samples. Anal. Chim. Acta 531, 299–305.

Papangelakis, V., Berk, D., Demopoulos, G., 1990. Mathematical modeling of an exothermic leaching reaction system: pressure oxidation of wide size arsenopyrite participates. Metall. Trans. B 21, 827–837.

Papangelakis, V., Demopoulos, G., 1991. Acid pressure oxidation of pyrite: reaction kinetics. Hydrometallurgy 26, 309–325.

Parada, F., Jeffrey, M.I., Asselin, E., 2014. Leaching kinetics of enargite in alkaline sodium sulphide solutions. Hydrometallurgy 146, 48–58.

Peters, E., 1992. Hydrometallurgical process innovation. Elsevier Sci. Publ. BV Amst. 431–459.

Peters, E., 1991. The mathematical modeling of leaching systems. JOM 43, 20–26.

Phillips, D.H., Johnson, M.J., 1959. Oxygen transfer in agitated vessels. Ind. Eng. Chem. 51, 83–88.

Pourbaix, M.J.., Muylder, V.J., Zoubov, N. d., 1956. Electrochemical properties of the Platinum metals. Cent. Belge Etude Corros., 3 3, 100–106.

Prosser, A.P., 1996. Review of uncertainty in the collection and interpretation of leaching data. Hydrometallurgy 41, 119–153.

Rappas, A.S., Waterman, B.T., 1990. Processes for the treatment of smelter flue dust. Patent US4891067.

Renner, H., 2001. Platinum Group Metals and Compounds,: Wiley & Co (Ed.), Ullmann’s Encyclopedia of Industrial Chemistry. Wiley-VCH Verlag GmbH & Co. KGaA, Weinheim, Germany.

Rieger, P.., 2012. Electrochemistry, 2nd ed. Springer Science & Business Media.

Rimstidt, J.D., Vaughan, D.J., 2003. Pyrite oxidation: a state-of-the-art assessment of the reaction mechanism. Geochim. Cosmochim. Acta 67, 873–880.

Robinson, R., Engel, A., 1967. Analysis of controlled cycling mass transfer operations. Ind. Eng. Chem. 59, 22–29.

Roxburgh, J., 1962. Studies on fermentation aeration: II. Catalyst effects on sulphite oxidation rates. Can. J. Chem. Eng. 40, 127–130.

Rubidge, G.R., 2007. Evaluation and optimisation of selected methods of arsenic removal from industrial effluent. PhD dissertation, Port Elizabeth Technical.

Ruiz, M.C., Grandon, L., Padilla, R., 2014. Selective arsenic removal from enargite by alkaline digestion and water leaching. Hydrometallurgy 150, 20–26.

Saydut, A., Duz, M.Z., Erdogan, S., Tonbul, Y., Hamamci, C., 2011. Chemical Leaching on Sulfur and Mineral Matter Removal from Asphaltite (Harbul, SE Anatolia, Turkey). Energy Sources Part Recovery Util. Environ. Eff. 33, 383–391.

Scott, M.J., 1991. Kinetics of adsorption and redox processes on iron and manganese oxides: reactions of As (III) and Se (IV) at goethite and birnessite surfaces. PhD dissertation, California Institute of Technology.

Shukla, S.K., 1958. The study of rhodium (III) complexes by paper electrophoresis and ion-exchange chromatography: III. Rhodium (III) in perchlroric acid. J. Chromatogr. A 1, 457–460.

Sill, H., 1960. Process for treating complex ores. U.S. Patent 2,951,741.

Smith, E., Shumate, K.., 1970. Sulphide to sulphate reaction mechanism. Water pollution control series. No. 14010 FPS. Ohio state university.

Steenekamp, N., Dunn, G., 1999. Operations of and improvements to the Lonrho platinum base metal refinery. Presented at the EPD Congress 1999, pp. 365–378.

Stenhouse, J.F., Armstrong, W., 1952. The aqueous oxidation of pyrite. Can Inst Min. Met Bull 49–53.

Stenstrom, M.K., Gilbert, R.G., 1981. Effects of alpha, beta and theta factor upon the design, specification and operation of aeration systems. Water Res. 15, 643–654.

Steyl, J., 2012. Simulating the medium temperature chalcopyrite oxidation system in batch and continuous autoclaves. PhD dissertation, Stellenbosch University.

Stokes, H.N., 1907. Experiments on the action of various solutions on pyrite and marcasite. J. Am. Chem. Soc. 29, 307–314.

Subramanian, K.N., Bell, M.C., Thomas, J.A., Nissen, N.C., 1980. Process for the recovery of metal values from anode slimes.

Subramanian, K.N., Illis, A., Nissen, N.C., 1979. Recovery of selenium. US. Patent 4,229,270.

Suresh, S., Srivastava, V., Mishra, I., 2009. Techniques for oxygen transfer measurement in bioreactors: a review. J. Chem. Technol. Biotechnol. 84, 1091–1103.

Taylor, P., Amoah-Forson, B., 2008. Kinetic behaviour of arsenopyrite in alkaline autoclave oxidation. Society of mining, Metallurgy and explorations. Colorado, 990-995.

Taylor, P.R., Martins, G., 1986. Reactor Design for Aqueous--Solid Reactions. Hydrometall. React. Des. Kinet. 105–119.

Thomas, J.A., Nissen, N.C., Bell, M.C., Illis, A., 1986. Hydrometallurgical processing of precious metal-containing materials. European Patent 0049169 A3.

Tromas, D., 1998a. Temperature and Pressure Dependence of Oxygen in water. Hydrometall. 48 3278–342.

Tromas, D., 1998b. Oxygen solubility modeling in inorganic solutions: concentration, temperature and pressure effects. Hydrometall. 50 279–296.

Viñals, J., Roca, A., Hernández, M.., Benavente, O., 2003. Topochemical transformation of enargite into copper oxide by hypochlorite leaching. Hydrometallurgy 68, 183–193.

Virčíkova, E., Fedor, J., 1991. Leaching behaviour of arsenic trisulphide with sodium hydroxide solution. Hydrometallurgy 27, 1–6.

Wadsworth, M.E., 1979. Rate Process of Extractive Metallurgy. Plenum Press. New York and London.

Watari, K., Imai, K., Takeshita, H., Hatsushiba, K., 1994. Adsorption of High Oxidation State Ruthenium Anions on Filter Paper. J. Nucl. Sci. Technol. 31, 253–254.

Westerterp, K., Van Dierendonck, L., De Kraa, J., 1963. Interfacial areas in agitated gas-liquid contactors. Chem. Eng. Sci. 18, 157–176.

Whitman, W.G., 1962. The two film theory of gas absorption. Int. J. Heat Mass Transf. 5, 429–433.

Wood, S.A., 1991. Experimental determination of the hydrolysis constants of Pt2+ and Pd2+ at 25°C from the solubility of Pt and Pd in aqueous hydroxide solutions. Geochim Cosmochin. Acta, 55 1759–1767.

Yang, J.D., Wang, N.S., 1992. Oxygen mass transfer enhancement via fermentor headspace pressurization. Biotechnol. Prog. 8, 244–251.

Yang, W.-J., 1982. Gas-liquid mass transfer in rotating perforated-disc contactors. Lett. Heat Mass Transf. 9, 119–129.

Yu, G., Zhang, Y., Zheng, S., Zou, X., Wang, X., Zhang, Y., 2014. Extraction of arsenic from arsenic-containing cobalt and nickel slag and preparation of arsenic-bearing compounds. Trans. Nonferrous Met. Soc. China 24, 1918–1927.

Zemaitis, J., Clark, D., Raphal, M., Scrivner, N., 1986. Handbook of Aqueous Electrolyte Thermodynamics. Design Institute for Physical Property Data (DIPPR), New York.

Zheng, Y., Chen, K., 2013. Leaching kinetics of selenium from selenium−tellurium-rich materials in sodium sulfite solutions. Trans Nonferrous Met Soc China 24, 536–543.

Appendix I

Thermodynamic data for E_h-pH diagrams

Table I 1: Thermodynamic data for S-H_2O at 25°C

ROUGH ESTIMATES	T (Cp)	H (25°C)	kcal/mol	S (25°C)	cal/(mol*K)	Cp	cal/(mol*K)
Chemical Formula	°C	Estimate	Database	Estimate	Database	Estimate	Database
H2O	25.00	-68.75	-68.32	8.47	16.72	17.99	17.98
H2O(l)	25.00	-52.99	-68.32	24.00	16.72	15.48	17.98
S	25.00	0.00	0.00	7.71	7.66	5.12	5.42
H2(a)	25.00	-19.50	-1.00	N/A	13.80	N/A	39.76
H(+a)	25.00	2.55	0.00	N/A	0.00	N/A	0.00
HS(-a)	25.00	1.14	-3.85	N/A	16.01	N/A	-22.38
HS2O7(-a)	25.00	-366.07	-299.67	N/A	313.40	N/A	0.00
O2(a)	25.00	-44.75	-2.80	N/A	26.51	N/A	54.77
O3(a)	25.00	-73.72	30.09	N/A	34.90	N/A	9.38
O(-a)	25.00	-33.18	8.94	N/A	-3.97	N/A	27.82
O2(-a)	25.00	-62.15	12.72	N/A	9.94	N/A	0.00
O2(-2a)	25.00	-74.55	120.00	N/A	46.40	N/A	0.00
O2(-3a)	25.00	-85.25	-2.80	N/A	26.51	N/A	0.00
OH(a)	25.00	-32.13	-1.19	N/A	15.49	N/A	0.00
OH(-a)	25.00	-49.53	-54.98	N/A	-2.56	N/A	-32.42
S2O4(-2a)	25.00	-198.86	-180.10	N/A	22.00	N/A	-49.64
S3O3(-2a)	25.00	-174.02	-227.39	N/A	28.20	N/A	0.00
S5O3(-2a)	25.00	-201.65	-277.17	N/A	39.20	N/A	0.00
S5O6(-2a)	25.00	-317.62	-281.00	N/A	40.00	N/A	-38.91

Table I 2: Thermodynamic data for Se-H_2O at 25°C

ROUGH ESTIMATES	T (Cp)	H (25°C)	kcal/mol	S (25°C)	cal/(mol*K)	Cp	cal/(mol*K)
Chemical Formula	°C	Estimate	Database	Estimate	Database	Estimate	Database
H2O	25.00	-68.75	-68.32	8.47	16.72	17.99	17.98
H2SeO3	25.00	-140.91	-125.40	26.96	20.00	23.42	0.00
Se	25.00	0.00	0.00	11.03	10.14	5.80	5.98
H2Se(a)	25.00	18.49	3.42	N/A	35.53	N/A	0.00
HSe(-a)	25.00	17.44	3.80	N/A	19.00	N/A	-19.55
HSeO3(a)	25.00	-104.97	-121.29	N/A	49.70	N/A	35.08
H2SeO3(a)	25.00	-121.32	-121.29	N/A	49.70	N/A	35.08
H2SeO4(a)	25.00	-142.45	-145.30	N/A	5.70	N/A	0.00
HSeO3(-a)	25.00	-122.37	-122.98	N/A	32.30	N/A	6.59
HSeO4(-a)	25.00	-143.50	-139.00	N/A	35.70	N/A	12.16
O2(a)	25.00	-44.75	-2.80	N/A	26.51	N/A	54.77
OH(-a)	25.00	-49.53	-54.98	N/A	-2.56	N/A	-32.42
Se(-2a)	25.00	21.38	30.91	N/A	20.00	N/A	0.00
SeO3(-2a)	25.00	-118.42	-121.70	N/A	3.10	N/A	-60.87
SeO4(-2a)	25.00	-139.56	-143.20	N/A	12.90	N/A	-55.10

Table I 3: Thermodynamic data for As-H_2O at 25°C

ROUGH ESTIMATES	T (Cp)	H (25°C)	kcal/mol	S (25°C)	cal/(mol*K)	Cp	cal/(mol*K)
Chemical Formula	°C	Estimate	Database	Estimate	Database	Estimate	Database
As	25.00	0.00	0.00	8.72	8.53	5.96	5.90
As2O3	25.00	-140.55	-156.50	27.88	27.96	24.41	23.15
As2O4	25.00	-179.61	-191.10	31.76	36.00	28.56	22.61
H2O	25.00	-68.75	-68.32	8.47	16.72	17.99	17.98
AsH3(a)	25.00	-95.48	11.76	N/A	30.20	N/A	44.53
AsO3(-3a)	25.00	-173.85	-158.70	N/A	-44.69	N/A	0.00
AsO4(-3a)	25.00	-202.83	-212.27	N/A	-38.90	N/A	-115.19
HAsO2(a)	25.00	-120.73	-109.11	N/A	30.10	N/A	2.96
H3AsO4(a)	25.00	-211.37	-216.20	N/A	44.00	N/A	25.73
HAsO3(-2a)	25.00	-179.50	-164.67	N/A	-3.59	N/A	0.00
HAsO4(-2a)	25.00	-208.47	-216.62	N/A	-0.40	N/A	-47.04
H2AsO3(-a)	25.00	-183.45	-172.32	N/A	26.40	N/A	-2.76
H2AsO4(-a)	25.00	-212.42	-217.39	N/A	28.00	N/A	-0.47
O2(a)	25.00	-44.75	-2.80	N/A	26.51	N/A	54.77
OH(-a)	25.00	-49.53	-54.98	N/A	-2.56	N/A	-32.42

Appendix II

Analytical methods

9.2.1 A. Inductively coupled plasma – optical emission spectroscopy (ICP-OES)

Inductively coupled plasma – optical emission spectroscopy (ICP-OES) was used for total metal concentration analysis (solution samples). ICP-OES is the oldest multi elemental atomic spectrometric technique. The analytical application is based on the spontaneous emission of photons from gaseous atoms and ions that have been generated from the sample and then thermally excited. The excited atom or ion only emits light of a certain wavelength. This leads to producing specific atomic or ionic spectra, enabling qualitative evaluation of elements in a sample. A calibration curve relating the intensity spectra line with the concentration can be used for the quantification of a given element. In principle, the emission source should provide a high rate of atomisation and excitation of as many elements as possible, including those with low and high excitation energy.

9.2.2 B. X-Ray Diffraction (XRD)

X-Ray Diffraction method was used to identify the atomic and molecular structure of crystals (feed and residue). This method is the most basic method for characterising the crystal structures. The method is based on measuring X-ray intensities scattered by the statistically distributed electrons belonging to the atoms in the material. X-ray diffractometers is made up of three basic elements: an X-ray tube, a sample holder, and an X-ray detector. The cathode ray tube generates the X-rays by heating a filament producing electrons. The electrons are accelerating towards a target by applying a voltage which bombards the target material with electrons. Characteristic X-ray spectra are produced when the electrons have enough energy to dislodge the inner shell electrons of the material. A detector records and processes the X-ray signal and converts the signal to a count rate, which is then output to a device such as a printer or computer monitor.

9.2.3 C. Scanning Electron Microscope (SEM)

Bulk elemental composition and backscattered electron (BSE) imaging

A representative sample (feed or residue) was mounted in resin which was polished and coated with carbon. The carbon coating was due to the fact that gold was an element of interest and as such the sample could not be coated with gold. In a scanning electron microscope (SEM), a tiny electron beam is focussed onto the sample. Simultaneous to scanning the beam across a selected sample area, generated signals are being recorded and thereby an image is formed pixel by pixel. Minerals possess different chemical compositions, and thus have different grey levels based upon the average atomic number. Heavier particles have higher, BSE brightness than gangue minerals, which are less dense. SEM does not need huge samples and as such, tiny and compact samples can thus be investigated by SEM. Valuable information about morphology, surface topology and composition were obtained using this method.

Appendix III

Wet chemistry

Standard solutions preparations

Starch indicator

- 1 g soluble starch was prepared by adding the soluble paste to boiling distilled water while constantly stirring.
- The starch solution was boiled for approximately 5 minute (until the solution became clear).
- The starch solution was allowed to cool to room temperature
- Approximately 3g of potassium iodide was added to preserve the starch indicator
- The starch solution was stored in a dark cupboard.

Iodine solution (0.2 N)

- 40 g of potassium iodide (KI) crystals, was dissolved in 30 mL water in a 1-litre glass-stoppered volumetric flask
- 25.5 g resublimed iodine (I2) was weighed and transferred to the KI solution.
- The flask was shaken after inserting the stopper until all the iodine crystals had dissolved (Visual observation).
- The solution was diluted to the 1-litre mark with distilled water

Standardising the iodine solution

Iodine crystals are known to be volatile. As such, it was necessary to standardise it before use. This was done using already prepared thiosulphate solution. The standardising procedure is as below:

- 10 mL of the prepared iodine solution was pipetted into a 500 mL conical flask to which 50 mL of distilled water was added.
- The solution in conical flask was titrated thiosulfate solution until a light yellow colour appeared
- 1 mL starch indicator was added and the solution turned dark blue

- The Titration was continued until the disappearance of the dark blue colour (solution was almost colourless)
- The volume of thiosulphate used was recorded at the end point and iodine concentration was calculated according to Equation below III-1.

$$2S_2O_3^{2-} + I_2 = S_4O_6^{2-} + 2I^- \qquad \text{III-1}$$

Thiosulfate solution (0.1 N)

- 25 g of sodium thiosulphate crystals ($Na_2S_2O.5H_2O$) was weighed and dissolved in boiled-out distilled water.
- 0.1g of 0.1 g sodium carbonate was added to the solution -recommended if the solution is to be kept for a few days (Jeffrey et al. 1989).
- The graduated flask was made up to a 1 L mark with boiled-out water.
- This resulting concentration of thiosulphate solution was approximately 0.1 mol/kg
- The solution was stored in a dark container

Hydrochloric acid (2 M)

- 171 mL of pure concentrated hydrochloric acid (37% w/w) was measured by means of a burette
- The acid was poured into a 1 L volumetric flask containing about 500 mL of distilled water.
- The flask was made up to the litre mark with distilled water and thoroughly mixes by shaking.
- This resulted into a solution that is approximately 2 M.

Sulfite ($SO3^{2-}$) titration

The titration of sulfite ion was used to determine the rate of interfacial oxygen mass transfer between the gas and solution phase in a reaction vessel. This section describes the iodometric back-titration method used to determine the residual sulfite concentration in a stirred reactor over time.

- 50 mL standardised 0.2 N iodine solution was added to a 10 mL acid solution (2 M HCl) in a 250 mL conical flask.
- The 4 mL aliquot sulfite sample was then added to the iodine solution (stoichiometric excess).
- The solution was swirled gently and left in a dark place for about 15 minutes. This permitted complete oxidation of sulfite ion to occur.
- The unreacted iodine in the flask was then titrated against thiosulfate solution (0.1N) until the dark yellow-orange colour of the tri-iodide ion had almost disappeared.
- A 3 mL starch solution was added at this point and caused solution to turn to the deep purple colour of the starch-tri-iodide complex.
- Titration was continued right up to a point when the solution changed to an almost colourless form.
- The end-point was recorded and the overall reaction stoichiometry was used to calculate the amount of iodine that had reacted with the sulfite aliquot. This value was, in turn, used to calculate the concentration of sulfite ion that was initially present in the sample from the reactor.

Appendix IV

Table A 1: Particle size analysis and surface area calculations of PGM-rich leach residue

Sieve Aperture Size	Mass % Undersize	Mean Sieve size	Mass fraction	Mass fraction between Sieves	$\sum q_r/-d_{Ar}$
d_{Ar}(µm)	$\sum q_r$	$-d_{Ar}$(µm)		q_r	
0.7	0.239	0.000	0.002	0.0000	0
0.8	0.920	0.748	0.009	0.0068	0.009
0.9	0.946	0.849	0.009	0.0003	0.009
1	0.946	0.949	0.009	0.0000	0.009
2	2.010	1.414	0.020	0.0106	0.017
3	3.096	2.449	0.031	0.0109	0.021
4	4.058	3.464	0.041	0.0096	0.024
5	4.970	4.472	0.050	0.0091	0.026
6	5.786	5.477	0.058	0.0082	0.028
7	6.463	6.481	0.065	0.0068	0.029
8	7.065	7.483	0.071	0.0060	0.030
9	7.669	8.485	0.077	0.0060	0.030
10	8.350	9.487	0.083	0.0068	0.031
20	14.868	14.142	0.149	0.0652	0.036
30	21.531	24.495	0.215	0.0666	0.038
40	28.845	34.641	0.288	0.0731	0.040
50	36.198	44.721	0.362	0.0735	0.042
53	38.348	51.478	0.383	0.0215	0.042
60	43.174	56.391	0.432	0.0483	0.043
70	49.429	64.807	0.494	0.0625	0.044
80	54.663	74.833	0.547	0.0523	0.045
90	58.973	84.853	0.590	0.0431	0.045
100	62.673	94.868	0.627	0.0370	0.046
120	68.972	109.545	0.690	0.0630	0.046
150	75.847	134.164	0.758	0.0687	0.047
200	84.132	173.205	0.841	0.0829	0.047
250	92.169	223.607	0.922	0.0804	0.048
300	97.655	273.861	0.977	0.0549	0.048
400	99.995	346.410	1.000	0.0234	0.048

Assuming particle is spherical, volume shape factor	6
S_v= volume specific surface area, m^2m^{-3}	0.288
Density of mineral, g/cm^3	3.8
A=Specific surface area, m^2/g	0.08

Appendix V

9.2.4 Mass transfer test results

This appendix is the summary of the oxygen mass transfer test results. The tests were carried out in the 2 litre autoclave Figure 6.1 which was aimed at identifying the physical absorption regime using the chemical (indirect) method.
The following gives the results generated to identify the physical absorption regime.

Table A 2: Mass transfer tests MT1 at 1 mg/L Co(II) and 500 rev/min

Test ID	Temp °C	Imp speed (rev/min)	Gauge pressure (Kpa)	Gas $\%O_2$	Co(II) mg/L
MT_1	~60	500	100	100	1

$[SO_3^{2-}]$ (mol/L)	Aliquot vol (mL)	[Iondine] (N)	Iodine vol (mL)	[Thiosulphate] (N)
~1.2	4	0.201	50	0.099

Time (min)	Temp °C	Thiosulphate (mL)	Density (g/L)	$[SO_3^{2-}]$ remaining (mol/kg)	O_2 reacted (mg/kg)	$[O_2]$* (mg/kg)
0	60	14.5	1129	1.07	0	22.4
5	60	20.5	1129	0.990	1357	22.4
10	60	25.0	1129	0.927	2359	22.4
15	60	30.5	1130	0.851	3577	22.4
20	60	36.5	1130	0.771	4867	22.4
30	60	46.3	1133	0.640	6953	22.4
40	60	56.7	1134	0.508	9072	22.4

Table A 3: Mass transfer tests MT2 at 1 mg/L Co(II) and 500 rev/min

Test ID	Temp °C	Imp speed (rev/min)	Gauge pressure (Kpa)	Gas $\%O_2$	Co(II) mg/L
MT_2	~60	750	100	100	1

$[SO_3^{2-}]$ (mol/L)	Aliquot vol (mL)	[Iondine] (N)	Iodine vol (mL)	[Thiosulphate] (N)
~1.2	4	0.201	50	0.099

Time (min)	Temp °C	Thiosulphate (mL)	Density (g/L)	$[SO_3^{2-}]$ remaining (mol/kg)	O_2 reacted (mg/kg)	$[O_2]^*$ (mg/kg)
0	60	34	1129	0.80	0	22.4
5	60	43	1129	0.686	1908	22.4
10	60	51.5	1130	0.575	3671	22.4
15	60	61.5	1130	0.450	5677	22.4
20	60	69.8	1130	0.349	7297	22.4
30	60	88.5	1133	0.129	10814	22.4

Table A 4: Mass transfer tests MT_{3A} at 5 mg/L Co(II) and 500 rev/min

Test ID	Temp °C	Imp speed (rev/min)	Gauge pressure (Kpa)	Gas $\%O_2$	Co(II) mg/L
MT_1	~60	500	100	100	5

$[SO_3^{2-}]$ (mol/L)	Aliquot vol (mL)	[Iondine] (N)	Iodine vol (mL)	[Thiosulphate] (N)
~1.2	4	0.201	50	0.099

Time (min)	Temp °C	Thiosulphate (mL)	Density (g/L)	$[SO_3^{2-}]$ remaining (mol/kg)	O_2 reacted (mg/kg)	$[O_2]^*$ (mg/kg)
0	60	20.0	1128	1.00	0	22.4
5	60	27.7	1129	0.890	1708	22.4
10	60	33.5	1129	0.812	2967	22.4
15	60	39.2	1129	0.735	4195	22.4
20	60	45.0	1130	0.659	5409	22.4
30	60	60.0	1130	0.467	8476	22.4
40	60	72.5	1133	0.315	10909	22.4

Table A 5: Mass transfer tests MT_{3B} at 5 mg/L Co(II) and 500 rev/min

Test ID	Temp °C	Imp speed (rev/min)	Gauge pressure (Kpa)	Gas $\%O_2$	Co(II) mg/L
MT_2	~60	500	100	100	5
$[SO_3^{2-}]$ (mol/L)	Aliquot vol (mL)	[Iondine] (N)	Iodine vol (mL)	[Thiosulphate] (N)	
~1.2	4	0.201	50	0.099	

Time (min)	Temp °C	Thiosulphate (mL)	Density (g/L)	$[SO_3^{2-}]$ remaining (mol/kg)	O_2 reacted (mg/kg)	$[O_2]$* (mg/kg)
0	60	20.6	1128	0.99	0	22.4
5	60	27.3	1128	0.896	1501	22.4
10	60	32.9	1129	0.820	2719	22.4
15	60	39.6	1129	0.729	4172	22.4
20	60	44.8	1131	0.661	5259	22.4
30	60	60.4	1131	0.462	8436	22.4
40	60	72.0	1133	0.321	10695	22.4

Table A 6: Mass transfer tests MT_{4A} at 5 mg/L Co(II) and 750 rev/min

Test ID	Temp °C	Imp speed (rev/min)	Gauge pressure (Kpa)	Gas $\%O_2$	Co(II) mg/L
MT_1	~60	750	100	100	5
$[SO_3^{2-}]$ (mol/L)	Aliquot vol (mL)	[Iondine] (N)	Iodine vol (mL)	[Thiosulphate] (N)	
~1.2	4	0.201	50	0.099	

Time (min)	Temp °C	Thiosulphate (mL)	Density (g/L)	$[SO_3^{2-}]$ remaining (mol/kg)	O_2 reacted (mg/kg)	$[O_2]$* (mg/kg)
0	60	32.0	1129	0.83	0	22.4
5	60	40.0	1130	0.724	1720	22.4
10	60	49.0	1131	0.607	3600	22.4
15	60	58.0	1131	0.493	5420	22.4
20	60	67.0	1133	0.382	7203	22.4
30	60	85.0	1134	0.169	10607	22.4

Table A 7: Mass transfer tests $MT4_B$ at 5 mg/L Co(II) and 750 rev/min

Test ID	Temp °C	Imp speed (rev/min)	Gauge pressure (Kpa)	Gas $\%O_2$	Co(II) mg/L
MT_2	~60	750	100	100	5

$[SO_3^{2-}]$ (mol/L)	Aliquot vol (mL)	[Iondine] (N)	Iodine vol (mL)	[Thiosulphate] (N)
~1.2	4	0.201	50	0.099

Time (min)	Temp °C	Thiosulphate (mL)	Density (g/L)	$[SO_3^{2-}]$ remaining (mol/kg)	O_2 reacted (mg/kg)	$[O_2]$* (mg/kg)
0	60	30	1129	0.86	0	22.4
5	60	38	1130	0.751	1731	22.4
10	60	47.2	1131	0.630	3664	22.4
15	60	58.6	1131	0.486	5973	22.4
20	60	65.2	1133	0.403	7287	22.4
30	60	82.9	1134	0.193	10653	22.4

Table A 8: Mass transfer tests MT5 at 5 mg/L Co(II) and 1000 rev/min

Test ID	Temp °C	Imp speed (rev/min)	Gauge pressure (kPa)	Gas $\%O_2$	Co(II) mg/L
MT_5	~60	1000	100	100	5

$[SO_3^{2-}]$ (mol/L)	Aliquot vol (mL)	[Iodine] (N)	Iodine vol (mL)	[Thiosulphate] (N)
~1.2	4	0.201	50	0.099

Time (min)	Temp °C	Thiosulphate (mL)	Density (g/L)	$[SO_3^{2-}]$ remaining (mol/kg)	O_2 reacted (mg/kg)	$[O_2]$* (mg/kg)
0	60	28.3	1129	0.88	0	22.4
5	60	49.5	1131	0.600	4507	22.4
10	60	67	1132	0.382	8002	22.4
15	60	91	1133	0.101	12504	22.4

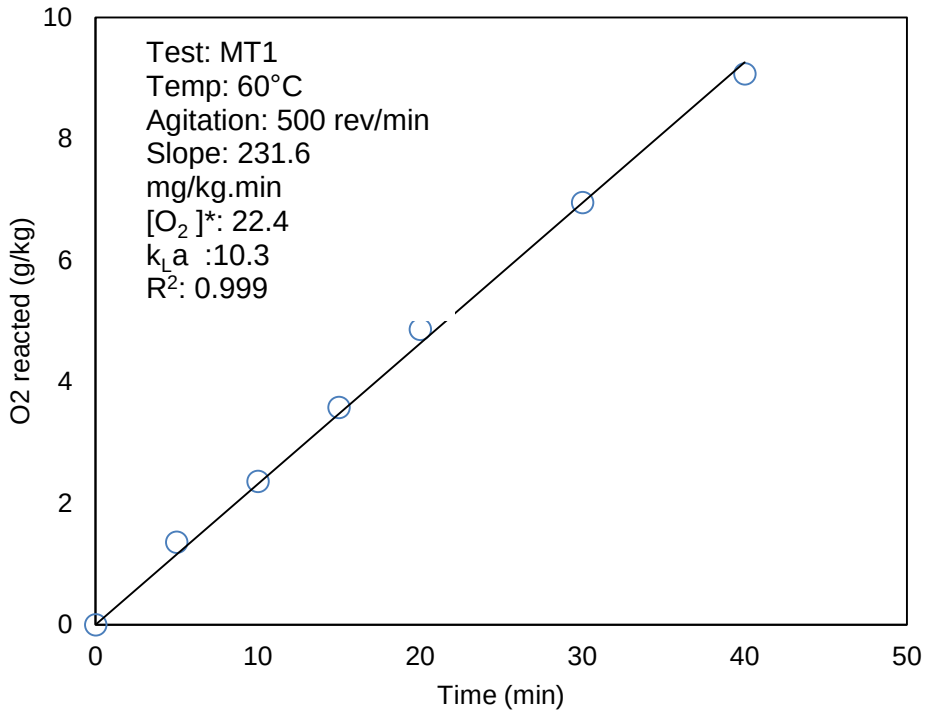

Figure A 1: Mass transfer Test with 1 mg/L Co^{2+} at 500 rev/min

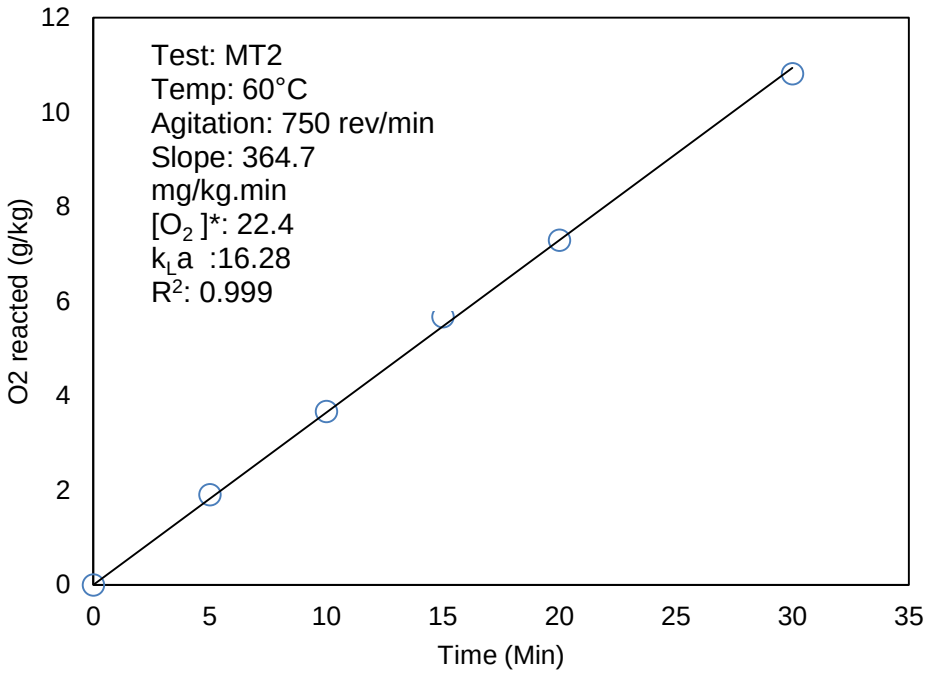

Figure A 2: Mass transfer Test with 1 mg/L Co^{2+} at 750 rev/min

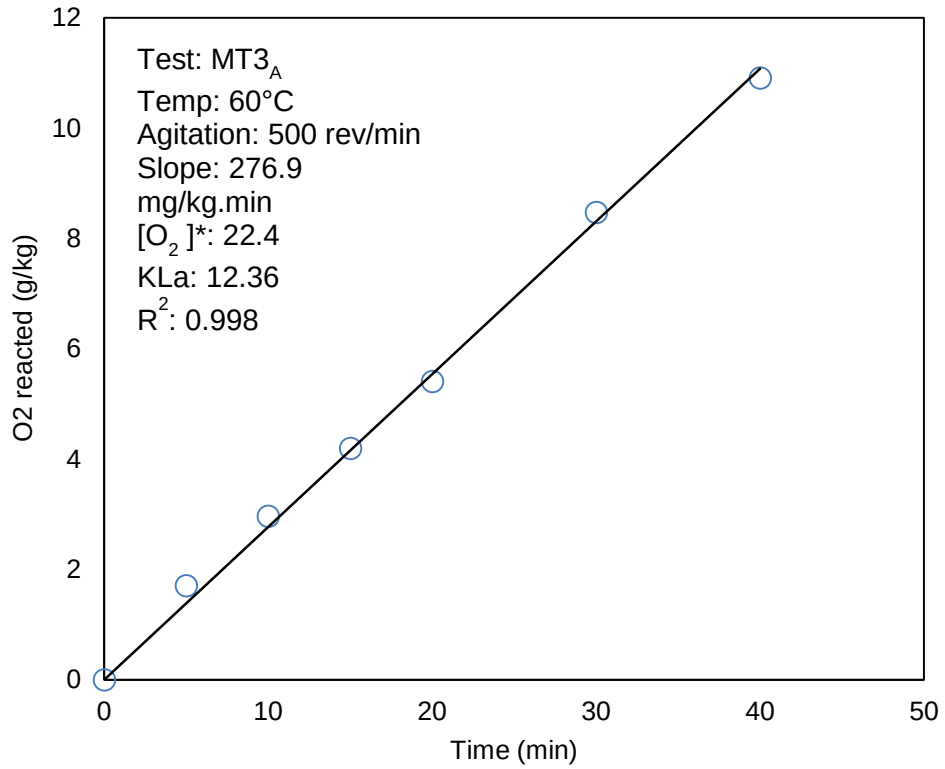

Figure A 3: Mass transfer Test with 5 mg/L Co^{2+} at 500 rev/min

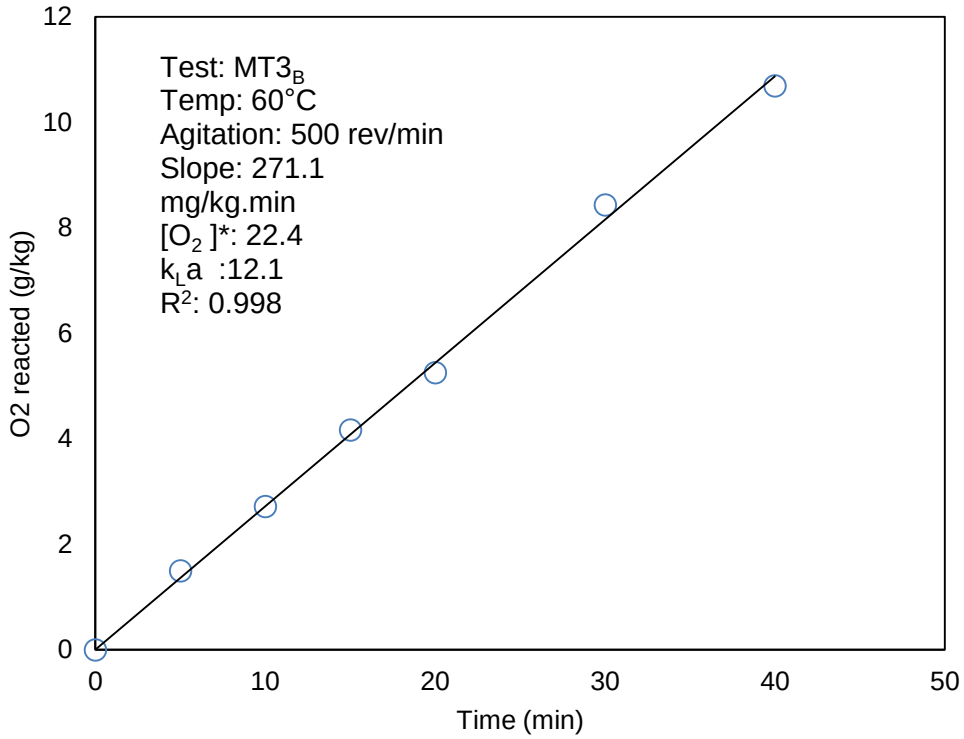

Figure A 4: Mass transfer Test with 5 mg/L Co^{2+} at 500 rev/min

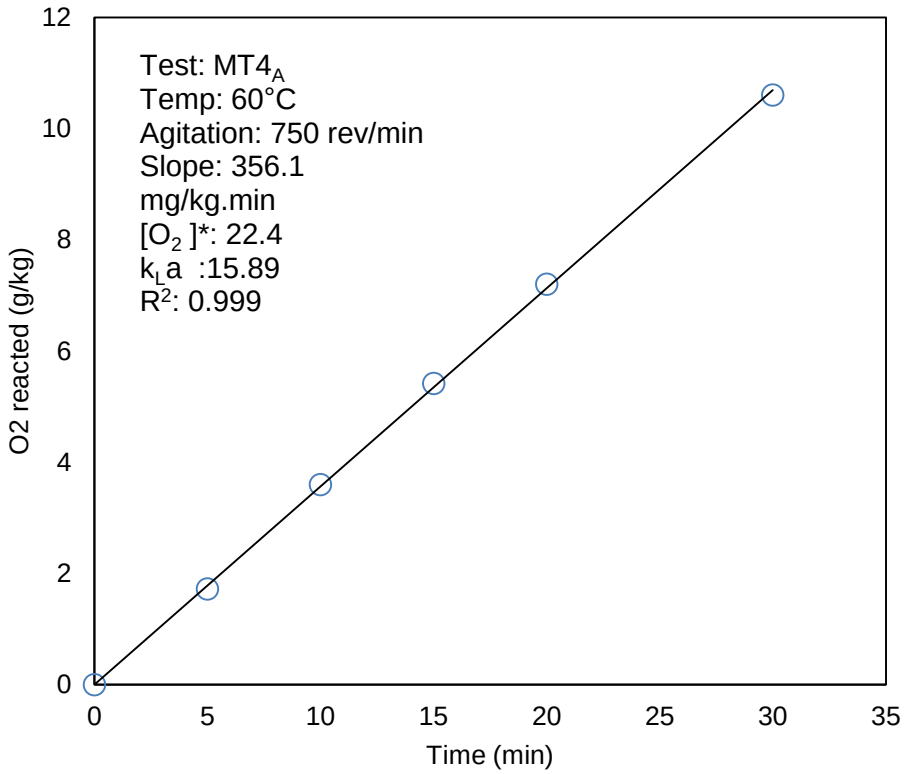

Figure A 5: Mass transfer Test with 5 mg/L Co^{2+} at 750 rev/min

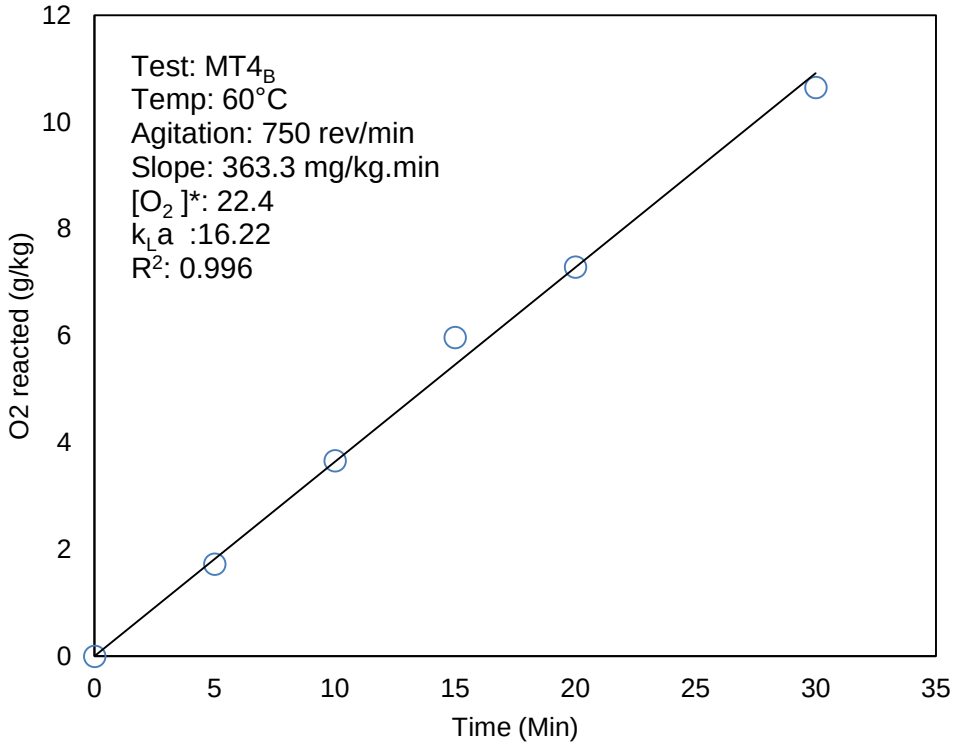

Figure A 6: Mass transfer Test with 1mg/L Co^{2+} at 750rev/min

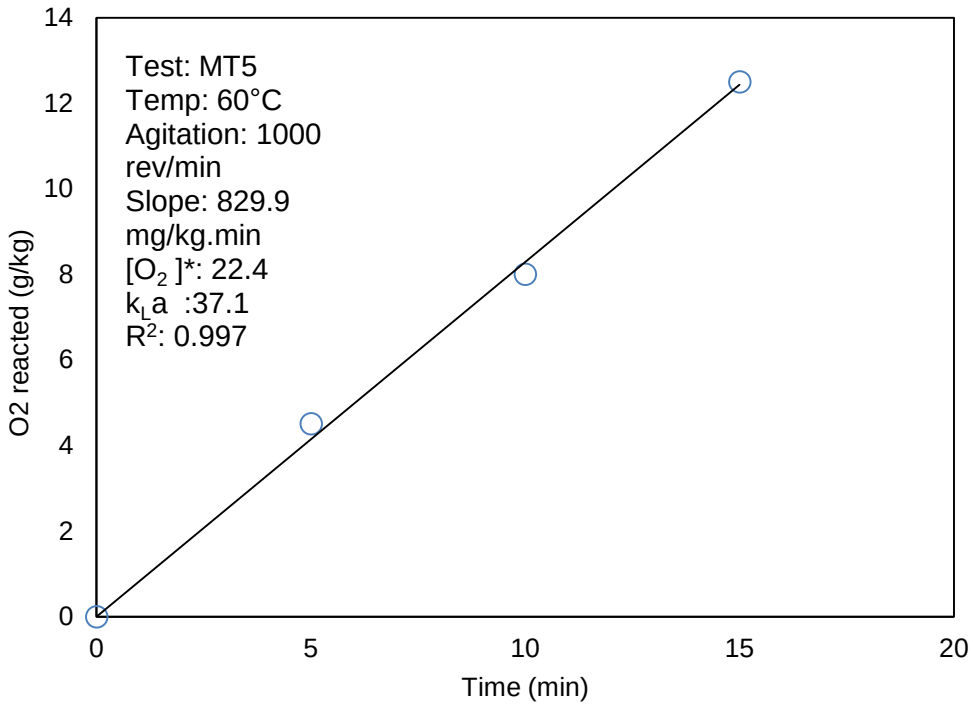

Figure A 7: Mass transfer Test with 1mg/L Co^{2+} at 500rev/min

Appendix VI

9.2.5 Leaching experimental data and results

Table A 9: Low pulp density leaching test at 0.125 mol/L, 160°C, 11 atm O_2 partial pressure

Test No	NaOH conc	Temp	P_g	PO_2	solids	solids	Density	Impeller speed
1	0.125 mol/L	160°C	20 atm	11 atm	1 wt %	10g	-	750 rev/min
Time	Temp	P_g	pH	Eh	Density	S extraction	Se extraction	As extraction
Min	°C	atm		mV	g/L	%	%	%
0	163	20	13.6	500	-	0.00	0.00	0.00
10	160	20	13.6	503	1.006	0.65	0.65	0.59
20	160	19	13.5	502	1.014	0.67	0.72	0.63
30	160	18	13.5	508	1.021	0.70	0.74	0.66
45	159	20	13.4	510	1.028	0.76	0.77	0.69
60	160	20	13.2	511	1.036	0.78	0.78	0.70

Table A 10: Low pulp density leaching test at 0.125 mol/L, 175°C, 11 atm O_2 partial pressure

Test No	NaOH conc	Temp	P_g	PO_2	solids	solids	Density	Impeller speed
2	0.125 mol/L	175°C	20 atm	11 atm	1 wt %	10g	-	750 rev/min
Time	Temp	P_g	pH	Eh	Density	S extraction	Se extraction	As extraction
Min	°C	atm		mV	g/L	%	%	%
0	175	20	13.3	506	-	0.00	0.00	0.00
10	174	20	13.2	500	1.012	0.67	0.78	0.62
20	175	20	13.0	512	1.018	0.71	0.81	0.65
30	175	20	12.8	516	1.022	0.74	0.84	0.68
45	175	20	12.6	518	1.027	0.77	0.87	0.71
60	175	20	12.5	515	1.038	0.81	0.91	0.72

Table A 11: Low pulp density leaching test at 0.125 mol/L, 190°C, 11 atm O_2 partial pressure

Test No	NaOH conc	Temp	P_g	PO_2	solids	solids	Density	Impeller speed
3	0.125 mol/L	190°C	20 atm	11 atm	1 wt %	10g		750 rev/min
Time	Temp	P_g	pH	Eh	Density	S extraction	Se extraction	As extraction
Min	°C	atm		mV	g/L	%	%	%
0	192	20	13.9	500	-	0.00	0.00	0.00
10	189	20	13.8	500	1.013	0.79	0.80	0.65
20	190	20	13.5	502	1.017	0.84	0.83	0.67
30	190	20	13.4	499	1.026	0.87	0.87	0.69
45	190	20	13.4	510	1.029	0.91	0.89	0.72
60	190	20	13.2	515	1.037	0.94	0.91	0.75

Table A 12: Low pulp density leaching test at 0.125 mol/L, 160°C, 11 atm O_2 partial pressure

Test No	NaOH conc	Temp	P_g	PO_2	solids	solids	Density	Impeller speed
4	0.25 mol/L	160°C	20 atm	11 atm	1 wt %	10g	-	750 rev/min
Time	Temp	P_g	pH	Eh	Density	S extraction	Se extraction	As extraction
Min	°C	atm		mV	g/L	%	%	%
0	162	20	14.5	500	-	0.00	0.00	0.00
10	160	19	14.5	510	1.016	0.66	0.69	0.62
20	160	20	14.3	517	1.021	0.68	0.73	0.65
30	160	20	14.3	521	1.026	0.72	0.75	0.69
45	160	20	14.2	525	1.028	0.78	0.78	0.70
60	160	20	14.1	527	1.040	0.81	0.81	0.72

Table A 13: Low pulp density leaching test at 0.25 mol/L, 175°C, 11 atm O_2 partial pressure

Test No	NaOH conc	Temp	P_g	PO_2	solids	solids	Density	Impeller speed
5	0.25 mol/L	175°C	20 atm	11 atm	1 wt %	10g		750 rev/min
Time	Temp	P_g	pH	Eh	Density	S extraction	Se extraction	As extraction
Min	°C	atm		mV	g/L	%	%	%
0	176	20	14.3	503	-	0.00	0.00	0.00
10	174	20	14.2	510	1.018	0.71	0.80	0.67
20	175	19	14.3	519	1.023	0.77	0.84	0.70
30	175	20	14.0	525	1.027	0.79	0.87	0.73
45	175	19	13.9	528	1.031	0.82	0.91	0.74
60	175	20	13.9	531	1.038	0.83	0.94	0.75

Table A 14: Low pulp density leaching test at 0.25 mol/L, 190°C, 11 atm O_2 partial pressure

Test No	NaOH conc	Temp	P_g	PO_2	solids	solids	Density	Impeller speed
6	0.25 mol/L	190°C	20 atm	11 atm	1 wt %	10g	-	750 rev/min
Time	Temp	P_g	pH	Eh	Density	S extraction	Se extraction	As extraction
Min	°C	atm		mV	g/L	%	%	%
0	190	20	14.0	507		0.00	0.00	0.00
10	190	20	14.1	510	1.021	0.81	0.83	0.67
20	190	20	13.9	512	1.026	0.86	0.85	0.71
30	190	20	13.8	506	1.032	0.88	0.87	0.73
45	190	20	13.9	513	1.037	0.91	0.91	0.75
60	190	20	13.7	516	1.044	0.95	0.94	0.76

Table A 15: Low pulp density leaching test at 0.5 mol/L, 160°C, 11 atm O_2 partial pressure

Test No	NaOH conc	Temp	P_g	PO_2	solids	solids	Density	Impeller speed
7	0.5 mol/L	160°C	20 atm	11 atm	1 wt %	10g	-	750 rev/min
Time	Temp	P_g	pH	Eh	Density	S extraction	Se extraction	As extraction
Min	°C	atm		mV	g/L	%	%	%
0	160	20	14.7	503		0.00	0.00	0.00
10	160	20	14.5	507	1.027	0.76	0.77	0.65
20	159	20	14.5	501	1.033	0.80	0.79	0.69
30	160	20	14.5	509	1.038	0.83	0.82	0.74
45	159	20	14.4	513	1.042	0.84	0.82	0.77
60	160	20	14.4	517	1.046	0.86	0.84	0.77

Table A 16: Low pulp density leaching test at 0.5 mol/L, 175°C, 11 atm O_2 partial pressure

Test No	NaOH conc	Temp	P_g	PO_2	solids	solids	Density	Impeller speed
8	0.5 mol/L	175°C	20 atm	11 atm	1 wt %	10g	-	750 rev/min
Time	Temp	P_g	pH	Eh	Density	S extraction	Se extraction	As extraction
Min	°C	atm		mV	g/L	%	%	%
0	174	21	14.9	510		0.00	0.00	0.00
10	175	20	14.7	511	1.031	0.75	0.81	0.69
20	175	19	17.7	511	1.034	0.80	0.86	0.73
30	175	20	14.6	513	1.037	0.83	0.89	0.76
45	175	20	14.7	507	1.045	0.87	0.91	0.79
60	175	20	14.6	509	1.049	0.89	0.95	0.80

Table A 17: Low pulp density leaching test at 0.5 mol/L, 190°C, 11 atm O_2 partial pressure

Test No	NaOH conc	Temp	P_g	PO_2	solids	solids	Density	Impeller speed
9	0.5 mol/L	190°C	20 atm	11 atm	1 wt %	10g	-	750 rev/min
Time	Temp	P_g	pH	Eh	Density	S extraction	Se extraction	As extraction
Min	°C	atm		mV	g/L	%	%	%
0	190	20	14.7	507		0.00	0.00	0.00
10	189	20	14.5	511	1.025	0.85	0.84	0.72
20	190	20	14.5	513	1.031	0.90	0.87	0.76
30	190	19	14.4	517	1.039	0.94	0.90	0.77
45	190	20	14.4	521	1.047	0.95	0.91	0.81
60	190	20	14.3	523	1.053	0.96	0.96	0.83

Table A 18: Low pulp density leaching test at 0.125 mol/L, 160°C, 11 atm O_2 partial pressure

Test No	NaOH conc	Temp	P_g	PO_2	solids	solids	Density	Impeller speed
1A	0.125 mol/L	160°C	20 atm	11 atm	1 wt %	10g	-	750 rev/min
Time	Temp	P_g	pH	Eh	Density	S extraction	Se extraction	As extraction
Min	°C	atm		mV	g/L	%	%	%
0	160	20	13.8	487		0.00	0.00	0.00
10	160	20	13.6	493	1.007	0.63	0.66	0.58
20	160	20	13.5	499	1.01	0.66	0.73	0.63
30	160	20	13.3	503	1.023	0.71	0.75	0.66
45	159	20	13.2	507	1.029	0.75	0.76	0.70
60	160	20	13.2	511	1.033	0.79	0.79	0.71

Table A 19: Low pulp density leaching test at 0.125 mol/L, 175°C, 11 atm O_2 partial pressure

Test No	NaOH conc	Temp	P_g	PO_2	solids	solids	Density	Impeller speed
2A	0.125 mol/L	175°C	20 atm	11 atm	1 wt %	10g	-	750 rev/min
Time	Temp	P_g	pH	Eh	Density	S extraction	Se extraction	As extraction
Min	°C	atm		mV	g/L	%	%	%
0	176	20	13.4	500		0.00	0.00	0.00
10	174	20	13.3	506	1.016	0.68	0.76	0.60
20	175	20	13.1	511	1.021	0.71	0.80	0.65
30	175	20	12.9	516	1.024	0.76	0.85	0.68
45	175	20	12.6	518	1.027	0.78	0.87	0.70
60	175	20	12.6	521	1.035	0.82	0.89	0.72

Table A 20: Low pulp density leaching test at 0.125 mol/L, 190°C, 11 atm O_2 partial pressure

Test No	NaOH conc	Temp	P_g	PO_2	solids	solids	Density	Impeller speed
3A	0.125 mol/L	190°C	20 atm	11 atm	1 wt %	10g	-	750 rev/min
Time	Temp	P_g	pH	Eh	Density	S extraction	Se extraction	As extraction
Min	°C	atm		mV	g/L	%	%	%
0	188	20	13.8	499		0.00	0.00	0.00
10	189	20	13.5	504	1.010	0.79	0.81	0.66
20	191	20	13.4	507	1.015	0.83	0.83	0.68
30	190	20	12.1	512	1.022	0.85	0.87	0.70
45	190	20	12.9	515	1.026	0.89	0.91	0.72
60	190	20	12.7	516	1.033	0.93	0.93	0.75

Table A 21: Low pulp density leaching test at 0.25 mol/L, 160°C, 11 atm O_2 partial pressure

Test No	NaOH conc	Temp	P_g	PO_2	solids	solids	Density	Impeller speed
4A	0.25 mol/L	160°C	20 atm	11 atm	1 wt %	10g	-	750 rev/min
Time	Temp	P_g	pH	Eh	Density	S extraction	Se extraction	As extraction
Min	°C	atm		mV	g/L	%	%	%
0	162	20	14.1	503		0.00	0.00	0.00
10	160	19	14.0	510	1.017	0.67	0.67	0.62
20	160	20	14.0	516	1.021	0.69	0.71	0.64
30	160	20	13.8	523	1.027	0.72	0.74	0.68
45	160	20	13.7	526	1.029	0.76	0.76	0.71
60	160	20	13.8	527	1.037	0.79	0.79	0.73

Table A 22: Low pulp density leaching test at 0.25 mol/L, 175°C, 11 atm O_2 partial pressure

Test No	NaOH conc	Temp	P_g	PO_2	solids	solids	Density	Impeller speed
5A	0.25 mol/L	175°C	20 atm	11 atm	1 wt %	10g	-	750 rev/min
Time	Temp	P_g	pH	Eh	Density	S extraction	Se extraction	As extraction
Min	°C	atm		mV	g/L	%	%	%
0	177	20	14.0	504		0.00	0.00	0.00
10	175	19	13.9	507	1.017	0.70	0.79	0.67
20	174	20	13.9	514	1.02	0.75	0.84	0.72
30	175	20	13.8	519	1.024	0.79	0.88	0.74
45	175	20	13.7	523	1.038	0.81	0.91	0.75
60	175	20	13.7	529	1.035	0.83	0.95	0.77

Table A 23: Low pulp density leaching test at 0.25 mol/L, 190°C, 11 atm O_2 partial pressure

Test No	NaOH conc	Temp	P_g	PO_2	solids	solids	Density	Impeller speed
6A	0.25 mol/L	190°C	20 atm	11 atm	1 wt %	10g	-	750 rev/min
Time	Temp	P_g	pH	Eh	Density	S extraction	Se extraction	As extraction
Min	°C	atm		mV	g/L	%	%	%
0	191	20	14.2	504		0.00	0.00	0.00
10	190	19	14.0	511	1.018	0.82	0.81	0.64
20	190	20	13.9	513	1.025	0.86	0.83	0.69
30	190	20	13.8	516	1.031	0.89	0.86	0.71
45	190	20	13.9	517	1.035	0.92	0.89	0.74
60	190	20	13.7	516	1.043	0.95	0.93	0.76

Table A 24: Low pulp density leaching test at 0.5 mol/L, 160°C, 11 atm O_2 partial pressure

Test No	NaOH conc	Temp	P_g	PO_2	solids	solids	Density	Impeller speed
7A	0.5 mol/L	160°C	20 atm	11 atm	1 wt %	10g	-	750 rev/min
Time	Temp	P_g	pH	Eh	Density	S extraction	Se extraction	As extraction
Min	°C	atm		mV	g/L	%	%	%
0	160	20	14.9	504		0.00	0.00	0.00
10	160	20	14.6	508	1.025	0.77	0.77	0.65
20	160	20	14.5	512	1.034	0.79	0.81	0.69
30	160	20	14.3	515	1.039	0.84	0.83	0.74
45	160	20	14.2	516	1.043	0.86	0.85	0.77
60	160	20	14.1	516	1.046	0.87	0.86	0.79

Table A 25: Low pulp density leaching test at 0.5 mol/L, 175°C, 11 atm O_2 partial pressure

Test No	NaOH conc	Temp	P_g	PO_2	solids	solids	Density	Impeller speed
8A	0.5 mol/L	175°C	20 atm	11 atm	1 wt %	10g	-	750 rev/min
Time	Temp	P_g	pH	Eh	Density	S extraction	Se extraction	As extraction
Min	°C	atm		mV	g/L	%	%	%
0	175	21	14.5	511		0.00	0.00	0.00
10	174	20	14.4	513	1.028	0.75	0.83	0.70
20	175	19	14.2	512	1.033	0.78	0.86	0.73
30	175	20	14.2	516	1.035	0.81	0.91	0.75
45	175	20	14.1	519	1.038	0.85	0.93	0.77
60	175	20	13.9	521	1.044	0.88	0.95	0.80

Table A 26: Low pulp density leaching test at 0.125 mol/L, 175°C, 11 atm O_2 partial pressure

Test No	NaOH conc	Temp	P_g	PO_2	solids	solids	Density	Impeller speed
9A	0.5 mol/L	190°C	20 atm	11 atm	1 wt %	10g	-	750 rev/min
Time	Temp	P_g	pH	Eh	Density	S extraction	Se extraction	As extraction
Min	°C	atm		mV	g/L	%	%	%
0	189	20	14.8	506		0.00	0.00	0.00
10	189	20	14.6	511	1.022	0.83	0.85	0.72
20	190	20	14.4	513	1.028	0.87	0.87	0.74
30	190	20	14.3	516	1.035	0.92	0.90	0.77
45	190	20	14.4	521	1.044	0.94	0.93	0.81
60	190	20	14.2	527	1.049	0.95	0.96	0.84

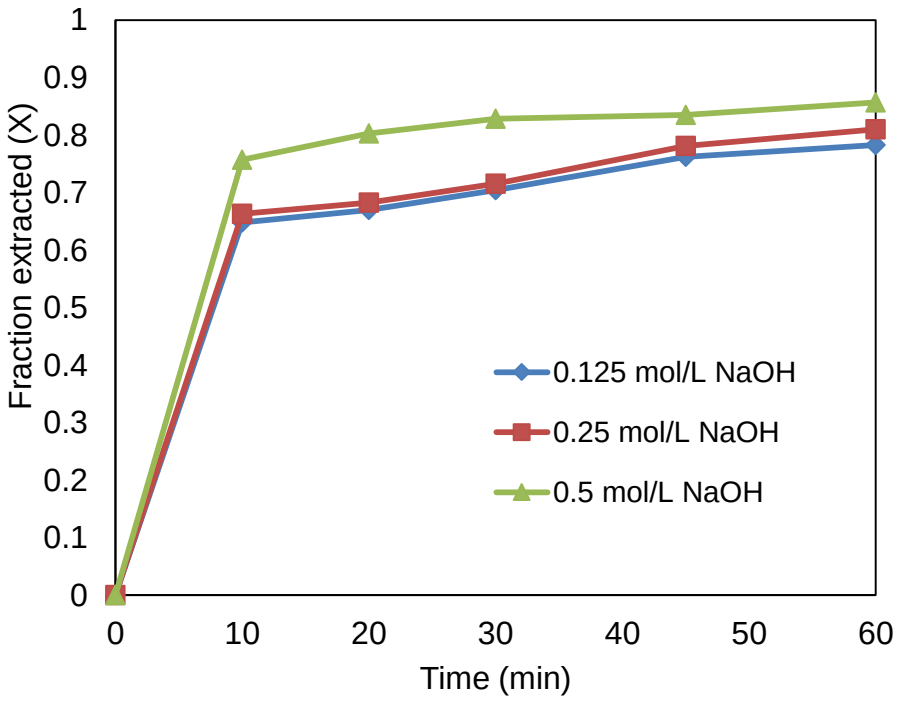

Figure A 8: Effect of NaOH concentration on sulphur extraction (Temperature 160°C; 10 g/L solids; 750 rev/min; 11 atm O_2 pressure)

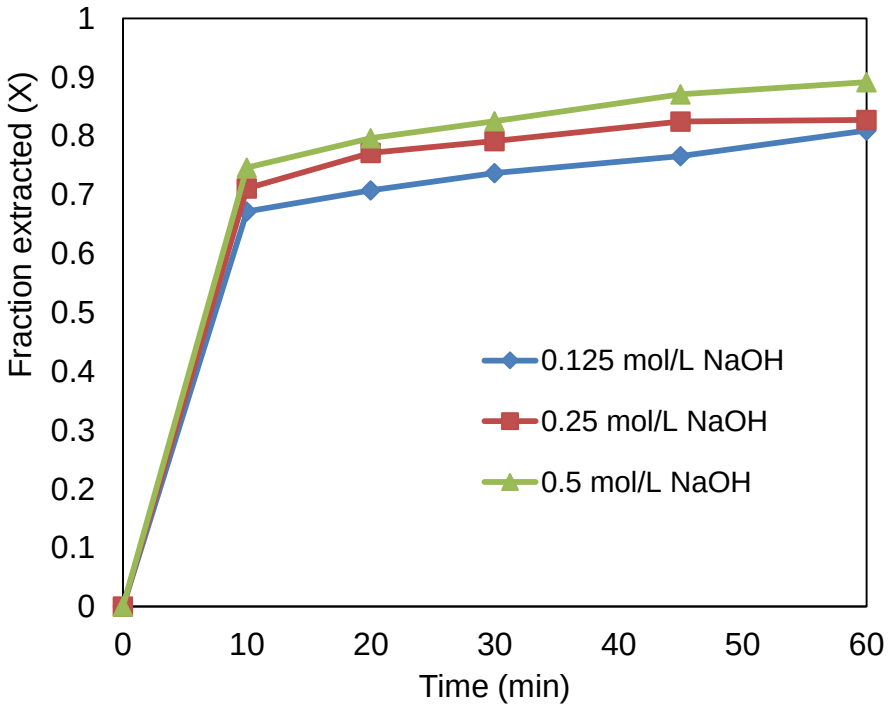

Figure A 9: Effect of NaOH concentration on sulphur extraction (Temperature 175°C; 10 g/L solids; 750 rev/min; 11 atm O_2 pressure)

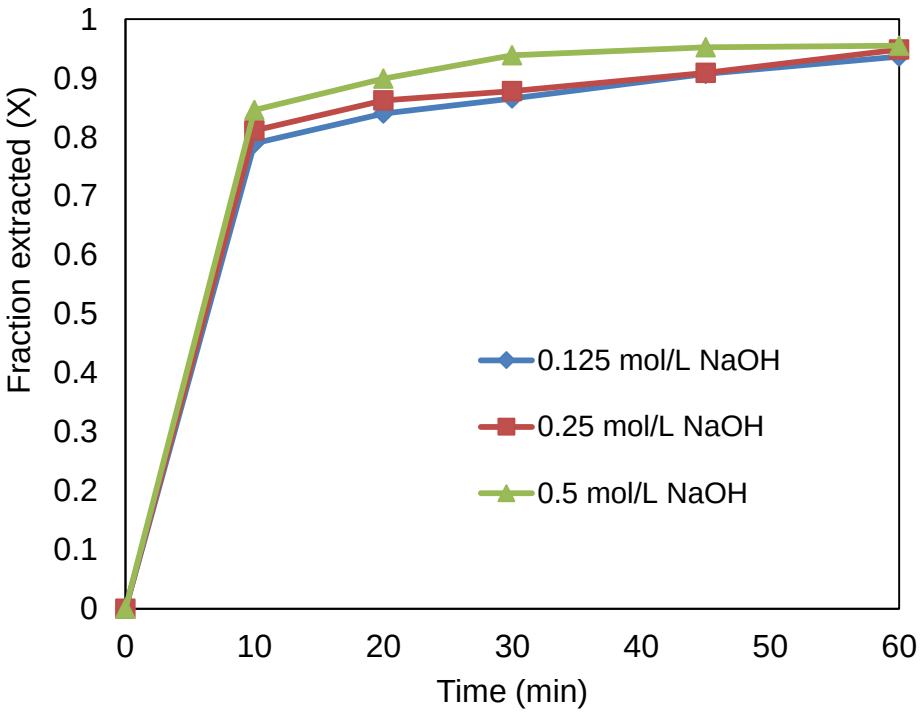

Figure A 10: Effect of NaOH concentration on sulphur extraction (Temperature 190°C; 10 g/L solids; 750 rev/min; 11 atm O_2 pressure)

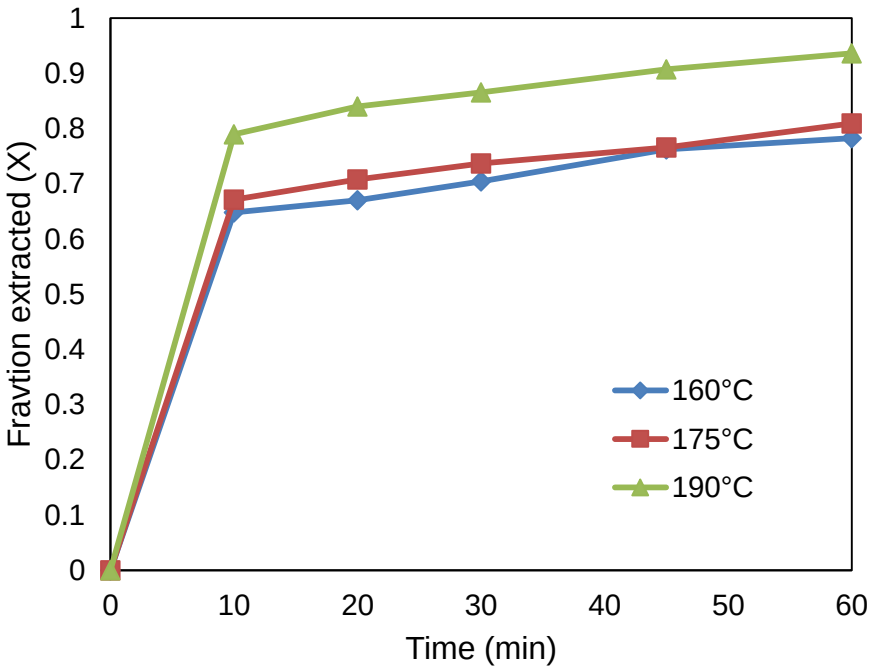

Figure A 11: Effect of temperature on sulphur extraction with 0.125mol/L NaOH (10 g/L solids; 750 rev/min; 11 atm O_2 pressure)

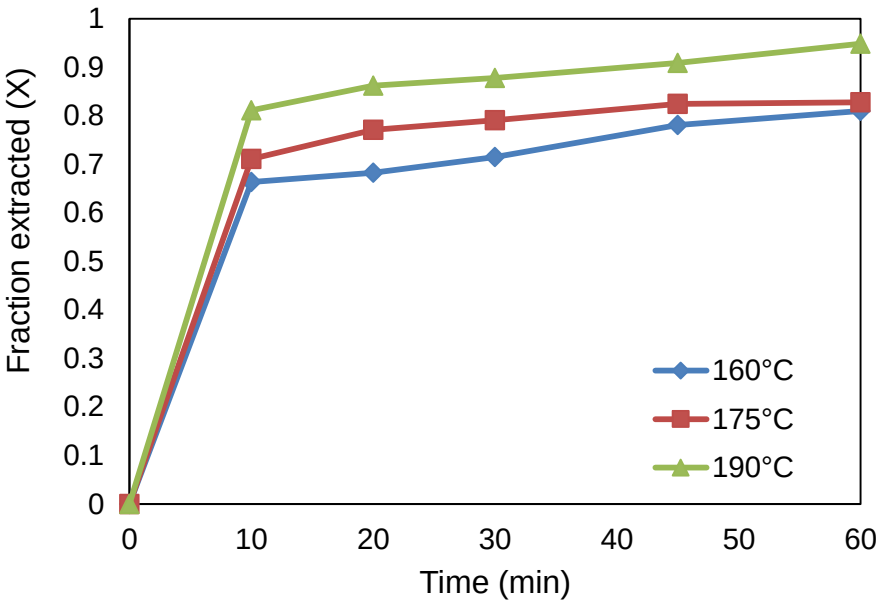

Figure A 12: Effect of temperature on arsenic extraction with 0.25 mol/L NaOH (10 g/L solids; 750 rev/min; 11 atm O_2 pressure)

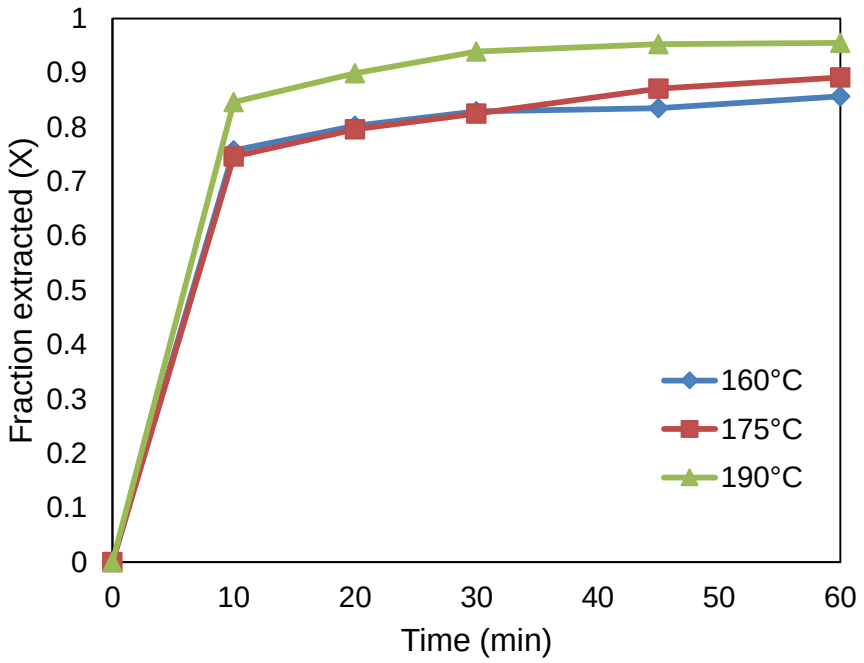

Figure A 13: Effect of temperature on sulphur extraction with 0.5 mol/L NaOH (10 g/L solids; 750 rev/min; 11 atm O_2 pressure)

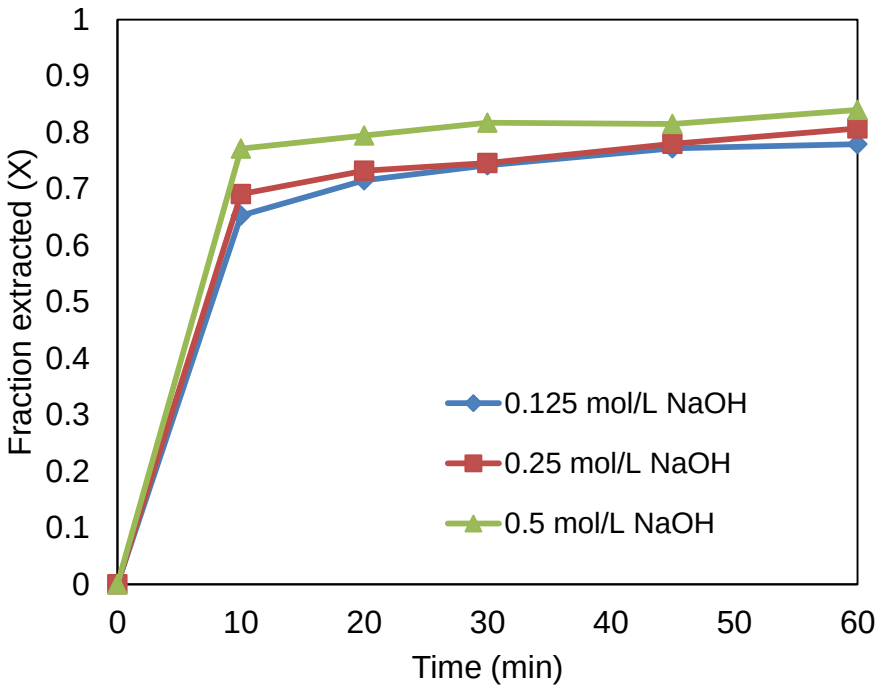

Figure A 14: Effect of NaOH concentration on selenium extraction (Temperature 160°C; 10 g/L solids; 750 rev/min; 11 atm O_2 pressure)

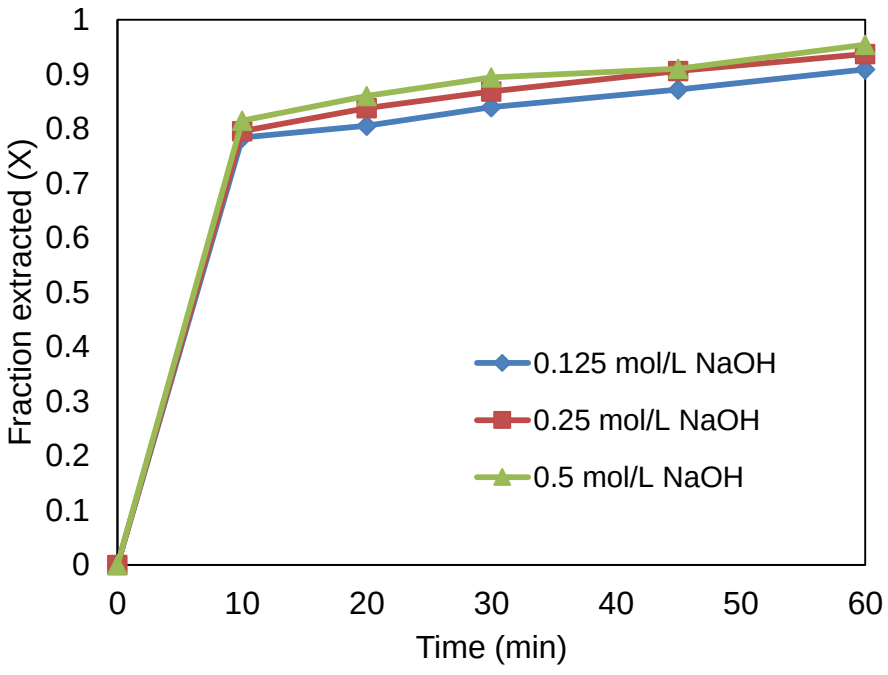

Figure A 15: Effect of NaOH concentration on selenium extraction (Temperature 175°C; 10 g/L solids; 750 rev/min; 11 atm O_2 pressure)

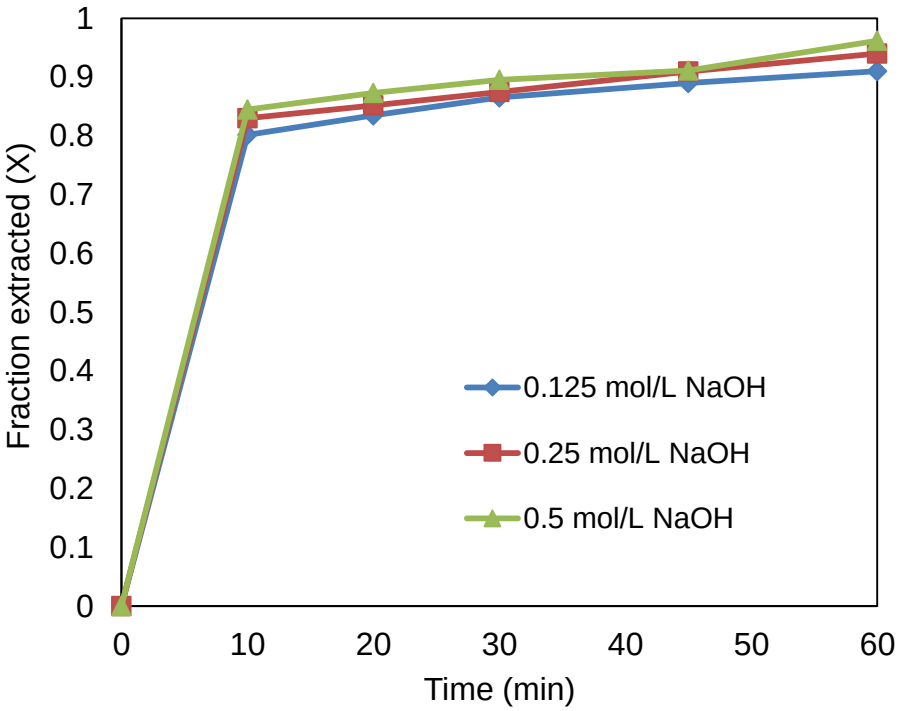

Figure A 16: Effect of NaOH concentration on selenium extraction (Temperature 190°C; 10 g/L solids; 750 rev/min; 11 atm O_2 pressure)

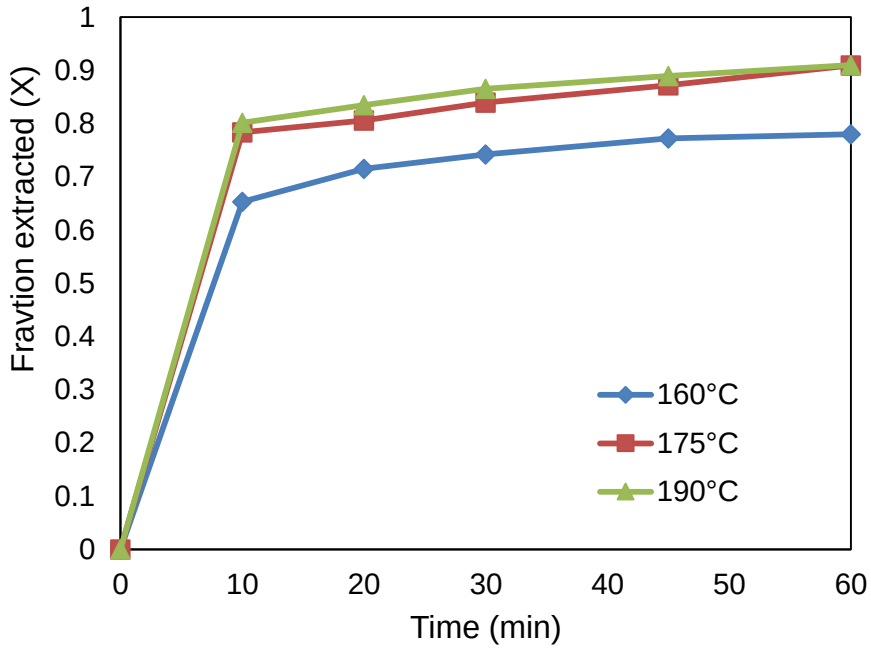

Figure A 17: Effect of temperature on selenium extraction with 0.125mol/L NaOH (10 g/L solids; 750 rev/min; 11 atm O_2 pressure)

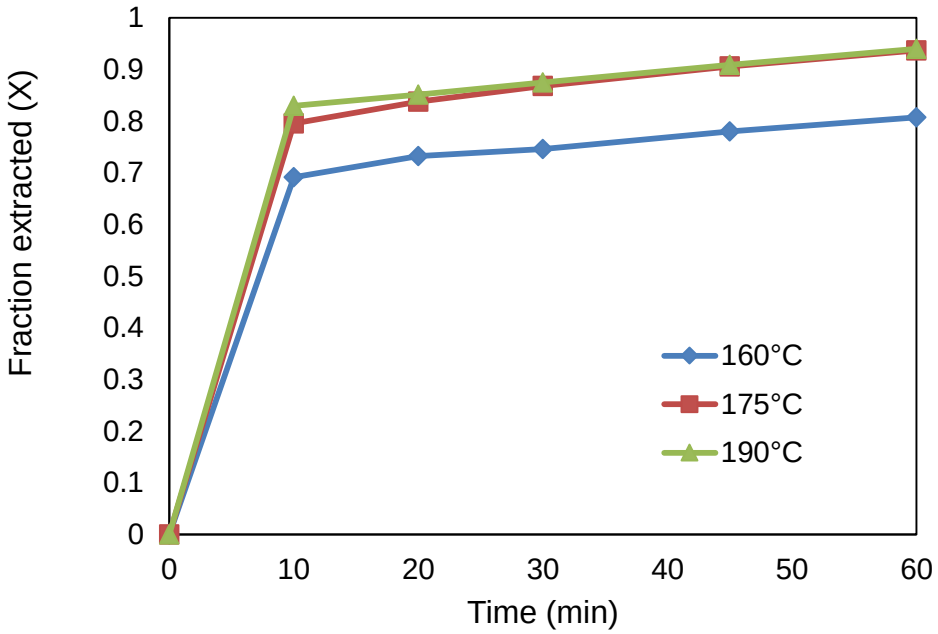

Figure A 18: Effect of temperature on selenium extraction with 0.25mol/L NaOH (10 g/L solids; 750 rev/min; 11 atm O_2 pressure)

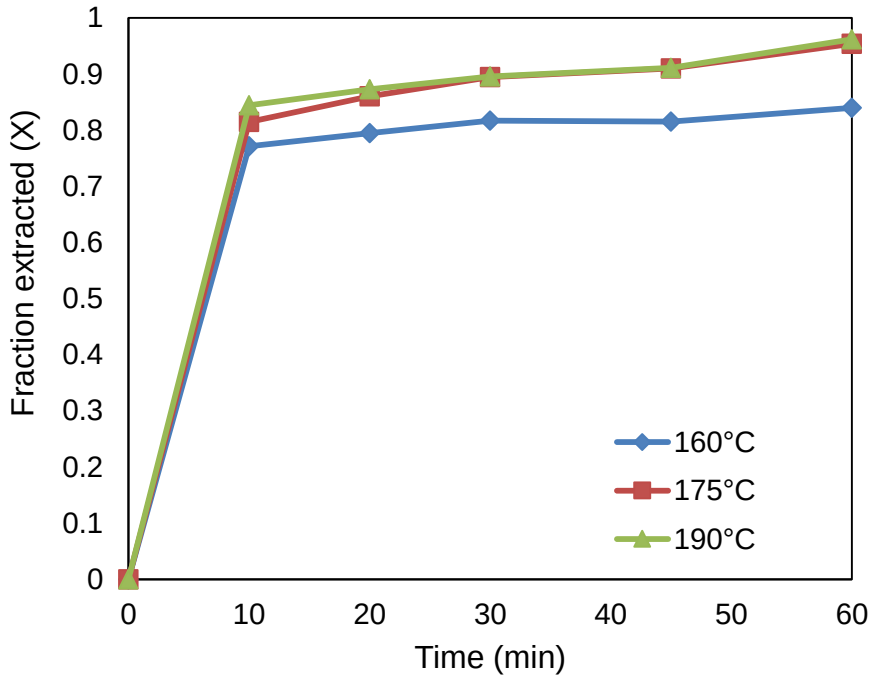

Figure A 19: Effect of temperature on selenium extraction with 0.5mol/L NaOH (10 g/L solids; 750 rev/min; 11 atm O_2 pressure)

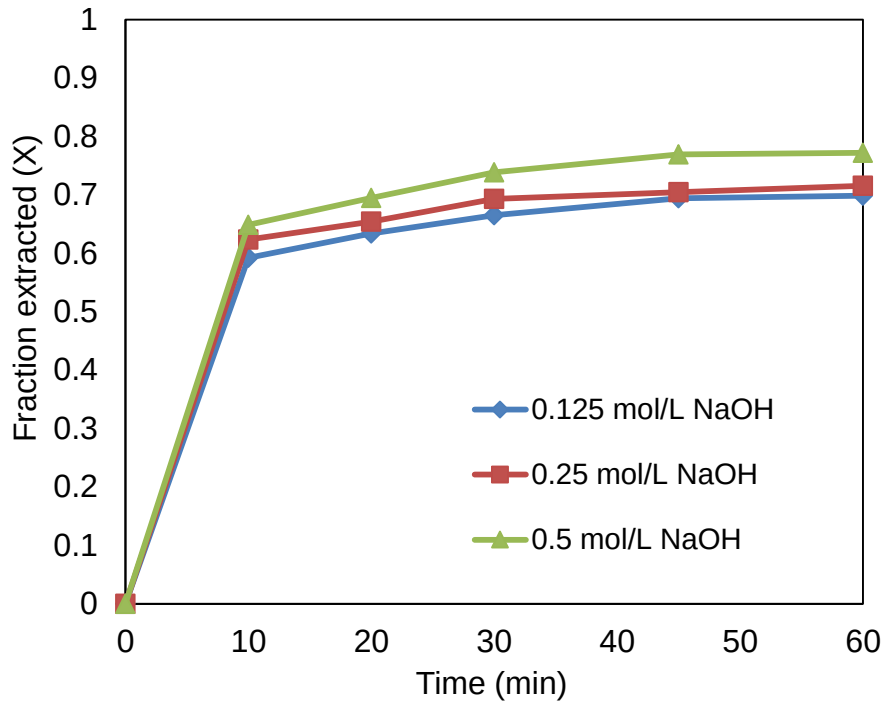

Figure A 20: Effect of NaOH concentration on arsenic extraction (Temperature 160°C; 10 g/L solids; 750 rev/min; 11 atm O_2 pressure)

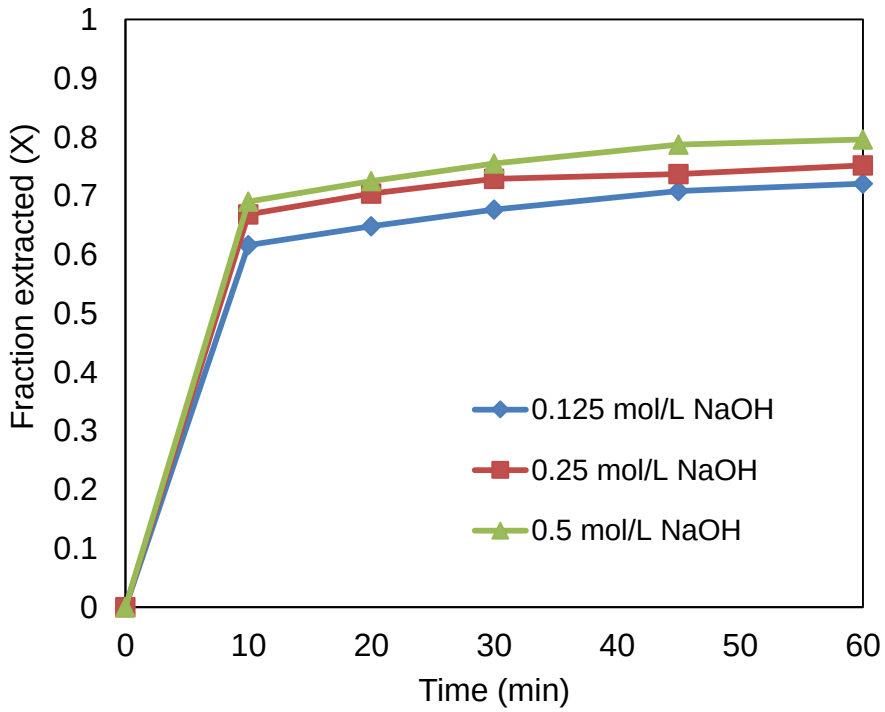

Figure A 21: Effect of NaOH concentration on sulphur extraction (Temperature 175°C; 10 g/L solids; 750 rev/min; 11 atm O_2 pressure)

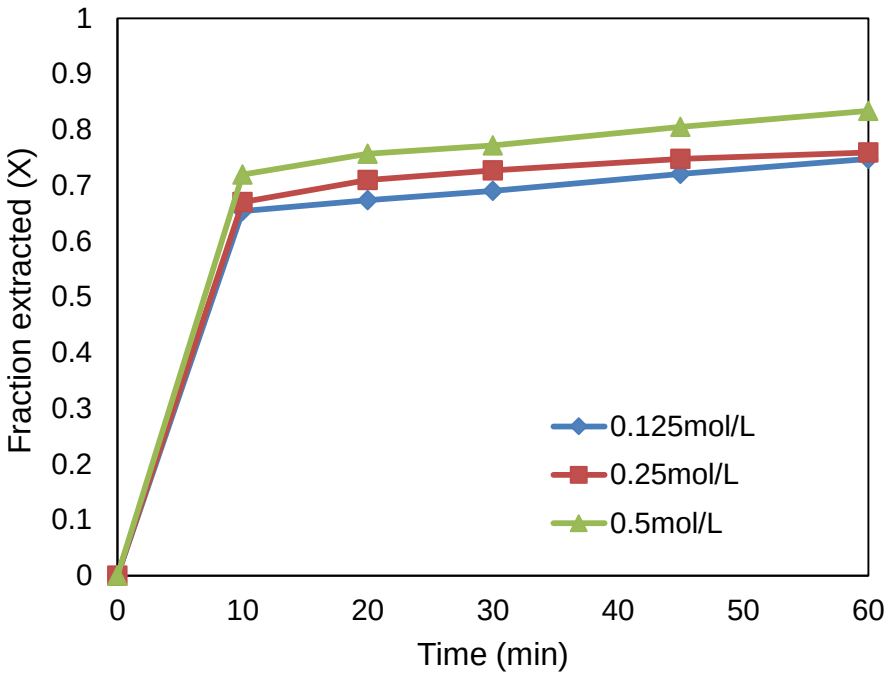

Figure A 22: Effect of NaOH concentration on arsenic extraction (Temperature 175°C; 10 g/L solids; stirring rate: 750 rev/min; 11 atm O_2 pressure)

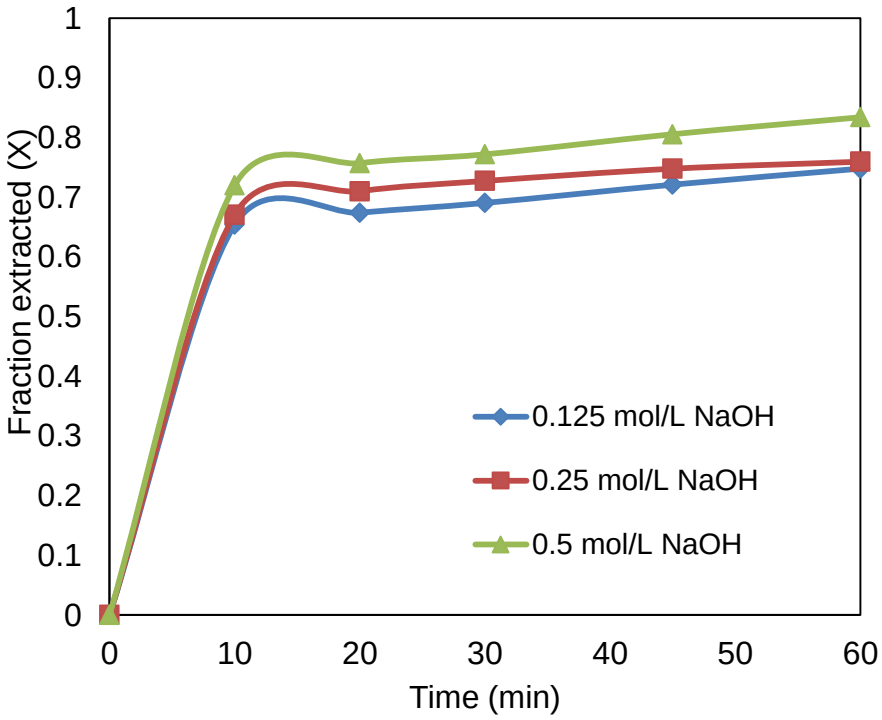

Figure A 23: Effect of temperature on arsenic extraction with 0.125mol/L NaOH (10 g/L solids; 750rev/min; 11 atm O_2 pressure)

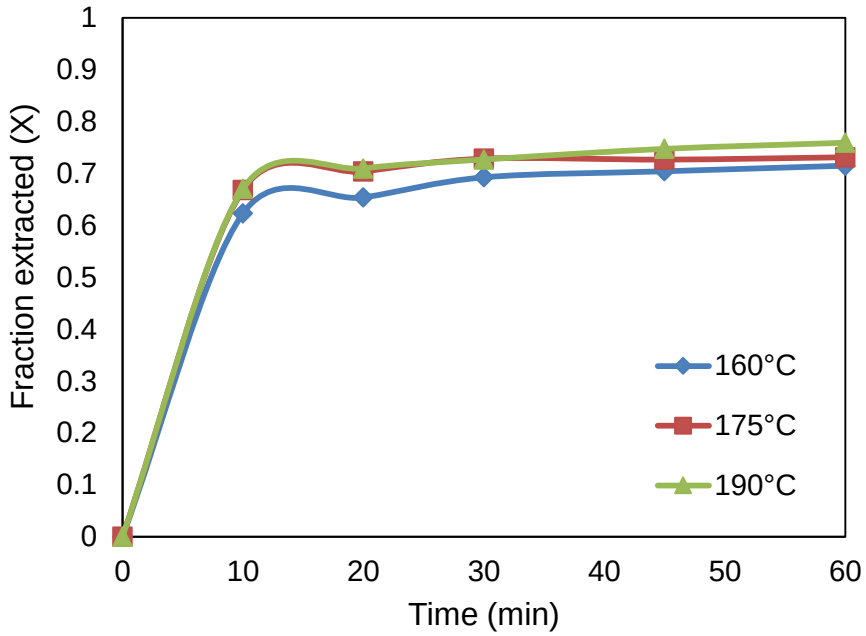

Figure A 24: Effect of temperature on arsenic extraction with 0.25mol/L NaOH (1 g/L solids; 750 rev/min; 11 atm O_2 pressure)

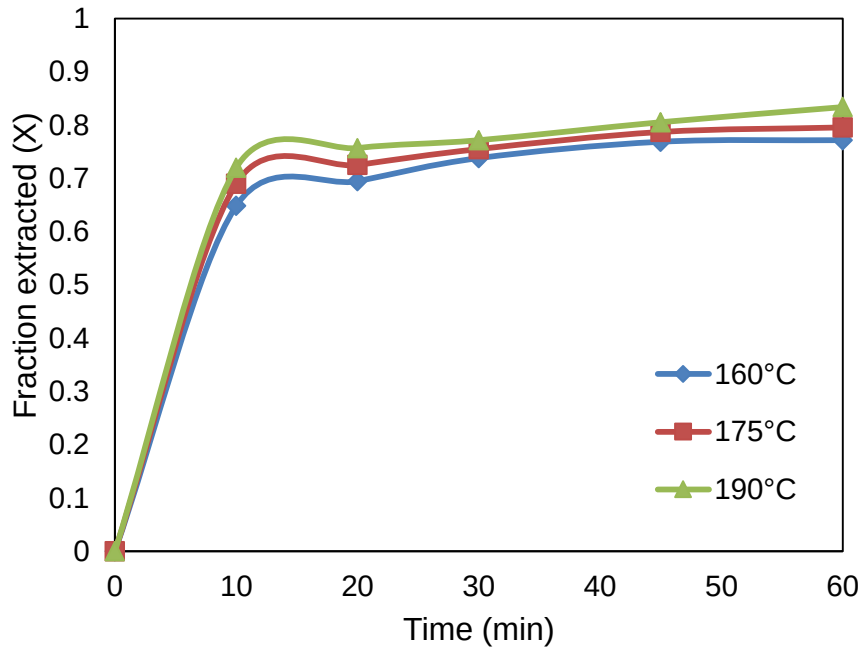

Figure A 25: Effect of temperature on arsenic extraction with 0.5mol/L NaOH (10 g/L solids; 750rev/min; 11 atm O_2 pressure)

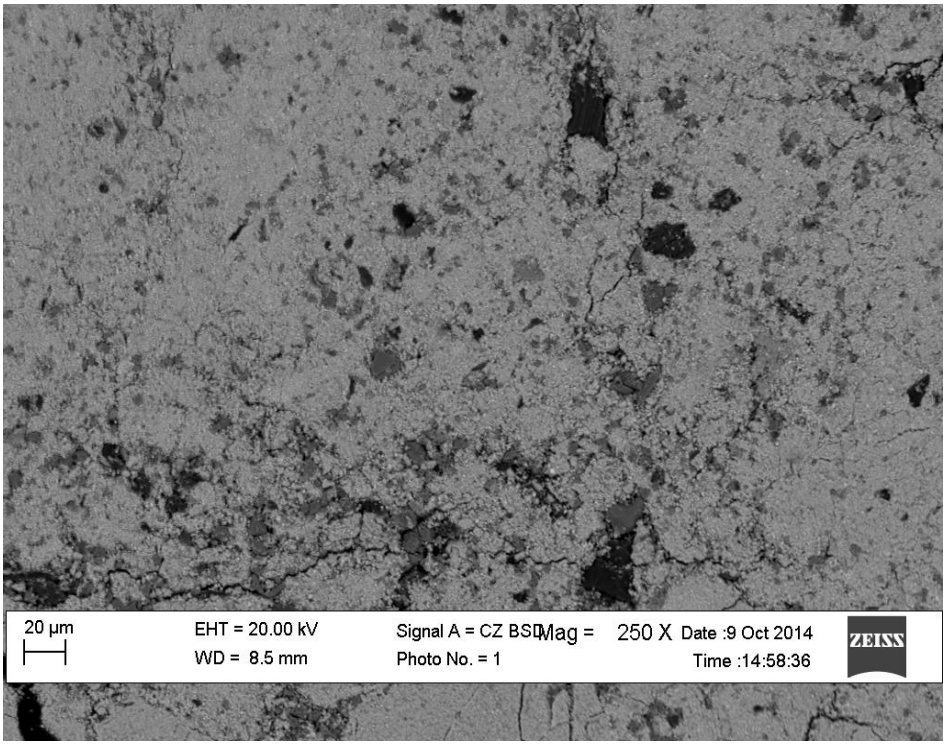

Figure A 26: Backscattered electron image of the leached residue grains of PGM rich leach reside (175°C, 0.5 mol/L NaOH, 11 atm O_2 pressure)

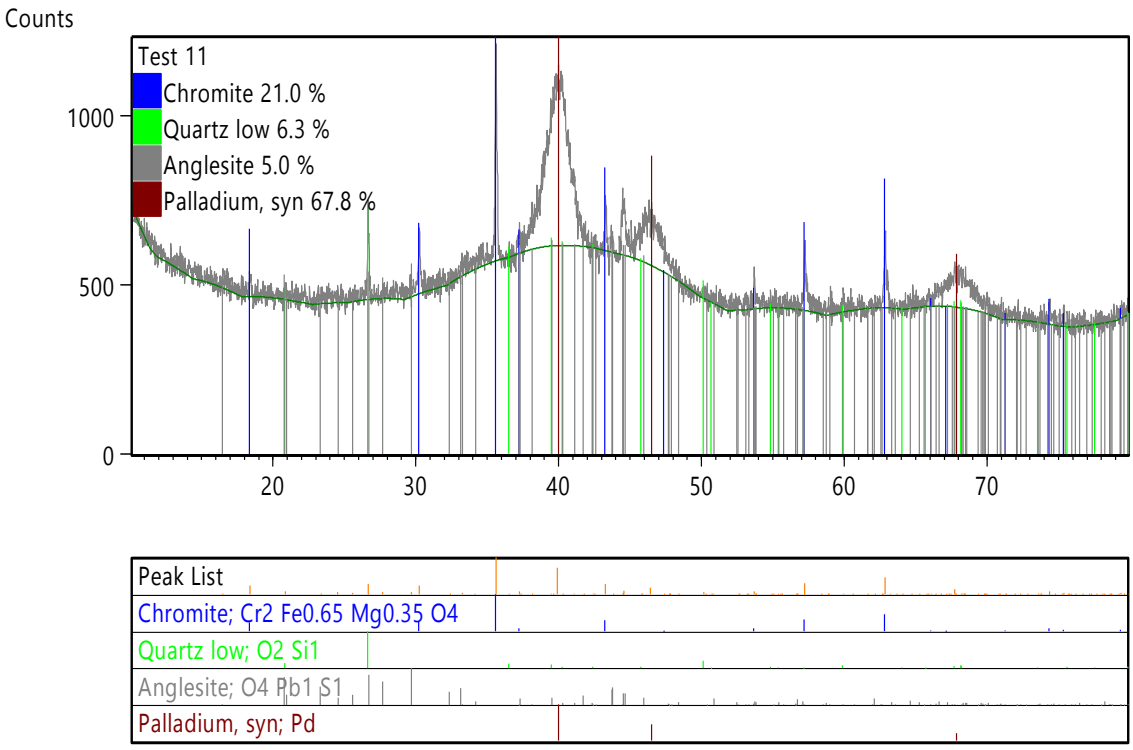

Figure A 27: XRD analysis of residue at 175°C, 0.5 mol/L NaOH, 750 rev/min and 11 atm O_2 partial pressure)

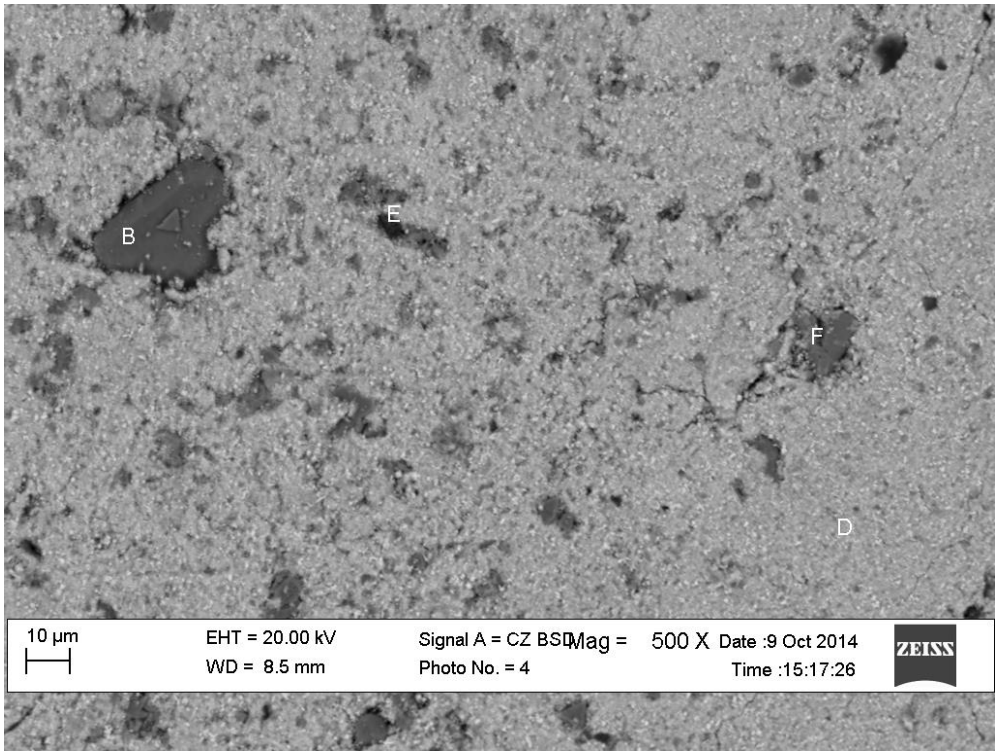

Figure A 28: Backscattered electron image of the leached residue grains of PGM rich leach reside (160°C, 0.5 mol/L NaOH, 11 atm O_2 pressure)

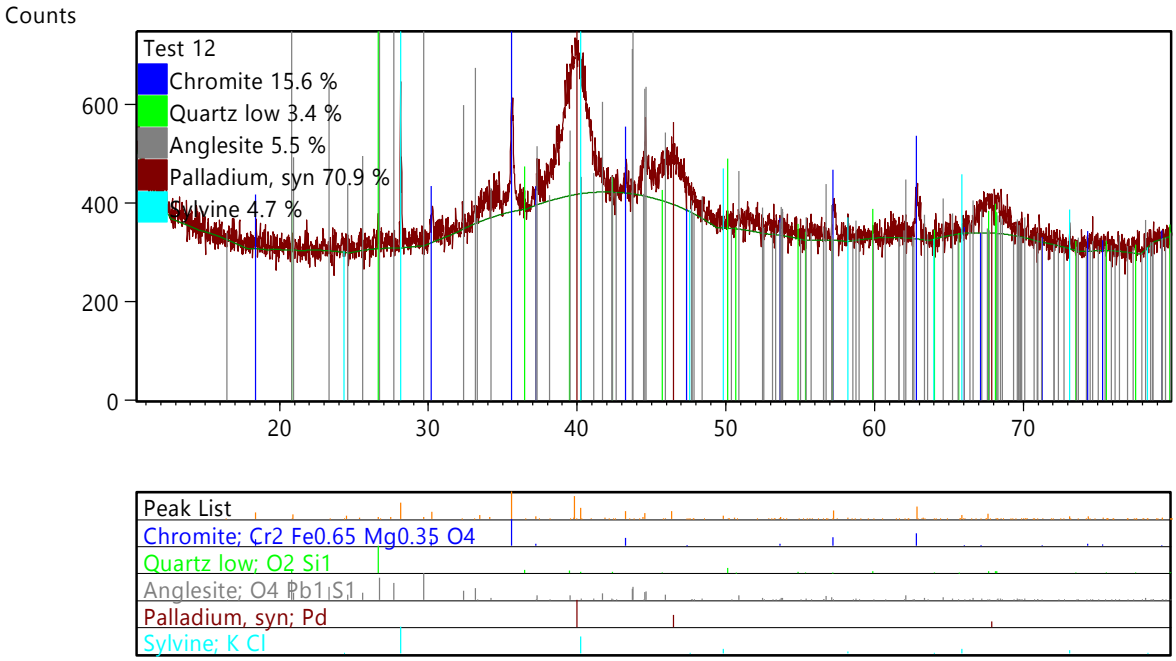

Figure A 29: XRD analysis of residue at 160°C, 0.5 mol/L NaOH, 750 rev/min and 11atm O_2 partial pressure)

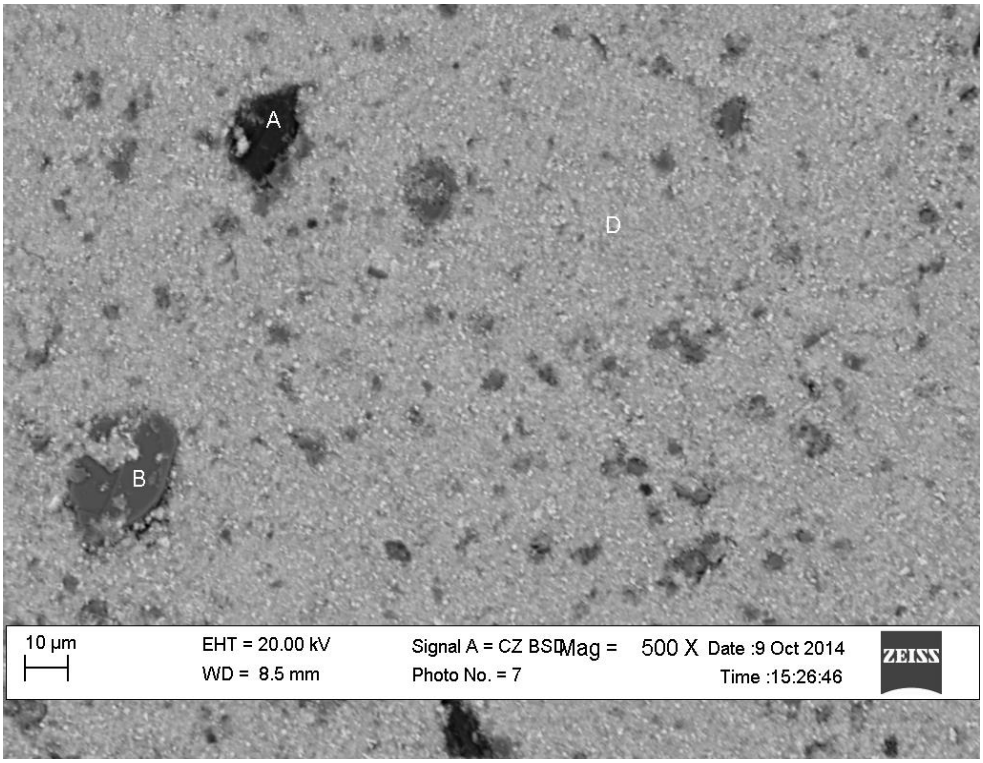

Figure A 30: Backscattered electron image of the leached residue grains of PGM rich leach reside (175°C, 0.25 mol/L NaOH, 11 atm O_2 pressure)

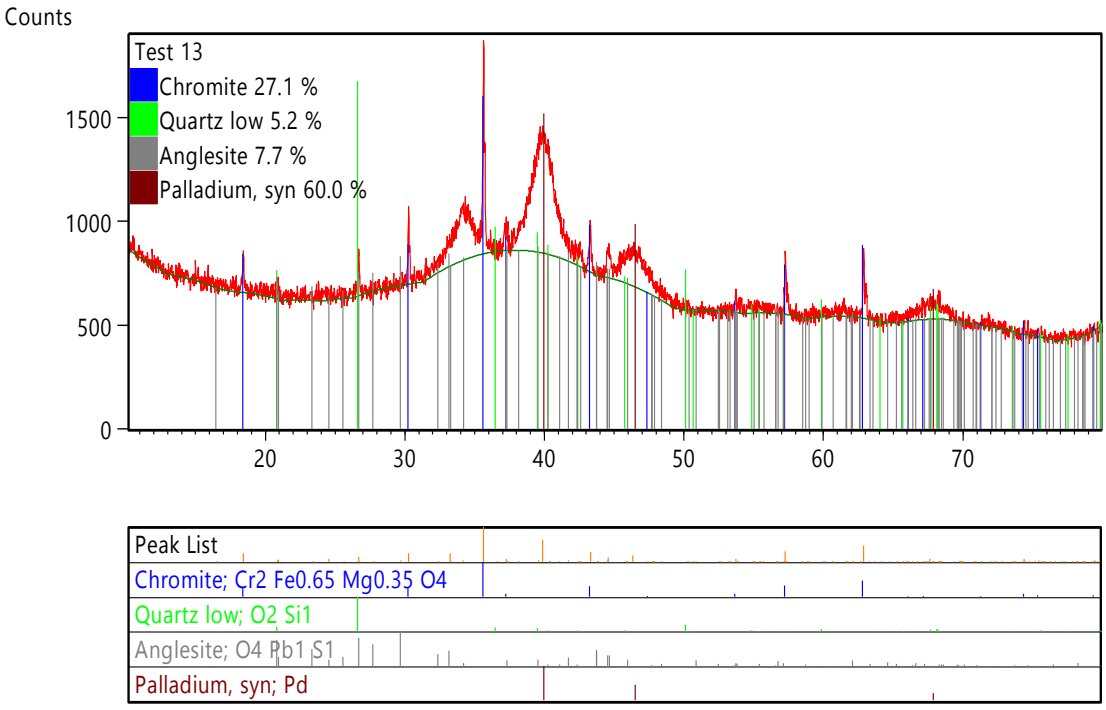

Figure A 31: XRD analysis of residue at 175°C, 0.25 mol/L NaOH, 750 rev/min and 11 atm O_2 partial pressure)

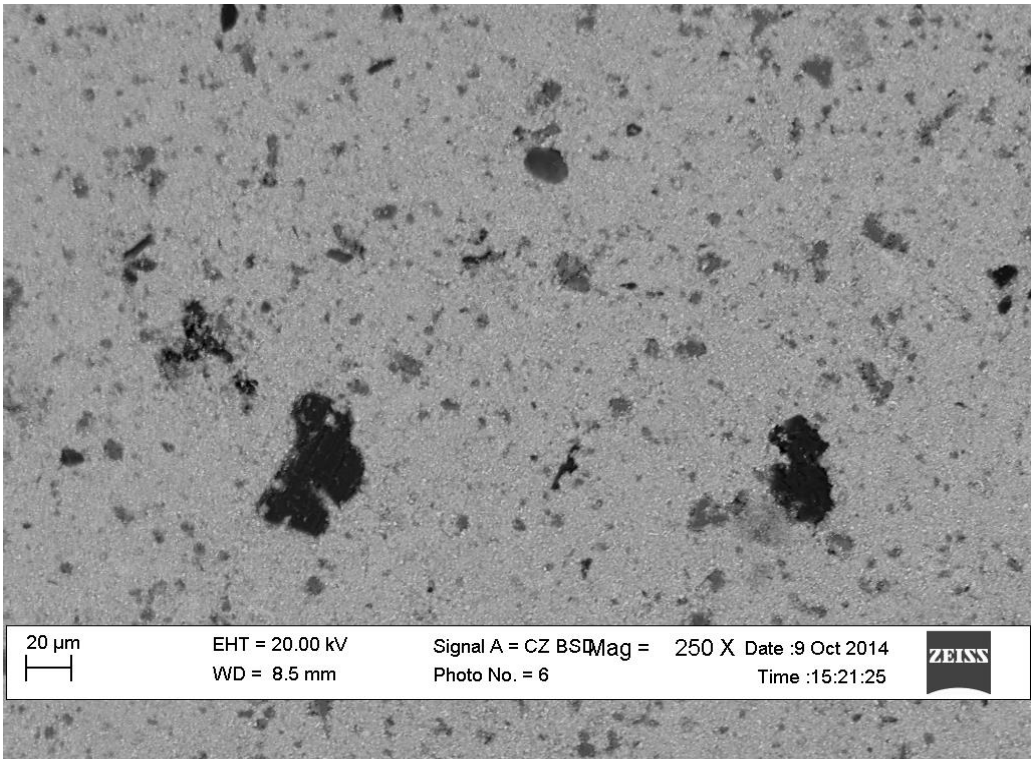

Figure A 32: Backscattered electron image of the leached residue grains of PGM rich leach (160°C, 0.25 mol/L NaOH, 11 atm O_2 pressure)

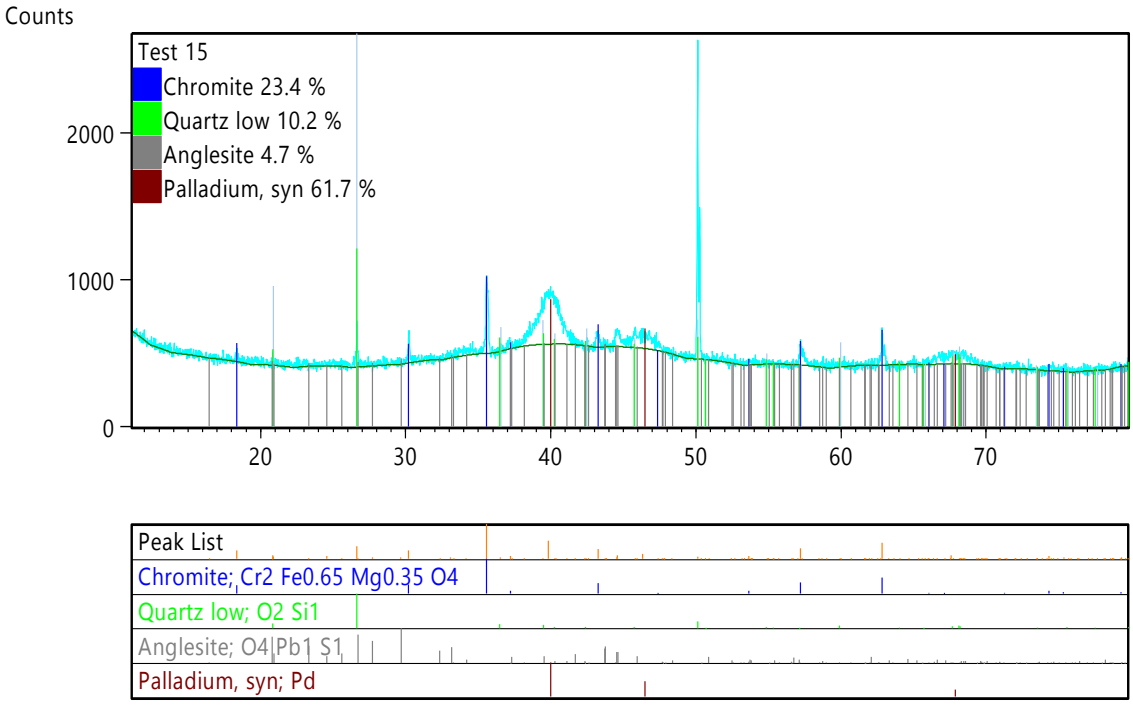

Figure A 33: XRD analysis of residue at 160°C, 0.25 mol/L NaOH, 750 rev/min and 11 atm O_2 partial pressure)

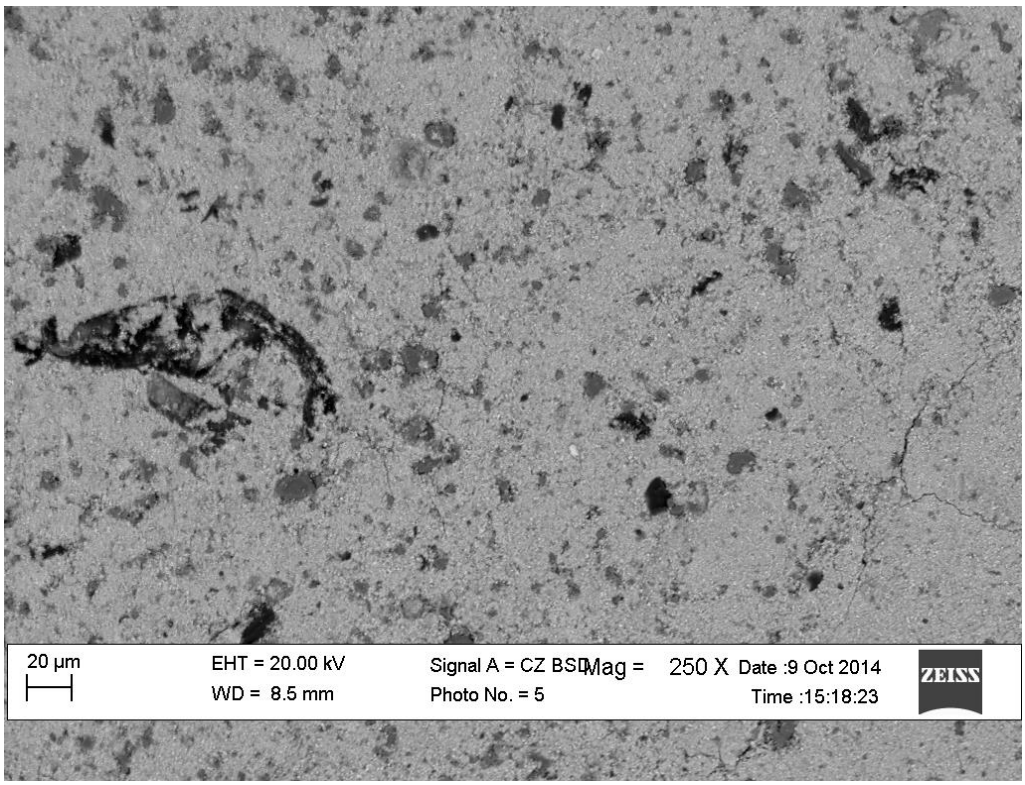

Figure A 34: Backscattered electron image of the leached residue grains of PGM rich leach reside (190°C, 0.25 mol/L NaOH, 11 atm O_2 pressure)

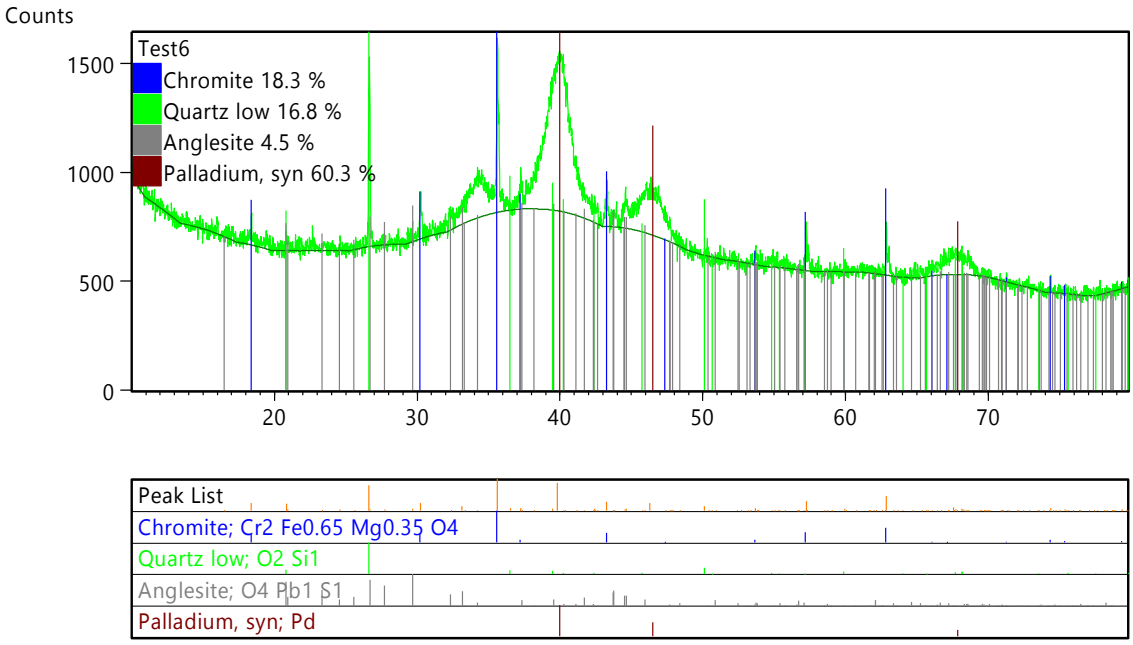

Figure A 35: XRD analysis of residue at 190°C, 0.25 mol/L NaOH, 750 rev/min and 11 atm O_2 partial pressure)

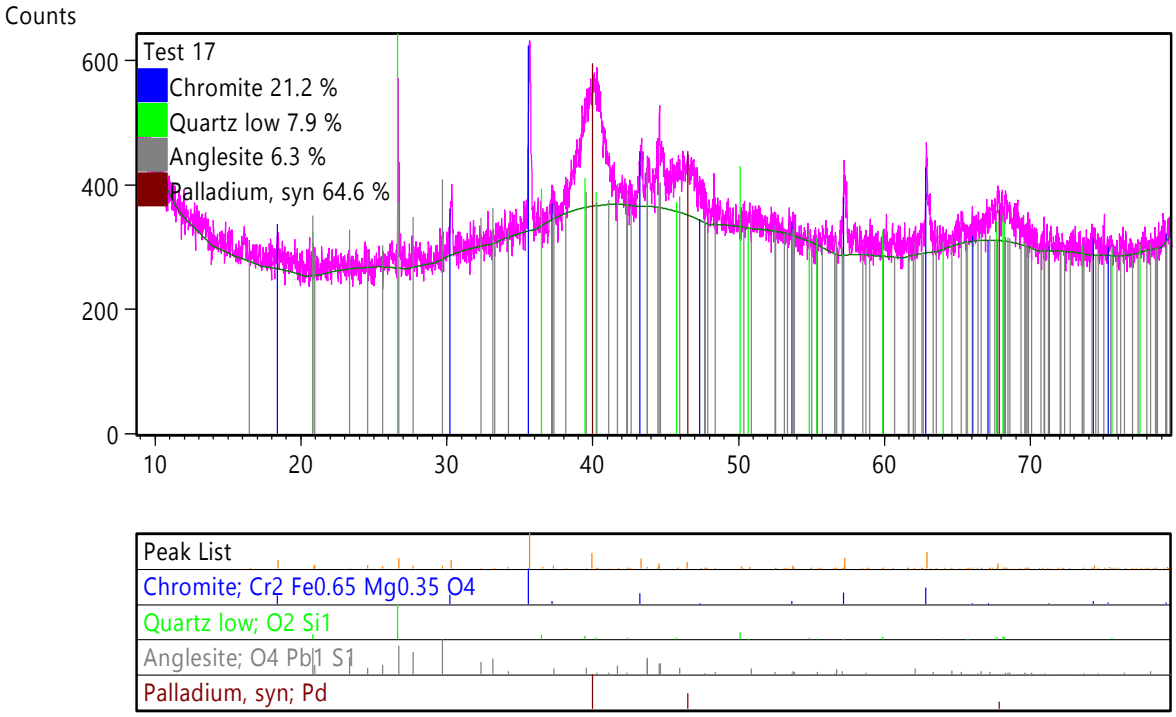

Figure A 36: XRD analysis of residue at 160°C, 0.125 mol/L NaOH, 750 rev/min and 11 atm O_2 partial pressure)

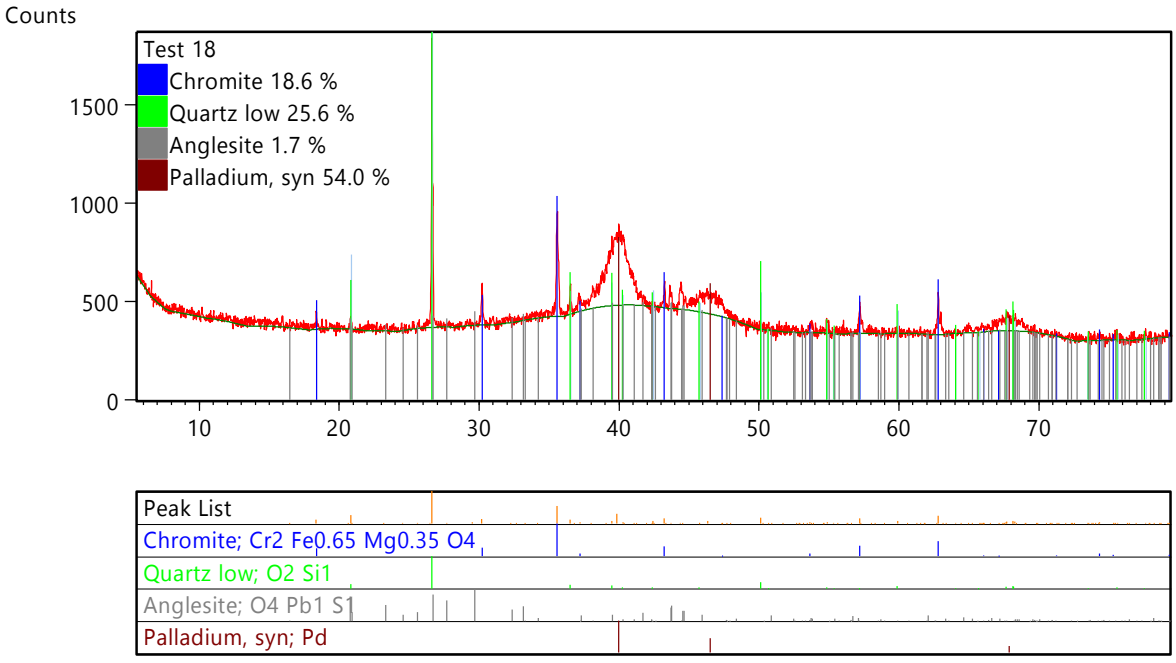

Figure A 37: XRD analysis of residue at 175°C, 0.125 mol/L NaOH, 750 rev/min and 11 atm O_2 partial pressure)

Appendix VII

Statistical analysis of experimental results

This section presents a detailed statistical analysis of the experimental results i.e. to support the effect of the process operating parameters discussed above. In order to statistically identify the factors influencing sulphur, selenium and arsenic dissolution, the experimental results were tested for statistical significance using different ANOVA analyses. Prediction and profiling plots are also discussed below.

The statistical significance of the leaching temperature and sodium hydroxide concentration and their interaction effects towards extraction was determined by fitting quadratic models to the experimental results and then perform an ANOVA analysis on the fitted models. The models are expressed in terms of their actual process parameters which consist of linear, quadratic and interaction terms. Generally the regression coefficient sign determines whether the influence of the model term has a positive effect or an antagonistic negative effect.

9.2.6 Statistical analysis of Sulphur response

Table A 27: ANOVA table (derived from Statistica 12.6) for sulphur extraction

Factor	Effect	Std.Err.	t(12)	p	-95.%	+95.%	Coeff.	Std.Err.	-95.%	+95.%
Mean/Interc.	0.847	0.003	278.660	0.000	0.840	0.853	0.847	0.003	0.840	0.853
(1) Temperature °C (L)	0.126	0.007	16.940	0.000	0.110	0.142	0.063	0.004	0.055	0.071
Temperature °C (Q)	-0.038	0.006	-6.014	0.000	-0.052	-0.024	-0.019	0.003	-0.026	-0.012
(2) NaOH conc (mol/L) (L)	0.076	0.007	10.299	0.000	0.060	0.092	0.038	0.004	0.030	0.046
NaOH conc (mol/L) (Q)	0.001	0.007	0.157	0.878	-0.013	0.015	0.001	0.003	-0.007	0.008
1L by 2L	-0.020	0.009	-2.310	0.039	-0.040	-0.001	-0.010	0.004	-0.020	-0.001

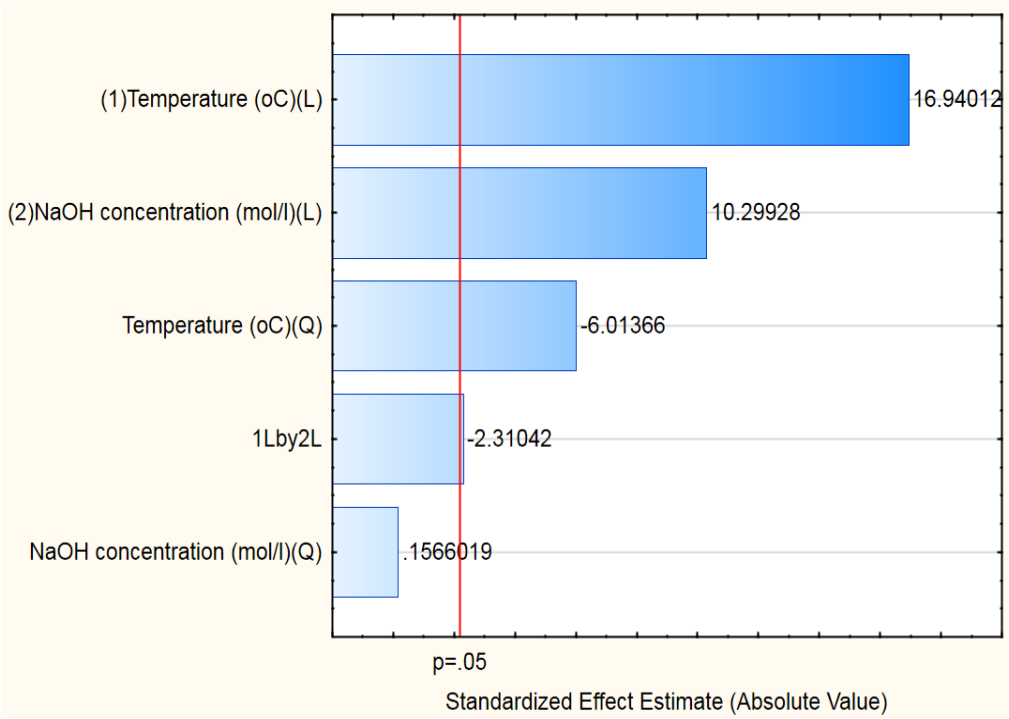

Figure A 38: Pareto chart for standardised effect on sulphur extraction

From the ANOVA table and Pareto chart above, it can be seen that the linear terms of temperature and caustic concentration both have positive effects on extraction. This supports the discussion in Section 7.2.1 and 7.2.2 where both temperature and sodium hydroxide concentration were observed to increase sulphur extraction. The Pareto plot also illustrates the degree of significance of these parameters. It can be seen that the temperature has the most significant (positive) effect on extraction. The significance of the analysis is captured by the p values obtained from the ANOVA analysis. Only the parameters with less than 0.05 p values have a significant effect. It can be concluded from the ANOVA analysis that only the sodium hydroxide quadratic term had an insignificant effect on extraction. The effect of these process parameters can also be seen from the contour plot in Figure A 39 where the temperature is seen to have the most significant effect. These statistical analyses support the discussion of the extraction trends observed in Section 7.2.1 and 7.2.2.

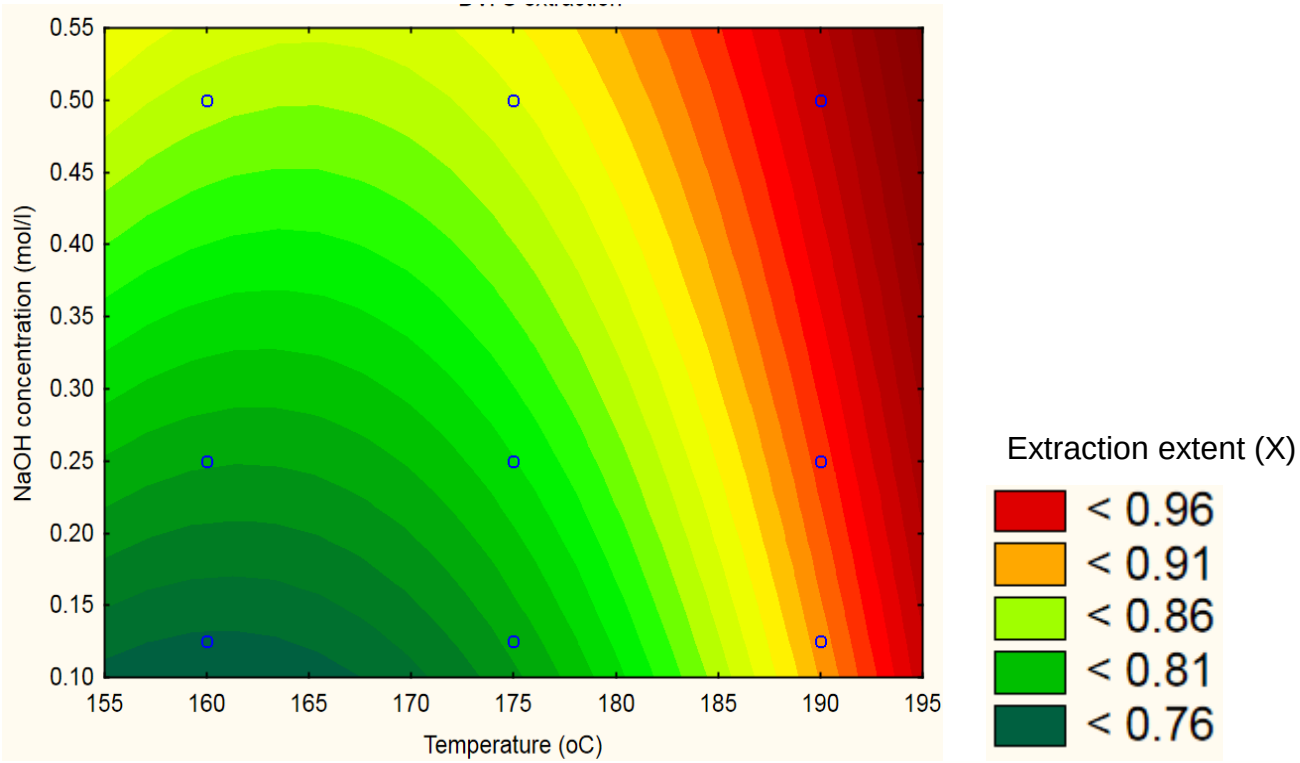

Figure A 39: Contour plot for sulphur extraction at 180 minutes

9.2.7 Statistical analysis of selenium response

Table A 28: ANOVA table (derived from Statistica 12.6) for selenium extraction

Factor	Effect	Std.Err.	t(12)	p	-95.%	+95.%	Coeff.	Std.Err.	-95.%	+95.%
Mean/Interc.	0.87	0.00	242.85	0.00	0.86	0.88	0.87	0.00	0.86	0.88
(1)Temperature °C (L)	0.11	0.01	13.03	0.00	0.10	0.13	0.06	0.00	0.05	0.07
Temperature °C (Q)	0.05	0.01	6.72	0.00	0.03	0.07	0.03	0.00	0.02	0.03
(2)NaOH conc (mol/l) (L)	0.05	0.01	5.28	0.00	0.03	0.06	0.02	0.00	0.01	0.03
NaOH conc (mol/l) (Q)	0.00	0.01	-0.35	0.73	-0.02	0.01	0.00	0.00	-0.01	0.01
1L by 2L	-0.02	0.01	-2.28	0.04	-0.05	0.00	-0.01	0.01	-0.02	0.00

The ANOVA analysis, Pareto charts and contour plots below show that both the temperature and caustic concentration have positive effects on selenium extraction,

with the most significant effect assigned to the temperature. The interaction effect of temperature and sodium hydroxide (1L by 2L) is shown to have a marginal effect as depicted in the Pareto chart.

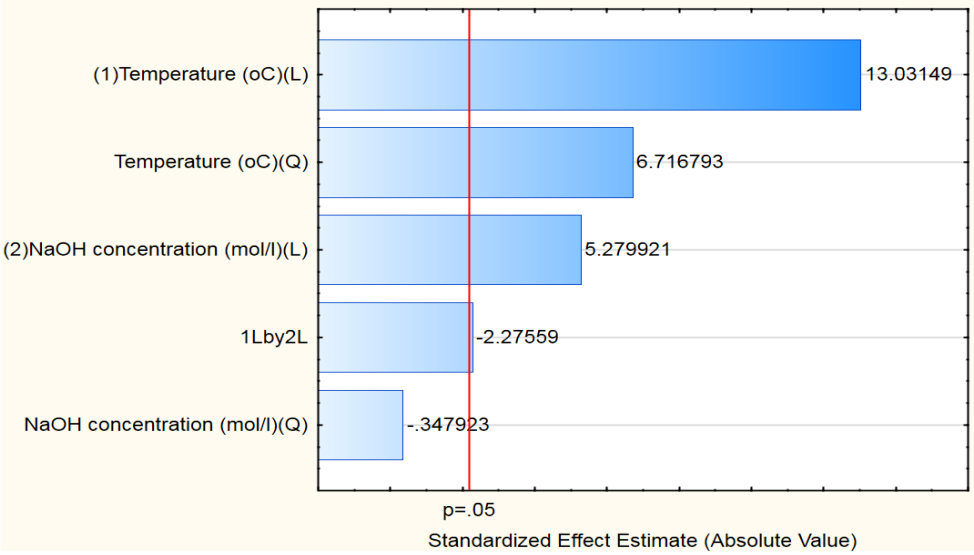

Figure A 40: Pareto chart for standardised effect on selenium extraction

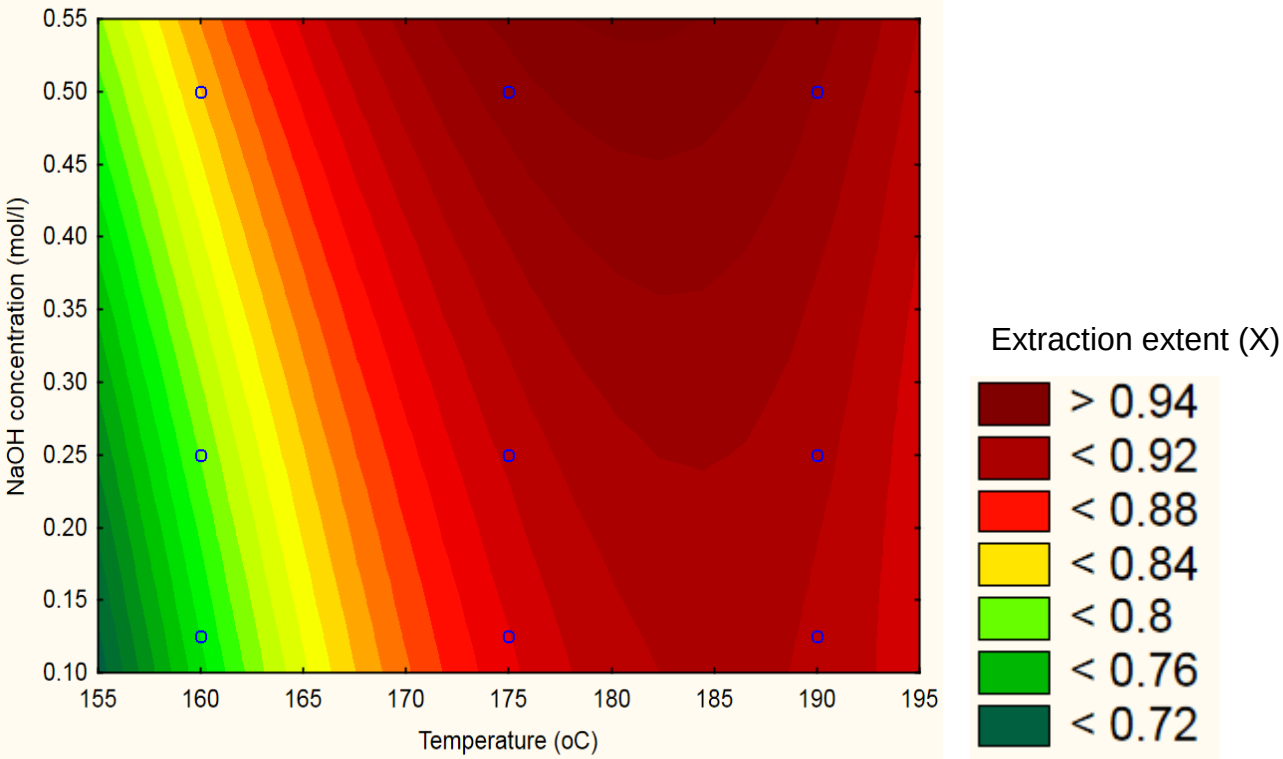

Figure A 41: Contour plot for selenium extraction at 180 minutes

9.2.8 Statistical analysis of arsenic response

Table A 29: ANOVA table (derived from Statistica 12.6) for arsenic extraction

Factor	Effect	Std.Err.	t(12)	p	-95.%	+95.%	Coeff.	Std.Err.	-95.%	+95.%
Mean/Interc.	0.75	0.00	365.64	0.00	0.74	0.75	0.75	0.00	0.74	0.75
(1)Temperature °C (L)	0.03	0.00	6.30	0.00	0.02	0.04	0.02	0.00	0.01	0.02
Temperature °C (Q)	0.00	0.00	0.09	0.93	-0.01	0.01	0.00	0.00	0.00	0.00
(2)NaOH conc (mol/L) (L)	0.08	0.00	15.61	0.00	0.07	0.09	0.04	0.00	0.03	0.04
NaOH conc (mol/L) (Q)	0.00	0.00	-0.41	0.69	-0.01	0.01	0.00	0.00	-0.01	0.00
1L by 2L	0.01	0.01	1.10	0.29	-0.01	0.02	0.00	0.00	0.00	0.01

The statistical results Table A 29, Figure A 42 and Figure A 43 show that only the linear temperature and caustic concentration have positive effects on arsenic extraction. The quadratic and interaction terms have a significant effect. It can also be seen from the Pareto plot that sodium hydroxide has the most significant effect. The contour plot also show that even at high temperature, the extraction of arsenic remains poor, but only increases when the caustic concentration is increased.

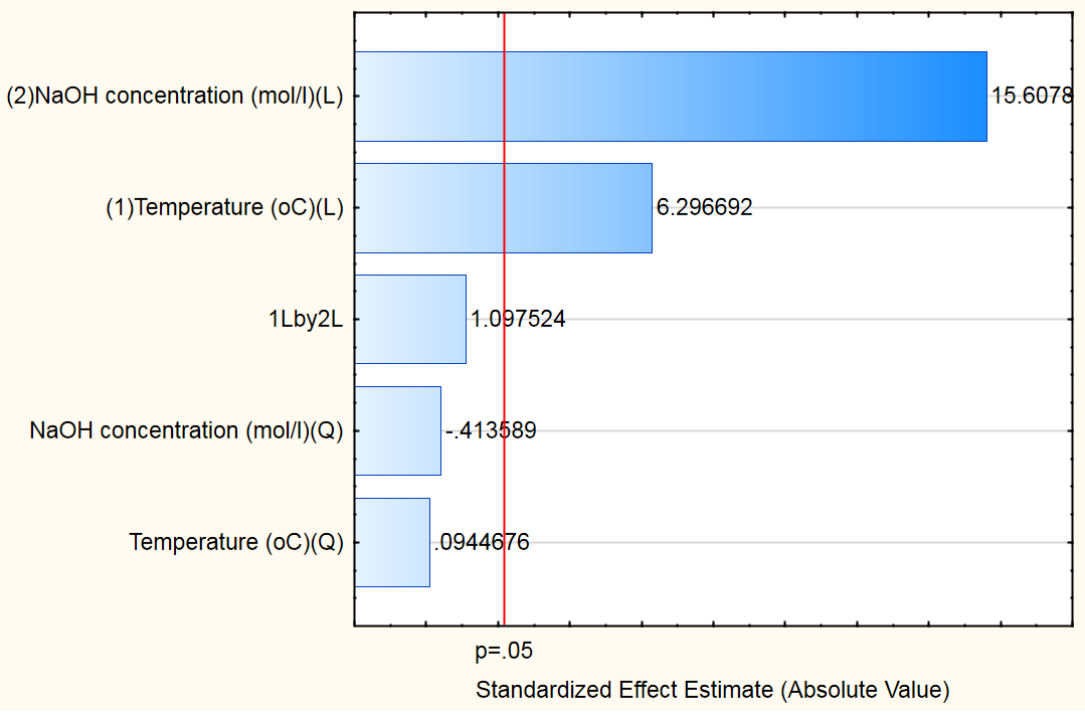

Figure A 42: Pareto chart for standardised effect on arsenic extraction

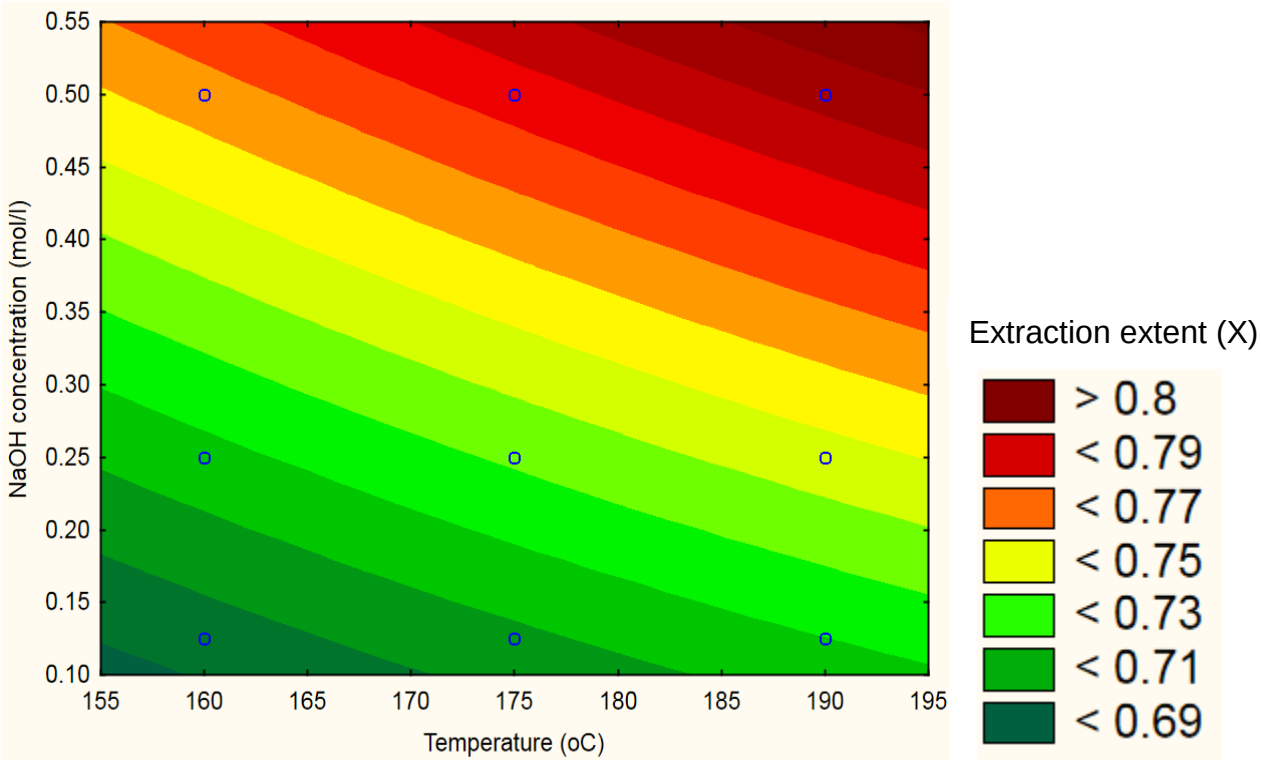

Figure A 43: Contour plot for arsenic extraction

9.2.9

9.2.10 Statistical analysis of platinum response

Table A 30: ANOVA table (derived from Statistica 12.6) for platinum dissolution

Factor	Effect	Std.Err.	t(12)	p	-95.%	+95.%	Coeff.	Std.Err.	-95.%	+95.%
Mean/Interc.	126.70	3.85	32.93	0.00	118.32	135.08	126.70	3.85	118.32	135.08
(1)Temperature °C (L)	-85.17	9.42	-9.04	0.00	-105.70	-64.64	-42.59	4.71	-52.85	-32.32
Temperature °C (Q)	7.21	8.09	0.89	0.39	-10.41	24.84	3.61	4.04	-5.20	12.42
(2)NaOH conc (mol/L) (L)	158.25	9.34	16.94	0.00	137.90	178.60	79.12	4.67	68.95	89.30
NaOH conc (mol/L) (Q)	23.22	8.24	2.82	0.02	5.27	41.16	11.61	4.12	2.64	20.58
1L by 2L	2.22	11.23	0.20	0.85	-22.26	26.69	1.11	5.62	-11.13	13.35

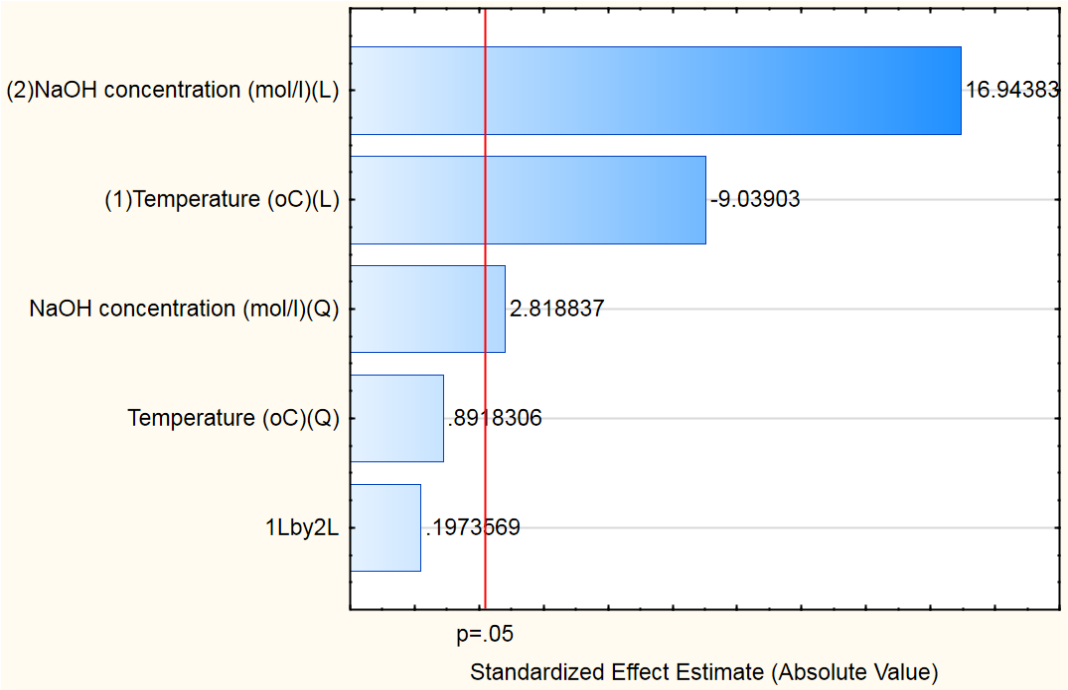

Figure A 44: Pareto chart for standardised effect on platinum dissolution

The effect of process parameters on the platinum dissolution is presented in Figure A 44 and Figure A 45. In this analysis, the positive effect (favouring dissolution) is in fact negative because the process has to lose as little precious metals as possible. The ANOVA table and Pareto plots depicted above show that sodium hydroxide favours platinum dissolution. The effect of temperature on dissolution is significantly negative, implying reduced dissolution with increased temperature. The contour plot in Figure A 45 below also shows a hot spot region where sodium hydroxide concentration is high at low temperature. Palladium response is similar to that of platinum, thus, no additional statistical analysis on palladium was conducted.

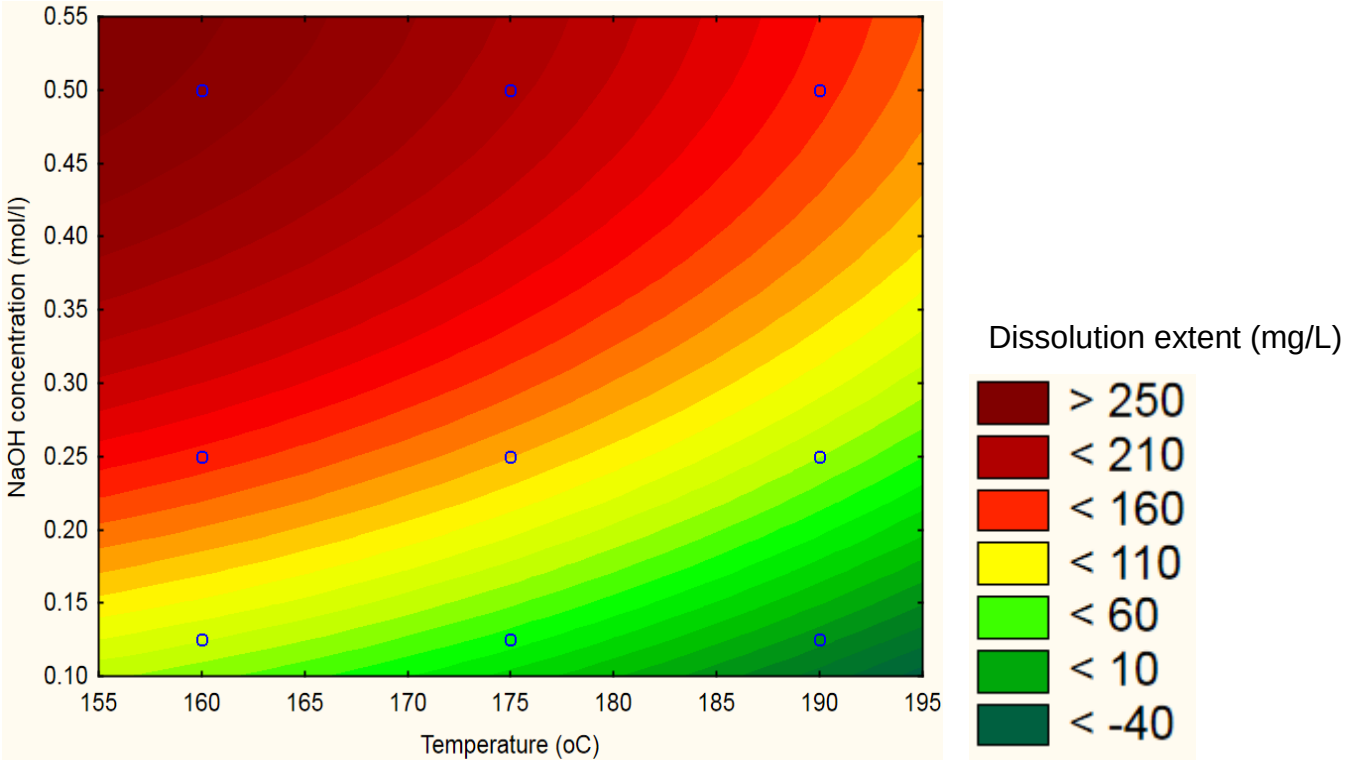

Figure A 45: Contour plot for platinum dissolution at 180 minutes

9.2.11 Statistical analysis of ruthenium response

Table A 31: ANOVA table (derived from Statistica 12.6) for ruthenium dissolution

Factor	Effect	Std.Err.	t(12)	p	-95.%	+95.%	Coeff.	Std.Err.	-95.%	+95.%
Mean/Interc.	118.61	5.01	23.65	0.00	107.68	129.53	118.61	5.01	107.68	129.53
(1)Temperature °C (L)	133.96	12.28	10.91	0.00	107.21	160.71	66.98	6.14	53.60	80.36
Temperature °C (Q)	-32.88	10.54	-3.12	0.01	-55.85	-9.92	-16.44	5.27	-27.92	-4.96
(2)NaOH conc (mol/L) (L)	132.63	12.17	10.90	0.00	106.11	159.14	66.31	6.08	53.05	79.57
NaOH conc (mol/L) (Q)	27.58	10.73	2.57	0.02	4.20	50.97	13.79	5.37	2.10	25.48
1L by 2L	74.65	14.64	5.10	0.00	42.76	106.54	37.32	7.32	21.38	53.27

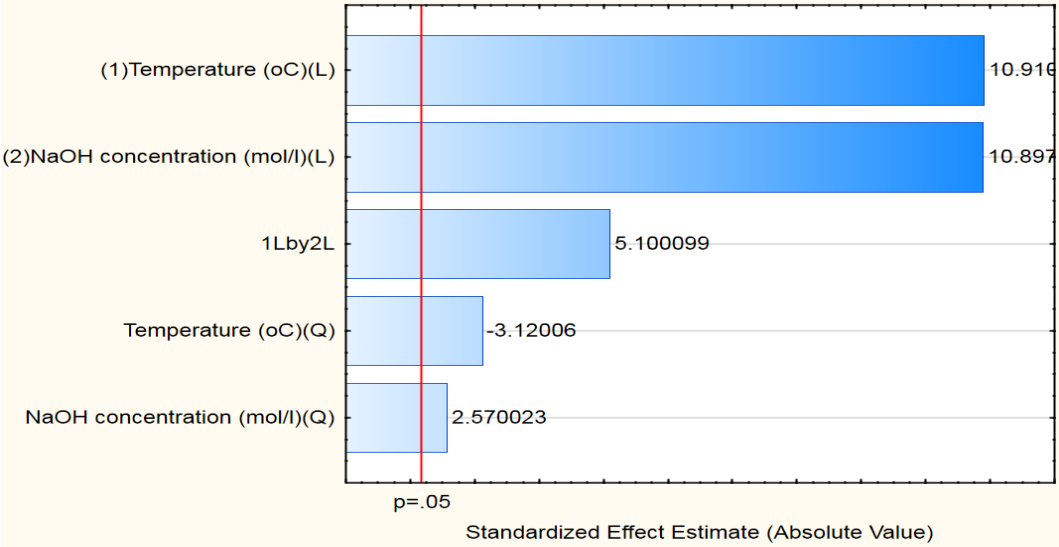

Figure A 46: Pareto chart for standardised effect on ruthenium dissolution

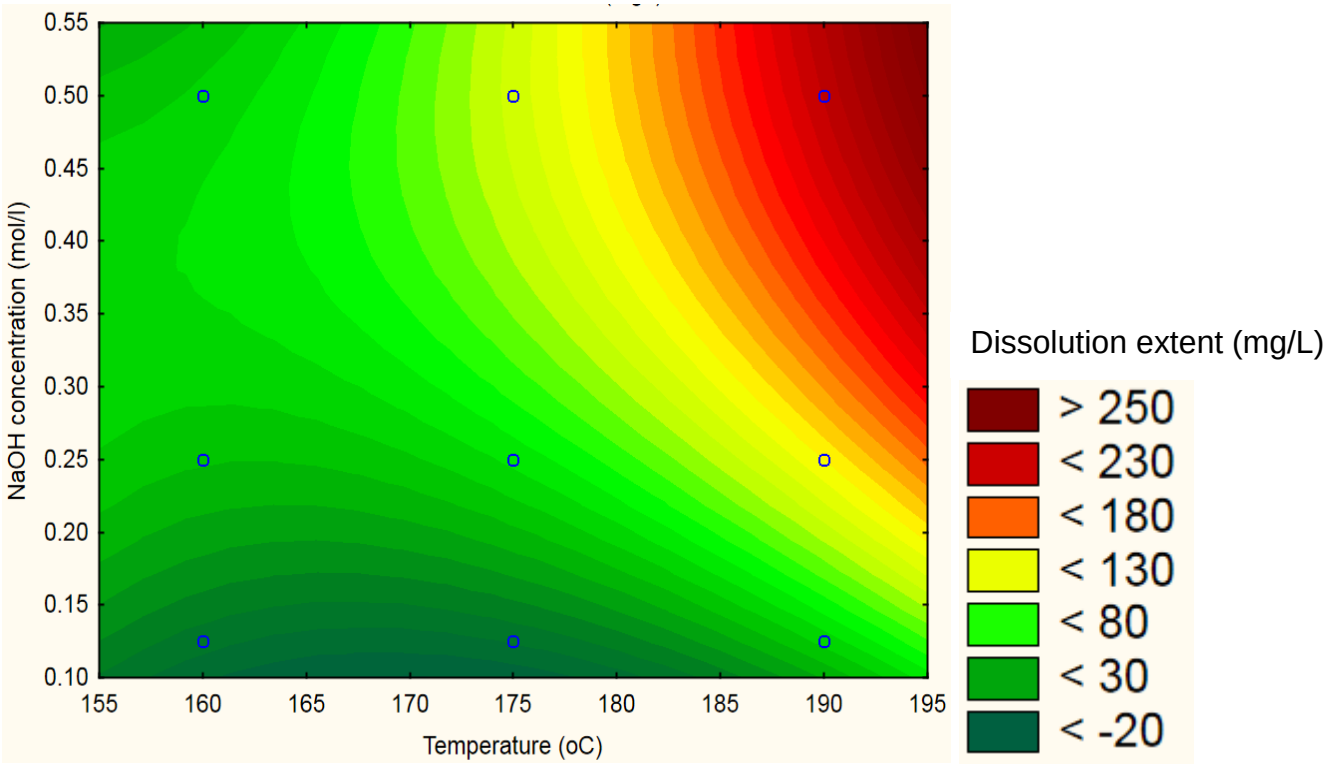

Figure A 47: Contour plot for ruthenium dissolution at 180 minutes

With regards to ruthenium dissolution, all the process parameters influenced the dissolution of ruthenium with sodium hydroxide and temperature being equally significant (Table A 31, Figure A 46 and Figure A 47). Maximum dissolution of ruthenium is obtained if both temperature and caustic concentration are increased.

Response Factor	Quadratic model equation	Degree of significance (Descending order)	R^2_{adj}
S extraction	$0.847 + 0.126X_1 + 0.076X_2 - 0.038X_1^2 - 0.02X_1X_2$	X_1, X_2, X_1^2, X_1X_2	0.96
Se extraction	$0.087 + 0.11X_1 - 0.05X_2 + 0.05X_1^2 - 0.02X_1X_2$	X_1, X_1^2, X_2, X_1X_2	0.93
As extraction	$0.75 + 0.03X_1 + 0.08X_2$	X_2, X_1	0.94
	X_1 is temperature		
	X_2 is NaOH concentration		

The quadratic models are checked for adequacy by comparing the observed vs predicted variables. This is represented in the **Error! Reference source not found.** to Figure A 52 below. As can be seen, the model is quite adequate as the measured values lie close to the predicted response line.

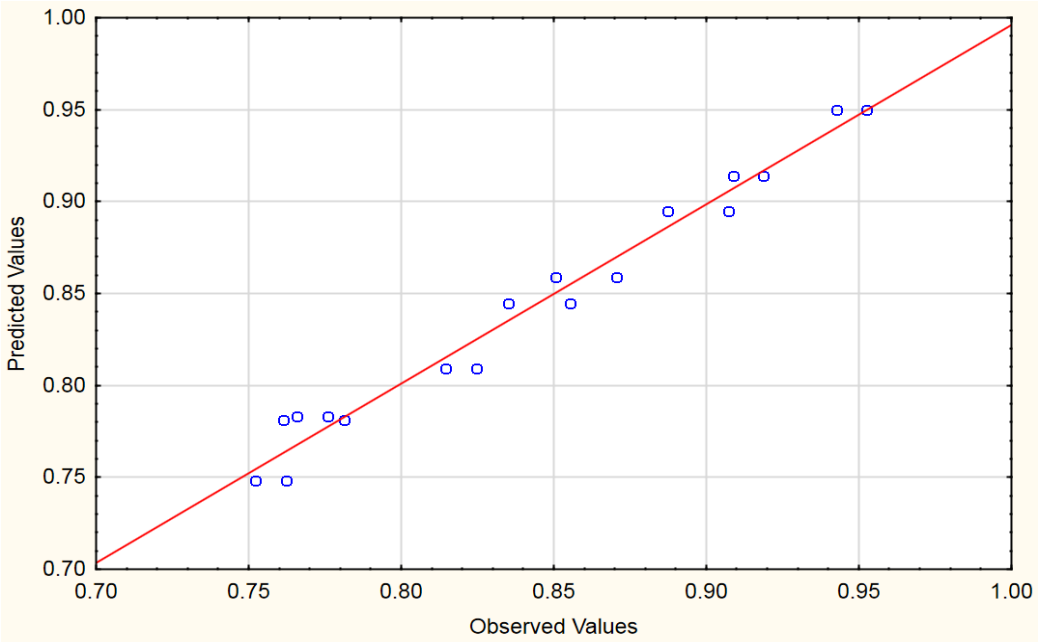

Figure A 48: Predicted (quadratic model) vs observed values for sulphur extraction

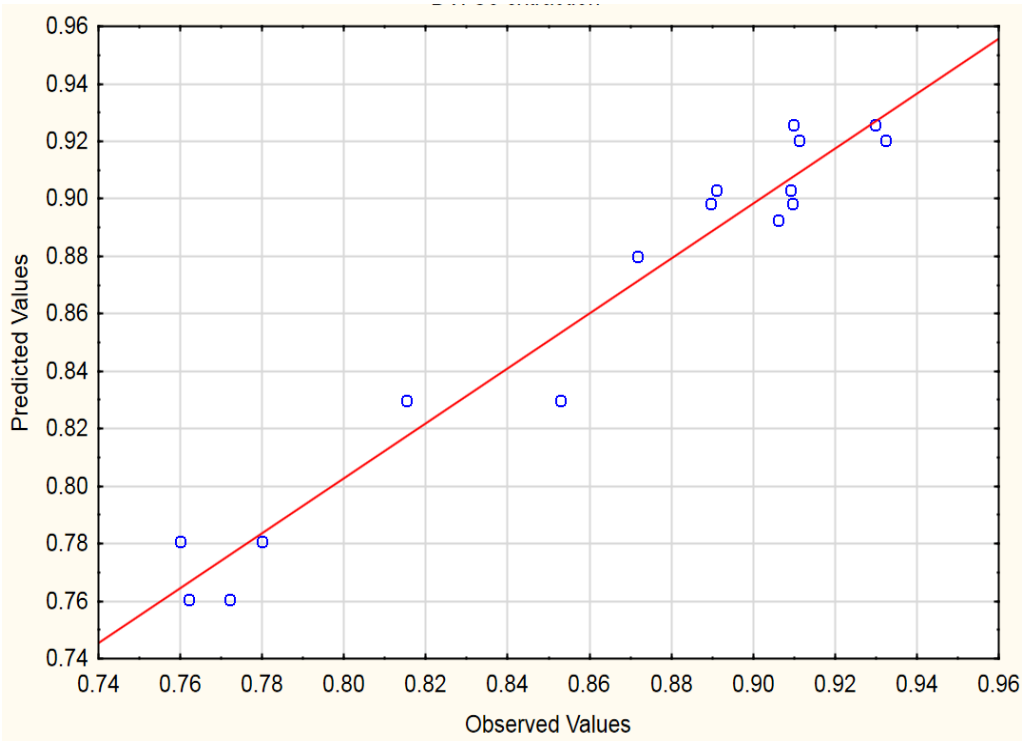

Figure A 49: Predicted (quadratic model) vs observed values for selenium extraction

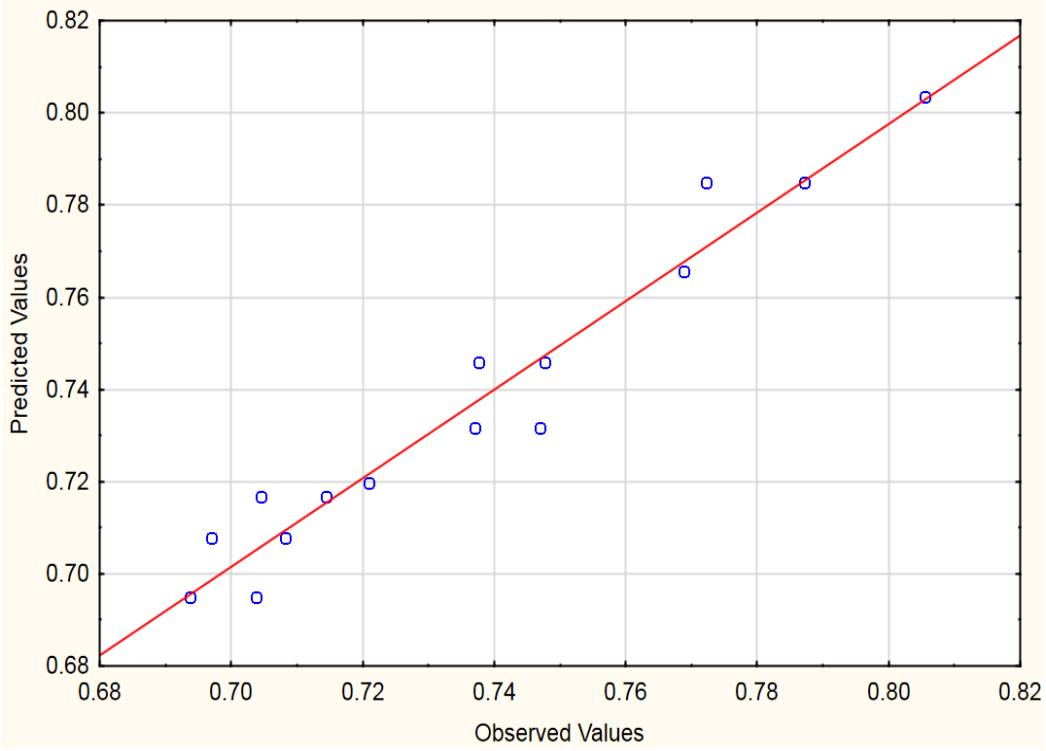

Figure A 50: Predicted (quadratic model) vs observed values for arsenic extraction

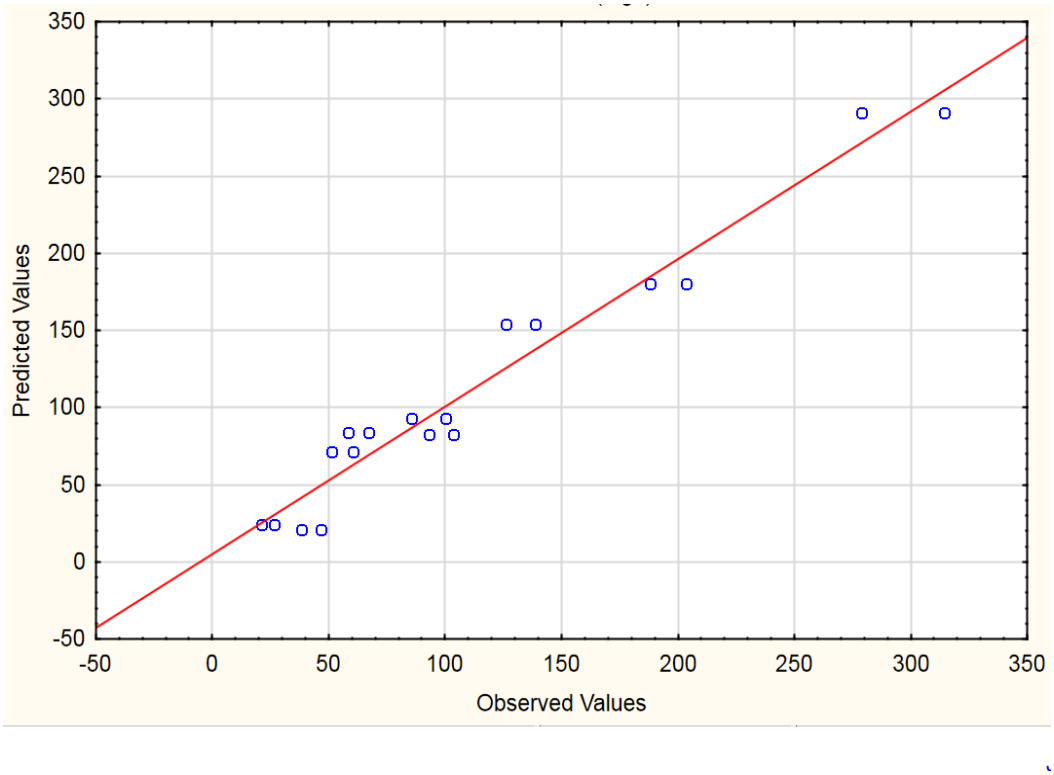

Figure A 51: Predicted (quadratic model) vs observed values for ruthenium extraction

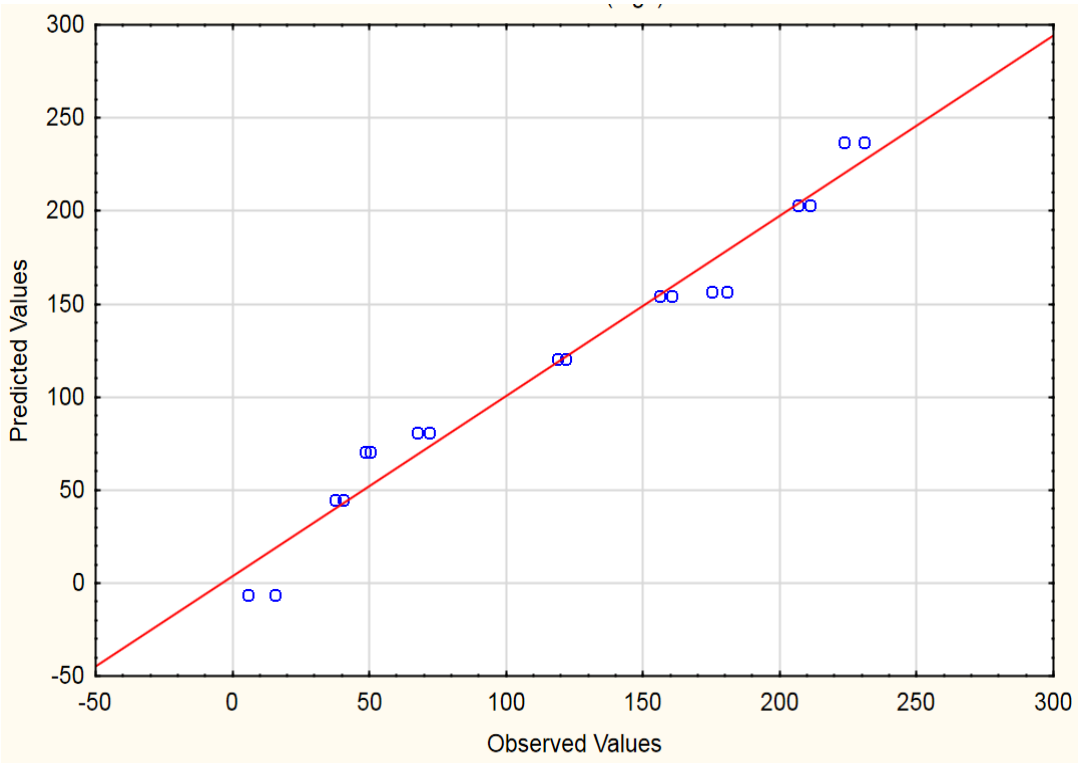

Figure A 52: Predicted (quadratic model) vs observed values for ruthenium extraction

Appendix VIII

Brunauer, Emmett and Teller (BET) Theory

The Brunauer Emmett and Teller (BET) theory aims to explain the physical adsorption of gas molecules on a solid surface and serves as the basis of for an important analysis technique for the measurement of the specific surface area of a material.

The concept of the theory is an extension of the Langmuir theory which is a theory of monolayer molecular adsorption, to multilayer adsorption with the hypothesis that gas molecules physically adsorb on a solid in layers infinitely and that there is no interaction between each adsorbed layer and that the Langmuir theory can be applied to each layer. See (Brunauer et al., 1938, Masel, 2001) for details.

Saturn DigiSizer 5200

The particle size distribution of the powder material was performed on a particle sizing instrument Saturn DigiSizer 5200, Micrometrics. The instrument gives the particle size distribution of a sample by detecting its light scattering pattern when the specimen is suspended in a specific solution. The instrument analyses samples in a liquid media and is capable of analysing particles in the range of 0.05 to 1000 micrometres. It is equipped with an ultra-sonic probe for internal dispersion of samples and auto sampler that can be set to run multiple samples automatically.

APPENDIX IX

Table A 32: Hazards identification

Hazard	Example of Hazard	Example of activity	Preventive action
Chemicals			
Sodium hydroxide, Sodium sulphite, Hydrochloric acid		Leaks during operation Loading reactor contents Sampling	Do regular leak tests, ensure all valves closed before operation Wear PPE, Handle material with care Wear ppe
Oxygen	Oxygen cylinder leaks		Close all regulator valves when not being used, Keep flammable substances away from cylinder
High temperatures	High temperature of reactor surface Fire Overheating	Increased fire hard near running reactor Programming and reprograming of temperature controller Cooling water not running in reactor	Allow reactor to cool before handling Set limit on temperature controller
High pressure			
Reactor vessel	Bursting Unexpected pressure release	Addition of oxygen gas to vessel Discharging of reactor	Put all reactor locking systems in place, Use protective shield Always depressurise reactor as part of shut down procedure